

**PHOTO-MEDIATED FENTON-LIKE PROCESS IN THE
REMOVAL OF MICRO-POLLUTANTS FROM AQUEOUS
SOLUTIONS USING HIGHLY ACTIVE NANO-CATALYST**

**A THESIS SUBMITTED IN PARTIAL FULFILMENT OF THE
REQUIREMENTS FOR THE DEGREE OF DOCTOR OF
PHILOSOPHY**

HIMANGSHU DIHINGIA

MZU REGISTRATION NUMBER : 1506749

Ph.D. REGISTRATION NUMBER: MZU/Ph.D./1103 of 24.04.2018



**DEPARTMENT OF CHEMISTRY
SCHOOL OF PHYSICAL SCIENCES
DECEMBER, 2022**

**PHOTO-MEDIATED FENTON-LIKE PROCESS IN THE
REMOVAL OF MICRO-POLLUTANTS FROM AQUEOUS
SOLUTIONS USING HIGHLY ACTIVE NANO-CATALYST**

BY
HIMANGSHU DIHINGIA
Department of Chemistry

Under the supervision of
Prof. DIWAKAR TIWARI

Submitted
In partial fulfilment of the requirement of the Degree of Doctor of Philosophy in
Chemistry of Mizoram University, Aizawl.



MIZORAM UNIVERSITY
Department of Chemistry
(A DST-FIST Supported Department)
Tanhril, Aizawl, Mizoram. PIN: 796004

Prof. Diwakar Tiwari, Dean (SPS)

Thesis Certificate

This is to certify that the thesis entitled '*Photo-mediated Fenton-like Process in the Removal of Micro-pollutants from Aqueous Solutions using Highly Active Nano-catalyst*' submitted by **Mr. Himangshu Dihingia** for the degree of **Doctor of Philosophy** in the Mizoram University, Aizawl, Mizoram, embodies the record of original investigations carried out by him under my supervision. He has been duly registered and the thesis presented is worthy of being considered for the award of the Ph.D. degree. This work has not been submitted for any degree in any other university.

Dated: 14th December, 2022.

(DIWAKAR TIWARI)

Supervisor

DECLARATION OF THE CANDIDATE

Mizoram University

December, 2022

I, HIMANGSHU DIHINGIA, hereby declare that the subject matter of this thesis is the record of work done by me, that the contents of this thesis did not form basis of the award of any previous degree to me or to do the best of my knowledge to anybody else, and that the thesis has not been submitted by me for any research degree in any other University/Institute.

This is being submitted to the Mizoram University for the degree of Doctor of Philosophy in Chemistry.

Dated: 14th December, 2022.

(HIMANGSHU DIHINGIA)

Candidate

(Prof. MUTHUKUMARAN, R)

Head

(Prof. DIWAKAR TIWARI)

Supervisor

ACKNOWLEDGEMENT

I would like to express my deepest and sincere gratitude to my research supervisor, *Prof. Diwakar Tiwari*, Department of Chemistry, Mizoram University, for allowing me to do research and giving helpful suggestions and guidance throughout this research. His vision, dynamism, motivation, and sincerity have deeply encouraged me. He has been a great teacher, a friend, and a guiding light to me. It was a great honor to work and study under his guidance. I would also like to express my gratitude for his compassion and good humor. I like to express my heartfelt thanks to his wife, and family for their support, acceptance, and endurance throughout the time he has devoted to my research work and thesis preparation.

I sincerely thank and give respect to *Prof. Muthukumaran, R., Head, Department of Chemistry, MZU*, and other faculty members *viz., Dr. Zodinpuia Pachuau, Dr. N. Mohondas Singh, Dr. Ved Prakash Singh, and Dr. A. Bimolini Devi*, for their constant encouragement and useful advice they have offered me throughout my academic career in the University. My heartfelt thanks go to *Dr. Lalhmunsiama* for his incentive and helpful suggestions in completing my research work.

I am grateful for the close cooperation and support I received from all of my colleagues in the Department of Chemistry. I'd like to thank *Dr. J. Lalmalsawm, Dr. R. Malsawmdawgnzela, Dr. Levia Lalthazuala, Ms. Ngainunsiami, Mr. CVL Hmingmawia, Mr. Ricky Lalawmpuia, Mr. Sarikokba, Ms. Melody Lalhruaitluangi, Ms. Swagata Goswami, Ms. Lalmalsawmdawngliani, Ms. Barsha Rabha* and *Mr. Lalruatkima Ralte* for assisting me with my laboratory work. I owe a deep sense of gratitude to the assistance of *Mr. Brojendro Singh Shagolsem*, Sr. Laboratory Technician, and *Mr. John Vanlalhruaia*, Technical Assistant, Chemistry Department.

It is my privilege to thank my parents and all of my family members for their love and support during my tenure for the degree, as well as their comforts and prayers; I can't repay them entirely, but I thank and appreciate them for the bottom of my heart.

After all, I thank Almighty God for blessing me with health, strength, and knowledge to accomplish this work. Without his grace and mercy, this work would not have been possible.

(HIMANGSHU DIHINGIA)

CONTENTS

	<i>Pages</i>
Title of the Thesis	i
Certificate	ii
Declaration of the Candidate	iii
Acknowledgments	iv
Contents	vi
List of Figures	x
List of Tables	xvi

CHAPTER 1

1. INTRODUCTION	1
1.1 Water resources	1
1.2 Contaminated water and water reuse	2
1.3 Advanced oxidation processes (AOPs)	3
1.3.1 Classical Fenton process and its modifications	5
1.3.2 Fenton-Like process and its modifications	8
1.3.3 Development of nano-Fenton-like catalyst (nFLC)	9
1.4 Emerging contaminants	9
1.4.1 Diclofenac (DCF)	13
1.4.2 Phenol	15
1.4.3 N-(n-propyl) Thiourea (NNPT)	16
1.4.4 Amoxicillin (AMX)	18
1.4.5 Sulfamethazine (SMZ)	19
1.5 Review of literature	21
1.5.1 Iron-based nFLC	21
1.5.2 Copper-based nFLC	27
1.6 Scope of the present investigation	32

CHAPTER 2

2. METHODOLOGY	35
2.1 Materials	35
2.1.1 Chemicals	35
2.1.2 Clay samples and real water samples	36
2.1.3 Reagents	38
2.1.4 Instruments	38
2.2 Preparation Of Materials	39
2.2.1 Preparation of guava leaf extract	39
2.2.2 Synthesis of nanocomposite materials	40
2.2.2.1 Preparation of <i>Ben@FeNPs</i> and <i>Ben@(FeNPs+AgNPs) nFLC</i>	40
2.2.2.2 Synthesis of <i>Ben@CuNPs</i> and <i>Ben@(CuNPs+AgNPs) nFLC</i>	41
2.3 Characterization of the materials	42
2.3.1 Phytochemical screening	42
2.3.2 Characterization of nanocomposite materials	44
2.4 Batch reactor Studies	47
2.4.1 Degradation of targeted organic pollutants	47
2.4.2 Effect of Solution pH	49
2.4.3 Optimization of initial H ₂ O ₂ and nanocomposite dose	50
2.4.4 Photo-Fenton-like degradation of micropollutants	50
2.4.5 Effect of initial concentration of the pollutant	51
2.4.6 Effect of co-existing ions	51
2.4.7 Degradation kinetics	52
2.4.8 Involvement of •OH radical	52
2.4.9 Mineralization of organic pollutants: TOC measurements	53
2.4.10 Determination of leached ion concentrations	54
2.4.11 Reutilization of the nanocatalyst	55
2.4.12 Real water experiments	55

CHAPTER 3

3. RESULTS AND DISCUSSION	57
3.1 Characterization of materials	57
3.1.1 Phytochemical studies of <i>P. Guajava</i> (guava) leaf extract	57
3.1.2 pH_{pzc} , band-gap energy, and BET surface area analysis	58
3.1.3 Surface morphology of nanocomposites	64
3.1.4 XRD and XPS analysis	69
3.2 Photo-Fenton-like degradation of diclofenac sodium (DCF), phenol, and n-(n-propyl) thiourea from aqueous solution	73
3.2.1 Effect of initial pH	73
3.2.2 Effect of H ₂ O ₂ dosage and nanocomposite dosage	75
3.2.3 Photo-Fenton-like degradation of DCF, Phenol, and NNPT	79
3.2.4 Concentration dependence abatement of DCF, phenol, and NNPT	82
3.2.5 Presence of several cations/anions	84
3.2.6 Degradation kinetics of DCF, phenol, and NNPT	87
3.2.7 Involvement of •OH radical	89
3.2.8 Mineralization of target organic pollutants	92
3.2.9 Determination of leached iron (II) concentrations	94
3.2.10 Reutilization of nanocatalyst	97
3.2.11 Real matrix water experiments	99
3.3 Degradation of Amoxicillin (AMX) and Sulfamethazine (SMZ) using Ben@(CuNPs+AgNPs) nFLC	103
3.3.1 Effect of initial pH	103
3.3.2 Effect of initial H ₂ O ₂ dosage and nanocomposite dosage	106
3.3.3 Photo-Fenton-like degradation of AMX and SMZ	108
3.3.4 Concentration dependence removal of AMX and SMZ	111
3.3.5 Presence of other cations/anions	112
3.3.6 Degradation kinetics of AMX and SMZ	114

3.3.7	Involvement of •OH radical	115
3.3.8	Mineralization of target organic pollutants	118
3.3.9	Determination of leached copper (II) concentrations	119
3.3.10	Reutilization of the nanocatalyst	121
3.3.11	Real matrix water experiments	123

CHAPTER 4

4. Conclusion	128
4.1 Future Perspective	131
REFERENCES	133
BIODATA	173
LIST OF PUBLICATIONS	174
PARTICULARS OF CANDIDATE	182

List of Figures:

Figure 1.1: Steps involved in an AOPs treatment of wastewater.

Figure 1.2. Schematics of the classical Fenton process.

Figure 1.3: Speciation diagram of iron in aqueous solution with different pH.

Figure 1.4: Chemical structure of diclofenac.

Figure 1.5: Chemical structure of phenol.

Figure 1.6: Chemical structure of N-(n-propyl) Thiourea.

Figure 1.7: Chemical structure of Amoxicillin.

Figure 1.8: Chemical structure of Sulfamethazine.

Figure 2.1: (a) Guava leaf powder; (b) Aqueous guava leaves extract.

Figure 2.2: Image of (a) Pristine bentonite clay ; (b) Ben@FeNPs, and (c) Ben@(FeNPs+AgNPs) nanocomposite.

Figure 2.3: Image of (a) Bentonite clay powder; (b) Ben@(CuNPs+AgNPs) nanocomposite.

Figure 2.4: Schematic of dark Cabinet for conducting the experiments.

Figure 3.1: FT-IR spectrum of aqueous *P. Guajava* (guava) leaf extract.

Figure 3.2: (a) The Tauc plots for determination of intermediate band-gap energy (E_g) of pristine bentonite, Ben@FeNPs, and Ben@(FeNPs+AgNPs) solids; (b) The Tauc plots for determination of intermediate band-gap energy (E_g) of pristine bentonite, Ben@CuNPs, and Ben@(CuNPs+AgNPs) solids.

Figure 3.3: (a) N_2 adsorption/desorption isotherms obtained for pristine bentonite (Ben), Ben@FeNPs, and Ben@(FeNPs+AgNPs) nanocomposites; (b) the pore size distribution graph for pure bentonite (Ben), Ben@FeNPs, and Ben@(FeNPs+AgNPs) nanocomposites.

Figure 3.4: (a) N₂ adsorption/desorption isotherms obtained for pristine bentonite (Ben), Ben@CuNPs, and Ben@(CuNPs+AgNPs) nanocomposites; (b) the pore size distribution graph for pure bentonite (Ben), Ben@CuNPs, and Ben@(CuNPs+AgNPs) nanocomposites.

Figure 3.5: SEM pictures of (a) pristine Bentonite (b) Ben@FeNPs (c) Ben@(FeNPs+AgNPs) (d) Ben@CuNPs and (e) Ben@(CuNPs+AgNPs) nanocomposite solids. EDX elemental spectra of (f) Pristine bentonite (g) Ben@FeNPs; and (h) Ben@(FeNPs+AgNPs) nanocomposite solids.

Figure 3.6: Transmission electron microscopy (TEM) pictures of (a) pristine bentonite; (b) Ben@FeNPs; (c) Ben@(FeNPs+AgNPs); (d) Ben@CuNPs; and (e) Ben@(CuNPs+AgNPs) nanocomposite solids; Particle size distribution of (f) Ben@CuNPs; and (g) Ben@(CuNPs+AgNPs) nanocomposite solids

Figure 3.7: (a) XRD spectra of pristine bentonite, Ben@FeNPs, and Ben@(FeNPs+AgNPs) nanocomposite solids [Inset: The XRD pattern of Ben@(FeNPs+AgNPs) nanocomposite material]; (b) X-ray diffraction pattern of the pristine bentonite; synthesized Ben@CuNPs and Ben@(CuNPs+AgNPs) nanocomposite solids.

Figure 3.8: (a) XPS survey for the Ben@(FeNPs+AgNPs) nanocomposite material [Inset: The XPS spectrum of iron (Fe) and silver (Ag) nanoparticles in the nanocomposite material]; (b) XPS survey for the Ben@(CuNPs+AgNPs) nanocomposite material [Inset: The XPS spectrum of copper (Cu) and silver (Ag) nanoparticles in the nanocomposite material].

Figure 3.9: Percentage degradation of DCF, phenol, and NNPT at different pH values under a dark environment [Catalyst dose = 200.0 mg/L; H₂O₂ dose (30%) = 0.2 mL/L; [Pollutant] = 2.0 mg/L; Reaction time = 2 hrs].

Figure 3.10: Percentage degradation of (a) DCF, (c) phenol & (d) NNPT at different dosages of H₂O₂ in a dark environment under reaction condition as [pH = 3.0; [Pollutant] = 2.0 mg/L; catalyst dose = 200.0 mg/L; reaction time = 2 hrs]; percentage degradation of (b) DCF, (d) phenol & (f) NNPT at different dosages of nanocatalyst in a dark environment under reaction condition as [pH = 3.0; [Pollutant] = 2.0 mg/L; peroxide dose = 0.2 mL/L; Reaction time = 2 hrs].

Figure 3.11: Disappearance of (a) DCF [pH = 3.0; [DCF] = 2.0 mg/L; catalyst dose = 250.0 mg/L; H₂O₂ dose = 0.4 mL/L; reaction time = 2 hrs] (b) Phenol [pH = 3.0; [Phenol] = 2.0 mg/L; catalyst dose = 100 mg/L; H₂O₂ dose = 0.15 mL/L; reaction time = 2 hrs] and (c) NNPT [pH = 3.0; [NNPT] = 2.0 mg/L; catalyst dose = 125 mg/L; H₂O₂ dose = 0.10 mL/L; reaction time = 2 hrs] vs. reaction time (min) in different reaction conditions.

Figure 3.12: Percentage degradation vs initial concentration of (a) DCF [pH= 3.0; Catalyst dose = 250.0 mg/L; H₂O₂ dose = 0.4 mL/L; Reaction time = 2 hr]; (b) phenol [pH= 3.0; Catalyst dose = 100.0 mg/L; H₂O₂ dose = 0.15 mL/L; Reaction time = 2 hrs] & (c) NNPT [pH= 3.0; Catalyst dose = 125.0 mg/L; H₂O₂ dose = 0.1 mL/L; Reaction time = 2 hrs] in different light ambiance.

Figure 3.13: Effect of coexisting ions in different light conditions for (a) DCF [pH = 3.0; [DCF]= 2.0 mg/L; [Co-existing ion] = 10.0 mg/L; Catalyst dose = 250.0 mg/L; H₂O₂ dose = 0.4 mL/L; Reaction time = 2 hr]; (b) phenol [pH = 3.0; [phenol]= 2.0 mg/L; [Co-existing ion] = 10.0 mg/L; Catalyst dose = 100.0 mg/L; H₂O₂ dose = 0.15 mL/L; Reaction time = 2 hrs] & (c) NNPT [pH = 3.0; [NNPT]= 2.0 mg/L; [Co-existing ion] = 10.0 mg/L; Catalyst dose = 125.0 mg/L; H₂O₂ dose = 0.1 mL/L; Reaction time = 2 hrs].

Figure 3.14: The kinetics of DCF [(a) and (b)], phenol [(c) and (d)], and NNPT [(e) and (f)] degradation using the PFO; and PSO models.

Figure 3.15: Effect on percentage degradation in the presence of scavengers [pH= 3.0; [pollutant] = 2.0 mg/L; [scavenger] = 0.1 mol/L (10 mL/L); Catalyst dose = 250.0 mg/L for DCF, 100.0 mg/L for phenol and 125.0 mg/L for NNPT;

H₂O₂ dose = 0.4 mL/L for DCF, 0.15 mL/L for phenol and 0.1 mL/L for NNPT; Reaction time = 2 hrs].

Figure 3.16: Mineralization(%) at different concentrations of (a) DCF [pH = 3.0; Catalyst dose = 250.0 mg/L; H₂O₂ dose = 0.4 ml/L; Reaction time = 2 hr]; (b) phenol [pH = 3.0; Catalyst dose = 100.0 mg/L; H₂O₂ dose = 0.15 ml/L; Reaction time = 2 hrs] and (c) NNPT [pH = 3.0; Catalyst dose = 125.0 mg/L; H₂O₂ dose = 0.1 ml/L; Reaction time = 2 hrs].

Figure 3.17: Leaching of iron concentration along with the disappearance of (a) DCF [pH = 3.0; Catalyst dose = 250.0 mg/L; H₂O₂ dose = 0.4 mL/L; Reaction time = 2 hr]; (b) phenol [pH = 3.0; Catalyst dose = 100.0 mg/L; H₂O₂ dose = 0.15 mL/L; Reaction time = 2 hrs] and (c) NNPT [pH = 3.0; Catalyst dose = 125.0 mg/L; H₂O₂ dose = 0.1 mL/L; Reaction time = 2 hrs] as a function of time.

Figure 3.18: Reusability of the Ben@(FeNPs+AgNPs) nanocomposite in the degradation of (a) DCF [pH = 3.0; Catalyst dose = 250.0 mg/L; H₂O₂ dose = 0.4 mL/L; Reaction time = 2 hr]; (b) phenol [pH = 3.0; Catalyst dose = 100.0 mg/L; H₂O₂ dose = 0.15 mL/L; Reaction time = 2 hrs] and (c) NNPT [pH = 3.0; Catalyst dose = 125.0 mg/L; H₂O₂ dose = 0.1 mL/L; Reaction time = 2 hrs] as a function of time.

Figure 3.19: photo Fenton-like degradation in the real water system for DCF [pH = 3.0; Catalyst dose = 250.0 mg/L; H₂O₂ dose = 0.4 mL/L; Reaction time = 2 hr]; phenol [pH= 3.0; Catalyst dose = 100.0 mg/L; H₂O₂ dose = 0.15 mL/L; Reaction time = 2 hrs] and NNPT [pH= 3.0; Catalyst dose = 125.0 mg/L; H₂O₂ dose = 0.10 mL/L; Reaction time = 2 hrs].

Figure 3.20: Degradation (%) of AMX and SMZ at different pH values under a dark environment [Catalyst dose = 300.0 mg/L; H₂O₂ dose (30%) = 0.2 mL/L; [Pollutant] = 2.0 mg/L; Reaction time = 2 hrs].

Figure 3.21: Percentage degradation of (a) AMX and (c) SMZ at different dosages of H₂O₂ in a dark environment under reaction condition as [pH = 3.0;

[Pollutant] = 2.0 mg/L; Catalyst dose = 200.0 mg/L; Reaction time = 2 hrs]; Percentage degradation of (b) AMX, & (d) SMZ at different dosages of nanocatalyst in a dark environment under reaction condition as [pH = 3.0; [Pollutant] = 2.0 mg/L; peroxide dose = 0.2 ml/L; Reaction time = 2 hrs].

Figure 3.22. Removal of (a) AMX [pH = 3.0; [AMX] = 2.0 mg/L; catalyst dose = 300.0 mg/L; H₂O₂ dose = 0.2 mL/L; reaction time = 2 hrs]; and (b) SMZ [pH = 3.0; [SMZ] = 2.0 mg/L; catalyst dose = 250.0 mg/L; H₂O₂ dose = 0.15 mL/L; reaction time = 2 hrs] vs. reaction time (min) at different reaction conditions in the photo-Fenton-like reactions.

Figure 3.23: Percentage degradation vs initial concentration of (a) AMX [pH= 3.0; Catalyst dose = 300.0 mg/L; H₂O₂ dose = 0.2 mL/L; Reaction time = 2 hrs] & (b) SMZ [pH= 3.0; Catalyst dose = 250.0 mg/L; H₂O₂ dose = 0.15 mL/L; Reaction time = 2 hrs] in different light ambiance.

Figure 3.24: Effect of coexisting ions in different light conditions for (a) AMX [pH=3.0; [AMX]= 2.0 mg/L; [Co-existing ion] = 10.0 mg/L; Catalyst dose = 300.0 mg/L; H₂O₂ dose = 0.2 mL/L; Reaction time = 2 hrs] & (b) SMZ [pH = 3.0; [SMZ]= 2.0 mg/L; [Co-existing ion] = 10.0 mg/L; Catalyst dose = 250.0 mg/L; H₂O₂ dose = 0.15 mL/L; Reaction time = 2 hrs].

Figure 3.25: The kinetics of AMX [(a) and (b)] and SMZ [(c) and (d)] degradation using the PFO; and PSO models.

Figure 3.26: Effect on percentage degradation in the presence of scavengers [pH = 3.0; [pollutant] = 2.0 mg/L; [scavenger] = 0.1 mol/L (10 mL/L); Catalyst dose = 300.0 mg/L for AMX and 250.0 mg/L for SMZ; H₂O₂ dose = 0.2 mL/L for AMX and 0.15 mL/L for SMZ; Reaction time = 2 hrs].

Figure 3.27: Mineralization (%) at different concentrations of (a) AMX [pH = 3.0; Catalyst dose = 300.0 mg/L; H₂O₂ dose = 0.2 ml/L; Reaction time = 2 hrs] and (b) SMZ [pH = 3.0; Catalyst dose = 250.0 mg/L; H₂O₂ dose = 0.15 ml/L; Reaction time = 2 hrs].

Figure 3.28: Leaching of copper concentration along with the disappearance of (a) AMX [pH = 3.0; Catalyst dose = 300.0 mg/L; H₂O₂ dose = 0.2 mL/L; Reaction time = 2 hrs] and (b) SMZ [pH = 3.0; Catalyst dose = 250.0 mg/L; H₂O₂ dose = 0.15 mL/L; Reaction time = 2 hrs] as a function of time.

Figure 3.29: Reusability tests for Ben@(CuNPs+AgNPs) nanocatalyst in the degradation of (a) AMX and (b) SMZ.

Figure 3.30: Photo Fenton-like degradation in the real water system for AMX [pH= 3.0; Catalyst dose = 300.0 mg/L; H₂O₂ dose = 0.2 mL/L; Reaction time = 2 hrs] and SMZ [pH= 3.0; Catalyst dose = 250.0 mg/L; H₂O₂ dose = 0.15 mL/L; Reaction time = 2 hrs].

List of Tables:

Table 1.1: An overview of different categories and main sources of known ECs.

Table 2.1: Details of various chemicals used for experimental works.

Table 2.2: GPS locations of real water samples collected.

Table 2.3: Physico-chemical properties of two real water samples.

Table 2.4: Different parameters for the quantification in HPLC.

Table 3.1: Qualitative identification of various phytochemicals present in *P. Guajava* leaf extract.

Table 3.2: BET-specific surface area, pore size, and pore volume of pristine bentonite (Ben), Ben@FeNPs, and Ben@(FeNPs+AgNPs) nanocomposite materials.

Table 3.3: BET-specific surface area, pore size, and pore volume of pristine bentonite (Ben), Ben@CuNPs, and Ben@(CuNPs+AgNPs) nanocomposite materials.

CHAPTER 1
INTRODUCTION

1. INTRODUCTION

1.1 Water resources

"There is a water crisis today. But the crisis is not about having too little water to satisfy our needs. It is a crisis of managing water so badly that billions of people - and the environment - suffer badly." (World Water Council).

Water, a need for life and a vital resource for mankind, is plentiful on Earth (about 1400 million km³). 97.5% of the water is, however, salt water. 70% of the remaining fresh water is frozen in the polar icecaps; the remaining 2.5% is mostly found as soil moisture or in inaccessible subsurface aquifers. Only around 1% of the world's freshwater resources are easily accessible for human use, and even that is unevenly distributed (United Nations Environment Programme and Earthscan, 2002).

Nearly 2 billion people acquired access to proper sanitation in 1990, and 2.3 billion have access to clean drinking water sources. According to a new WHO/UNICEF research, 1.6 billion of these individuals are having access to pipe water connections in their houses or complexes. A closing gap in access to clean water and proper sanitation is usually between the rural and urban regions (WHO and UNICEF, 2013). More than half of the world's population lives in cities, which still have greater access to clean water and sanitation than rural regions. In 1990, more than 76% of urban residents had better sanitation, compared to only 28% of rural residents. In 1990, 95% of urban residents had access to clean water, compared to only 62% of rural residents. By 2012, 96% of urban residents and 82% of rural residents had increased access to water (WHO and UNICEF, 2013). Despite this significant increase, there are still significant regional, sociocultural, and economic disparities in access to drinking water and sanitation facilities all across the world. Aside from the differences in access between urban and rural regions, there are also noticeable inequalities in access inside towns and cities. Low-income people, those living in informal or illegal settlements, and those living on the outskirts of cities or small towns are less likely to have access to clean water and proper sanitation (WHO and UNICEF, 2013).

Furthermore, 884 million people still lack access to clean drinking water, and 2.6 billion people (two in every five) lack adequate sanitation. Diseases including

cholera, diarrhea, dysentery, hepatitis A, and typhoid are directly related to the quality of water and sanitation. Moreover, insufficient or inadequate water and sanitation services in healthcare institutions are caused several infectious diseases (3.5 million people die prematurely each year as a result of water-related diseases).

The situation is grim due to the shortage of water as a result of climate change and the increased exploitation of available resources. By 2050, the world population is expected to reach 9 billion, an increase of 4 billion from 1990. Water shortage is a natural as well as a manmade occurrence. There is enough fresh water on the earth for seven billion people, but it is unequally distributed, and much is wasted, contaminated, or managed in an unsustainable manner. Increased demand for energy and food as a result of population growth and expanding economies puts even more stress on limited water and land resources, while also providing an opportunity for new technology to more efficiently utilize water. To address the global problem of water shortages, a concerted effort from all sectors is required and reutilization of water is one of the possible solutions.

1.2 Contaminated water and water reuse

Implementing appropriate treatment technology, which is efficient in eliminating pollutants and providing clean water is a possible contribution to the field of Environmental Engineering to address amicably the problem of water shortages. The largest threat to the world's freshwater supply, aside from global water shortages, is the dumping of contaminants into water bodies that affects adversely both human health and the environment. Wastewater treatment facilities (WWTPs) are being constructed to reduce contaminants loads on water bodies (Meneses et al., 2010a). The complexity of the effluent of a wastewater treatment plant, on the other hand, renders the definition of a conclusive treatment scheme unfeasible. As a result, a traditional water treatment plan may not always be adequate to remove the pollution charge. To avoid this, a thorough examination of the influent quality is required. As a result, specialized treatments capable of degrading refractory contaminants that cannot be removed by regular treatments may be required in WWTPs, especially when reuse is the goal.

Preliminary and primary (physical and chemical) treatment, as well as secondary (biological) treatment, are the two degrees of treatment used in typical WWTPs. Suspended particles, biodegradable organics, harmful microorganisms, and nutrients are significantly reduced by these treatments. Furthermore, because the water cycle promotes sustainability, WWTPs should recover water resources (reclaimed water), energy (methane from anaerobic digestion), and materials (biosolids and nutrients). Normally, treated wastewater is discharged into the sea or rivers, rather than being reused. A WWTP can obtain a resource from wastewater by performing tertiary treatment on the treated wastewater, which is then reused (Meneses et al., 2010a). The basic goal of wastewater reclamation and reuse is to provide high-quality water for all non-potable purposes (uses that do not require drinking water quality standards). Reclaimed water would save a lot of freshwaters that would otherwise be discarded (Iglesias Esteban and Ortega de Miguel, 2008; Meneses et al., 2010b). Traditional practices such as agricultural and landscape irrigation, industrial applications, environmental applications, recreational activities, urban cleaning, and construction, among others, could be benefitted from reclaimed water (Meneses et al., 2010a; Petala et al., 2006; Yang and Abbaspour, 2007).

1.3 Advanced oxidation processes (AOPs)

In light of the dwindling global water supply, ECs (emerging contaminants) have attracted attention owing to their extremely harmful effects on human health, even at low levels. It is thus imperative that an efficient and safe treatment method is to be developed to remove efficiently the recalcitrant contaminants. Further, the conventional WWTPs are not efficient enough in eliminating emerging water contaminants hence, advanced treatment technologies are required to better tune the existing wastewater treatment technology.

In order to eliminate emerging and persistent water contaminants, an overdose of chemicals results in excessive toxic wastes. Advanced treatment technology, such as nanofiltration (NF), ultrafiltration (UF), reverse osmosis (RO), membrane bioreactors (MBRs), and catalytic oxidation, are effective in removing ECs, but their high operating costs are key issues associated with these approaches (Guo et al., 2020). It is also reported that ecologically sustainable procedures use less energy and produce

fewer hazardous byproducts (Rahim Pouran et al., 2014). Therefore, researchers are exploring newer and more efficient alternative methods for the treatment of recalcitrant contaminants.

Advanced oxidation processes (AOPs) are a novel approach for efficient and accelerated degradation of resistant micropollutants that are used in conjunction with a variety of treatment methods. Advanced oxidation processes (AOPs), defined as oxidation processes including the formation of hydroxyl radicals ($\bullet\text{OH}$) in sufficient quantities to influence water purification, were initially proposed for potable water treatment in the 1980s (Glaze et al., 1987). The AOP idea was further applied to oxidative reactions using sulfate radicals ($\text{SO}_4^{\bullet-}$). AOPs can thus be defined as all chemical treatment procedures based on the production of very reactive species (especially hydroxyl radicals) in atmospheric temperature and pressure conditions with or without catalyst and/or reactive energy (electrochemical, UV-Vis, or ultrasounds) in atmospheric conditions. Several organic compounds can be oxidized and mineralized by AOPs, resulting in CO_2 and inorganic ions as end products.

A wide range of methods are used under AOPs, including Fenton: Iron(II)/ H_2O_2 (Kallel et al., 2009), Photo-Fenton: Iron(II)/ H_2O_2 /UV, ozonization (O_3) (Amat et al., 2003), $\text{H}_2\text{O}_2/\text{O}_3$ (Lee et al., 2011), H_2O_2 /UV (Lucas and Peres, 2009), hetero-/homogeneous Fenton-like processes, TiO_2 /UV (Lalhriatpuia et al., 2015), AuNPs/ TiO_2 (Lalliansanga et al., 2020b), ZnO/UV (Karunakaran and Anilkumar, 2007), supplemented with the light (Tiwari et al., 2018a) or microwave, electrical energy, cavitation field, etc. (Molina et al., 2006; Rajesh Banu et al., 2019).

Advanced oxidation is divided into many phases, which are given in Figure 1.1 and explained as follows:

- (i) Strong oxidants are formed (e.g. hydroxyl radicals).
- (ii) Biodegradable intermediates are produced when these oxidants react with organic molecules in water.

(iii) Mineralization is the reaction of biodegradable intermediates with oxidants (i.e. production of water, carbon dioxide, and inorganic salts).

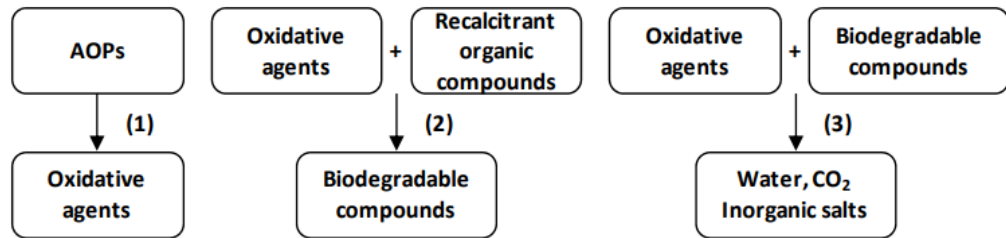
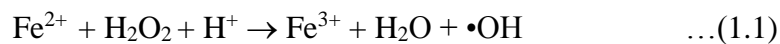


Figure 2.1. Steps involved in an AOPs treatment of wastewater.

The success of AOPs is, in reality, highly reliant on several factors, including the stream's composition and concentration load, as well as the treatment itself.

1.3.1 Classical Fenton process and its modifications

The classic Fenton reaction uses ferrous (Fe^{2+}) ions and peroxides (often H_2O_2) to form reactive oxygen species (ROS), which oxidizes the organic and inorganic molecules alike. H.J.H. Fenton initially developed the Fenton reaction in 1894, when he researched the redox processes that occurred during the oxidation of tartaric acid (Fenton, 1894). The mechanism of the reaction was studied by many researchers and it was described most commonly as (Equation 1.1) Figure (1.2) (Gupta et al., 2016; Kremer, 1999; Thomas et al., 2009; Zhang et al., 2019) :



Various Physicochemical parameters *viz.*, pH, the dose of the Fenton reagent, amount of H_2O_2 , and initial organic pollutant concentrations are the driving factors for the Fenton processes. However, an extremely important parameter is the solution pH of the treatment (Wang et al., 2016). In aqueous solutions, although iron (II) species remain in dissolved form even at neutral pH, however, the iron (III) species start forming hydroxo species at $\text{pH} \geq 4$, and thereby, the efficiency of the Fenton processed diminished (Salgado et al., 2013). The speciation diagram of iron shows that pH 2.8 to 3.2 is the optimum pH range for the Fenton process (Figure 1.3) (Bokare and Choi, 2014). Some other researchers also found that the pH range 2-4 is optimum for

achieving greater efficiency in the Fenton reaction (Barb et al., 1949; Pignatello et al., 2006; Rodríguez et al., 2003; Utset et al., 2000). The wastewater samples are not often found within this pH range, therefore, to attain the optimal pH range of the Fenton process, a high amount of acid is added for adjusting wastewater pH within the pH range of 2-4 before processing, which eventually increases the treatment cost.

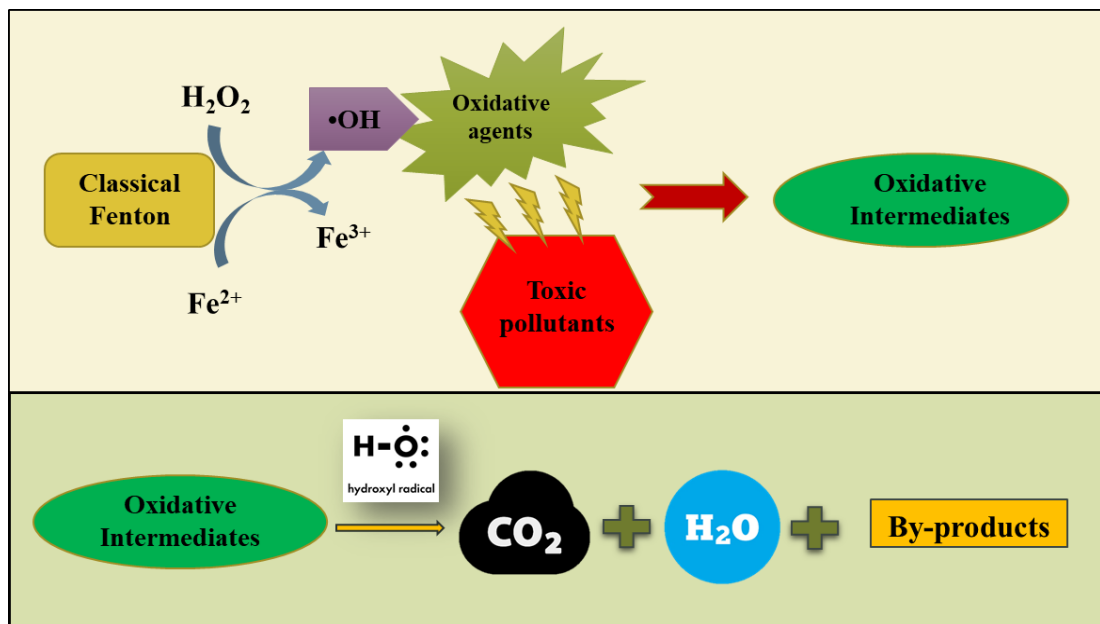


Figure 1.2. Schematics of the classical Fenton process.

Depending on the catalyst used, the Fenton process was categorized into two types, homogeneous and heterogeneous Fenton process. In the homogeneous process, whole reacting species are in the same phase (i.e., liquid phase). But homogeneous Fenton reactions are having few disadvantages as it requires a relatively higher iron dose (50-80 ppm) with a limited pH region to carry out the process (Neyens and Baeyens, 2003). On the other hand, the heterogeneous Fenton process is contained different phases i.e., the catalyst and target pollutants are in different phases. The reactions mainly occur on the heterogeneous catalyst surface, where adsorption, as well as diffusion processes, are occurred (Escher et al., 2006). This heterogeneous Fenton process is carried out at a wide pH range and enables reutilization of the iron used. Furthermore, the efficiency of the process is rendered with several physical

field(s)/phenomena as successfully coupled with photo, electro, microwave, cavitation, ultrasound, etc.

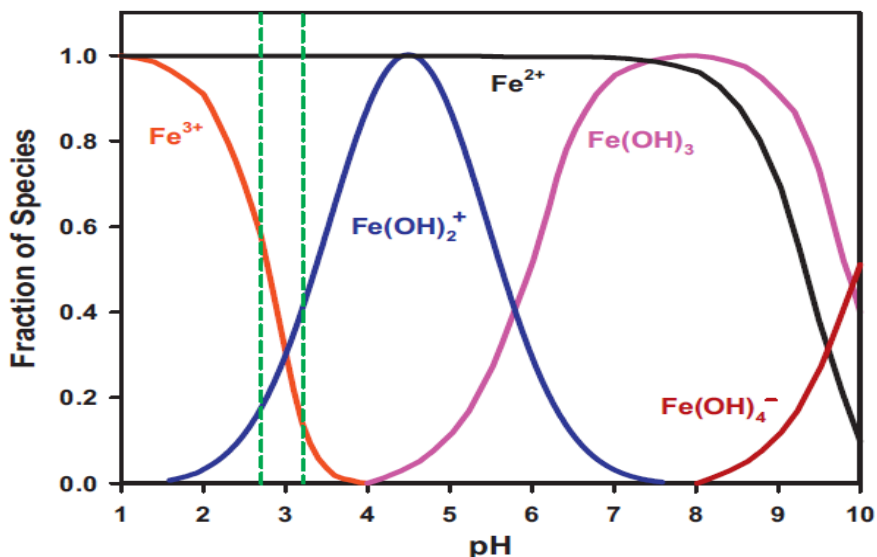


Figure 1.3: Speciation diagram of iron in aqueous solution with different pH (Bokare and Choi, 2014).

Some researchers have shown that the production of organic radical (R•) is from organic substrates (R-H) since the •OH radical eliminates a hydrogen atom from R-H. The R• radical consequently takes part in the reaction process as a moderate oxidizing agent (Neyens and Baeyens, 2003; Nidheesh et al., 2013). In the absence of other competitive scavengers for •OH or R• in the reaction processes, the organic compounds are mineralized into CO₂ and water by the classical Fenton reagents, i.e Fe²⁺ and H₂O₂.

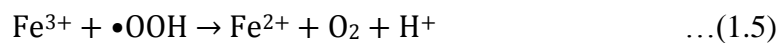
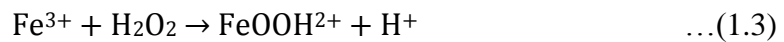
Furthermore, some reports have shown that at neutral pH, the generation of HO• radical in the Fenton reaction is replaced by the formation of ferryl-oxo species (Fe^{IV}) which is highly reactive and selective compared to •OH radical (Equation 1.2) (Hug and Leupin, 2003; Pang et al., 2011):



1.3.2 Fenton-Like process and its modifications

Although the Fenton process has been utilized extensively in wastewater treatment plants, however; the process inherently showed several shortcomings such as high operational cost, a short optimum pH range, leaching of a large amount of iron which exceeds the limit of 2.0 mg/L as directed by the European Union (EU) for direct injection to the surroundings (Sabhi and Kiwi, 2001). Because of that, alternative processes of the classical Fenton process were encouraged using different kinds of homo/heterogeneous catalysts including the Fe^{3+} (Fan et al., 2013), $\text{Cu}^{2+}/\text{Cu}^+$ (Maekawa et al., 2014), pyrite (Shinya and Bergwall, n.d.), nano zero-valent iron (NZVI) (Babuponnusami and Muthukumar, 2012), schorl (Xu et al., 2014), posnjakite (Wen et al., 2021), etc. These customized systems are collectively named the “Fenton-like” processes.

The Fenton-like reactions are mediated with the Fe^{3+} reactions which are demonstrated with the Equations (1.3-1.5) :



Similar to the Fenton process, the modified Fenton processes are also differentiated from the hetero/homogenous Fenton-like systems based on the catalyst phase. Furthermore, either one or more than one different physical field/phenomenon(s) is attributed to the Fenton-like process to achieve its high efficiency in wastewater treatments. Some typical examples of Fenton-like processes for various physical fields in terms of both homo/heterogeneous Fenton-like processes are photo@Fenton-like processes (Dehghani et al., 2014; Fei et al., 2014; Rahim Pouran et al., 2015), electro@Fenton-like processes (Alfaya et al., 2015; Balci et al., 2009; Brillas et al., 2009), cavitation@Fenton-like processes (Chand et al., 2009; ElShafei et al., 2014; Wang & Shih, 2015), and microwave@Fenton-like processes (Atta et al., 2012; Carta and Desogus, 2013), etc. Iron-impregnated heterogeneous catalysts are used in both Fenton and Fenton-like processes using natural and synthetic zeolites (Navalon et al.,

2010), mesoporous materials (Hartmann et al., 2010; Xu et al., 2021), pillared interlayered clays (Herney-Ramirez et al., 2010), Nafion films (Gumy et al., 2005), polymeric resins (Liou et al., 2005), activated carbon (Ramirez et al., 2007), ashes (Flores et al., 2008), biochar (Wang et al., 2021), pumice particles (Kitis and Kaplan, 2007), aluminates (Muthuvel and Swaminathan, 2008), etc. as supporting materials. Their adsorption capacity as well as their porosity helps to enhance the suitability and efficiency of the Fenton process.

1.3.3 Development of nano-Fenton-like catalyst (nFLC)

As both hetero/homogeneous Fenton processes have revealed several practical drawbacks hence, the challenge lies for researchers to develop newer and practically suitable, low-cost catalysts that can generate $\bullet\text{OH}$ radical from H_2O_2 in the Fenton-like system. To attain efficient generation of $\bullet\text{OH}$ radicals through the transfer of electrons to H_2O_2 , the alternative of the classical Fenton catalyst need to be modified in such a way that the catalyst is capable of attaining variable oxidation states. To prevent the precipitation of the catalytic species, both the active/inactive form should be stable at a wide pH range. Similarly, the surface properties of the nanoparticles allow significantly the bulk properties of catalysts (Theng and Yuan, 2008). The catalytic performance, and the nature of nanocatalysts, such as activity and selectivity, are strongly dependent on the shape, size, and surface structure, as well as on bulk compositions of catalysts (Bell, 2003; Perez, 2007).

Therefore, the role of several nano-metallic or nanocomposites-based nFLC, and the importance of supporting materials are discussed extensively, also their feasibility, and practical applicability toward various micro-pollutants are elaborated in the following sections. The mechanism followed by the reaction pathways in the degradation processes is further included to understand the insights into the catalytic processes.

1.4 Emerging contaminants

Current research in environmental pollution prevention, detection, control, and removal measures are extensively studied based on current practice and experience.

Moreover, it seems that the overall pollution in the environment is controlled by existing laws. The lengthy list of chemical pollutants continues to grow as new emerging contaminants are found and identified with time. Therefore, the majority of chemicals that are present in the environment are excluded from national and international lists of regulated chemicals, however; these chemicals are presumed to be the most important and pose the greatest risk to the environment, human health, and the economy. The selection of the most harmful chemical contaminants will remain a matter of debate. The previous 10-15 years have also shown that a large number of chemicals that has yet to be recognized will most likely be discovered in the near future because of advances in research in these fields.

It has long been considered that sewage treatment plants eliminate all potential contaminating substances. However, not all polluting substances are eliminated with typical treatment processes (Ginebreda et al., 2010; Teijon et al., 2010). A variety of chemicals are detected in the treated municipal effluents and receiving waters are seemingly contaminated with these residual contaminants (Kolpin et al., 2002; Phillips et al., 2010). Among these persistent compounds is the emerging polluting agents, which are made up of chemicals from a wide range of sources and are distinguished by their high production and consumption, implying their constant presence in the environment (Ginebreda et al., 2010; Teijon et al., 2010). Emerging contaminants or contaminants of emerging concern (ECs) are a broad category of substances that are identified as contaminants (Lapworth et al., 2012) or are discovered in the environment (Lindsey et al., 2001; Petrovic and Barceló, 2006). This phrase includes medications, diagnostic goods, steroids and hormones, antiseptics, personal care products, gasoline additives, heavy metals and metalloids, surfactants, endocrine disruptors, etc. Despite the low concentrations found in the environment, concern about these contaminants arises from their bioaccumulation and persistence (Hernando et al., 2007; Kasprzyk-Hordern et al., 2008; Kim et al., 2007; Miranda-García et al., 2010), and also their resistance to traditional wastewater treatments plants (Brooks et al., 2003; Crane et al., 2006; Planas et al., 1997).

Although risk assessments appear to indicate that trace levels of pharmaceuticals in drinking water pose a health threat, the World Health Organization noted that there are still knowledge gaps in assessing risks associated with long-term

exposure to low levels of pharmaceuticals and the combined effects of pharmaceutical mixtures (WHO).

Table 1.1: An overview of different categories and main sources of known ECs (Shahid et al., 2021).

Category of ECs	Sub-category	Sources	Major contaminants
Personal care products	Insect repellants, synthetic musk, sunblock agents/UV filters.	WWTPs effluent, landfill leachates, and surface water	Diethyltoluamide, 4-benzophenone, Galaxolide, Tonalide.
Pharmaceutically active complexes	Nonsteroidal anti-inflammatory medicines, antibiotics, anticonvulsants, lipid regulators, b-blocker, and hormones.	The effluent of a medicine manufacturing facility, hospitals and health centers, livestock farms, and domestic wastewater.	Diazepam, ciprofloxacin, metoprolol, diclofenac, carbamazepine, clorfibric acid, testosterone.
EDCs	Bisphenol, xenohormone, and phthalates.	Drinking water, surface water, sediments, soil, and secondary sludge.	Bisphenol A, xenoestrogen, and dioctyl phthalate
Regulated compounds	Pesticides and poly aromatic hydrocarbons.	Agricultural runoffs, sewage	Chlorpyrifos and phenanthrene

		treatment plants, sediments, soil, and surface water	
Biocides	Herbicides, fungicides, and molluscicide	Surface water, aquafarming, and agricultural runoff	Metaldehyde, butachlor, and epoxiconazole
Industrial chemical	Plasticizers and fire retardants.	Domestic and industrial wastewater	Dimethyl adipate and Tris (1- chloro-2- propyl) phosphate
Perfluorinated alkylated matters	Perfluorocarboxylic acids and perfluorosulfonic acids.	Sediments, groundwater, surface water, and wastewater.	Perfluorooctanoic acid and perfluorooctanesulfonate
Surfactants	Ionic and nonionic surfactants.	Domestic and industrial wastewater.	Tweens (Polysorbates) and sodium lauryl sulfate

1.4.1 Diclofenac (DCF)

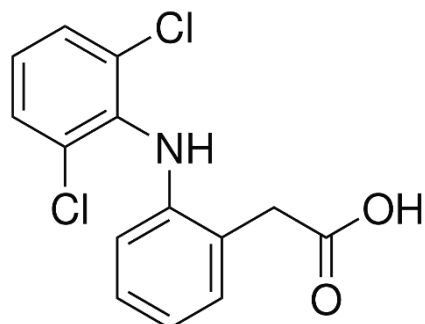


Figure 1.4: Chemical structure of diclofenac

Since the 1970s, diclofenac, a nonsteroidal anti-inflammatory medication with pain-relieving properties, has been utilized for both humans and domestic animals (Barbosa et al., 2016; Barra Caracciolo et al., 2015). It is a "contaminant of growing concern" that was included in the earlier EU Decision 2015/495 Watch List (Li et al., 2019; Lonappan et al., 2016a; Sousa et al., 2018) to acquire appropriate monitoring information on surface waters (Li et al., 2019; Lonappan et al., 2016a). In general, diclofenac is continuously introduced into the environment by pharmaceutical industries, hospitals, and household drainage, which pollutes the environment as a parent molecule or in its metabolite forms, and thus is a source of concern (Cardoso et al., 2014; Chiffre et al., 2016; Lindholm-Lehto et al., 2016). A major fraction of the diclofenac that is utilized ends up in the water and soil. In addition, it is reported that diclofenac accumulates in edible fruits and vegetables (Bartrons and Peñuelas, 2017; González et al., 2018), which impacts directly human health. Furthermore, the partial degradation of diclofenac in the treatment operations of WWTPs leaves residual diclofenac in the effluent waters, resulting in record-high diclofenac levels that harm inland aquatic habitats (Balakrishna et al., 2020; Thelusmond et al., 2018).

Further, *in vitro*/or *in vivo* studies showed diclofenac toxicity in birds, mammals, aquatic species, and plants. Diclofenac is hazardous to aquatic creatures even at low concentrations (ng/L) (Fontes et al., 2017). Apart from the chronic and acute toxicity caused by medications, biomagnification in the food chain constitute an ecological danger to non-targeted creatures (*Circling In on a Vulture Killer*, 2005). Diclofenac is cardiotoxic, hepatotoxic, nephrotoxic, neurotoxic, genotoxic, and

hematotoxic effects in animals as demonstrated elsewhere (Sriuttha et al., 2018; Tomic et al., 2008). Dass & Sattigeri (2018) investigated the hepatotoxic effects of diclofenac in albino rats and found an increase in liver enzymes including ALT, alkaline phosphatase (ALP), and aspartate aminotransferase (AST) in serum, confirming diclofenac's hepatotoxicity. Similarly, changes in renal functional indicators such as urea, creatinine, uric acid, and cytokines in diclofenac-administered in the albino rats were systematically investigated that conformed to the diclofenac's nephrotoxicity (S & Evan Prince, 2018). In diclofenac-administered rats, pyramidal cells and brain cells were lost in the Cornu ammonis areas of the hippocampus (Yurt et al., 2017). Many studies have shown the toxicity of diclofenac in numerous aquatic species. When compared to other pharmaceuticals, diclofenac has the highest toxicity in fish liver, kidneys, and gills (Triebkorn et al., 2007). Diclofenac exposure significantly affected the antioxidant mechanism of freshwater fish (*Rhamdia quelen*) (Guiloski et al., 2017). Similarly, other than delayed egg-laying times, diclofenac-exposed fish embryos demonstrated statistically negligible embryotoxicity and proteotoxicity (Hallare et al., 2004). The impact of trophic exposure was also taken into account because it had a strong impact on ecological risk assessments. The immunosuppressive impact and hemotoxicity of diclofenac were shown that mimicked diclofenac trophic exposure in fish (*Hoplias malabaricus*) (Chen et al., 2015; Ribas et al., 2016). Chen et al. (2015) studied diclofenac toxicity in the arthropod *Folsomia candida*, which is found in soils. Diclofenac decreased *F. candida* survival and reproduction rates in soil, and it was also reported that diclofenac is extremely hazardous to non-target soil invertebrates. Diclofenac and its metabolites were introduced into the soil environment through the treated wastewater and sludge (Carter et al., 2016) hence, caused for pollution in the soil and affecting the soil arthropods and organisms. Li et al. (2019) classified diclofenac as a high-priority drug among 100 pharmaceuticals in order to monitor its ecological danger in China's aquatic environment, followed by European nations. Diclofenac was found in freshwaters at the ecotoxicological danger threshold (Acuña et al., 2015). Moreover, numerous groups have published reviews on the presence of diclofenac (Barbosa et al., 2016; Fijalkowski et al., 2017; Jo et al., 2017; Lonappan et al., 2016b; Mzukisi et al., 2017; Vieno and Sillanpää, 2014) in particular emphasized

the need for more data to analyze the presence of diclofenac in the environment and the threats it poses to the terrestrial ecosystem.

1.4.2 Phenol

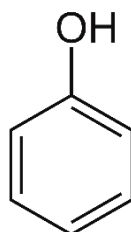


Figure 1.5: Chemical structure of phenol.

Phenol and its chemical derivatives are widely employed as precursors for a wide range of materials and compounds in a variety of industries. Phenol is a critical component in the production of fine chemicals, including medicines, herbicides, detergents, plastics, flame retardants, epoxy resins, and nylon. More than ten billion kilograms of phenol are produced from petroleum each year, with an estimated market value of about \$32 billion (Markets, 2019).

Phenol is a water-soluble aromatic organic compound. The deprotonation of the alcohol group results in resonance stabilization of the phenoxide anion, which accounts for its mild acidity ($pK_a = 9.95$) as shown in acid-base equilibrium (Equation 1.6) (Nogueira and Pliego, 2018; Silva, 2009). Phenol is a basic chemical in the phenolic family and serves as its primary representation. The major reaction involving hydroxyl radical and active chlorine species occurs when phenol is exposed to electrophilic aromatic substitution.



The environmental effect, industrial importance, representational structure, and reactivity to oxidants generated during the treatment of effluent using advanced oxidation processes (AOPs), phenol is regarded as one of the prominent pollutants in water research (Ahmed et al., 2010; Jun et al., 2019; Lado Ribeiro et al., 2019).

One of the most common organic contaminants detected in industrial wastewater is phenol. Textile processing, coal gasification, petroleum refining, leather manufacturing, resin synthesis, coconut retting, perfume creation, and pharmaceutical

manufacture are the common source of phenol (Arya et al., 2011; Gianfreda et al., 2006; Kiliç, 2009; Van scnte and Young, 2000). Chemical spills can also potentially raise the risk of phenol contamination in the ocean. In the port of Gothenburg, Sweden, for example, a cistern into which the phenol was stored was abruptly broken, leaking 400 tonnes of phenol down a quay and into the seas in 1973 (Galieriková et al., 2021). Because of its toxicity, even at a low level, phenol poses a major ecological risk when introduced into aquatic environments. Surface waters across the world are found to contain phenol at levels as low as a few $\mu\text{g/L}$ (Duan et al., 2018), while the highest concentrations have been recorded at 2110 $\mu\text{g/L}$. Phenol causes dermatitis in the eyes, skin, and respiratory system. Health issues that impact the central nervous system, heart, liver, and kidneys are linked to long-term exposure to phenol (Ayeni, 2014; Brillas and Garcia-Segura, 2020; Duan et al., 2018; Weisburger, 1992).

1.4.3 N-(n-propyl) Thiourea (NNPT)

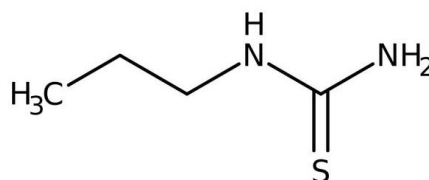


Figure 1.6: Chemical structure of N-(n-propyl) Thiourea

The sulfur-containing chemical thiourea (NH_2CSNH_2) is widely used in a variety of industries. Under specific conditions, thiourea reacts with hydrogen peroxide to generate a potent reductive bleaching agent that is widely employed in the textile industry (Cegarra et al., 1988). In industrial equipment such as boilers, thiourea and its derivatives are utilized as corrosion inhibitors (Ayres, 1970), and corrosion-related scaling (Sahu et al., 2011). The accumulation of corrosion products over time harms the effectiveness of the boilers (L and L, 1971). A thiourea solution in dilute hydrochloric acid is employed as a catalyst for eliminating scales from boilers, using a complexing agent. Apart from that, some thiourea derivatives are utilized for agricultural and analytical uses, including use as accelerators in the rubber industry, as

fixing agents and to remove stains from negatives in photography, and as fungicides, herbicides, and rodenticides in agriculture (Sahu et al., 2011). The use of thiourea in an aqueous solution as a gold-leaching agent is well-documented in the literature (Yang et al., 2011). Thiourea is also employed in the spectrophotometric reagent to determine the presence of certain metal ions (Snell, 1978). The presence of thiourea in the urine was described as a non-specific cancer indication (Sahu et al., 2011). Because of its effect on glucose metabolism, thiourea is a potential hazard (Lewis, 1996). Furthermore, it has been classified as carcinogenic (Sahu et al., 2011) and cautioned to avoid direct human exposure.

Thiourea, an antioxidant, is entirely absorbed and eliminated unaltered by the kidneys following oral administration to humans and animals. Biological oxidants, however, cause metabolic oxidation in some cases (Sahu et al., 2011). In the presence of iodine or iodide and hydrogen peroxide, thyroid gland peroxidase oxidizes formamidine disulfide to produce formamidine. At $\text{pH} > 3.0$, formamidine disulfide decomposes into cyanamide, elemental sulfur, and thiourea, which are all unstable. Both cyanamide and thiourea are demonstrated to inhibit thyroid peroxidase *in vitro* and *in vivo* studies (Davidson et al., 1979). Because thiourea is hazardous and a cancer-promoting substance, environmental concerns are prompted research on its destruction. ETU, the most toxic and carcinogenic metabolite of the commonly used ethylene bis-dithiocarbamate fungicides was extensively investigated in terms of oxidative degradation (Sahu et al., 2011). Using oxidants such as potassium permanganate (Sahoo et al., 2010), sodium hypochlorite (Marshall, 2002), or hydrogen peroxide, this is normally decomposed. The oxidants, on the other hand, either include heavy metals or halogen atoms, resulting in undesirable byproducts (De Zacchini and De Agazio, 2001).

1.4.4 Amoxicillin (AMX)

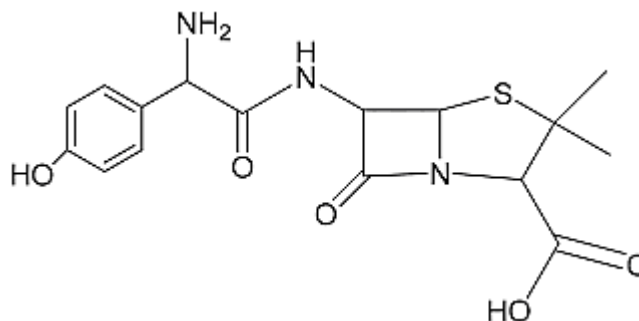


Figure 1.7: Chemical structure of Amoxicillin

Amoxicillin (AMX) is a beta-lactam antibiotic and is one of the most prescribed antibiotics in the penicillin family for both animal and human medications (Bound and Voulvoulis 2006; Lissemore et al., 2006). It is used to cure and avoid respiratory disorders, gastrointestinal, and urinary tract infections, skin bacterial infections, pharyngitis, tonsillitis, as well as helicobacter pylori infection, and duodenal ulcer disease. It is widely recommended for the management of chlamydia trachomatis infection due to its pharmacological and pharmacokinetic properties (Deng et al., 2008). It is highly resistant to bacteria such as *Escherichia coli*, *Neisseria gonorrhoeae*, *Haemophilus influenza*, *Streptococci*, *Pneumococci*, and certain *Staphylococci* strains (Fazelirad et al., 2015; Bebu et al., 2011).

Amoxicillin is having a molecular weight of 365.40 g/mol, log K_{ow} (partition coefficient of octanol-water) of 0.87, and acid dissociation constants (pK_a) of 9.41 (Windholz, 1976; Carless, 1966). It is considered a major water contaminant due to its pharmacological characteristics, ingestion rate, environmental toxicity, chemical composition, and solubility (Baghapour et al., 2014; Homem et al., 2013). Despite the fact that amoxicillin is hydrolysis sensitive under varying pH conditions, however, complete degradation of amoxicillin is not achieved in conventional wastewater treatment plants (Nägele and Moritz 2005; Zia et al., 1977). As a consequence, amoxicillin and its hydrolyzed and metabolized byproducts are detected in both urine and feces (Putra et al., 2009). It has been documented that the oral ingestion of amoxicillin (500.0 mg) in humans results in the release of 86.8% through excretion,

which further causes a significant risk to many marine organisms (Sun et al., 2012; Pan et al., 2008). It was also demonstrated that amoxicillin compounds are harmful to the algae *Synechocystis sp.*, especially by inhibiting the algae's photosynthesis process (Pan et al., 2008). Amoxicillin concentrations in household wastewater vary from ng/L to mg/L (Putra et al., 2009).

Amoxicillin seems to cause adverse effects on the natural environment due to its persistence and bioaccumulation. Amoxicillin is a commonly used antibiotic in Australia, and it is detected at ng/L levels in river water and hospital effluents (Watkinson et al., 2009). In waste/effluent water, the existence of amoxicillin causes unpleasant smells and microbial resistance to pathogenic or microorganism deaths. The resistant bacteria then cause various diseases, which normal antibiotics do not cure (Kanakaraju et al., 2015). Amoxicillin promotes the spread of bacteria immune to β -lactam antibiotics (Martinez, 2009). Since amoxicillin is not sufficiently treated in conventional water and wastewater treatment facilities, it reaches both surface and groundwater, affecting marine habitats. Additionally, it contributes to bacterial tolerance and, as a result, failure to treat infections with traditional antibiotics (Ding et al., 2012; Fatta et al., 2007). This allows researchers to further realize the prevalence of resistant genes in drinking and surface waters (Vaz-Moreira et al., 2014). As a result of these findings, it is imperative that amoxicillin be fully removed from the marine environment.

1.4.5 Sulfamethazine (SMZ)

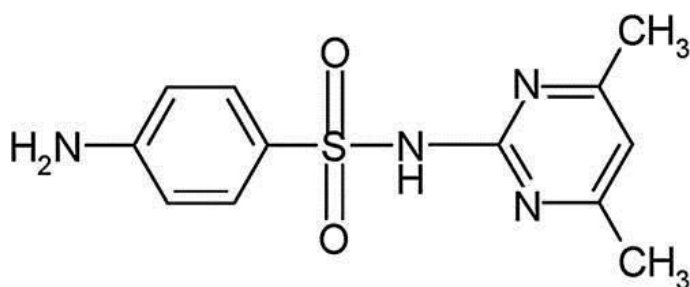


Figure 1.8: Chemical structure of Sulfamethazine

Sulfamethazine is a sulfonamide with sulfanilamide and para-amino groups and is a commonly prescribed sulfonamide drug. Due to its low cost and efficient

antibiotic impact, sulfamethazine is also a commonly used medication for the treatment of infectious diseases in humans and animals, for the promotion of animal development in agricultural processing, for the treatment and prevention of influenza, and also used as a feed additive in the dairy processing industry (Zhao et al., 2017; Lin and Wu 2018; Wang et al., 2019).

Sulfamethazine is a strongly hydrophilic substance and it is poorly metabolized by microorganisms; about 90% of the ingested SMZ is excreted by humans and livestock such that the concentrations of sulfamethazine vary from ng/L to µg/L in the treated wastewater (Wen et al., 2018; Tang and Wang 2019; Lin and Wu 2018). Moreover, this endless drive also contributed to the extensive presence of SMZ in farmlands, due to long-term agricultural activities. Subsequently, the SMZ is reintroduced into ground and drinking waters, surface water, and ultimately to the aquatic ecosystems through surface runoff/leaching (Dolliver and Gupta 2008; Davis et al., 2006). SMZ is not eliminated by traditional wastewater treatment systems due to its antibacterial properties and low biodegradability (Lin and Chen 2018; Tzeng et al., 2016). Along with other classes of sulfonamides, it is frequently detected in the aquatic environment such as surface water, drinking water, groundwater, and effluent of wastewater treatment plants (Huang et al., 2012). SMZ is detected in a broad variety of environmental matrices due to its high mobility and water solubility, with concentrations up to 20 mg/kg in animal wastes, 323 ng/L in water, and 15 g/kg in agricultural soils (Kaczala and Blum 2016; Larsbo et al., 2008). Additionally, SMZ accumulated in soils and sediments or spread across the food chain, resulting in antibiotic resistance growth. As a consequence, a reduction or lack of antibiotic drug efficacy against human pathogens results in public health problems (Heberer 2002; Batt et al., 2006). In humans, sulfamethazine exhibits a trimodal form of polymorphic acetylation. In rats, it induces thyroid gland enlargement (goiter), and in both mice and rats, it causes diffuse hypertrophy and hyperplasia. Sulfamethazine administration to rats under bioassay conditions is known to induce tumors and alter thyroid hormone homeostasis (Finch et al., 2006). The reversible suppression of thyroid peroxidase function is the fundamental cause of these changes. Sulfamethazine caused decreased reproduction in both males and females in a continuous breeding trial in mice and shows little effect on sperm parameters (Brezina et al., 2012). Further, it was reported

that sulfonamide antibiotics possibly inhibit the development of several *Gram-negative* as well as most *Gram-positive* bacteria (Wan & Wang, 2016; Liu & Wang, 2013).

1.5 Review of literature

The occurrence of micro-pollutants in wastewater, surface water, sediments, groundwater, or even in drinking water is a serious environmental concern. The main aim of wastewater purification by means of AOP methods is the reduction of the chemical pollutants and their toxicity to such an extent that cleaned wastewater is reintroduced into receiving streams.

The most investigated AOPs was the Fenton process in which highly reactive hydroxyl radicals ($\bullet\text{OH}$) are *in situ* generated through the catalytic reaction of Fe(II)/Fe(III) with hydrogen peroxide. The Fenton or Fenton-like processes showed widespread applicability due to their robust operation and flexibility in nature as well as reasonably cost-effective, (iron and H_2O_2) in unit operations (Bokare and Choi, 2014).

1.5.1 Iron-based nFLC

Fe(II)/Fe(III) redox couple is the driving force that is utilized for the electron transfer processes in the generation of $\bullet\text{OH}$ radicals from H_2O_2 as demonstrated in Equations (1.1-1.5). It was noted that in the classical Fenton process, a relatively higher amount of iron is required, which causes excessive sludge production, hence; its disposal is an additional environmental burden. However, nano zero-valent iron (Fe^0) has shown innumerable properties and offers efficient Fenton-like processes with a minimal dose of iron hence, sludge production is significantly reduced (Crane & Scott, 2012; Lücking et al., 1998; Scaria et al., 2021; Segura et al., 2013). Therefore, the use of zero-valent iron (ZVI) in a Fenton-type process has received greater and considerable interest in recent times because of its excellent performance in the catalytic processes (Bergendahl and Thies, 2004; Doong and Chang, 1998) and less environmental load as in the form of sludge. Moreover, the catalyst possessed a high specific surface area to volume ratio which eventually enabled high photocatalytic reactivity having fast kinetics in eliminating quite a large number of micro-pollutants

from aquatic environments (Tang & Lo, 2013). It is mentioned that several pollutants are being efficiently remediated by using nano zero-valent iron, however, the major drawback was reported to be the low mineralization rate of micro-pollutants especially antibiotics (Xue et al., 2009; Zhang et al., 2017). However, even a small dose of hydrogen peroxide enhances significantly the mineralization of micro-pollutants (Xue et al., 2009). Further, it was pointed out that a higher concentration of H₂O₂ is hazardous for transportation and handling, and expensive in bulk utilization (Zhang et al., 2017). Therefore, a novel role of EDTA was explored as it is capable of activating the dioxygen and *in situ* generations of H₂O₂ in the Fe²⁺/EDTA system (Seibig and van Eldik, 1997). This was known to be the “Greener Reagent” in operation (Noradoun et al., 2003; Noradoun & Cheng, 2005).

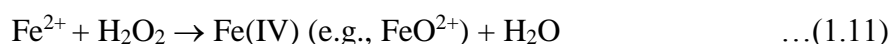
A novel nZVI/H₂O₂ Fenton-like system was introduced coupled with acoustic ultrasound effects (Bremner et al., 2008), for the removal of 2,4-dichlorophenoxyacetic acid. In line, many researchers have explored the suitability and applicability of nZVI/Fenton-like systems (Babuponnusami & Muthukumar, 2012; Bao et al., 2020; Chen et al., 2020; ElShafei et al., 2017; Morshed et al., 2019; Raji et al., 2021; Yang et al., 2019). A small-sized nZVI (20.0 nm, specific surface area = 39.2 m²/g) was synthesized by the borohydride reduction process and the material was optimized for the degradation of norfloxacin under the Fenton-like process. Adjusting the pH to around 3.0-4.0 enabled the degradation of norfloxacin *Ca.* 95% within 40 mins (Zhang et al., 2017). Similarly, the degradation of 4-chloro-3-methyl phenol (Xu & Wang, 2011), nitrobenzene (Yao et al., 2019), carbothiolate herbicide, molinate (Joo et al., 2004), Methyl tert-butyl ether (Bergendahl and Thies, 2004) were demonstrated elsewhere. The nano zero-valent iron utilized a Fenton-like process and was impacted in presence of several cations/anions hence, the presence of Cu²⁺ and Mg²⁺ is greatly studied in the degradation of amoxicillin (Liu et al., 2017). The removal percentage was increased with increasing Cu²⁺ concentration however, a reverse trend was obtained in the presence of Mg²⁺. The insight studies conducted with XPS indicated that the Cu²⁺ was reduced to Cu⁰ by the Fe⁰ with nano zero-valent iron and formed the bimetallic (Fe/Cu), which accelerated the removal of amoxicillin (Liu et al., 2017). Simultaneous removal of EDTA and 4-chlorophenol was investigated in the ultrasound/Fenton system using a heterogeneous zerovalent iron catalyst. The *in*

situ production of H₂O₂ via iron/EDTA reactions was demonstrated and the ferryl-EDTA complex ([Fe^{IV}O]EDTA) was the predominant oxidant identified in the degradation of 4-chlorophenol (4-CP) and EDTA (Zhou et al., 2009). The possible mineralization reactions were as given in equation (1.7):



(LMW: Low molecular weight).

The introduction of different methods with synergistic effects of AOPs enabled the efficient degradation of micro-pollutants (Babuponnusami and Muthukumar, 2011). The nano zero-valent iron (nZVI) catalyzed (photo-electro)@Fenton-like process was introduced in the degradation of phenol. The impact of various Physicochemical parameters *viz.*, the effect of pH, phenol concentration, catalyst dose, H₂O₂ concentration, etc., were studied and the optimized catalyst dose and H₂O₂ concentration were established to be 0.5 g/L and 500.0 mg/L, respectively. Further, pH 3.0 was an optimum pH for the degradation of phenol, which was demonstrated by the fact that the production of ferrous (Fe²⁺) ion involved three stages: (i) production of electrical energy using stainless steel as a cathode; (ii) oxidation via two-electron transfer; and (iii) leaching of iron(II) through photolytic reaction. At first, in presence of H₂O₂, the nano zero-valent iron was oxidized (Eq. 1.8) followed by the generation of •OH by the Fenton process (Eq. 1.9) and photolytic degradation of pollutants (Eq. 1.10). pH values >5.0, the ferryl ions (FeO²⁺) are formed which are comparatively weaker oxidants as well as more selective than •OH radical which slowed down the overall reaction (Equation 1.11) (Babuponnusami and Muthukumar, 2012).



An interesting study was conducted with the bimetallic additive using the Cu/nZVI-Fenton process for the degradation of trichloroethylene. It was eventually observed that the bimetallic Fenton system Cu/nZVI possessed the following four

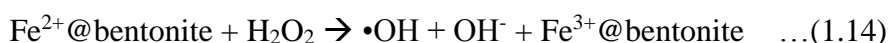
steps in the oxidative removal of trichloroethylene: (i) nZVI releases Fe^{2+} via redox cycle from Fe(0) in the presence of Cu(II); (ii) Fe(0) reduces Cu species on the catalyst surface; (iii) generation of $\bullet\text{OH}$ via oxidation of Fe(II) by hydrogen peroxide followed by radical-induced degradation of trichloroethylene in Cu/nZVI suspension; and (iv) hydrogen peroxide oxidizes Fe(0) from nZVI to Fe(II), which enables sustained generation of hydroxyl radicals to degrade completely the trichloroethylene (Choi and Lee, 2012). Similarly, the bimetallic Cu/nZVI was found efficient in the degradation of ciprofloxacin under a weak magnetic field. The Cu(II) species enhances the leaching of Fe(II) ions from the surface of nZVI, which gives rise to an increase in $\bullet\text{OH}$ production via reaction with H_2O_2 . Additionally, the regeneration of nZVI/Cu was conducted using the tea extracts and employed for multiple operations in the removal of ciprofloxacin (Chen et al., 2020).

Though the presence of nanoparticles favors greatly the degradation of potential micro-pollutants in the Fenton-like processes, however; the major disadvantage over nanoparticles is that it keeps the tendency to get agglomerated easily and suppresses the catalytic activity of the catalyst. Hence, to overcome the problems, researchers tried to stack nanoparticles on the surface of some supporting solid materials. A few widely used supporting materials include iron exchanged with Nafion membranes (Maletzky et al., 1999), thin-film (Lalliansanga et al., 2020a; Tiwari et al., 2015), modified clays (De León et al., 2008; Iurascu et al., 2009), sand (Lee et al., 2012; Tiwari et al., 2011), etc. Some other modified materials such as silica fabric (Bozzi et al., 2002), carbon shell (Ahsan et al., 2020), zeolites (Rios-Enriquez et al., 2004), resins (Lv et al., 2005), and cotton (Tryba, 2008) are used to immobilize the nZVI on the substrate surface at varied experimental conditions in the removal of several micro-pollutants including the phenol, 4-chlorophenol, cationic or anionic dyes, oxalic acid, 2,4-xylidine, etc. Similarly, the zero-valent iron nanoparticles are impregnated with the bentonite solid and the composite material was employed in the decontamination of phenol. Further, the Fenton-like removal of phenol showed that a maximum of 450 mg/g of phenol was removed under suitable experimental conditions. Additionally, the removal pathways of degradation were demonstrated in two steps (Bao et al., 2020):

(i) Adsorption of BPA (bisphenol A) by the composite material

(ii) Fenton-Like degradation of BPA by the material

Using the nano zerovalent iron-bentonite composite (nZVI@bentonite) showed greater advantages since leachates (contained with iron) were produced which eventually reduced the load of secondary waste. The EPR studies demonstrated the reaction mechanism having the reactions (Bao et al., 2020) (Equations (1.12- 1.16)) :



Indigenously collected laterite which is enriched with iron was used to obtain the iron nanoparticles (FeNPs) utilizing the eucalyptus leaf extracts (Sangami and Manu, 2017). The iron nanoparticles were contained with Fe^0 , Fe_2O_3 , and Fe_3O_4 and had a specific surface area of $36.62 \text{ m}^2/\text{g}$. The Fe(NPs) catalyzed Fenton-like process and used for the degradation of ametryn (2-ethylamino-4-(isopropylamino)-6-(methylthio)-s-triazine) from an aqueous medium. Moreover, the optimized physicochemical conditions were 2.125, 6.0, 3.5, and 135.0 min for pH, H_2O_2 :COD ratio, H_2O_2 :Fe ratio, and reaction time, respectively having the H_2O_2 dose of 17.0 and 2.83 mg/L of catalyst (Raji et al., 2021). Similarly, Pirsahab et al., (Pirsahab et al., 2019) created a novel nanocomposite using nZVI particles encapsulated on carbon dot films and utilized as a nanocatalyst in the Fenton-like process for the degradation of two widely used antibiotics *viz.*, amoxicillin and ciprofloxacin. It was stated that encapsulating nZVI particles on biopolymer-based carbon dots boosts air/water stability and enhances the reactivity of nZVI with H_2O_2 . The role of carbon dots in the process is to keep intact the nZVI particles against agglomeration, and oxidation, and enable slow discharge to the aqueous medium over time. Similarly, the carbon-based material biochar-supported nZVI-catalyzed Fenton-like process was used for the remediation of antibiotics. Biochar is a microporous structure that is attributed to the impregnation of nZVI (Tang & Wang, 2018). The synthesis of iron-based magnetic nanoparticles implanted with the mesoporous carbon-based hybrid material (Fe@MesoC) was strategically synthesized in a metal-organic framework (MIL-

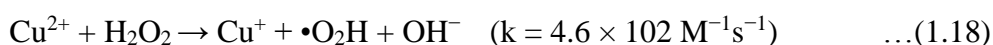
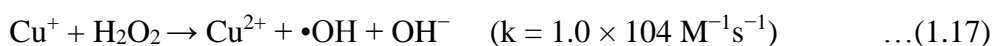
100(Fe)). This novel nano-Fenton-like catalytic system was intended to utilize for the elimination of sulfamethoxazole (SMX). In a line, the Fe-based metal-organic framework MIL-88B-Fe (Mei et al., 2019), MIL-53(Fe) (Rasheed et al., 2018), MIL-100(Fe)@Fe₃O₄/ CA(MNPCs) (Zhang et al., 2020) derived catalysts were obtained and utilized as a proficient Fenton-like catalyst for the elimination of various organic pollutants from aqueous solutions.

Iron oxides are chemical compounds containing iron and oxygen. It occurs on the earth's surface as the mineral magnetite. In investigating the catalytic performance of nanoparticles of iron(III) oxides in the Fenton-like process in the degradation of ethylene glycol and phenol in absence of UV irradiation (Zelmanov and Semiat, 2008). Results indicated that the degradation rate was considerably higher than that of the photo-implemented conventional Fenton process (Zelmanov and Semiat, 2008). Iron oxide nanoparticles supported on the hydroxylated surface of modified diamond nanoparticles were obtained. Further, the visible light-assisted heterogeneous catalyst was utilized for the Fenton-like reactions in the removal of phenol. It was reported that a superior catalytic activity of the catalyst was obtained as compared to the equivalent carbon-based catalysts such as activated carbon, graphite, or the standard Fe_{ox}/TiO₂ photocatalyst (Espinosa et al., 2018).

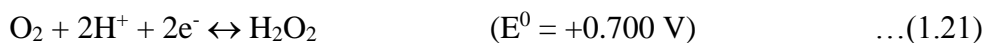
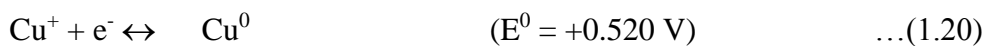
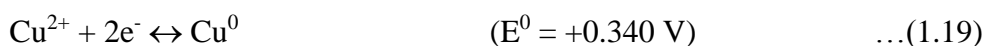
It is noted that the iron-based nano Fenton-like catalyst has attracted greater attention in recent times and shown catalytic efficiency and reusability in reactor operations. However, the implications of laboratory-scale trials and technology development need further large-scale or pilot-scale treatment. The challenges are ahead with the real or complex matrix treatment at a large-scale treatment. Moreover, the sludge contained in iron is a great challenge for recycling such leachates in the cost-effective sustainability of the reactor operations. Moreover, the greener method of synthesis devoid of harmful chemicals is the need of the hour, however, the optimization of reaction for technology development is an additional challenge lying ahead.

1.5.2 Copper-based nFLC

Similar to zero-valent iron, nano zero-valent copper has attracted greater attention in the recent past because of its unique properties and stability in the dispersed medium (Xu et al., 2019; Zhou, Zhang, Liu, et al., 2016). Compared to iron (-0.44 V, Fe^{2+}/Fe), copper possesses a relatively higher redox potential ($+0.34$ V, Cu^{2+}/Cu) vs the normal hydrogen electrode (NHE). Therefore, it can't react with hydrogen ions (H^+) to generate H_2 . Hence, useful for triggering O_2 to produce H_2O_2 ($+0.70$ V, $\text{O}_2/\text{H}_2\text{O}_2$) on the surface of the catalyst (Xu et al., 2019). The reactions involved are given in Equations 1.17-1.18 (Stumm and Morgan, 2012):

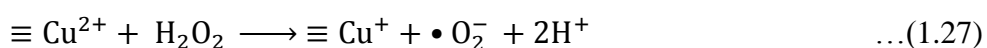
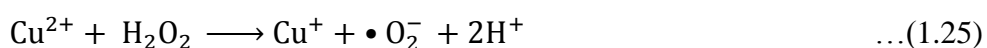


Several studies are conducted utilizing the nano zero-valent copper heterogeneous catalyst in the Fenton-like processes for the degradation of several micro-pollutants from aqueous solutions. The diethyl phthalate (DEP) was completely degraded by the zero-valent copper (nZVC) in 120 min at pH 2.5 in the reactor operations. The mechanism was investigated and showed that under aerobic atmospheric conditions, the possible redox reactions are as followed (Equations (1.19-1.21)) (Wen et al., 2014):



Similarly, the commercial nanosized zero-valent copper (nZVC) was utilized in the degradation of norfloxacin (NOR) under the Fenton-like process along with ultrasonic reactor operations. The US/nZVC/ H_2O_2 (US: ultrasonic irradiation) system favoured greatly the degradation of NOR compared to the conventional Fenton process. The leaching of Cu^+ ions from the nZVC was assumed to be the predominant species that give rise to activate the H_2O_2 for producing $\bullet\text{OH}$ radicals. The mechanism

of NOR degradation due to the different Cu species along with H₂O₂ present in the reaction system was underlined as Equations (1.22-1.29) (Ma et al., 2018):



Further, it is reported that the use of ultrasound in aqueous solutions produces the radical species which provides a synergistic influence in the elimination of micropollutants (Chand et al., 2009; Henglein, 1987). The nZVC-assisted Fenton-like process using 20, 300, and 520 kHz ultrasonic was introduced for the degradation of phenol. Further, the operating frequency of 300 kHz in ultrasound showed a maximum phenol removal per unit of power dissipation and the extent of total organic carbon elimination (Chand et al., 2009). Macroporous graphene-supported zero-valent copper nanoparticles modified 3D structure (3D-GN@Cu⁰) was obtained by a simple liquid-phase reduction process. Moreover, the formation of macropores (>50 nm) was indicated by the hysteresis loop of Cu⁰, as it was shifted to P/P0 ≈ 1.0 (Xu et al., 2019). Without adding extra hydrogen peroxide, very high efficiency in the degradation of metronidazole (MNZ) was obtained by the novel 3D nanocatalyst in a wide pH range from 3.2 to 9.8 (Xu et al., 2019). Approximately 2.33 ppm of Cu leached out from the nanocatalyst i.e., about 2.33% dissolution rate, which was considerably less compared to Cu(NPs) (55.36 ppm and the combination of Cu⁰ and 3D-GN (35.72 ppm). The reusability of the catalyst turned out to be worthy as the degradation was above 60% even after the third cycle of MNZ degradation.

Three different nano zero-valent metals (nZVMs) viz. iron (Fe⁰), copper (Cu⁰), and nickel (Ni⁰) were utilized in the ultrasound-assisted heterogeneous nano Fenton-like process in the degradation of nonylphenol. Each of these nZVMs was subjected

to reactor operations at neutral pH conditions. The ability of various nZVMs in the degradation of nonylphenol (6.0 ppm) was found in the order of $\text{Fe}^0 > \text{Cu}^0 > \text{Ni}^0$ (ElShafei et al., 2017). Further, the nZVC/ H_2O_2 system was assessed in the degradation of benzoic acid. It was noted that acidic conditions and higher doses of catalyst favored greatly the degradation of benzoic acid. Moreover, the aid of H_2O_2 accelerates the corrosion of nZVC to release Cu^+ ions, which eventually generate $\bullet\text{OH}$ radicals via a Fenton-like reaction (Zhou, Zhang, Zhang, et al., 2016). The identification of major reactive oxidant $\bullet\text{OH}$ was identified by using an excess amount of isopropyl alcohol as a quencher as its reaction rate constant ($6.0 \times 10^8 \text{ M}^{-1}\text{s}^{-1}$) is very high (Buxton et al., 1988). Do et al., (Do et al., 2017) synthesized a novel yolk-like magnetic structured Fenton-like catalyst which is encapsulated in a silica shell and wrapped with copper nanoparticles. In the presence of H_2O_2 , the synthesized Cu(NPs) decorated $\text{Fe}_3\text{O}_4@\text{SiO}_2$ nanocatalyst showed efficient catalytic activity, which resulted in the complete elimination of acetaminophen within 60 min of operation while Fe_3O_4 , $\text{Fe}_3\text{O}_4@\text{Cu}$, and $\text{Fe}_3\text{O}_4@\text{SiO}_2$ exhibited 58.8, 65.3, 67.0% degradation, respectively, within 120 min of reactor operations.

CuFeO_2 nanoplates and nanocubes having different surface manifestations {012} and {110}, respectively were synthesized and characterized by the SEM, TEM, and HRTEM methods. The CuFe-012 nanoplate was found with a width and thickness of about 1 μm and 50 nm having a lattice fringe of 0.251 nm in HR-TEM. On the other hand, cubic-structured CuFe-110 has a lattice fringe of 0.152 nm in the HR-TEM image. The materials were intended to utilize in the Fenton reaction in degrading the ofloxacin (OFX). The degradation of OFX by CuFeO_2 {012} was about four times faster than that of CuFeO_2 {110}. It was demonstrated that the electron transfer from CuFeO_2 {012} facet results in the suitable O-O bond elongation (1.472 Å), i.e. bond length in H_2O_2 which leads to the production of reactive oxidant $\bullet\text{OH}$ radicals. In the case of CuFeO_2 {110}, O-O bond length is stretched from 1.468 Å to 3.290 Å, which causes the formation of OH^- ions (Dai et al., 2018). $\text{Cu}@\text{Fe}_3\text{O}_4$ core-shell nanoparticles (n- $\text{Cu}@\text{Fe}_3\text{O}_4$) were obtained and employed in pre-treated landfill leachates for oxytetracycline (OTC) degradation. Almost complete removal of 20 ppm OTC was obtained within 30 minutes through the n- $\text{Cu}@\text{Fe}_3\text{O}_4/\text{H}_2\text{O}_2$ Fenton-like reaction at a pH of 3.0. The reusability and stability performance of the catalyst showed a gradual

decrease in the removal of OTC for five consecutive runs at 99.2%, 92.4%, 71.3%, 68.3%, and 66.2%, respectively (Pham et al., 2018). Utilization of novel magnetic CuFe_2O_4 spinel nanoparticles mediated Fenton-like oxidation of sulfanilamide was conducted. It was reported that the Cu(II) on the CuFe_2O_4 nanocomposite caused an enhanced degradation of sulfanilamide at around neutral pH conditions. A comparative evaluation of the rate constant concerning the different catalytic systems such as CuO (2.60×10^{-2} L/m/min), CuFe_2O_4 NPs (2.58×10^{-3} L/m/min), Fe_3O_4 (1.92×10^{-3} L/m/min), and $\alpha\text{-Fe}_2\text{O}_3$ (7.30×10^{-4} L/m/min) were concluded that the activation by the H_2O_2 , the reactivity of solid Cu(II) was efficient than that of Fe(III) at the neutral pH conditions. Further, the LCMS/MS studies enabled the 11 degradation products devoid of sulfanilic acid. Therefore, the possible pathway was obtained through the cleavage of the C-S bond rather than the S-N bond cleavage and subsequently the mineralization of sulfanilic acid (Feng et al., 2016). The inert surface of conditioned diamond nanoparticles (D) is greatly enabled to generate and diffuse freely $\bullet\text{OH}$ within the solution and interact feebly with the pollutant molecules (Espinosa and Navalón, 2015). Further, the inert D surface is useful as support media for the Ag, Au, or even Cu nanoparticles and enhances the suitability of materials in the catalyzed reactions (Litter, 1999; Navalon et al., 2013; Sempere et al., 2013). In a line, a novel Fenton-like catalyst consists of copper nanoparticles propped up on diamond nanoparticles (DNPs) as-synthesized by polyol reduction of $\text{Cu}(\text{NO}_3)_2$ in the presence of DNPs and utilized in the degradation of phenol (Espinosa et al., 2016). CuNPs/DNPs catalyst-mediated Fenton-like system enables an enhanced degradation efficiency than analogous catalytic systems *viz.*, CuNPs/activated carbon, CuNPs/carbon nanotubes, and CuNPs/ $\text{TiO}_2\text{-P25}$. The catalyst was having relatively less stability and activity upon reuse, although it is possible to recover by reducing the catalyst again by the polyol method. Fenton-like elimination of enrofloxacin (EFN) at concentration level ($\mu\text{g/L}$) was conducted using several nanocatalysts *viz.*, copper oxides, titanium carbide, and silicon nitride nanoparticles. The $\text{CuO}/\text{H}_2\text{O}_2$ and $\text{TiC}/\text{H}_2\text{O}_2$ catalytic systems showed $>90\%$ degradation of the EFN in 12 hrs. In the presence of sodium halide salts, the reaction rate was found to be accelerated in the case of CuO nanoparticles-mediated Fenton-like degradation. This increase in reaction rate was explained by two possible mechanisms: (i) An additional reaction pathway was provided by the salts

which contained the radical species which degrades ENF readily; and (ii) otherwise, the presence of salts inherently accelerates the non-radical mechanism for the degradation of enrofloxacin (Fink et al., 2012).

The catalytic degradation of alachlor and phenanthrene was conducted using the nano-sized copper oxide in the presence of H₂O₂. Rapid degradation of these micro-pollutants was obtained and the presence of several oxidants or salts inhibited the degradation rate of alachlor. However, very high concentrations (>1 M) of NaCl favored significantly the reaction rate of degradation (Ben-Moshe et al., 2009). Several studies intended to assess the unsupported nanoparticles of copper oxide in the oxidative removal of nitrophenols (Bandara et al., 1996), production of H₂O₂ (Bandara et al., 2005), and inactivation of bacteria (Paschoalino et al., 2008).

Fe(NPs), Cu(NPs), and Fe/Cu bimetallic nanoparticles were employed in three different electro-Fenton catalytic systems for the degradation of nafcillin (NFC). The NFC drug was completely removed by Fe/Cu bimetallic nanoparticles mediated Fenton-like systems having less electrolysis time than that of Fe and Cu nanoparticles. Moreover, the reusability of Fe/Cu bimetallic nanocatalyst has shown about 77% degradation of the NFC even after three consecutive cycles (Campos et al., 2020). The use of nano zero-valent copper showed a greater drawback for its bulk particles and hence, the activity is reduced significantly since the active surface area is reduced for bulk particles (Li et al., 2015; Tamilvanan et al., 2014). This affects the Fenton reaction for the degradation of several micro-pollutants. However, the support media enables to restriction of the agglomeration of nanoparticles and enhances the suitability/applicability of materials (Jain et al., 2015).

Clay media in the Fenton-like reaction is attractive for the remediation of water contaminated with a variety of contaminants. Sanabria et al. (2008) observed 100% removal of phenol in 2 hrs of operation by a Fenton-like reaction, using Fe-pillared interlayer clay (PILC) made up of natural bentonite. Similarly, Giordano et al. (2007) were able to eliminate 97% of polyphenols from olive oil mill wastewater within 3 hrs, using Cu-PILC in a wet oxidation process with H₂O₂.

1.6 Scope of the present investigation

The contamination of the aquatic environment with a variety of micro-pollutants is ubiquitous and found serious global concern. This is, perhaps, due to the large-scale use of personal care products (PCPs) (e.g., shampoos, soaps, toothpaste, creams, cosmetics, medical skin care products, deodorants, etc.) that are primarily contained preservatives, biocides, musks or UV-filters [Yuval et al., (2018)]. Similarly, the widespread use of drugs *viz.*, antibiotics, antipyretic/analgesic drugs, potential environmental estrogens, and disinfectants poses a serious environmental threat since these compounds are found relatively persistent and often escape through the existing urban wastewater or sewage water treatment plants and readily detected, at a low level, in the aquatic environment (Bester, 2005; Heidler et al., 2006; Liu et al., 20013)]. Moreover, the presence of these micro-pollutants even at a low level impacted adversely and showed a potential risk to human and animal health (Lehutso et al., 2017). Therefore, these pollutants are, in recent times, known to be emerging water pollutants that need to be eliminated from the water bodies.

Advanced oxidation processes (AOPs) are found to be effective and efficient processes to degrade a variety of organic species from water bodies and provide a useful way of eliminating contaminants from aqueous solutions. The Fenton process is a widely used process among all the AOPs in such water strategies. The Fenton processes, which include $\text{H}_2\text{O}_2/\text{Fe}^{2+}$, $\text{UV}/\text{H}_2\text{O}_2/\text{Fe}^{2+}$, Sono-Fenton-like process, and Electro-Fenton-like are, therefore, used in the treatment of aquatic environments contaminated with micro-pollutants. However, the Fenton or Fenton-like processes are shown their limitations hence, the upgraded Fenton-like processes are likely to show enhanced applicability to tune the wastewater treatment plants with the required efficiency. Moreover, the use of natural and greener methods is ever-demanding to address effectively the associated environmental issues.

Therefore, the present investigation is specifically intended to upgrade the Fenton-like process to achieve the required efficiency and to eliminate the persistent micro-pollutants, *viz.* diclofenac sodium, phenol, N-(n-propyl)thiourea, amoxicillin, sulfamethazine, etc. from aqueous solutions. Moreover, it also focuses on the greener synthesis of heterogeneous nanocomposites contained in natural clay materials with

nZVI and nanoparticles of stable metals such as copper and silver. The nanoparticles of iron, copper, and silver are obtained by the greener synthetic route using the *Psidium guajava* (guava) leaf extracts. Bentonite is utilized as a supporting medium for the development of nanocomposite materials. The presence of bimetallic heterojunction enhances the reactivity towards H₂O₂/Visible solar light and improves the overall efficiency of Fenton-like processes in the treatment of various water pollutants *viz.*, diclofenac sodium, phenol, N-(n-propyl)thiourea, amoxicillin, sulfamethazine. Further, the practical applicability of the method is assessed in real-water samples collected from two different natural water sources.

CHAPTER 2
METHODOLOGY

2. METHODOLOGY

2.1 Materials

2.1.1 Chemicals

All chemicals and reagents obtained are preferably analytical or equivalent grade and are used without further purification. Details of all the chemicals are listed in Table 2.1.

Table 2. 5. Details of various chemicals used for experimental works.

Sl. No.	Chemicals used	Formula	Company	CAS number
1	Iron nitrate nonahydrate purified	$\text{Fe}(\text{NO}_3)_3 \cdot (\text{H}_2\text{O})_9$	Merck	7782-61-8
2	Silver nitrate	AgNO_3	Sigma Aldrich, USA	7761-88-8
3	Copper sulfate	CuSO_4	Merck	7758-99-8
4	Diclofenac sodium salt	$\text{C}_{14}\text{H}_{10}\text{Cl}_2\text{NNaO}_2$	Sigma Aldrich, USA	15307-79-6
5	Phenol	$\text{C}_6\text{H}_5\text{OH}$	HiMedia, India	108-95-2
7	Amoxicillin	$\text{C}_{16}\text{H}_{19}\text{N}_3\text{O}_5\text{S}$	Merck	26787-78-0
8	Sulfamethazine	$\text{C}_{12}\text{H}_{14}\text{N}_4\text{O}_2\text{S}$	Sigma Aldrich, USA	57-68-1
9	Glycine	$\text{C}_2\text{H}_5\text{NO}_2$	Himedia, India	56-40-6
10	Sodium acetate	CH_3COONa	Merck	127-09-3
11	Cadmium nitrate tetrahydrate	$\text{Cd}(\text{NO}_3)_2 \cdot 4\text{H}_2\text{O}$	Merck	10022-68-1
12	Disodium hydrogen phosphate anhydrous	Na_2HPO_4	Merck	7558-79-4

13	Ethylenediamine-tetraacetic acid	$C_{10}H_{16}N_2O_8$	Qualigens Fine Chemicals, India	60-00-4
14	Ethanol	CH_3CH_2OH	Qualigens Fine Chemicals, India	64-17-5
15	Ferric chloride hexahydrate	$FeCl_3 \cdot 6H_2O$	Himedia, India	7705-08-0
16	Chloroform	$CHCl_3$	Himedia, India	67-66-3
17	Conc. Sulphuric acid	H_2SO_4	Himedia, India	7664-93-9
18	Sodium hydroxide	$NaOH$	Himedia, India	1310-73-2
19	Nickel chloride	$NiCl_2$	Merck	7718-54-9
20	Hydrochloric acid	HCl	Merck	7647-01-0
21	N-(n-propyl) thiourea	$C_4H_{10}N_2S$	Thermo Scientific™	927-67-3
22	Hydrogen peroxide	H_2O_2	Merck	7722-84-1
23	2-propanol	C_3H_8O	Himedia, India	67-63-0
24	Lead Nitrate	$Pb(NO_3)_2$	Merck	10099-74-8
25	Oxalic acid	$C_2H_2O_4$	Merck	6153-56-6

2.1.2 Clay samples and real water samples

The pristine bentonite clay used in the preparation of nanocomposite was purchased from HiMedia, India. The clay powder was washed several times with deionized water (DW) and dried in the hot-air oven (Relitech Co., India) at 90°C and crushed to a fine powder to obtain 100 BSS (British Standard Sieve).

Two real water samples were collected from two different sources located at Aizawl City, Mizoram, India, for real water experiments. Table 2.2 provides locations of two different locations. One of them is spring water and another water is from the tank of the university's water supply. It was filtered using Whatman filter paper (pore size 20 µm) and tested for quality before being used. These water samples were

subjected to a variety of Physico-chemical parametric investigations (*cf* **Table 2.7**). A multiparameter instrument was used to test the water quality, including pH, conductivity, resistivity, salinity, and total dissolved solids, utilizing a variety of parameters. The AAS (Atomic Absorption Spectrometer) was used to check several metals in these water samples. The TOC analyzer is used to obtain the NPOC (Non-purgeable Organic Carbon) and IC (inorganic carbon).

Table 2.6: GPS locations of real water samples collected.

Locations	Code	Water Source	GPS Location
Six miles, Tanhril, Aizawl	R1	Spring	Latitude = 23°44'3"N Longitude = 92°40'33"E Elevation = 833 m
University water-supply tank	R2	Stock water	Latitude = 23°44'16"N Longitude = 92°40'10"E Elevation = 884 m

Table 2.7 Physico-chemical properties of two real water samples

Source	TOC (mg/L)	Cations (mg/L)	Anions	Physical properties
R ₁	NPOC=1.349 TC = 18.851 IC = 17.502	Cu = 0.0036 Ca = 2.3582 Zn = 0 Pb = 0.0752 Ni = 0.0195 Fe = 0 Mn = 0	Sulphate = 11 mg/L Phosphate = 0.1 mg/L Nitrate = 9 µg/L	pH = 8.21 Salinity = 0.1 PSU Oxd. & red. Potential = 160.7 MV Resistivity = 0.0045 MΩcm ⁻¹ Conductivity = 199 µScm ⁻¹ TDS = 100 ppm
R ₂	NPOC=0.976 TC = 8.443 IC = 7.466	Cu = 0.01 Ca = 3.4589 Zn = 0.0054 Pb = 0.0442 Ni = 0.0239 Fe = 0 Mn = 0	Sulphate = 7 mg/L Phosphate = 0.1 mg/L Nitrate = 20 µg/L	pH = 7.9 Salinity = 0.07 PSU Oxd. & red. Potential = 194.5 MV Resistivity = 0.0078 MΩcm ⁻¹ Conductivity = 129 µScm ⁻¹ TDS = 65 ppm

2.1.3 Reagents

- i) Sample stock solutions: 50.0 mg/L stock solutions of different micropollutants were prepared in purified distilled water. An accurate amount of the analyte (extra pure ~ 99.99%) was dissolved in purified water to prepare the stock solutions. Other required concentrations were made with the help of successive dilutions.
- ii) Standard buffer solutions (pH 4.01, 7.00, 10.01) (Hanna Instruments) were utilized for calibrating the pH meter.
- iii) Freshly prepared standard 0.1 mol/L HCl and 0.1 mol/L NaOH solutions were utilized for modifying the pH of the sample solutions.
- iv) Standard TOC calibration solutions were prepared using potassium hydrogen phthalate solution for calibrating the TOC instrument.

2.1.4 Instruments

Electronic balance (HPB220, Wensar, India) was employed for weighing solid chemicals. A digital pH meter (Labtronics, Model: LT-50 microprocessor pH meter, India) was utilized to measure the pH of solutions. The Fourier transform infrared spectrometer (FT-IR-Shimadzu, Model: IR Affinity-1S, Japan) was used to characterize the guava extract, which enables identifying the possible functional groups responsible for reducing the novel metal ions. The diffuse reflectance spectra (DRS) for the solids were obtained using a UV-Visible Spectrophotometer (Thermo Scientific, Model: Evolution 220, USA). Brunauer-Emmett-Teller (BET) method was used to measure the specific surface area of the nanocomposite materials utilizing the BET Surface area analyzer (Micromeritics, Model: ASAP 2010, USA). A transmission electron microscope (TEM; JEOL, Model: JEM 2100, Japan) examines the materials' morphology. A field emission scanning electron microscope (FE-SEM; Hitachi, Model: S-4700, Japan) was used to analyze the materials' surface images. X-Ray Diffraction (XRD) patterns were obtained by using an X-ray diffraction machine (PANalytical, Model: X'Pert PRO MPD, Netherland) equipped with Cu K α radiation ($\lambda=1.5414 \text{ \AA}$) as the X-ray source. To study the composition and oxidation states of elements present in the catalyst, the X-ray photoelectron spectroscopy (XPS; Thermo Fisher Scientific Pvt. Ltd., Model: Nexsa XPS system, UK) was employed. The total organic carbon (TOC) in all the water samples was measured using a TOC analyzer (Shimadzu, Model: TOC-VCPH/CPN, Japan). A multiparameter photometer (Hanna

Instrument, Model: HI98914, USA) and an atomic absorption spectrophotometer (AAS; Shimadzu, Model: AA-7000, Japan) were used to determine the quality of natural water samples. AAS was used for the quantitative determination of metals such as Zn, Ni, Cu, Pb, Mn, Fe, etc. whereas, a multiparameter gives a quantitative estimation of several anionic species present in the water samples.

A LED (light emitting diode) bulb (Havells- Adore LED 9W, India) and a UV-A lamp ($\lambda_{\text{max}} = 360 \text{ nm}$, Philips, 9W, Model: PLS9W BLB/2P 1CT, South Korea) were used as a light source for photo-Fenton-like reactions.

2.2 Preparation Of Materials

2.2.1 Preparation of guava leaf extract

Fresh guava (*Psidium guajava*) leaves were collected from the university campus (Mizoram University, India). A facile and simple procedure was used to get the leaf extract. 10 g dried and finely ground guava leaves were accurately weighed and put in a 250 mL conical flask filled with 100 mL of purified water. The mixture was heated at 80°C for 20 minutes, cooled, and filtered using Whatman no. 1 filter paper. Filtrates were stored at 4°C for further use.

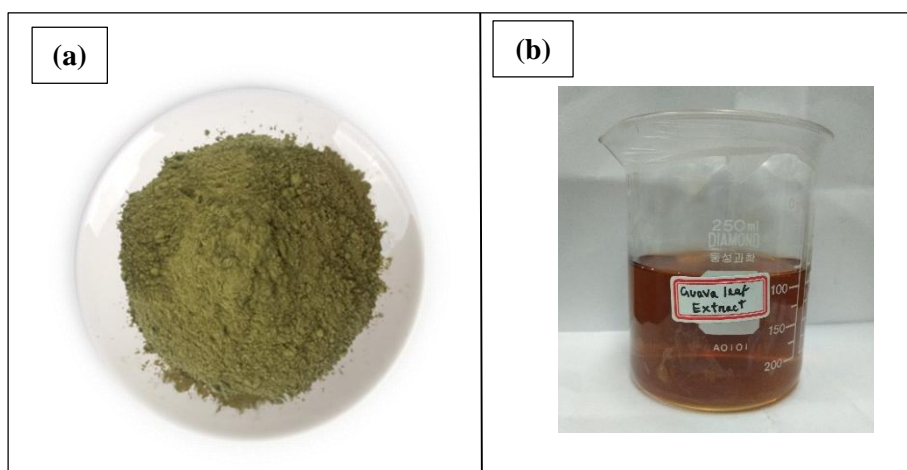


Figure 2.1: (a) Guava leaf powder; (b) Aqueous guava leaves extract

2.2.2 Synthesis of nanocomposite materials

2.2.2.1 Preparation of Ben@FeNPs and Ben@(FeNPs+AgNPs) nFLC

Freshly prepared guava leaf extract was utilized as a green, reducing agent in the *in situ* synthesis of nanoparticles *viz.*, iron, silver, and copper nanoparticles. The optimal quantity of guava extract was determined by adjusting the volumetric ratio of precursor ions and guava leaf extract. A facile procedure was adopted to synthesize the Ben@FeNPs and Ben@(FeNPs+AgNPs) nano Fenton-like catalysts (nFLC). Bentonite (15 g) was suspended for 8 hrs in 250 mL 0.1 mol/L Fe(NO₃)₃ solution with slow stirring at room temperature, centrifuged (1500 rpm), and the supernatant was discarded. 75 mL of guava leaf extract was dropped into the refined Fe³⁺-bentonite at the ratio of 1:5 (clay: guava leaf extract) and agitated for around 12 hrs. The bentonite-supported iron nanoparticle (Ben@FeNPs) is obtained. The black-colored aggregation of iron nanoparticles on the bentonite clay is obtained (*Cf.* Figure 2.2)

Further, the nanocomposite Ben@(FeNPs+AgNPs) was obtained as: the Fe³⁺-bentonite suspension was suspended in 250 mL 2.5 mmol/L AgNO₃ solutions for 6 hrs. The solid was transferred to round bottom flasks. The pH of the suspension was measured and found to be 8.12. 75 mL of guava leaf extract was added dropwise to the (Ben@Fe³⁺-Ag⁺) suspension, and the suspension was agitated for 6 hrs. The supernatant was discarded after centrifugation of the suspension. Several piles of washing of solid enabled the removal of the excess of NO₃⁻ ions. The solid residue was kept in a hot air oven at 50°C for 5 hrs. The bimetallic nanoparticles supported bentonite were crushed into a fine powder and kept in an airtight polyethylene container for future use.

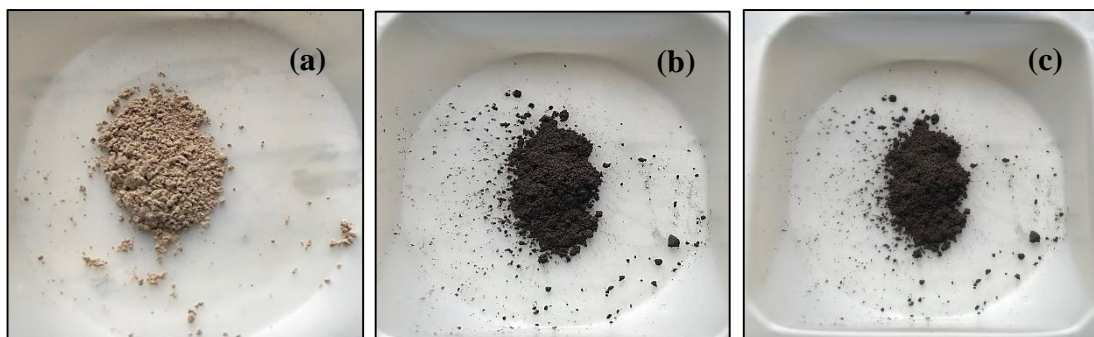


Figure 2.2: Image of (a) Pristine bentonite clay ; (b) Ben@FeNPs, and (c) Ben@(FeNPs+AgNPs) nanocomposite

2.2.2.2 Synthesis of Ben@CuNPs and Ben@(CuNPs+AgNPs) nFLC

The Ben@CuNPs and Ben@(CuNPs+AgNPs) nano-Fenton-like catalysts (nFLC) were synthesized using a similar procedure described previously for the Ben@FeNPs and Ben@(FeNPs+AgNPs). Bentonite (15 g) was suspended for 8 hrs with slow stirring at room temperature in 250 mL 0.1 mol/L CuSO₄ solution, then centrifuged (1500 rpm) and the supernatant was discarded. 75 mL guava leaf extract was added to the solid (Cu²⁺-bentonite) at a 1:5 (solid: guava leaf extract) ratio and agitated for 12 hrs. This prepared nanocomposite is named as Ben@CuNPs. Furthermore, the Cu²⁺-bentonite suspension was suspended in 250 mL 2.5 mmol/L AgNO₃ solutions for 6 hrs to obtain the nanocomposite Ben@(CuNPs+AgNPs). The suspension was transferred to round bottom flasks followed by adding 75 mL of guava leaf extract dropwise to the (Ben@Cu²⁺-Ag⁺) solid and the suspension was agitated for 6 hrs. The final pH of the suspension was found to be 9.03. After centrifuging the suspension, the supernatant was discarded. The excess NO₃⁻ ions were removed using several stacks of solid washing with purified water. The solid residue was heated for 5 hrs in a hot air oven at 50°C. The bentonite-supported bimetallic nanoparticles were crushed into a fine powder and stored in an airtight polypropylene container for later use.



Figure 2.3: Image of (a) Bentonite clay powder; (b) Ben@(CuNPs+AgNPs) nanocomposite.

2.3 Characterization of the materials

2.3.1 Phytochemical screening

The Fourier transform infrared spectrometer (FT-IR-Shimadzu, Model: IR Affinity-1S, Japan) was used to characterize the guava extract, which enables identifying the possible functional groups responsible for reducing the silver, iron, and copper ions. The aqueous guava extract sample was exposed to infrared light from the FT-IR instrument that ranges in wavelength from 10,000 to 100 cm^{-1} , some of which is absorbed and some of which passes through. The sample molecules transform the absorbed radiation into rotational and/or vibrational energy. The resultant signal, which appears as a spectrum at the detector and ranges from 4000 cm^{-1} to 400 cm^{-1} , represents the sample's molecular fingerprint. Because each molecule or chemical structure will provide a distinct spectral fingerprint, FT-IR analysis is a fantastic technique for identifying specific chemicals.

Screening of phytochemical contents of the aqueous extract was performed qualitatively based on coloring and precipitation reactions. Various tests for the phytochemical contents of the extract were conducted using the standard protocols reported elsewhere (Chandraker et al., 2020; Auwal et al., 2014; Obouayeba et al., 2015).

1) Test for alkaloids: In 1 mL extract solution, slowly 6-8 drops of Mayer's reagent were added. This gives a cream precipitate which confirmed the presence of alkaloids.

Mayer's reagent is prepared by dissolving 5 g of potassium iodide and 1.358 g of mercuric chloride in 100 mL of distilled water (Sanghani, 2017).

2) Test for flavonoids: 1 mL of the extract was taken in a test tube and a few drops of neutral ferric chloride solution was added to it. The formation of black-red precipitate confirmed the presence of flavonoids.

3) Test for tannins: 2 mL of 5% ferric chloride and 1 mL of the extract are vigorously mixed in a test tube. This gives a greenish-black/dark blue color, which confirms the presence of tannins in the extract solution.

4) Test for phlobatannins: 10 mL of extract solution is boiled with 2-3 mL of 10% HCl for 5 minutes. The formation of a red precipitate is the confirmation of phlobatannins contents in the extract solution.

5) Test for triterpenes: The test is done with Salkowski test where equal volumes of chloroform and leaf extract are shaken with a few drops of concentrated H_2SO_4 . The lower layer turns yellow, which confirmed the presence of triterpenes.

6) Test for saponins: 1 mL extract is shaken vigorously with 2 mL distilled water and the persistence of foam indicated the presence of saponin contents.

7) Test for glycosides: 1 mL extract is added with 2-3 drops of Molisch's reagent followed by a few drops of concentrated H_2SO_4 . A reddish-purple ring on the junction showed the presence of glycosides.

Molisch's reagent is prepared by dissolving 20 g naphthol in 100 mL of ethanol (Yogesh & Sanghani, 2017).

8) Test for anthocyanins: 2 mL of plant extract is mixed with 2 mL of 2 mol/L HCl. The presence of anthocyanins is indicated by the development of a pink-red tint that becomes purple-blue when ammonia solution is added.

9) Test for reducing sugars: In a test tube, 2 mL of aqueous leaf extract solution is taken and 5 mL of a mixture solution containing equal volumes of Fehling's solutions A and B is added slowly (Fehling's solution A is an aqueous blue solution of copper

(II) sulphate, while Fehling's solution B is a clear solution of aqueous potassium sodium tartrate and a strong base, mostly sodium hydroxide). The solution mixture is heated for about 2 mins in a water bath. The presence of reducing sugars is confirmed by the occurrence of the brick-red precipitate.

10) Test for polyphenols: Two drops of alcoholic solution of 2 percent ferric chloride are added with 2 mL of plant extract. The presence of polyphenolic chemicals is indicated by a more or less dark blackish-blue or green color.

2.3.2 Characterization of nanocomposite materials

The 'point of zero charge' (pH_{PZC}) is the pH value at which the surface acidic and basic functional groups no longer contribute to the pH value of the solution (Igberase and Osifo, 2015). The point of zero charge determination of these solids is also important in elucidating the adsorption mechanism involved at a solid solutions interface. At a pH lower than the pH_{PZC} , the solid carries a net positive surface charge, and at a pH higher than the pH_{PZC} , the surface carries a net negative charge because of the acidic dissociation of surface functional groups. The pH_{PZC} (point of zero charges) of the solids, *viz.* pristine bentonite, Ben@FeNPs, Ben@CuNPs, Ben@(FeNPs+AgNPs), and Ben@(CuNPs+AgNPs) were obtained by the pH drift method as demonstrated previously (Lalhriatpuia et al., 2015; Tiwari et al., 2015): A 1000 mL Erlenmeyer flask was filled with 500 mL of distilled water, the top was covered with cotton, and the water was slowly and gradually heated till boiling for 20 minutes to extract the dissolved CO_2 . To prevent air CO_2 from being reabsorbed, the flask was promptly capped. Using the CO_2 -free water, 50 mL of 0.01 mol/L NaCl solutions were created. The pH of each flask's solution was then changed by adding dropwise additions of 0.1 mol/L HCl or 0.1 mol/L NaOH solutions to achieve varied pH values of 2.0, 4.0, 6.0, 8.0, 10.0, and 12.0. Each flask was filled with 100 mg of the solid sample, which was then firmly sealed before being shaken for 24 hours at 25°C. The final pH of the solutions was noted, and graphs were created between $pH_{Initial}$ and pH_{Final} . This curve's junction point indicated the point of zero charge.

The band-gap energy (E_g) is important for the catalysts, especially in the photo-induced degradation of pollutants. Diffuse reflectance spectroscopy (DRS) is a more

valuable approach for characterizing powdered samples than UV-Vis absorption spectroscopy because it provides an enhanced scattering phenomenon in powder materials (Morales et al., 2007). A UV-Visible Spectrophotometer (Model: Evolution 220, Thermo Scientific, USA) was used to produce diffuse reflectance spectra (DRS) for the solids, *viz.* pristine bentonite, Ben@FeNPs, Ben@CuNPs, Ben@(FeNPs+AgNPs), and Ben@(CuNPs+AgNPs). Using diffuse reflectance data, the absorption coefficient was calculated using the Kubelka-Munk equation to estimate the solid band gap energy (Equation 2.1). The Kubelka-Munk equation was used to transform the reflectance into a Kubelka-Munk function ($F(R)$) (Abdullahi et al., 2016). The absorbance is directly proportional to the values of $F(R)$. Tauc plots, which include extrapolating the linear section of a graph of $(F(R) \times h\nu)^{1/2}$ vs the energy of a photon of light, may be used to determine the band gap energy of the nanocomposite materials.

$$F(R) = (1 - R)^2 / 2R \quad \dots(2.1)$$

where R represents the sample's reflectance regarding a reference at each wavelength.

The specific surface area of the pristine bentonite and other synthesized nanocomposites was obtained using the Brunauer-Emmett-Teller (BET) analyses (Micromeritics, USA) based on liquid N₂ adsorption-desorption isotherms. It provides significant information about their physical structure. Many characteristics, such as dissolution rates, catalytic activity, moisture retention, and shelf life, are frequently demonstrated with the surface area of a material. According to the BET theory, the adsorption of an inert gas yields an atomic-level determination of a particle's real or specific surface area, including surface imperfections and pore walls. The solid substance needs to be chilled, usually using a cryogenic liquid, because most gases and solids interact with each other very weakly. While the pressure or concentration of the adsorbing gas is raised, the temperature of the solid sample is maintained at a constant level or under isothermal circumstances. The BET findings revealed the pore size, specific surface area, and pore volumes of all the pristine as well as synthesized materials.

Field emission Scanning Electron Microscope (SEM) (FE-SEM: JEOL JSM 7100F; Oxford Xmax) (Operation condition: SEI Resolution used: 15kV,

Magnification: 10-1000000, Accelerating Voltage: 0.2-30 kV, Probe Current: 1pA-400nA and Electron Gun used: In-Lens Schottky field emission gun) was employed to achieve the surface morphology of nanocomposite. Furthermore, the elemental composition was determined using energy-dispersive X-ray (EDX, Oxford instruments X-Max^N) spectroscopy in conjunction with a scanning electron microscope (SEM). Similarly, Transmission electron microscopy (TEM; Model: JEM 2100, JEOL, Japan) was used to analyze the bulk morphology of the particles. The nanocatalyst powder was dispersed in isopropyl alcohol by sonication and drop cast on the TEM grid (Lacey carbon-coated copper grid-300 Mesh). The grid was dried in a vacuum desiccator and then coated with gold (2.0 nm). The samples were analyzed using the secondary electron detector at 30 kV acceleration voltage. In addition, the interplanar distance of Ag(NPs) or Fe(NPs), or Cu(NPs) was computed, and the particle size was determined. X-ray diffraction (XRD) pattern of the nanocomposite materials was carried out using an XRD machine (i.e., X'Pert PRO MPD; PANalytical, Netherlands). The X-ray diffraction data were collected at a scan rate of 0.033 of 2 θ illuminations and with the generator set to 30 mA and 40 kV. To study the composition and oxidation states of elements present in the catalyst, the X-ray photoelectron spectroscopy (XPS; Thermo Fisher Scientific Pvt. Ltd., Model: Nexsa XPS system, UK) was employed. The source of the X-ray was monochromatic Al K α (1486.6 eV) along with beam size 400 μ m, base pressure 2.0 x 10⁻⁷ Torr, and pass energy 50 eV. The TOC analyzer (Shimadzu, Model: TOC-VCPH/CPN, Japan) was used to measure the total organic carbon (TOC) in both treated and untreated water samples. The TOC Analyzer used in this study is based on the catalytic oxidation/NDIR (680° C combustion) method and has extremely high responsiveness and dependability for analyzing parameters like total carbon (TC), inorganic carbon (IC), and Non-Purgeable Organic Carbon (NPOC) with measuring ranges and detection limits of TC: 4.0 ng/L to 25000.0 mg/L and IC: 4.0 ng/L to 30000.0 mg/L. The mineralization of the contaminants under photo-Fenton-like operations was represented by the change in NPOC values with the photocatalytic process.

2.4 Batch reactor Studies

2.4.1 Degradation of targeted organic pollutants

Stock solutions of diclofenac sodium (DCF) (50.0 mg/L), phenol (50.0 mg/L), N-(n-propyl) thiourea (NNPT) (50.0 mg/L), amoxicillin (AMX) (50.0 mg/L), and sulfamethazine (SMZ) (50.0 mg/L) were prepared using purified water. The solutions were sonicated for 10 minutes to increase the solubility of these contaminants in purified water. Additionally, the experimental concentrations were obtained by successive dilution of the stock solutions. Drop-by-drop addition of HCl (1 mol/L)/or NaOH (1 mol/L) solutions allowed the pH of these solutions to be adjusted from 2.0 to 7.0.

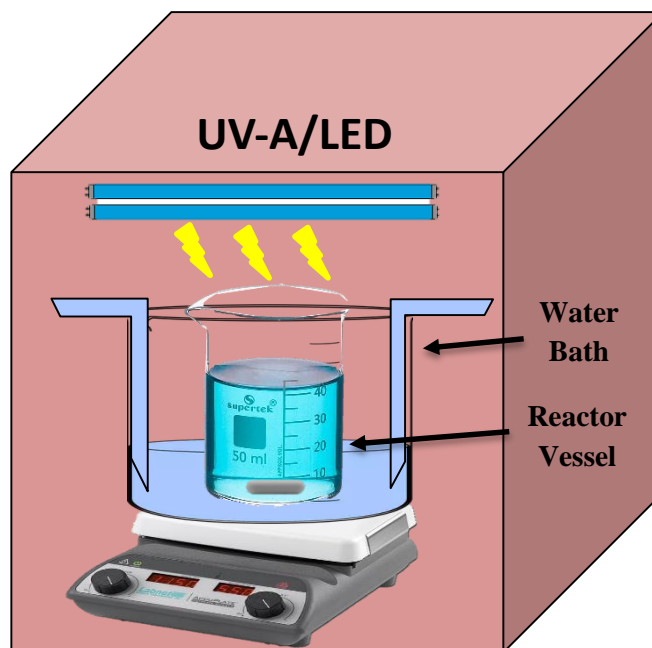


Figure 2.4: Schematic of dark Cabinet for conducting the experiments

The experiments were carried out at $25^{\circ}\pm 1^{\circ}\text{C}$ using a self-assembled water bath. The degradation studies were carried out in a 100 mL borosilicate glass beaker kept on a magnetic stirrer plate with a continuous stirring speed of 300 rpm. The beaker is suitably wrapped with parafilm and stored inside a self-made dark cabinet (Figure 2.4). The specific pollutant solution was taken along with an appropriate amount of nanocatalyst; the suspension was agitated in the dark for 60 mins to achieve adsorption/desorption equilibrium. The optimized H_2O_2 amount was introduced just

after the equilibrium time was reached. The quantitative estimation of each pollutant solution was obtained using a UV-VIS spectrophotometer (Shimadzu, Japan, model: UV-1800), and some cross-checks were carried out using an HPLC system (High-Performance Liquid Chromatography, Waters, Model: Waters 515 HPLC pump) equipped with a UV detector (Waters, Model: Waters 2489 UV/VIS Detector; USA). A C18 analytical column (4.6X250 mm, pore size 100 Å) was used to evaluate unknown pollutant concentrations using water (HPLC grade, Himedia), methanol (HPLC grade, Himedia), and acetonitrile (HPLC grade, Himedia) as mobile phases. The treated pollutant samples' supernatant was collected to analyze concentrations at various intervals of time (e.g., 10, 20, 30, 45, 60, 90, and 120 mins). The supernatant solution was filtered using a syringe filter (0.22 µm; Whatman, USA) before being subjected to either a UV-Vis Spectrophotometer or HPLC to determine unknown pollutants' concentrations. The UV-Vis spectrophotometer was adjusted to the specific λ_{\max} for each pollutant. The λ_{\max} for DCF, phenol, NNPT, AMX, and SMZ were determined to be 275, 270, 236, 228, and 260 nm, respectively. As a result, each pollutant's calibration lines were obtained at their respective wavelength. For the UV-Vis spectrophotometer, the standard solutions of each pollutant at various concentrations (0.5 to 20.0 mg/L) were used to obtain the calibration line by plotting a graph of absorbance vs. known concentrations of the particular pollutant solution. Similarly, to achieve the calibration curve for the HPLC instrument, a graph of peak area vs various pollutant concentrations (0.5 to 20.0 mg/L) was plotted for each pollutant. The details of different parameters used for the quantification in HPLC instruments were mentioned in table 2.4. Pollutant samples were taken from the reactor at specified time intervals, and the calibration curve was used to calculate the unknown concentrations of the pollutants. Using equation 2.2, the percentage degradation for various contaminants was estimated:

$$\text{Percentage degradation} = \frac{C_i - C_t}{C_i} \times 100 \quad \dots(2.2)$$

where C_i stands for the initial pollutant concentrations whereas C_t stands for the concentration of the pollutant at the time “t”. All the experiments were repeated three times and standard errors are obtained.

Table 2.8. Different parameters for the quantification in HPLC.

Name of pollutant	Mobile phase	Wavelength (nm)	Injection volume (μL)	Flow rate (mL/min)	Retention time (min)
DCF	Water: Acetonitrile (80:20)	275	20	0.5	9.25
Phenol	Water: Acetonitrile (65:35)	270	20	0.5	6.05
NNPT	Water: Methanol (60:40)	236	20	1	2.50
AMX	Acetonitrile: water (90:10)	228	20	1	6.47
SMZ	Acetonitrile: water (55: 45)	275	20	1	2.94

2.4.2 Effect of Solution pH

The influence of the solution pH is a regulating parameter in deducing the process of pollutant degradation in aqueous media. The generation of $\bullet\text{OH}$ radicals and breakdown of zero-valent Fe(NPs) or Cu(NPs) and the speciation of pollutant molecules is predominantly governed by the pH of the solution (Song et al., 2017). The pH of the solution affects the catalyst's surface charge and the size of the catalyst aggregates. The Fenton process is significantly impacted by the sorption of contaminants on the surface of the nanocatalyst. The pH of sorptive liquids substantially influences the sorption process (Chong et al., 2010). Therefore, the solution pH strongly affects the degradation efficiency of organic pollutants in Fenton or Fenton-like reactions.

The pH-dependent degradation of the targeted micropollutants was carried out in a wide range of pH 2.0 to 7.0. Pollutant degradation percentage as a function of solution pH was used to express the results.

2.4.3 Optimization of initial H₂O₂ and nanocomposite dose

In order to produce •OH radicals during the degradation of micropollutants, the oxidant (H₂O₂) dose as well as the Fenton-catalyst dose, are considered to be crucial operational parameters. Several researchers indicated that the degradation percentage of pollutants increases with the increase in oxidant and catalyst dose up to a certain point after which the degradation percentage decreases gradually (Mitsika et al., 2013a; H. Zhang et al., 2005). To monitor the effect of H₂O₂, different doses of H₂O₂ (30% v/v) were employed at a constant pH, nFLC dose, and pollutant concentrations. The experiments were performed for each pollutant inside a dark box. Similarly, the optimized nanocomposite dose was determined by monitoring the effect of different doses of nanocomposite by keeping the H₂O₂ amount, pollutant concentrations, and pH values of the solution constant. The experiments were performed for each pollutant inside a dark box. The dosage of the oxidant and nanocomposite that results in the maximum removal efficiency of the target pollutant was deemed to be the ideal dose and employed in the remaining experiments.

2.4.4 Photo-Fenton-like degradation of micropollutants

Light irradiation synergized the removal efficiency of the Fenton process by stimulating the formation of •OH radicals (Sapach and Viraraghavan, 1997) as shown in (Eq. 2.2):



The photo-Fenton-like procedure was carried out at 25°±1°C using a self-assembled water bath inside the dark cabinet. An appropriate dosage of nanocatalyst was added to the solution containing the particular pollutant solution, and the suspension was stirred in the dark for 60 minutes to reach adsorption/desorption isotherms. After that, the optimal amount of H₂O₂ was added to the pollutant solution. Immediately after the addition of the optimal H₂O₂ dose, the pollutant solution was subjected to light irradiation (LED and UV-A) for definite time intervals (2 hrs). Pollutant samples were collected from the reactor at definite time intervals (e.g., 10,

20, 30, 45, 60, 90, and 120 mins), and the unknown concentrations of the pollutant were calculated.

2.4.5 Effect of initial concentration of the pollutant

The initial concentration of pollutants is an important parameter that demonstrates the mechanistic aspects of degradation (Nasseri et al., 2017). According to the literature, the concentrations of micropollutants in aquatic environments ranged from ng/L to µg/L (Sousa et al., 2018). The percentage degradation of pollutants used to be higher at a lower initial concentration and become less with an increase in pollutant concentrations. Therefore, at constant solution pH, the effect of the initial concentration of pollutants in photo-Fenton-like degradation of organic pollutants was investigated by increasing the initial concentrations from 2.0 mg/L to 30.0 mg/L. The degradation experiments were conducted for both LED and UV-A-mediated Fenton-like degradation of the targeted pollutants. After a specific reaction time i.e., 2 hrs, the results were obtained as percent pollutant degradation as a function of pollutants' initial concentrations.

2.4.6 Effect of co-existing ions

Wastewater contains a range of dissolved inorganic and organic cations and anions that can either have a detrimental or positive impact on the rate of photo-Fenton-like degradation of organic contaminants. Studies on the photo-Fenton-like degradation of various organic pollutants under UV-A and visible light irradiations using the synthesized nano-Fenton-like catalyst were conducted in the presence of several coexisting ions, *viz.*, oxalate, phosphate, sulphate, glycine, palladium, cadmium, nickel, copper, lead, etc. to replicate the natural wastewater matrix. Under UV-A and LED light irradiation and optimal reaction conditions, a comparable removal of contaminants was obtained. The pollutant concentration and cations/anions were kept constant at 2.0 mg/L and 10.0 mg/L, respectively.

2.4.7 Degradation kinetics

The Fenton or Fenton-like reactions are complicated, making kinetic investigations challenging. The Fenton or Fenton-like processes have multiple-step reactions, each with a specific rate constant. However, the reaction involving the degraded component and •OH radicals is regarded as the primary reactants for establishing the overall rate constant (Mitsika et al., 2013b). The time-dependent change in pollutant concentrations is observed and predicted using known kinetic equations. The degradation kinetics was investigated using both pseudo-first-order and pseudo-second-order kinetics models, with the best-fitted model being used to investigate the degradation kinetics of each pollutant. The pseudo-first-order (Equation 2.3) and pseudo-second-order (Equation 2.4) rate equations were shown using the experimental data for pollutant degradation.

$$\ln \frac{C_t}{C_0} = -k_f t \quad \dots(2.3)$$

$$\frac{1}{C_t} - \frac{1}{C_0} = k_s t \quad \dots(2.4)$$

where C_t (mg/L) and C_0 (mg/L) are the pollutant concentrations at time t and t_0 (initial reaction time), respectively. Similarly, the k_f and k_s are the experimental rate constants for the pseudo-first-order and pseudo-second-order reactions, respectively. The values of k_f and k_s are obtained by plotting the linear plots between the $\ln C_t/C_0$ vs. reaction time (t) and $(1/C_t - 1/C_0)$ vs. t , respectively (Gopal et al., 2020).

2.4.8 Involvement of •OH radical

H_2O_2 produces hydroxyl (•OH) radicals and breaks down the pollutant molecule's unsaturated double bonds. Hydroxyl radicals break down the conjugated system in macromolecules into tiny intermediates (Wu et al., 2015). Intermediates are readily mineralized as CO_2 and H_2O . To reaffirm the participation of •OH radicals in the degradation pathway, the study was extended, introducing a few widely known •OH radical quenchers. The isopropanol and HCO_3^- are described to be good quenchers of •OH radicals (Lalliansanga et al., 2020; Tiwari et al., 2018b). Similarly, sodium

azide (NaN_3) quenches another important reactive oxygen species (ROS), singlet oxygen produced due to the reaction of $\cdot\text{O}_2^-$ radicals and photo-generated holes. This singlet oxygen is extremely reactive toward the organic compounds in aqueous media (Barka et al., 2010). Hence photo-Fenton-like degradation of 2.0 mg/L of each targeted pollutant (100.0 mL) in the presence of 1.0 mL (0.1 mol/L) isopropanol, HCO_3^- and NaN_3 was conducted utilizing the synthesized nano Fenton-like catalyst maintaining the optimum reaction conditions. The decrease in the percentage of degradation signifies the participation of $\cdot\text{OH}$ radicals in the degradation of the pollutant.

2.4.9 Mineralization of organic pollutants: TOC measurements

The extent of mineralization of pollutants in the photo-Fenton-like treatment demonstrates the efficiency/applicability of operation as it indicates the total elimination of dissolved harmful organic compounds from the contaminated aqueous solutions. As a result, the TOC (total organic carbon) analyzer was used to measure the extent of mineralization in the photo-Fenton-like degradation process. The mineralization of pollutants was obtained at different initial concentrations (2.0 mg/L to 30.0 mg/L), at a constant solution pH (~3.0). The NPOC (Non-Purgeable Organic Carbon) values were obtained for the treated and untreated pollutant solutions, hence; the percentage removal of NPOC was calculated. Further, the percentage mineralization was plotted against the initial pollutants' concentrations.

To analyze the TOC data, the treated pollutant samples' supernatant was collected at the final hour, i.e. 120 min. The supernatant solution was filtered using a syringe filter (0.22 μm ; Whatman, USA). NPOC values were obtained for the final sample solutions and their corresponding blank solutions using a TOC analyzer (Shimadzu, TOC-VCPH/CPN). The decrease in the NPOC value of treated samples compared to blanks shows the amount of decomposition of the organic species under photo-Fenton-like treatment. The NPOC data is then converted into percent elimination by using the pollutant's initial TOC value (blank). The NPOC value indicates the extent of mineralization of organic compounds in the aqueous medium. As a result, the percent mineralization was calculated and plotted as a function of the initial concentration at the optimized reaction conditions.

2.4.10 Determination of leached ion concentrations

The disappearance of organic contaminants in the photo-Fenton-like process might be correlated with the Fe^{2+} or Cu^{2+} leaching from the reaction mixture. The main hypothesis of the classical Fenton process was the involvement of Fe^{2+} or Cu^{2+} and H_2O_2 . In the case of Ben@[FeNPs+AgNPs] nanocatalyst, as iron leaching progresses, the concentration of Fe^{2+} rises (Cf Eq. (2.5-)), and the Fenton-like reaction of Fe^{2+}/Fe^{3+} with H_2O_2 generates $\bullet OH$ radicals. In a heterogeneous system, it was established that the presence of H_2O_2 with Fe(NPs)/Ag(NPs) in Ben@[FeNPs+AgNPs] nanocatalyst is the principal source producing ROS in the system. Therefore, the decomposition of H_2O_2 is determined by the affinity of H_2O_2 towards the catalyst surface, the average available surface sites for the adsorption of H_2O_2 , and the rate of reduction of $\equiv Fe(III)$. Similarly, the concentration of Cu^{2+} increases as leaching advances, and the Fenton-like reaction of Cu^+/Cu^{2+} with H_2O_2 generates $\bullet OH$ radicals. In a heterogeneous system, the presence of H_2O_2 with Cu(NPs) or Ag(NPs) in Ben@[CuNPs+AgNPs] is a primary source of reactive oxygen species generation.



The concentration of Fe(II) leached out to the solution from the nano-catalyst Ben@[Fe(NPs)+Ag(NPs)] after corrosion of the nZVI was measured by complexometry using the 1,10-phenanthroline by monitoring the absorbance of the complex species at 510 nm as described previously (Sétifi et al., 2019; Zuo, 1995). Similarly, the amount of Cu(II) that was corroded from the Ben@[Fe(NPs)+Ag(NPs)] nanocomposite and leached into the mixture is determined by the AAS (LOD = 10 $\mu g/L$). The main idea behind the Fenton process is the involvement of Cu^{2+} and H_2O_2 . Cu^{2+} concentration is rising. When leaching intensifies, the concentration of Cu^{2+} rises, and $\bullet OH$ radicals are produced via the Fenton-like reaction of Cu^+/Cu^{2+} with H_2O_2 .

2.4.11 Reutilization of the nanocatalyst

Nanocatalyst's capacity is dependent on prolonged and repeated photo-Fenton-like processes. The nanocomposite material's stability is one of the important aspects. As a consequence, the batch reactor's repeated catalytic processes used nanocomposite material. Under UV-A irradiation, the photo-Fenton-like degradation of DCF, phenol, NNPT, AMX, and SMZ in an aqueous solution was conducted 4 to 5 times. The nanocomposite material was washed with distilled water after each cycle of operation, and it was then dried at 80°C in a drying oven. The next photocatalytic cycle used the crushed, finely ground catalyst after it had cooled to room temperature. For each cycle of operations, the starting pollutant concentration (2.0 mg/L) and pH (pH~3) were taken as constant.

2.4.12 Real water experiments

In order to utilize the synthesized material's applicability in real applications, the photo-Fenton-like remediation of DCF, phenol, NNPT, AMX, and SMZ from the actual water matrix, two real water samples were collected from natural sources and used in the experiment. Real water was collected in a polyethylene water container, filtered to remove the suspended solid particles, and subjected to different parametric analyses before the experiment was conducted. Using a multi-photometer device, several water quality parameters, including pH, conductivity, resistivity, salinity, total dissolved solids, phosphate, sulphate, nitrate, and fluoride, were measured. Using an atomic absorption spectrometer, the metal concentrations of Fe, Zn, Mn, Ca, Pb, and Cu were determined. The total carbon (TC), inorganic carbon (IC), and non-purgeable organic carbon (NPOC) readings of the real water samples were obtained using a TOC analyzer. The stock solution (50.0 mg/L) for each pollutant was prepared using both real water samples separately. Three different concentrations (2.0, 4.0, and 6.0 mg/L) for each pollutant were prepared from the stock pollutant solutions and subjected to the photo-Fenton-like degradation process maintaining the optimum reaction conditions of each particular pollutant. In the end, the degradation percentages were calculated, and the outcomes were compared to the degradation percentages of contaminants prepared with purified distilled water.

CHAPTER 3
RESULTS AND DISCUSSION

3. RESULTS AND DISCUSSION

3.1 Characterization of materials

3.1.1 Phytochemical studies of *P. Guajava* (guava) leaf extract

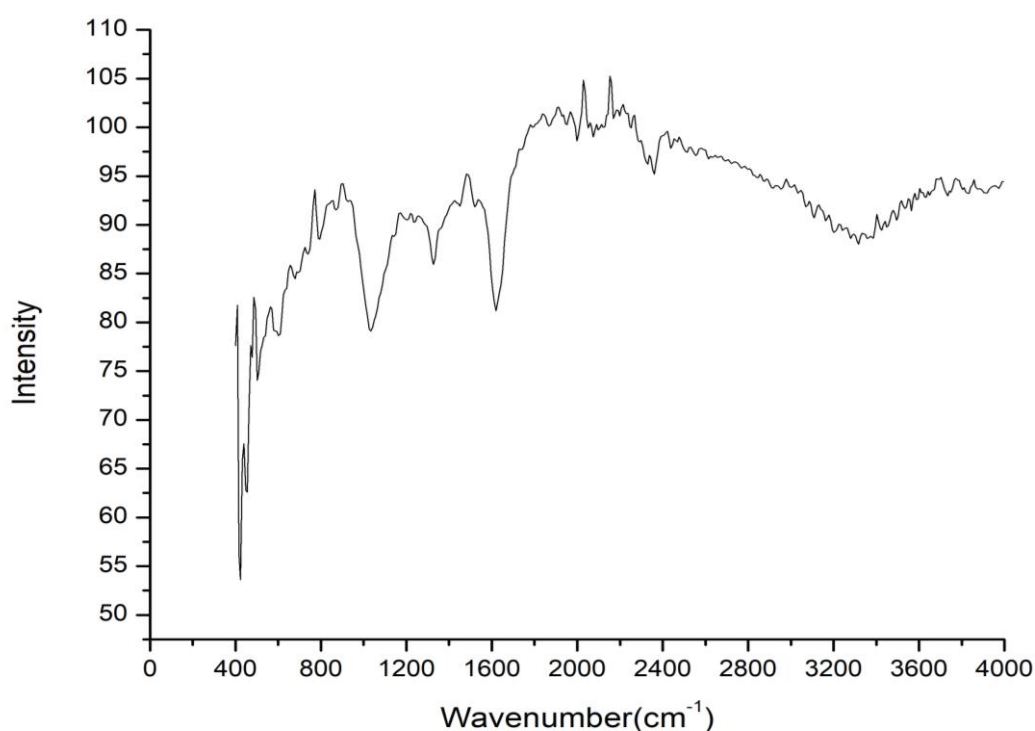


Figure 3.1: FT-IR spectrum of aqueous *P. Guajava* (guava) leaf extract.

The results of the FT-IR analysis enabled the identification of possible functional groups in the *P. Guajava* leaf extract, which are responsible for the reduction of metal cations (i.e., Fe^{3+} , Cu^{2+} & Ag^+). The stretching and bending bands 3378.98 (-OH), 2348.25 (CN), 1609.90 (C=C), 1353.89 (N-O), and 1050.90 cm^{-1} (C-O) in the IR spectral analysis of *P. Guajava* leaf extract reveal the existence of several functional groups present in *P. Guajava* leaf extract (Cf Figure 3.1). A broad peak around 3200-3400 cm^{-1} indicates the presence of the -OH group, which is common in tannins and flavonoids (Parashar et al., 2011). This peak indicates that antioxidants and flavonoid components such as ascorbic acid and gallic acid are likely to be present in the leaf extract, which is primarily responsible for metal ion reduction (Wang et al., 2018). Standard qualitative procedures were used to identify the significant phytochemicals in the aqueous leaf extract (Archana et al., 2012; Chandraker et al., 2020), and the results are shown in Table 3.1. Results indicated that alkaloids and

flavonoids are present in the leaf extract. The flavonoids are predominantly caused to reduce the precursor Ag^+ , Fe^{3+} , or Cu^{2+} ions to their zero-valent species.

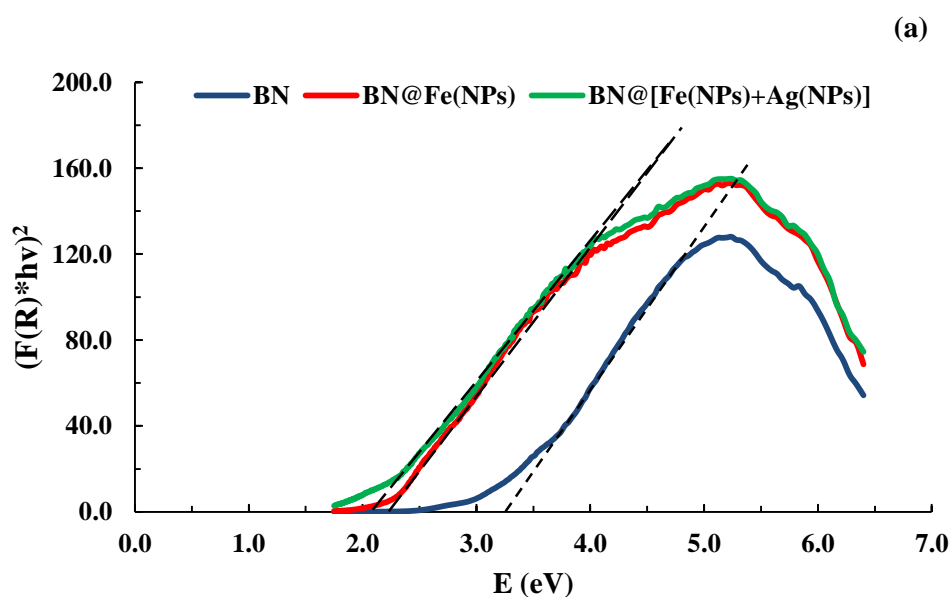
Table 3.1: Qualitative identification of various phytochemicals present in *P. Guajava* leaf extract.

S. No.	Phytochemicals	Test	Result
1	Alkaloids	Mayer's test, Wagner's test	+ve
2	Flavonoids	Ferric chloride test, lead acetate test	+ve
3	Tannins	Ferric Chloride test	+ve
4	Phlobatannins	HCl test	-ve
5	Triterpenes	Salkowski test, Liberman test	+ve
6	Diterpenes	Copper acetate test	+ve
7	Steroids	Salkowski test	+ve
8	Saponins	Foam test	-ve
9	Cardiac glycoside	Keller Killani test	+ve

3.1.2 pH_{pzc} , band-gap energy, and BET surface area analysis

The pH_{PZC} (point of zero charge) of bentonite, Ben@FeNPs, Ben@(FeNPs+AgNPs), Ben@CuNPs, Ben@(CuNPs+AgNPs) nanocomposites were obtained by a simple acid-base titration method as demonstrated previously (Lalhriatpuia et al., 2015; Tiwari et al., 2015). The pH_{PZC} of these solids was found to be 7.1, 6.4, 6.8, 6.2, and 6.6 respectively for the bentonite, Ben@FeNPs, Ben@(FeNPs+AgNPs), Ben@CuNPs, and Ben@(CuNPs+AgNPs) solids.

The band-gap (E_g) energy of the solids *viz.*, bentonite, Ben@FeNPs, Ben@(FeNPs+AgNPs), Ben@CuNPs, Ben@(CuNPs+AgNPs) nanocomposites were obtained using the Tauc plots generated from DRS data obtained by the UV-Visible spectrophotometer (Barron & Torrent, 1986; Lalliansanga et al., 2020). Further, using *Tauc's* relation, plots were drawn between the $h\nu$ vs. $(F(R) \times h\nu)^2$ as depicted in figure 3.2(a&b)). The band-gap energy of the bentonite, Ben@FeNPs, and Ben@(FeNPs+AgNPs) nanocomposites were found to be 3.25, 2.25, and 2.17, respectively, whereas, for Ben@CuNPs, Ben@(CuNPs+AgNPs) the values were 2.58 and 2.32. The band-gap energy of solids Ben@FeNPs, Ben@(FeNPs+AgNPs), Ben@CuNPs, and Ben@(CuNPs+AgNPs) was significantly decreased compared to the pristine bentonite. The changes in the electrical configuration of various metals have a major impact on the band gap energy of composite materials. The lowering of the band gap energy is due to the presence of zero-valent metal nanoparticles (Chitra et al., 2020). Further, the low band-gap energy of nanocomposite is favorable in visible-light-induced photo-Fenton-like operations utilizing visible or solar light sources (Chatterjee & Dasgupta, 2005; Lalliansanga et al., 2020c). A similar lowering of the band gap energy in the “bentonite modified with Nb₂O₅” photocatalyst was obtained (Hass Caetano Lacerda et al., 2020). The substrate present in the ZnO/bentonite composite caused a decrease in the band gap energy of the composite material (Hakimi et al., 2018).



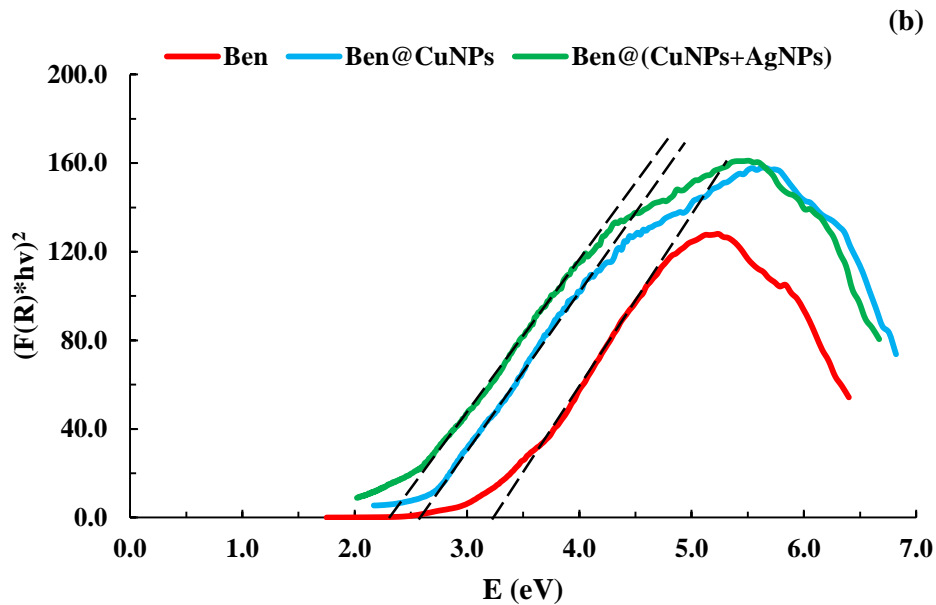


Figure 3.2: (a) The Tauc plots for determination of intermediate band-gap energy (E_g) of pristine bentonite, Ben@FeNPs, and Ben@(FeNPs+AgNPs) solids; (b) The Tauc plots for determination of intermediate band-gap energy (E_g) of pristine bentonite, Ben@CuNPs, and Ben@(CuNPs+AgNPs) solids.

The estimation of pore volume, pore size, and specific surface area is done using the N_2 adsorption/desorption data to illustrate the physical properties of pristine and modified materials. The N_2 adsorption/desorption isotherms as well as the pore size distribution curve of pristine bentonite, Ben@FeNPs, and Ben@(FeNPs+AgNPs) are shown in Figure 3.3 (a & b). It is evident from the figure that all these solids possessed Type IV type isotherms that have H3 type hysteresis loop. Further, Table 3.1 included the specific surface area, pore volume, and pore size of the pristine bentonite Ben@FeNPs, and Ben@(FeNPs+AgNPs) nanocomposites. These results revealed that the materials contained a mesoporous structure with a chaotic pore-size pattern (Bounab et al., 2017; Paul et al., 2011). Immobilization of Fe(NPs) and Ag(NPs) on the bentonite surface led to a considerable decrease in the specific surface area of solids because of the preferential distribution of nanoparticles on the bentonite surface and pores. It is evident from the pore size distribution plot that all these solids showed a desorption peak around the pore width of around 40 Å. Moreover, the

adsorption pore distribution results showed magnificent peaks had occurred around 15 Å of the solids Ben@FeNPs, and Ben@(FeNPs+AgNPs).

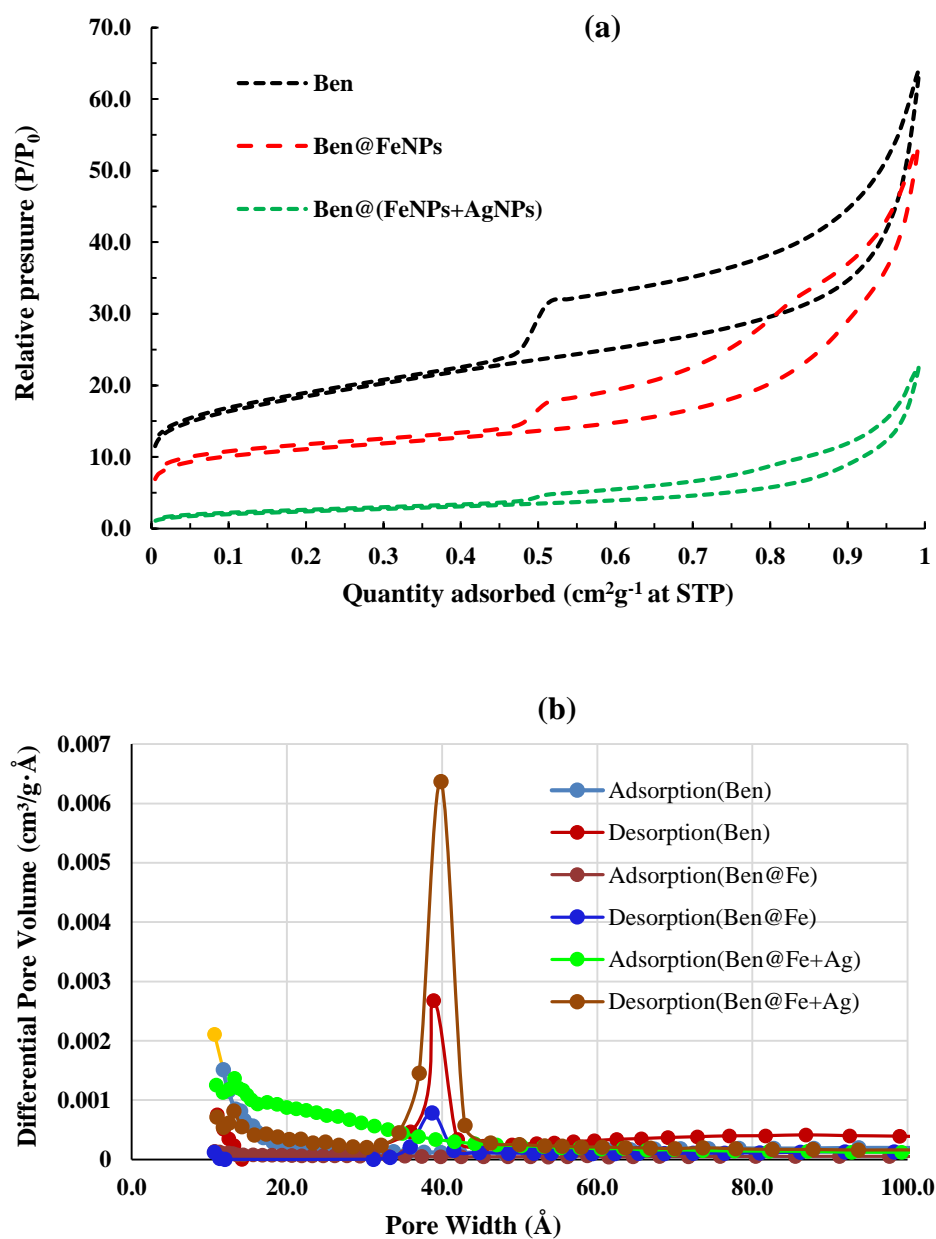


Figure 3.3: (a) N₂ adsorption/desorption isotherms obtained for pristine bentonite (Ben), Ben@FeNPs, and Ben@(FeNPs+AgNPs) nanocomposites; (b) the pore size distribution graph for pure bentonite (Ben), Ben@FeNPs, and Ben@(FeNPs+AgNPs) nanocomposites.

Table 3.2: BET-specific surface area, pore size, and pore volume of pristine bentonite (Ben), Ben@FeNPs, and Ben@(FeNPs+AgNPs) nanocomposite materials.

Parameters	Catalyst samples		
	Ben	Ben@FeNPs	Ben@(FeNPs+AgNPs)
BET Surface Area (m²/g)	62.67	36.50	8.61
Pore volume BJH method (cm³/g)	0.0929	0.0824	0.0344
Average pore volume (cm³/g)	0.0993	0.0831	0.0351
Average pore diameter (Å)	63.38	91.09	163.01
Average pore width BJH method (Å)	62.37	89.13	124.43

Similarly, Figure 3.4 (a&b) depicts the N₂ adsorption/desorption as well as the pore size distribution graph for Ben@CuNPs, and Ben@(CuNPs+AgNPs) nanocomposite material, respectively. Using BET analysis data, the pore size, pore volume, and specific surface area of the nanocomposite materials were calculated. The results are displayed in table 3.3. The figure shows that all these solids had Type IV type isotherms with H3 hysteresis loops. These findings demonstrated that the materials have a mesoporous structure with a random pattern of pore size (Lalchhingpuii et al., 2017). Since nanoparticles were preferentially distributed and immobilized within the pores and surfaces of the bentonite, this caused a significant decrease in the specific surface area of nanocomposite solids *viz.*, Ben@CuNPs, and Ben@(CuNPs+AgNPs). The pore size distribution graph shows that these solids displayed a desorption peak around the pore width of 3.8 nm. The solids Ben@CuNPs, and Ben@(CuNPs+AgNPs) displayed small peaks of *Ca* 5.0 nm in the adsorption pore distribution data.

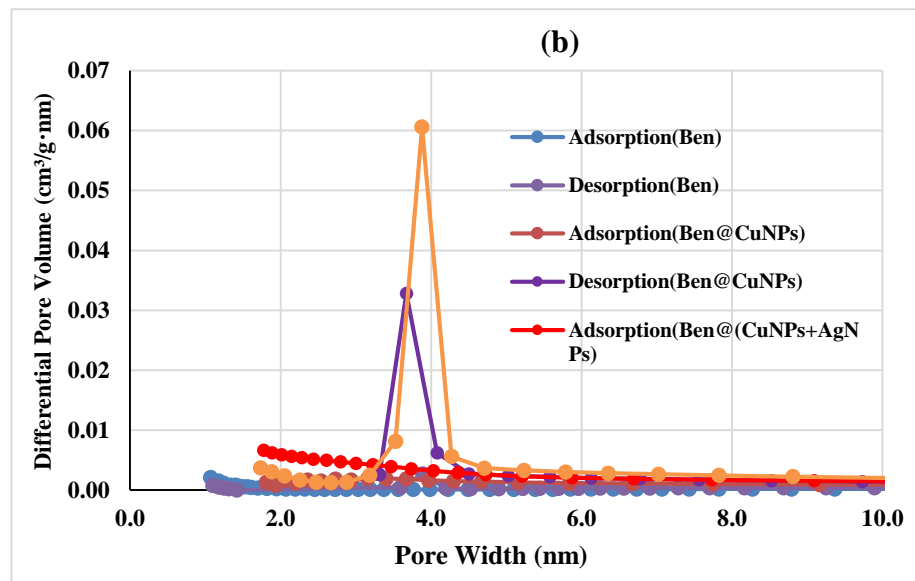
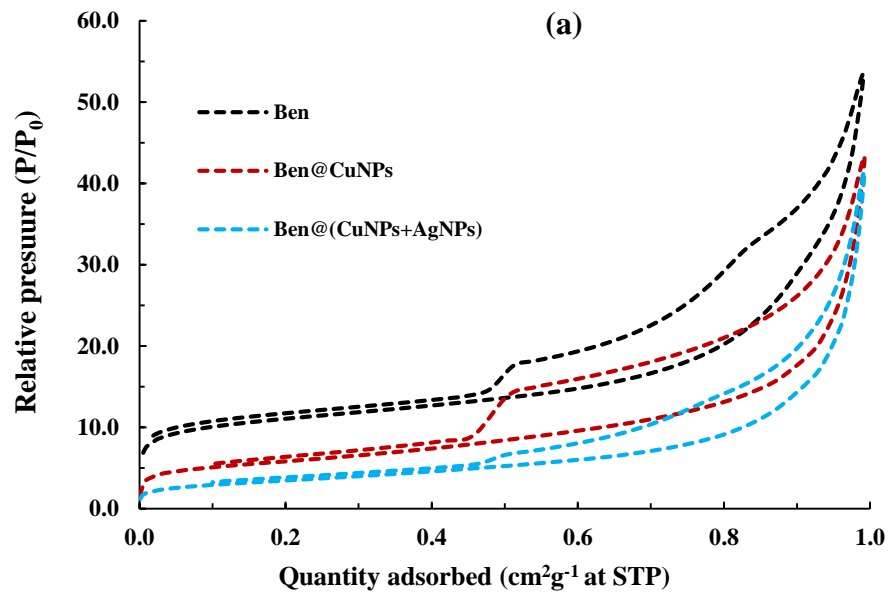


Figure 3.4: (a) N_2 adsorption/desorption isotherms obtained for pristine bentonite (Ben), Ben@CuNPs, and Ben@(CuNPs+AgNPs) nanocomposites; (b) the pore size distribution graph for pure bentonite (Ben), Ben@CuNPs, and Ben@(CuNPs+AgNPs) nanocomposites.

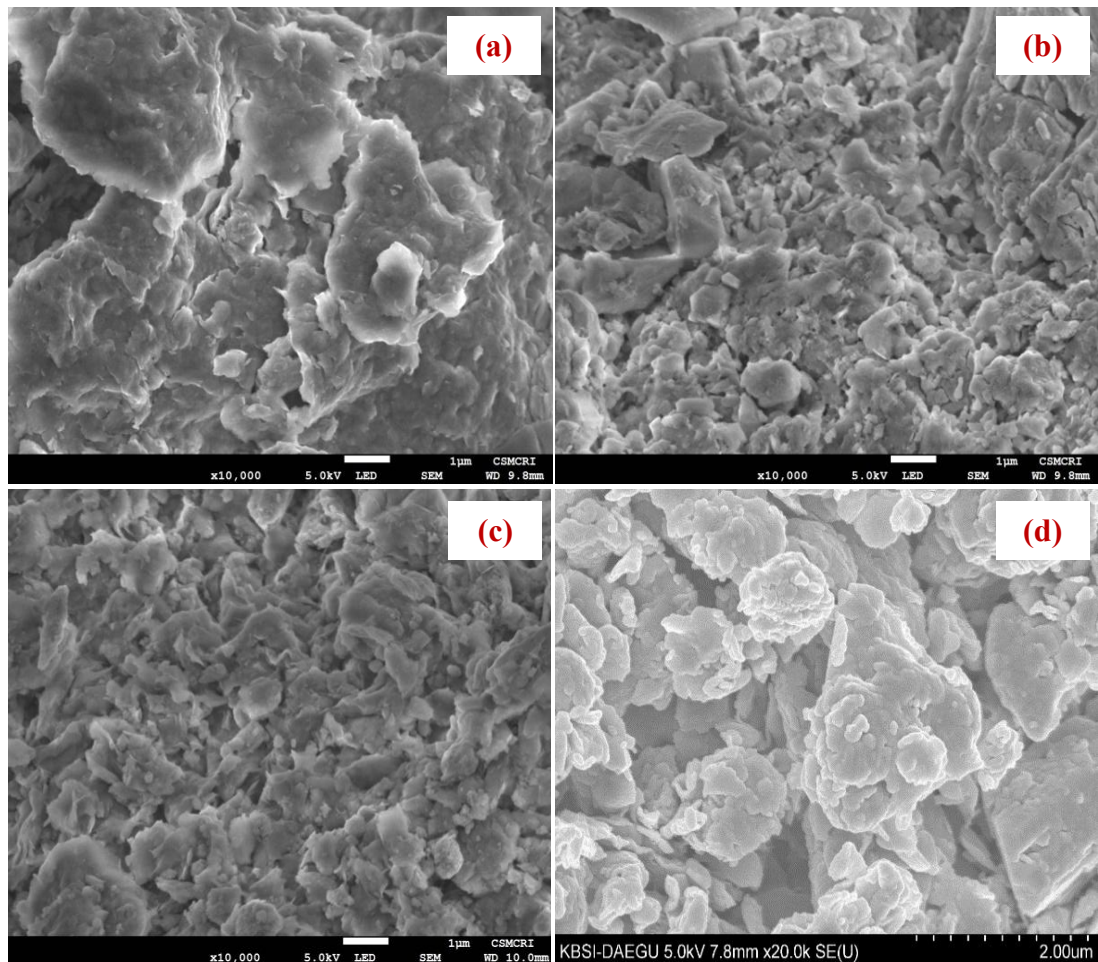
Table 3.3: BET-specific surface area, pore size, and pore volume of pristine bentonite (Ben), Ben@CuNPs, and Ben@(CuNPs+AgNPs) nanocomposite materials

Parameters	Catalyst samples		
	Ben	Ben@CuNPs	Ben@(CuNPs+AgNPs)
BET Surface Area (m²/g)	62.67	36.40	20.55
Pore volume BJH method (cm³/g)	0.0929	0.061980	0.07860
Average pore volume (cm³/g)	0.0993	0.066899	0.099504
Average pore diameter (Å)	63.38	1.302177	0.586478
Average pore width BJH method (Å)	62.37	1.63128	0.98383

3.1.3 Surface morphology of nanocomposites

The SEM images of bentonite, Ben@FeNPs, and Ben@(FeNPs+AgNPs) nanocomposites were shown in figure 3.5. The SEM image of bentonite revealed a heterogeneous and layered structure. The surface has voids and uniform pores widely distributed on the surface of solids (*Cf* Figure 3.5(a)). Furthermore, the nanocomposite solids Ben@FeNPs and Ben@(FeNPs+AgNPs) showed a more dense structure, with the Fe or Ag nanoparticles completely covering the surface (*Cf* Figure 3.5(b&c)). The spaces are occupied with small-sized Fe or Ag nanoparticles, resulting in a compact surface structure. Hence, the surface of nanocomposites becomes very heterogeneous and disordered. Similarly, The SEM images of Ben@CuNPs and Ben@(CuNPs+AgNPs) nanocomposites were shown in figure 3.5(d&e). The surface morphology of the Ben@CuNPs and Ben@(CuNPs+AgNPs) nanocomposites is significantly changed. The pores are occupied by the Cu or Ag nanoparticles; hence, exhibiting a denser surface structure. Liu et al. (2018) described the appearance of small spherical particles in the bentonite-supported nZVI material compared to the smooth and porous surface of pristine bentonite. Similarly, the SEM images of bentonite modified with Nb₂O₅ showed that the aggregation of Nb₂O₅ particles on the

surface of the pristine bentonite caused a raw disordered surface morphology of the solid (Hass Caetano Lacerda et al., 2020). In addition, figure 3.5 (f, g & h) showed the EDX spectra of Ben@FeNPs and Ben@(FeNPs+AgNPs) solids. The EDX results revealed that these solids are contained the common elements of Si, Fe, Al, C, O, Na, K, Ti, etc. However, an additional peak of the Ag is obtained in the EDX spectrum of Ben@(FeNPs+AgNPs), confirming the existence of Ag in the nanocomposite solid (Cf Figure 3.5(h)). Since bentonite contains Fe, it is indiscriminate to distinguish the iron in the Ben@FeNPs and Ben@(FeNPs+AgNPs) solids.



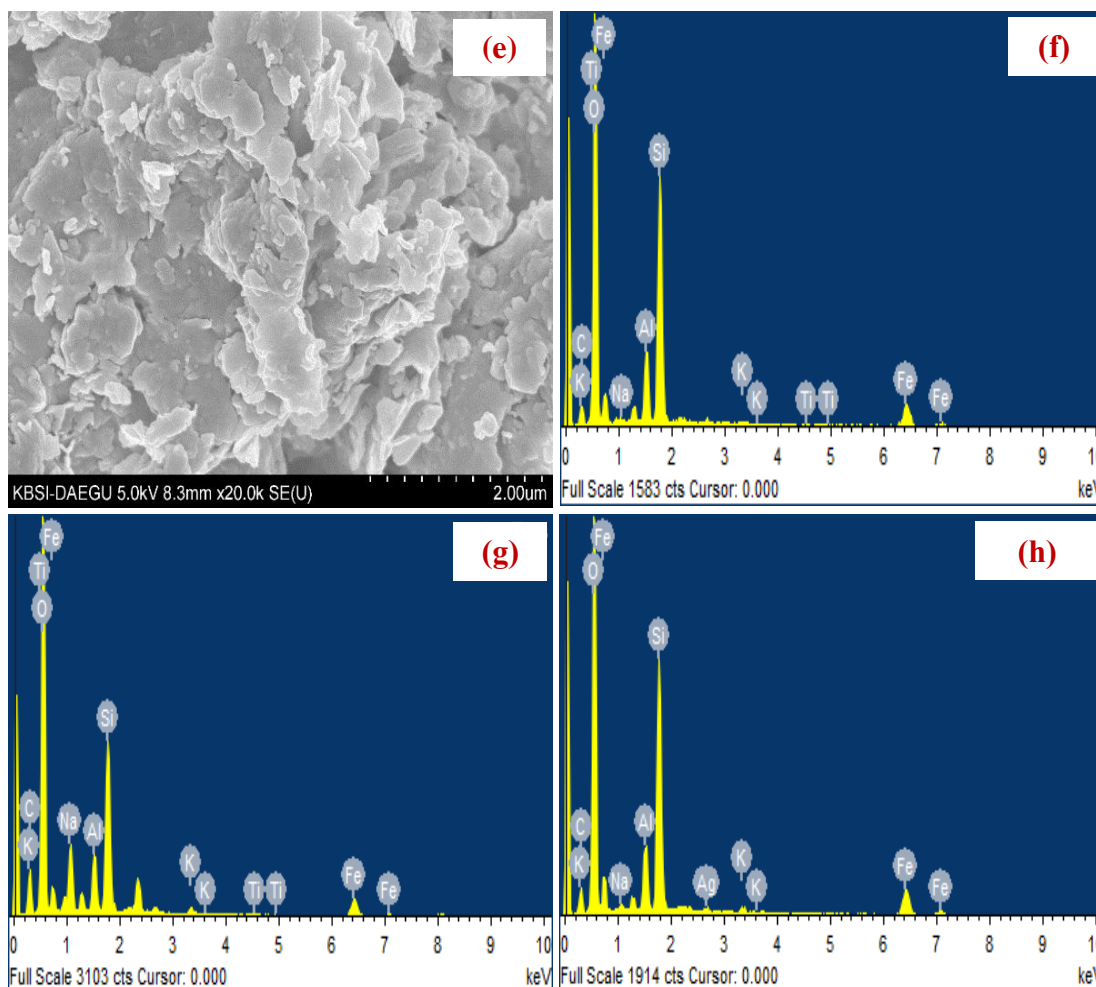
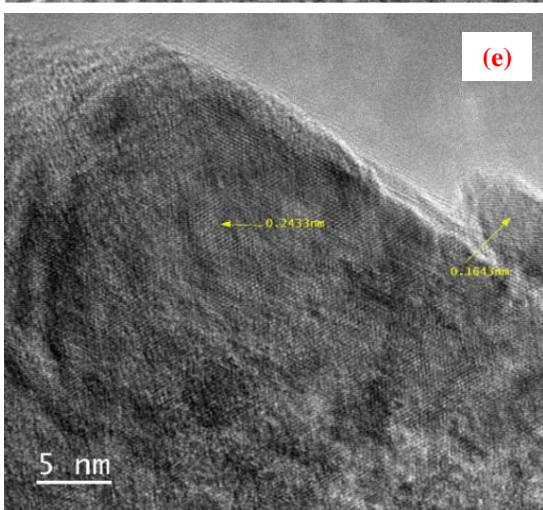
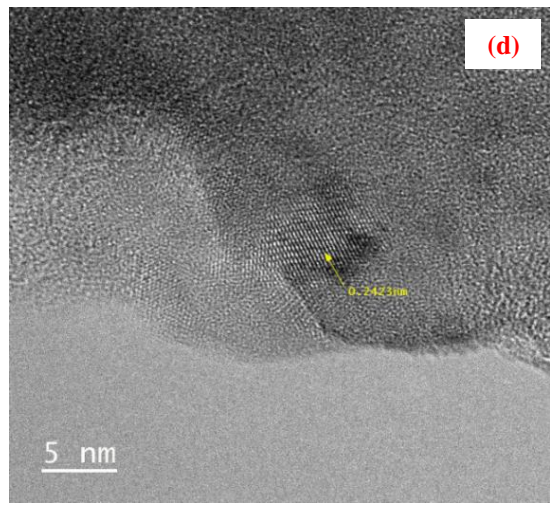
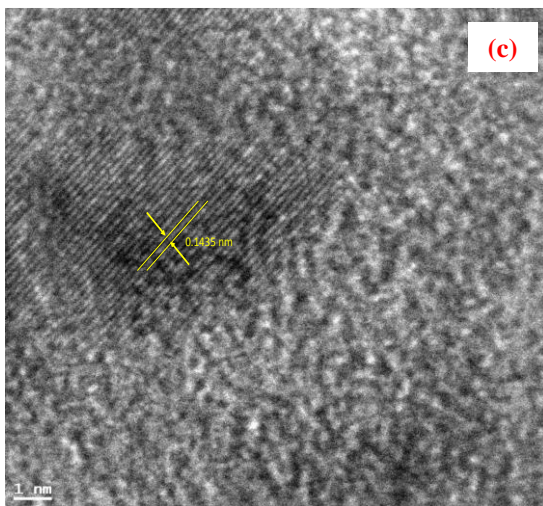
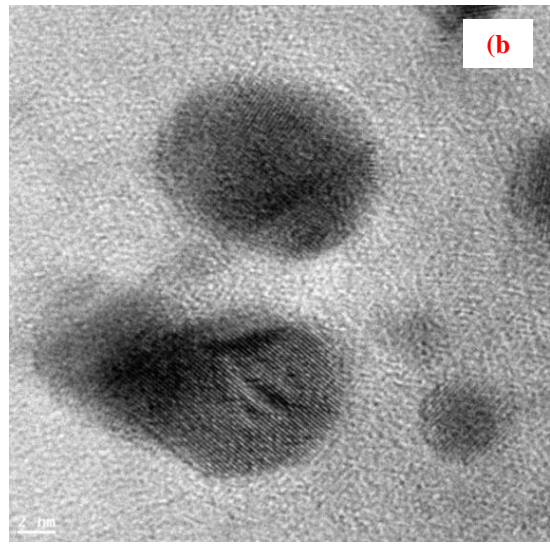
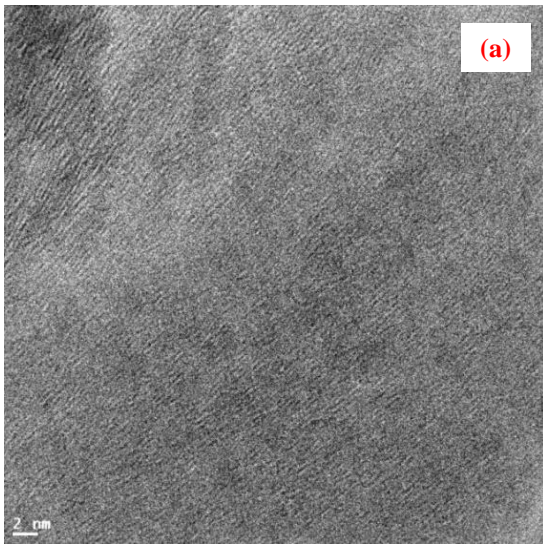


Figure 3.5: SEM pictures of (a) pristine Bentonite (b) Ben@FeNPs (c) Ben@(FeNPs+AgNPs) (d) Ben@CuNPs and (e) Ben@(CuNPs+AgNPs) nanocomposite solids. EDX elemental spectra of (f) Pristine bentonite (g) Ben@FeNPs; and (h) Ben@(FeNPs+AgNPs) nanocomposite solids.

The TEM images of bentonite, Ben@FeNPs, and Ben@(FeNPs+AgNPs) solids were shown in Figure 3.6. Figure (3.6(a)) shows that bentonite is a compact, layered, and heterogeneous structure. The Ben@FeNPs solid, on the other hand, clearly demonstrated a distinct distribution of Fe(NPs) onto the surface of bentonite, with an average particle size of *ca.* 16 nm. The iron nanoparticles are equally dispersed and do not agglomerate on the substrate surface. Similarly, the Ag nanoparticles in the nanocomposite Ben@(FeNPs+AgNPs) solid (*Cf* figure 3.6(c)) are evenly dispersed over the bentonite surface. The particle's average size is calculated to be *Ca* 10 nm. At

the surface of bentonite, the particles are spherical and not aggregated or clustered on the surface. Ag(NPs) were determined to have a d-spacing of 0.1435 (Cf Fig. 3.6(c)), which results from diffraction from the (220) plane of Ag (NPs). The *in situ* generations of iron or silver nanoparticles on the bentonite support media; enabled fair distribution of nanoparticles that are not agglomerated on the surface. Likewise, Figure 3.6 (d & e) displays the TEM images of Ben@CuNPs and Ben@(CuNPs+AgNPs) solids. The TEM image showed Cu(NPs) fine particles are spatially distributed on the bentonite's surface. Moreover, Cu(NPs) showed fringes with d spacings of 0.242 nm (Cf 3.6(d)). On the other hand, the TEM image of Ben@(CuNPs+AgNPs) solid showed the heterogenous surface structure, and the fringes indicated the d-values of 0.243 and 0.164 nm, respectively, for the Cu(NPs) and Ag(NPs) (Cf figure 3.6(e)). Further, the computed average particle size for the Ben@CuNPs and Ben@(CuNPs+AgNPs) solids is 4.207 and 2.518 nm, respective for the Ben@CuNPs and Ben@(CuNPs+AgNPs) solids. It is worth to be noted that the *in situ* impregnation of Cu and Ag nanoparticles with the support medium enabled a fair distribution of nanoparticles on the surface of bentonite. Previously, Shahwan et al., 2010 presented the TEM images of Bentonite-supported iron nanoparticles and explained as the iron nanoparticles were uniformly distributed on the bentonite surface. The modified bentonite-supported MnFe_2O_4 nanocomposite showed that the MnFe_2O_4 nanoparticles were distributed throughout the bentonite clay and were well dispersed. Further, the material's electrical conductivity allows an electron to move from the conduction band (C.B.) of MnFe_2O_4 nanoparticles to the bentonite clay if the two components come into close contact with each other (Almahri, 2022).



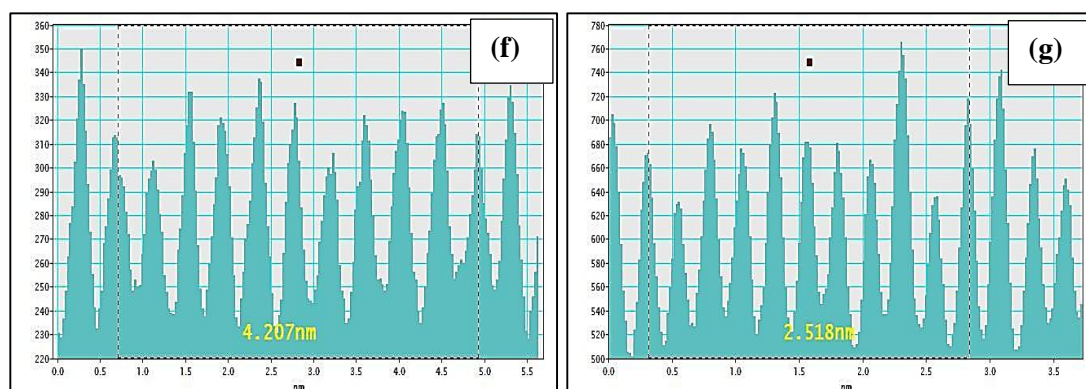
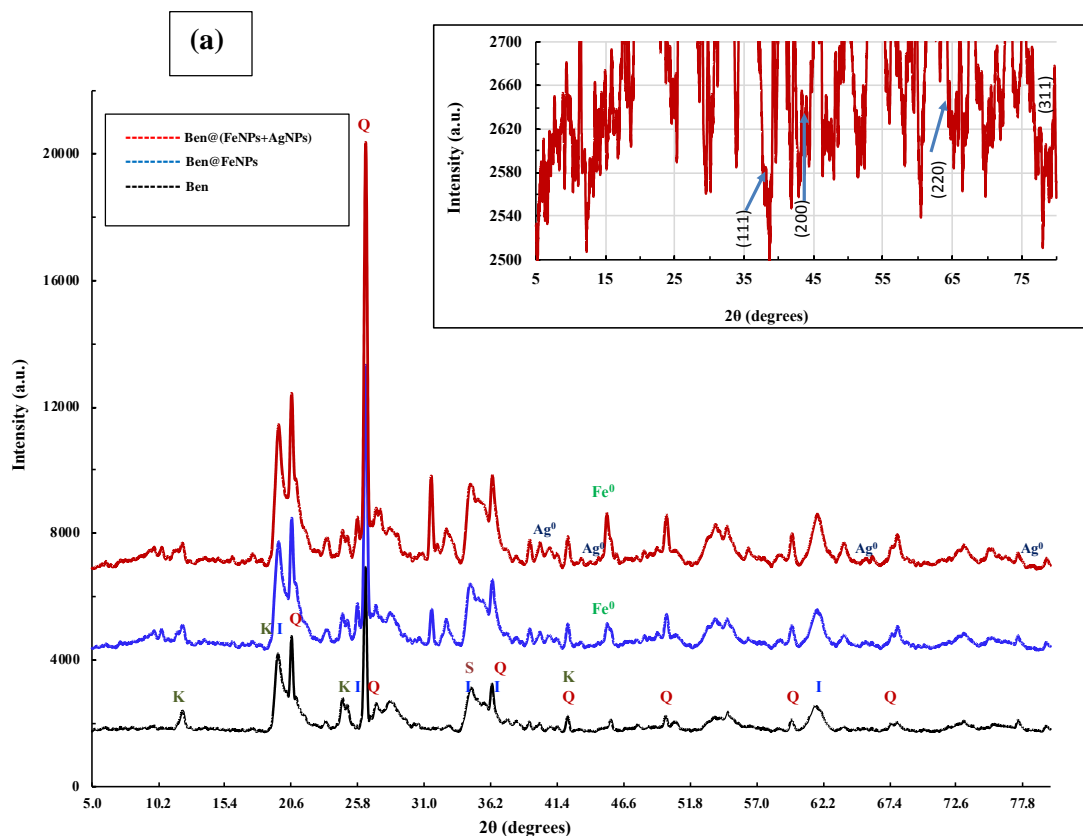


Figure 3.6: Transmission electron microscopy (TEM) pictures of (a) pristine bentonite; (b) Ben@FeNPs; (c) Ben@(FeNPs+AgNPs); (d) Ben@CuNPs; and (e) Ben@(CuNPs+AgNPs) nanocomposite solids; Particle size distribution of (f) Ben@CuNPs; and (g) Ben@(CuNPs+AgNPs) nanocomposite solids

3.1.4 XRD and XPS analysis

The X-ray diffraction data of the raw bentonite and the bentonite-supported Fe and Ag nanoparticles are shown in Figure 3.7(a). The bentonite shows characteristic diffraction peaks of kaolinite, illite, quartz, and smectite. The diffraction peaks observed at the 2θ values of 20.95, 26.78, 36.68, 50.26, and 68.36, suggesting the presence of quartz. Similarly, the illite diffraction peaks are observed at the 2θ values of 19.85, 36.62, and 50.0 (Malsawmdawngzela and Tiwari, 2021). The kaolinite peaks are observed at the 2θ value of 12.44° (Sdiri et al., 2016). Figure 3.7(a) further shows a prominent diffraction peak at around 2θ value of 45° for the solids Ben@FeNPs and Ben@(FeNPs+AgNPs), which confirms the presence of iron nanoparticles $\text{Fe}^0(\text{NPs})$ in these nanocomposite materials (Sulaiman and Al-Jabari, 2021). Further, the solid Ben@(FeNPs+AgNPs) showed additional diffraction peaks at the 2θ values of 38.89, 44.53, 64.34, and 77.71, which are attributed to the (111), (200), (220), and (311) planes of Ag(NPs) in the solid, respectively (JCPDS file No. 01-087-0719) (Cf Figure 3.1(a) Inset). The presence of bio-organic phases due to the use of guava leaf extract, possibly, shows additional peaks occurred at 2θ values of 27.55° , 32.03° , and 46.07° (Kumar et al., 2017). Further, for the Ben@CuNPs, and Ben@(CuNPs+AgNPs) nanocomposite solids (Cf figure 3.7(b)), the distinct peaks at 2θ values of 43.25, 50.39, and 74.23° referred to the (111), (200), and (220) planes of $\text{Cu}^0(\text{NPs})$ (JCPDS file No.

04-0836). This demonstrated that the Cu⁰(NPs) are *in situ* impregnated with the bentonite support medium using the phytochemicals. Similarly, the Ben@(CuNPs+AgNPs) nanocomposite also showed additional diffraction peaks at the 2θ values of 38.55, 44.91, 64.55, and 77.59, which are due to the (111), (200), (220), and (311) planes, respectively of Ag(NPs) in the solid (JCPDS file No. 01-087-0719). Palygorskite-supported bimetallic Fe/Ni nanocomposite presented the XRD pattern and confirmed the presence of iron nanoparticles and quartz impurities from the characteristic peaks occurred at 2θ value of around 45° and 36.6° (Ezzatahmadi et al., 2019). Rostami-Vartooni et al. (2015) revealed that the montmorillonite (M) and quartz (Q), whose characteristic diffraction peaks were obtained at 2θ = 19.84, 34.80, and 61.84° were indexed to (020), (130), and (060) planes of montmorillonite and 2θ = 26.81, 36.25, and 48.84° were indexed to (101), (110), and (201) planes of quartz, respectively, are the two main components of the natural clay. They also pointed out that the missing of predicted peaks for nanoparticles is due to a low concentration or high level of dispersion of nanoparticles in the bentonite matrix.



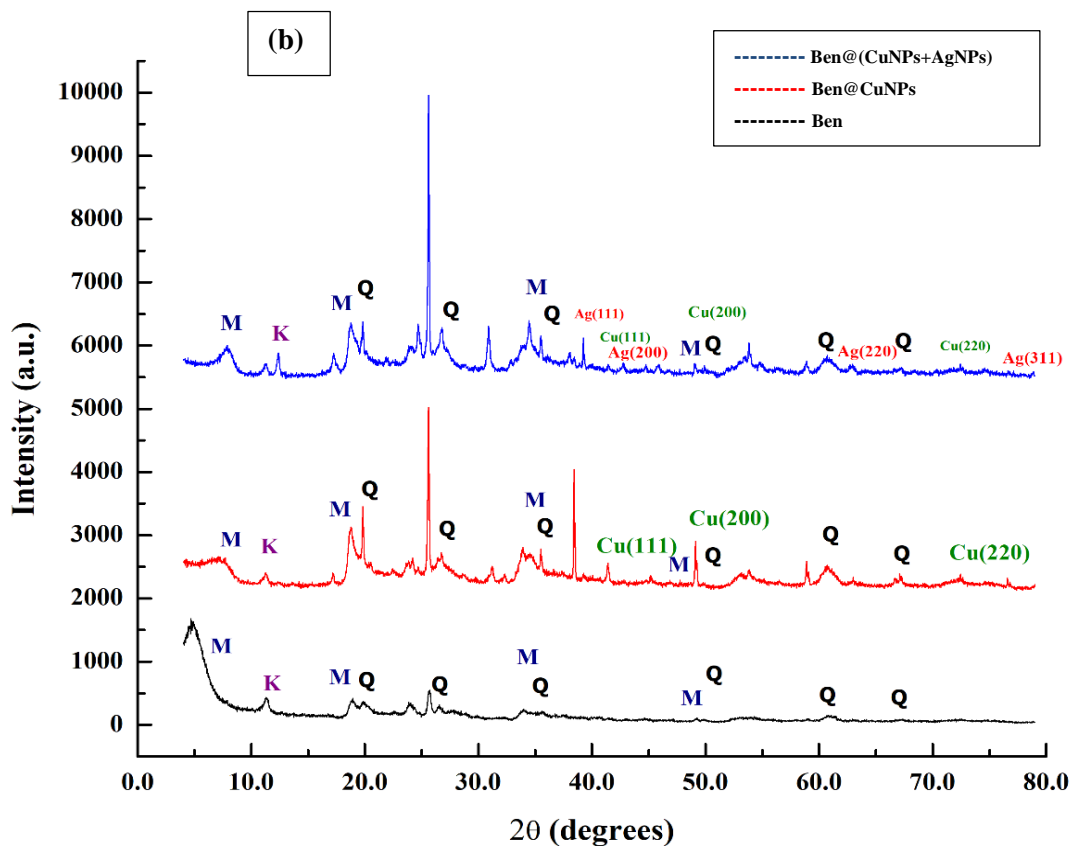
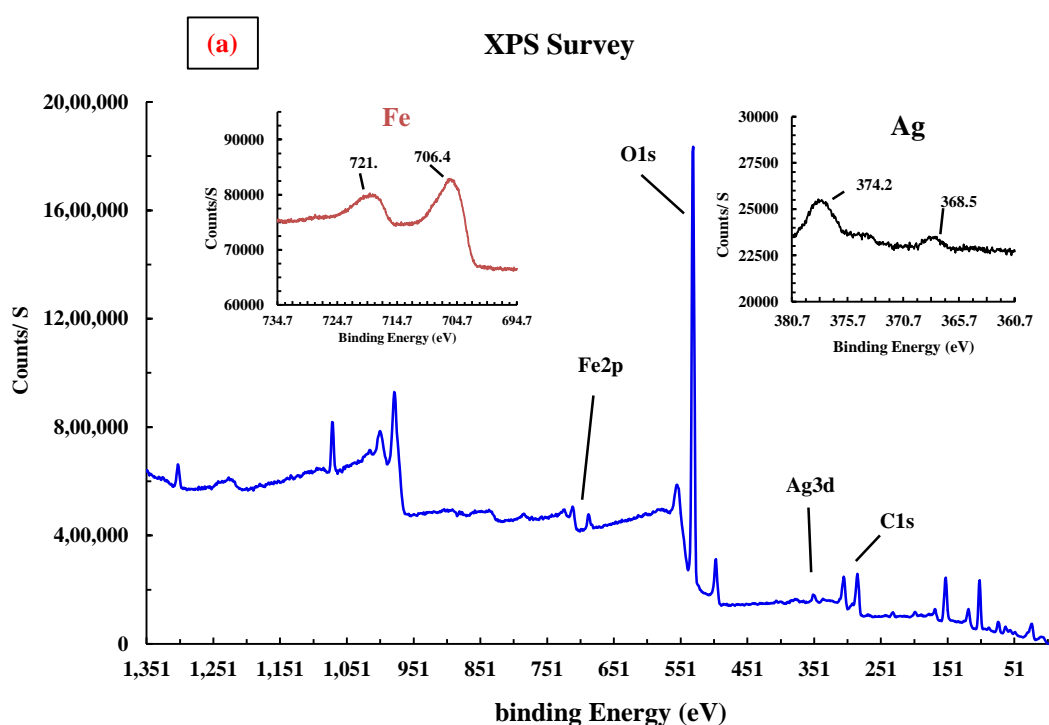


Figure 3.7: (a) XRD spectra of pristine bentonite, Ben@FeNPs, and Ben@(FeNPs+AgNPs) nanocomposite solids [Inset: The XRD pattern of Ben@(FeNPs+AgNPs) nanocomposite material]; (b) X-ray diffraction pattern of the pristine bentonite; synthesized Ben@CuNPs and Ben@(CuNPs+AgNPs) nanocomposite solids.

The presence of Fe(NPs) and Ag(NPs) with their oxidation states was obtained using the X-ray photoelectron (XPS) spectrum of the Ben@(FeNPs+AgNPs) nanocomposite. Figure 3.8(a) shows the results of the XPS scan. The XPS survey spectrum showed clearly the presence of Fe (2p), Ag (3d), and O (1s) peaks in the nanocomposite solid. Further, the photopeaks of Fe(2p) and Ag(3d) peaks were resolved and shown in Figures 3.8(a) (inset). The binding energy of a chemical species is associated with its chemical state. The photoelectron peak at 706.4 eV was shown in the spectra, indicating the presence of Fe(0) in the nanocomposite material (Ye et al., 2021). Similarly, the peaks of 3d electrons of Ag in the nanocomposite are clearly seen in the spectra. At the binding energies of 368.5 eV and 374.2 eV, respectively, a doublet of 3d peaks appeared, corresponding to the $3d_{5/2}$ and $3d_{3/2}$ energy levels of

elemental silver (Prieto et al., 2012). Therefore, silver and iron are present in their reduced state in the nanocomposite solid Ben@(FeNPs+AgNPs). Similarly, X-ray photoelectron (XPS) spectra of the Ben@(CuNPs+AgNPs) nanocomposite revealed the impregnation of Cu(NPs) and Ag(NPs) along with their oxidation states. Figure 3.8(b) provides the survey spectrum and individual spectra for both copper (Cu) and silver (Ag). The XPS peaks for Cu2p, Fe2p, Ag3d, O1s, and C1s are clearly identified in the nanocomposite's XPS survey spectra. The chemical species' binding energy is linked to its chemical states. The photoelectron peaks at 932.7 eV (Cu2p_{3/2}) and 952.5 eV (Cu2p_{1/2}) were evident (Cf figure 3.8(b) (Inset)), indicating the presence of Cu(0) in the nanocomposite material (Shah et al., 2020). Similarly, a pair of 3d peaks corresponding to the 3d_{5/2} and 3d_{3/2} energy levels of elemental silver appeared at the binding energies of 368.5 eV and 374.2 eV, respectively (Prieto et al., 2012). Thus, these XPS data revealed that Cu and Ag are in their reduced states in the nanocomposite material. Thus, the XPS spectra reaffirmed the existence of Cu(NPs) and Ag(NPs) in their zero-valent oxidation states in the nanocomposite solid.



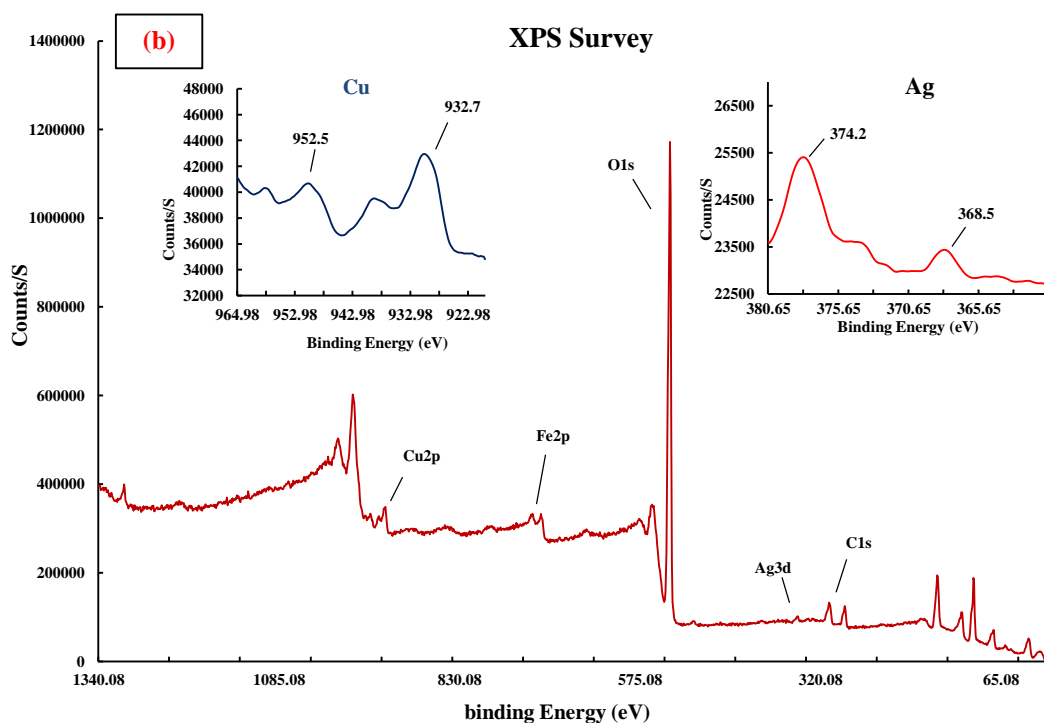


Figure 3.8: (a) XPS survey for the Ben@(FeNPs+AgNPs) nanocomposite material [Inset: The XPS spectrum of iron (Fe) and silver (Ag) nanoparticles in the nanocomposite material]; (b) XPS survey for the Ben@(CuNPs+AgNPs) nanocomposite material [Inset: The XPS spectrum of copper (Cu) and silver (Ag) nanoparticles in the nanocomposite material].

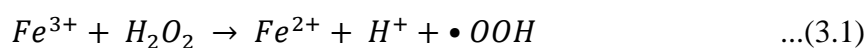
3.2 Photo-Fenton-like degradation of diclofenac sodium (DCF), phenol, and n-(n-propyl) thiourea from aqueous solution

3.2.1 Effect of initial pH

The impact of the solution pH is a controlling factor in deducing the mechanism of pollutant degradation in aqueous media since the formation of $\bullet\text{OH}$ radicals, surface properties of the catalyst, and speciation of pollutant species is primarily regulated by the pH of the solution. Therefore, the solution pH significantly impacts the degradation efficiency of organic contaminants in Fenton or Fenton-like reactions (Song et al., 2017). The pH-dependent experiments are carried out to assess the influence of pH on the removal of diclofenac, phenol, and N-(n propyl) thiourea (NNPT) using Ben@(FeNPs+AgNPs) nanocatalyst. A series of experiments were

carried out, varying pH from 2.0 to 7.0 at a constant pollutant concentration (2.0 mg/L) using a fixed dosage of nanocatalyst (200.0 mg/L) and H₂O₂ (0.2 mL/L). The percentage degradation of all the pollutants under a dark environment is illustrated in figure 3.9. It is evident from figure 3.9 that the acidic pH region favored the degradation efficiency (between pH 2.0-4.0) of these pollutants. Without using any external light source, i.e., under dark conditions, the DCF (2.0 mg/L) degraded *Ca.* 56%. In contrast, with an increase in pH from pH 3.0 to 7.0 the percentage removal of DCF decreased from 56% to 10%, respectively. A similar trend was obtained for the phenol and NNPT also. The percentage removal of phenol (2.0 mg/L) was found *Ca.* 44% of degradation within 2 hours of reaction time at pH 3.0. On the other hand, the NNPT degraded *Ca.* 73% in the dark condition. It is evident from the results that from pH 5.0 to 7.0, the degradation of these pollutants was inhibited significantly. The formation of buffer-iron (II) complexes and the precipitation of ferric oxyhydroxides possibly, inhibited the formation of hydroxyl radicals at pH >4.0, which caused suppression in degradation efficiency (Madani et al., 2015). The corrosion of nZVI producing •OH radicals favors the acidic pH region, and hence the results indicated that acidic conditions (pH=3.0) were more favorable for the degradation of both pollutants. Therefore, pH=3.0 was chosen for further studies in photo-Fenton-like reactions.

The potential decrease in the nanocatalyst's degrading efficiency at alkaline pH is owing to a blockage in Fe(II) discharge to the bulk of the solution, which inhibits the generation of •OH radicals (Guo et al., 2019) as shown in Eq. (3.1). In alkaline solutions, the oxidation potential of •OH radicals decreases (Fida et al., 2017).



Previous studies indicated that at pH >3.0, the oxidation efficiency was decreased rapidly due to the instability of H₂O₂ as it decomposes into molecular oxygen with less number of •OH radicals (Hassan & Hameed, 2011). At extremely low pH (~2.0), however, [Fe(H₂O)₆]²⁺ iron complex species formed, which hampered the reaction of Fe(II) with H₂O₂, resulting in a slight drop in the nanocatalyst's degrading efficiency (Fida et al., 2017). Furthermore, with the excess of H⁺ ions at low

pH, the hydroxyl species are quickly reduced, inhibiting the $\bullet\text{OH}$ radical-induced degradation of pollutions (Cf equation (3.2)).

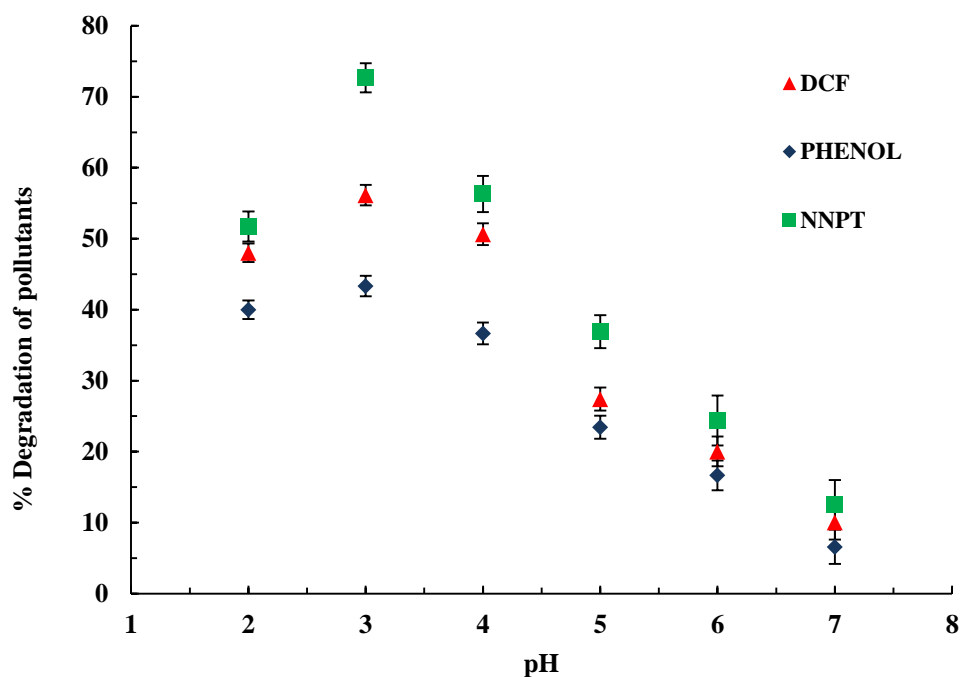
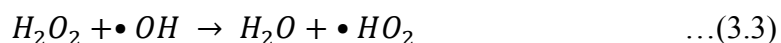


Figure 3.9: Percentage degradation of DCF, phenol, and NNPT at different pH values under a dark environment [Catalyst dose = 200.0 mg/L; H_2O_2 dose (30%) = 0.2 mL/L; [Pollutant] = 2.0 mg/L; Reaction time = 2 hrs].

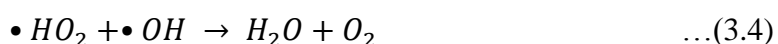
3.2.2 Effect of H_2O_2 dosage and nanocomposite dosage

The optimal dosage of hydrogen peroxide is a critical parameter for optimizing and maximizing degradation efficiency in the Fenton-like process. Therefore, to monitor the effect of H_2O_2 doses, different doses of H_2O_2 (30% v/v) were employed by keeping constant nFLC dose (200.0 mg/L), pollutant concentrations (2.0 mg/L), and pH (pH 3.0). The experiments were performed for each pollutant under dark conditions. Fig. 3.10 (a, c & e) illustrates the influence on the percentage degradation of the targeted pollutants at the different doses of H_2O_2 , and results are shown in figure 3.10 (a). It is evident from Figure 3.10(a) that by increasing the dose of H_2O_2 (30%

v/v) from 0.25 to 0.4 mL/L, the percentage degradation of DCF was increased from 46.15% to 56.14%, respectively. The increase in H₂O₂ favored the generation of •OH radicals, which caused the increase in DCF degradation efficiency. However, a further increase in H₂O₂ dose i.e., from 0.40 to 0.50 mL/L caused to decrease in the percentage degradation of DCF from 56.14 to 50.99% in the Fenton-like removal of DCF (Cf Figure 3.10(a)). Similarly, with an increase in hydrogen peroxide dose from 0.05 mL/L to 0.15 mL/L, the degradation efficiency of phenol was increased from Ca 41.4% to 43.3% at the reaction time of 2 hrs (Cf Figure 3.10 (c)). Further, increase in the peroxide dose >0.15 mL/L had caused a slight decrease in the degradation efficiency of DCF. On the other hand, by increasing the H₂O₂ dose from 0.05 mL/L to 0.1 mL/L, the degradation efficiency of NNPT was improved slightly from 70.54% to 72.68% at 2 hrs of reaction time (Cf Figure 3.10(e)). However, a further increase in H₂O₂ doses >0.1 mL/L led to a decrease in the degradation efficiency of NNPT. These results inferred that an increase in H₂O₂ concentrations significantly favored the formation of hydroxyl free radicals (•OH radicals). However, with much increase in H₂O₂ concentration, the degradation percentage of these pollutants was decreased because hydrogen peroxide reacted with •OH radicals, producing water (H₂O) and hydroperoxyl radical (•HO₂) (Cf Equation (3.3)). As a result, the reactive •OH radicals were readily consumed prior to taking part in the Fenton oxidation reaction (Hassan et al., 2020; Sétifi et al., 2019).



Furthermore, Fida et al. (Fida et al., 2017) mentioned that the •OH radicals are quenched by the •HO₂ radicals (Cf Equation (3.4)).



Therefore, the pollutant molecules were less degraded due to the rapid dissipation of radical species at much-enhanced hydrogen peroxide doses. The results are in line with those reported previously in the Fenton-like degradation of naproxen utilizing a goethite-montmorillonite nanocomposite (Paul et al., 2011).

Similarly, the effect of nanocatalyst dosages was studied in the removal of DCF, phenol, and NNPT under the Fenton-like process. The H₂O₂ amount, pollutant concentrations, and pH values of the solution were kept constant. The degradation efficiency was increased by increasing the nanocatalyst dosages up to the optimal dose (250.0 mg/L for DCF, 100.0 mg/L for phenol, and 125.0 mg/L for NNPT), as shown in Figure 3.10 (b, d & f). The increase of the nanocatalyst amount provides an enhanced available adsorption site, which favored the degradation efficiency of the catalyst. However, it was noted that the percentage degradation of these pollutants was decreased, increasing the dosages of Ben@(FeNPs+AgNPs) nanocatalyst (dose > 250.0 mg/L for DCF, dose >100.0 mg/L for phenol and dose >125.0 mg/L for NNPT). The negative effect on the degradation of these pollutants at higher dosages of nanocatalyst was because of the scavenging effect, in which the generated •OH radicals are consumed by the excess catalyst (*Cf* Equation (3.5))(Hassan & Hameed, 2011).



Similar findings were reported in the Fenton-like degradation of naproxen utilizing montmorillonite clay modified with nanoparticles of iron oxyhydroxides (MGO) (Sétifi et al., 2019). An optimum amount (0.1 g/L) of catalyst is required for fast Fenton-like reactions to occur in the Fenton-like degradation of phenol (Kurian and Sugunan, 2006).

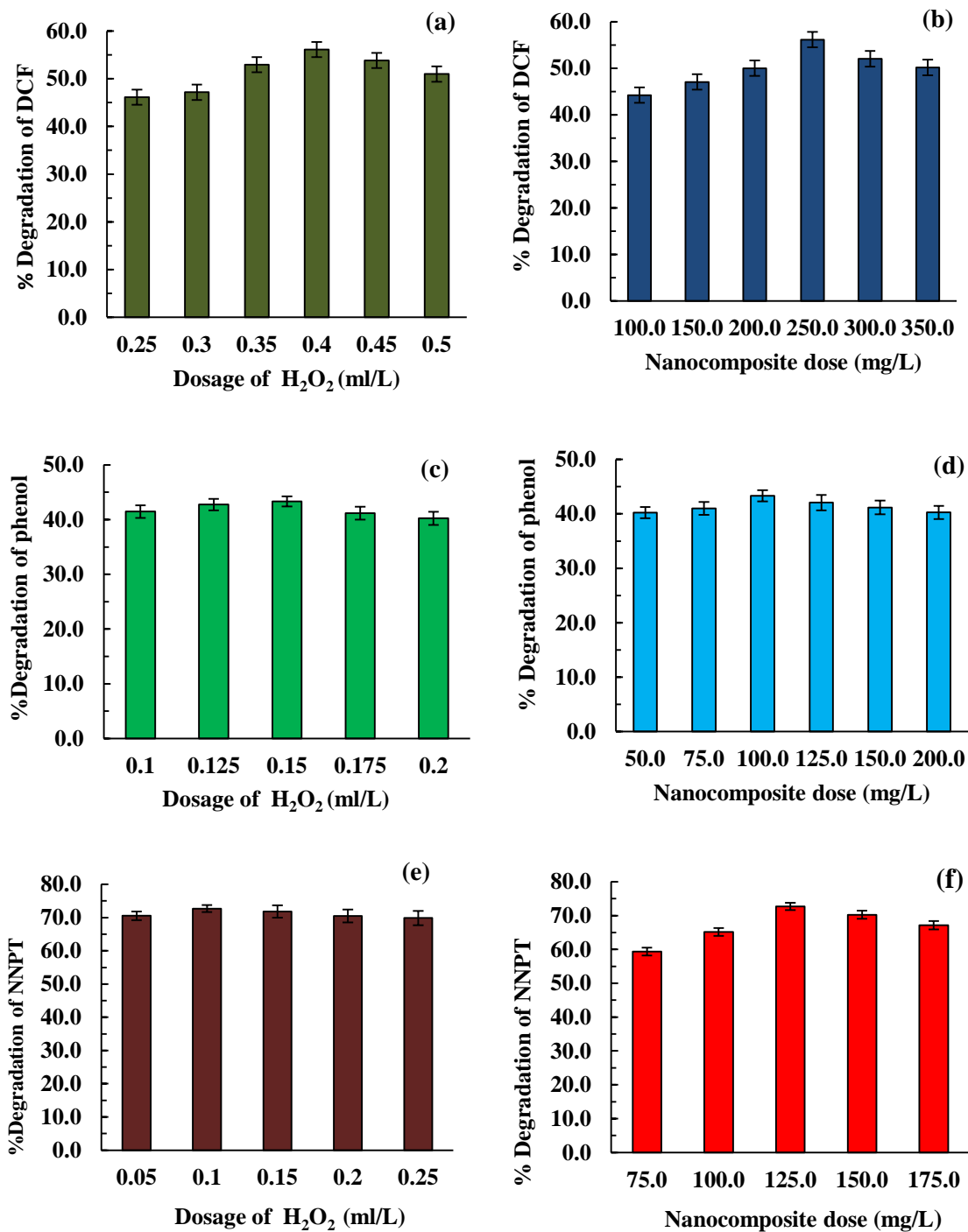


Figure 3.10: Percentage degradation of (a) DCF, (c) phenol & (d) NNPT at different dosages of H₂O₂ in a dark environment under reaction condition as [pH = 3.0; [Pollutant] = 2.0 mg/L; catalyst dose = 200.0 mg/L; reaction time = 2 hrs]; percentage degradation of (b) DCF, (d) phenol & (f) NNPT at different dosages of nanocatalyst

in a dark environment under reaction condition as [pH = 3.0; [Pollutant] = 2.0 mg/L; peroxide dose = 0.2 ml/L; Reaction time = 2 hrs]

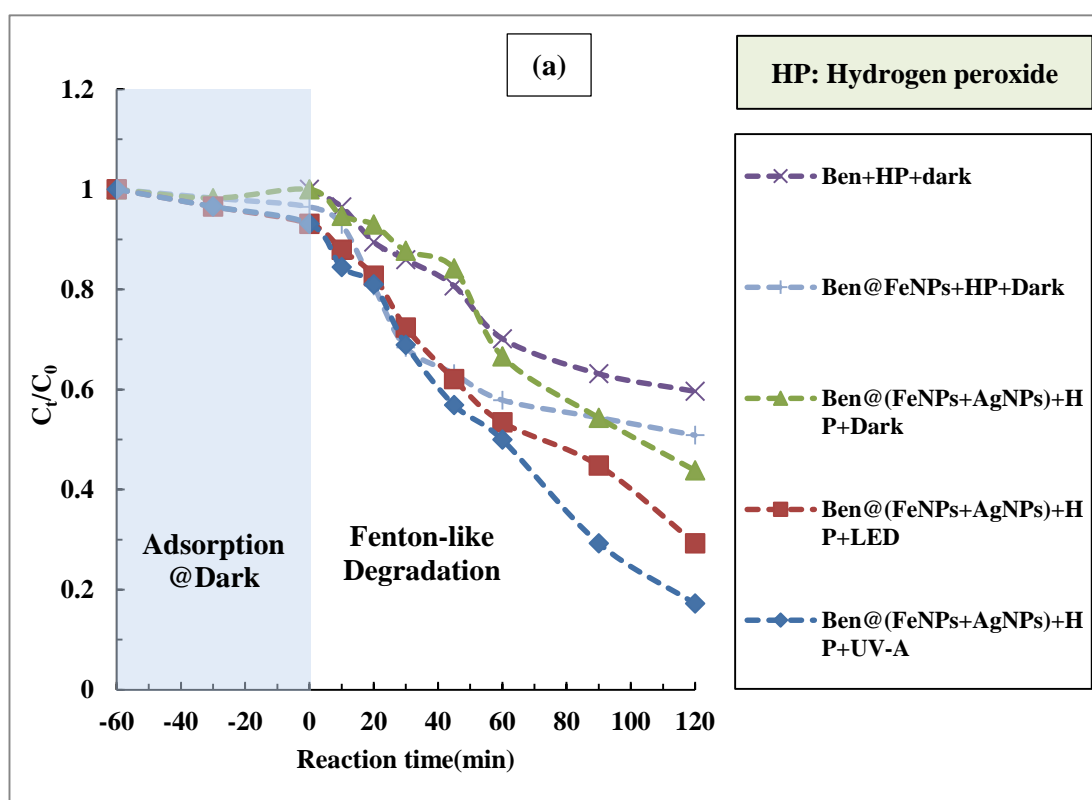
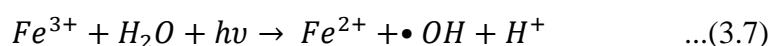
3.2.3 Photo-Fenton-like degradation of DCF, Phenol, and NNPT

Under optimized experimental conditions, a comparative investigation was carried out to investigate the influence of photo illuminations (using LED visible and UV-A light sources) on Fenton-like reactions. It was observed that light irradiation synergized the removal efficiency of these pollutants (*Cf* Figure 3.11). The effect of various light sources was studied, and the degradation efficiency of the targeted pollutants was decreased in the following order: (Fenton-like/ UV-A) > (Fenton-like/ LED) > (Fenton-like/Dark). Figure 3.11 shows a comparative disappearance of DCF, phenol, and NNPT as a function of reaction time under different light environments. Irradiation stimulates the formation of •OH radicals (Sapach and Viraraghavan, 1997) as shown in (Equation 3.6):



It is obvious from figure 3.11(a) that the Fenton-like treatment of DCF utilizing the Ben@[FeNPs+AgNPs] nanocatalyst achieved the removal efficiency of 83% and 70% using UV-A and LED(Visible) light illumination, respectively. However, the dark conditions enabled degradation of only 56% degradation within 2 hrs of reaction time. Similarly, using the Ben@FeNPs nanocatalyst, the degradation efficiency of DCF was achieved *Ca.* 68% and 57% by employing UV-A and LED light illuminations, respectively. Under UV-A and LED (visible) light, the Fenton-like degradation of phenol employing Ben@[FeNPs+AgNPs] nanocatalyst enabled to achieve the removal efficiency of 73.3% and 60.0%, respectively, whereas, in the dark conditions, 43.3% degradation occurred during 120 minutes of reaction time (*Cf* figure 3.11 (b)). Within 120 minutes of reaction time, the Fenton-like degradation of NNPT employing Ben@[FeNPs+AgNPs] nanocatalyst reached *Ca.* 95.1% and 84.9% using UV-A and LED light irradiations, respectively. Whereas, in the absence of light, the degradation of NNPT was only 72.7% (*Cf* figure 3.11 (c)). The light irradiation provides the needed energy (activation energy) which synergizes the degradation

efficiency of these pollutant molecules in the aqueous medium. On the other hand, the dark environment caused only 36.7% and 61.4% degradation of phenol and NNPT, respectively, utilizing the Ben@FeNPs nanocatalyst. Results inferred that the inclusion of Ag(NPs), enabled the degradation efficiency significantly. It was previously reported that an acidic pH favors the formation of •OH radicals (He et al., 2014). Furthermore, photocatalytic reactions on the active sites of the catalyst surface are known to occur in the heterogeneous phase. The formation of complexes between the catalyst's surface and H₂O₂ results in the generation of •OH radicals. The photolysis of H₂O₂ (Equation 3.7) is aided by light energy, which also enhances the catalytic activity of the iron leached from the nanocomposite, as shown below (Equation 38) (Sétifi et al., 2019):



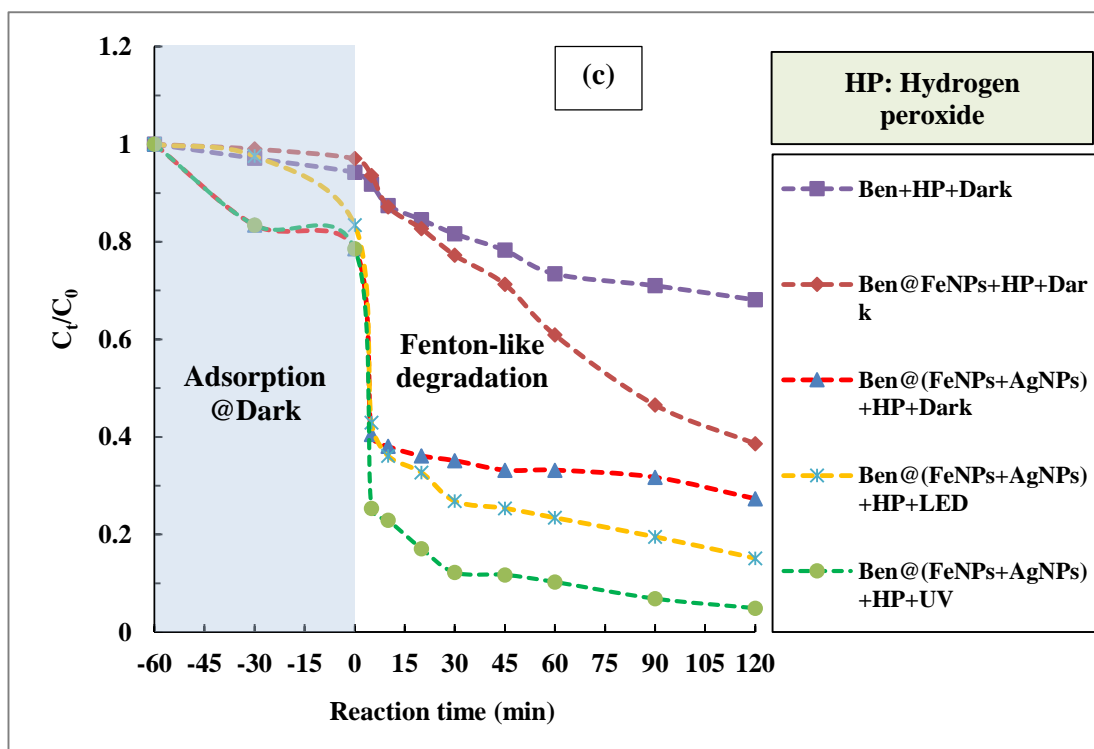
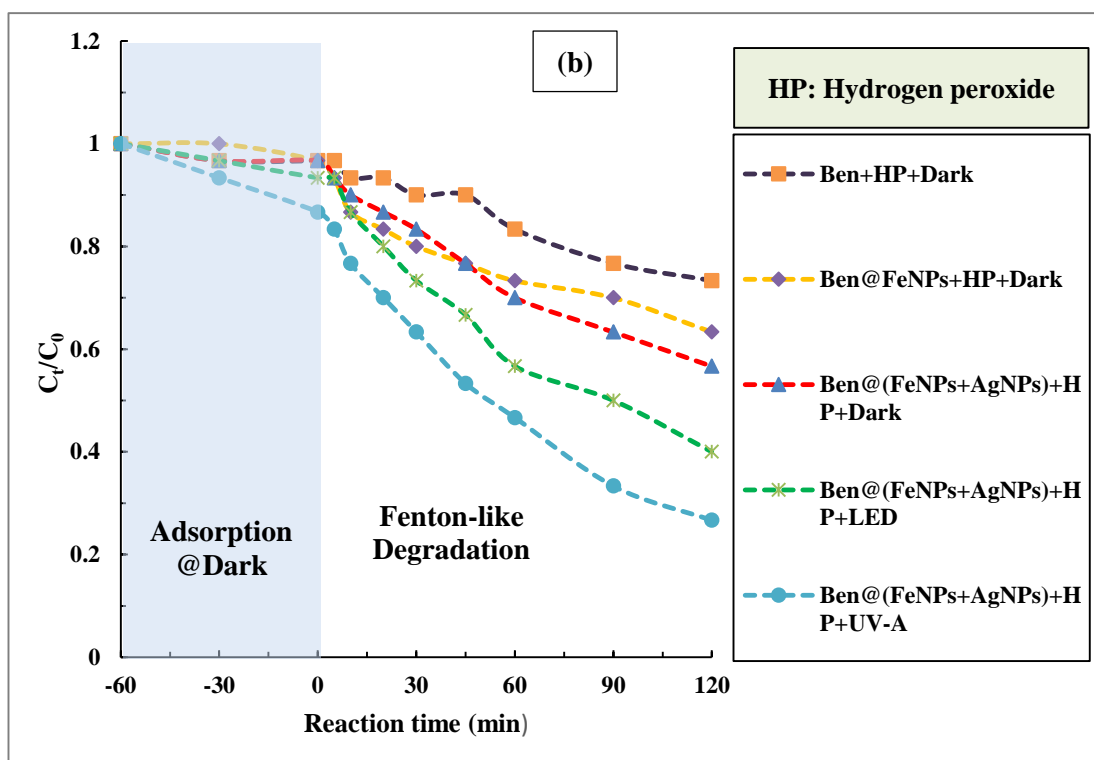
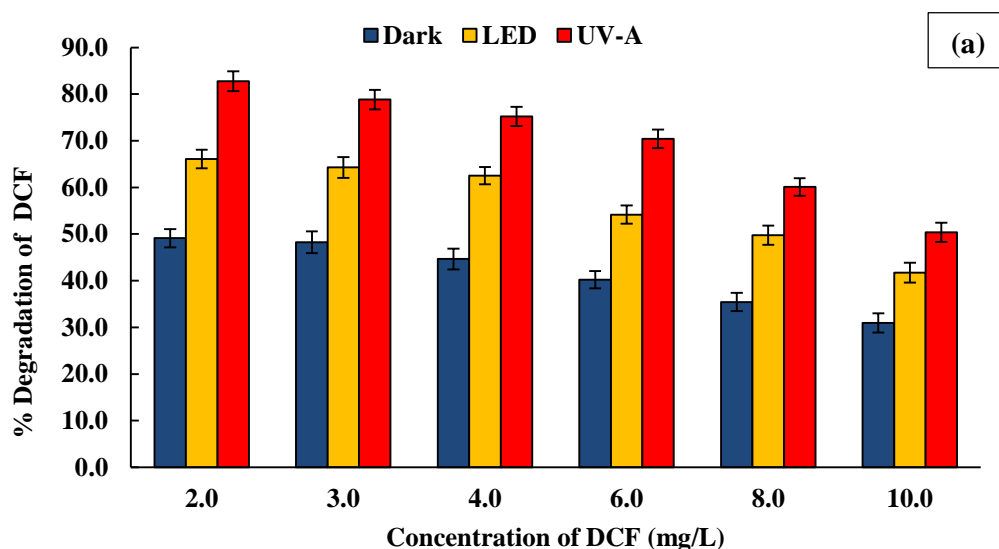


Figure 3.11: Disappearance of (a) DCF [pH = 3.0; [DCF] = 2.0 mg/L; catalyst dose = 250.0 mg/L; H₂O₂ dose = 0.4 mL/L; reaction time = 2 hrs] (b) Phenol [pH = 3.0;

[Phenol] = 2.0 mg/L; catalyst dose = 100 mg/L; H₂O₂ dose = 0.15 mL/L; reaction time = 2 hrs] and (c) NNPT [pH = 3.0; [NNPT] = 2.0 mg/L; catalyst dose = 125.0 mg/L; H₂O₂ dose = 0.10 mL/L; reaction time = 2 hrs] vs. reaction time (min) in different reaction conditions.

3.2.4 Concentration dependence abatement of DCF, phenol, and NNPT

The effect of the initial concentration of pollutants on the degradation efficiency of the Ben@(FeNPs+AgNPs) nanocatalyst was studied. The pollutant concentration was increased from 2.0 to 10.0 mg/L (for DCF & phenol) and 2.0 to 30.0 (for NNPT) while keeping the other optimized reaction conditions constant.



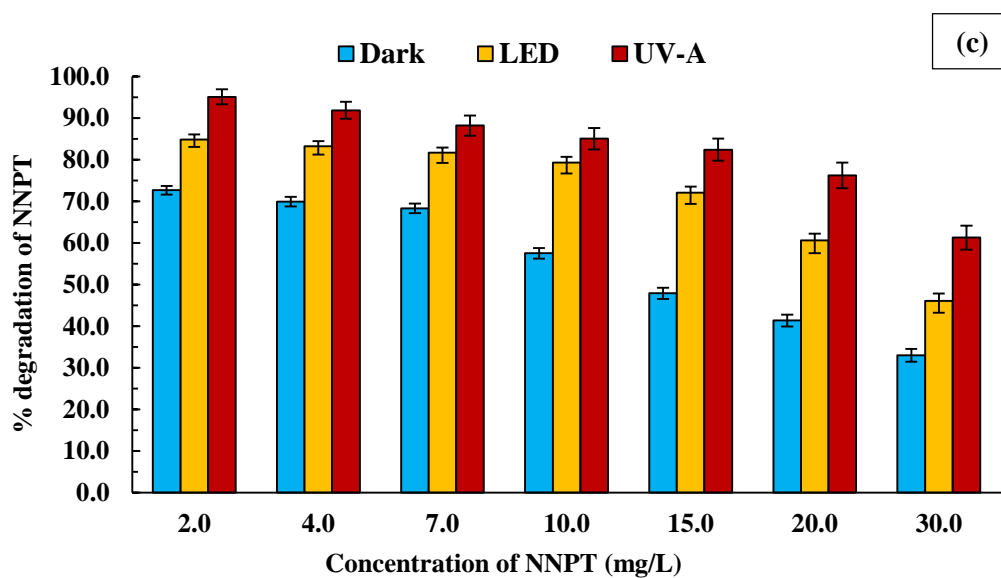
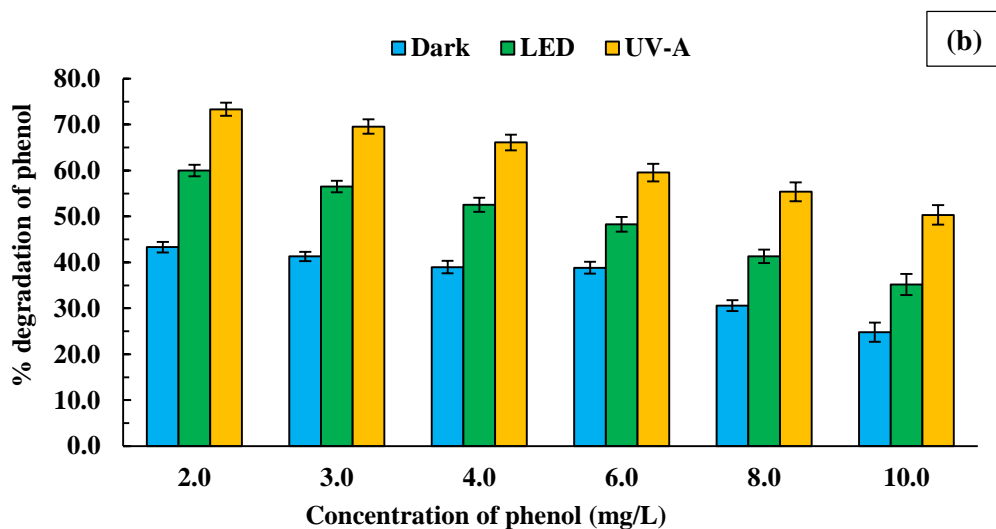


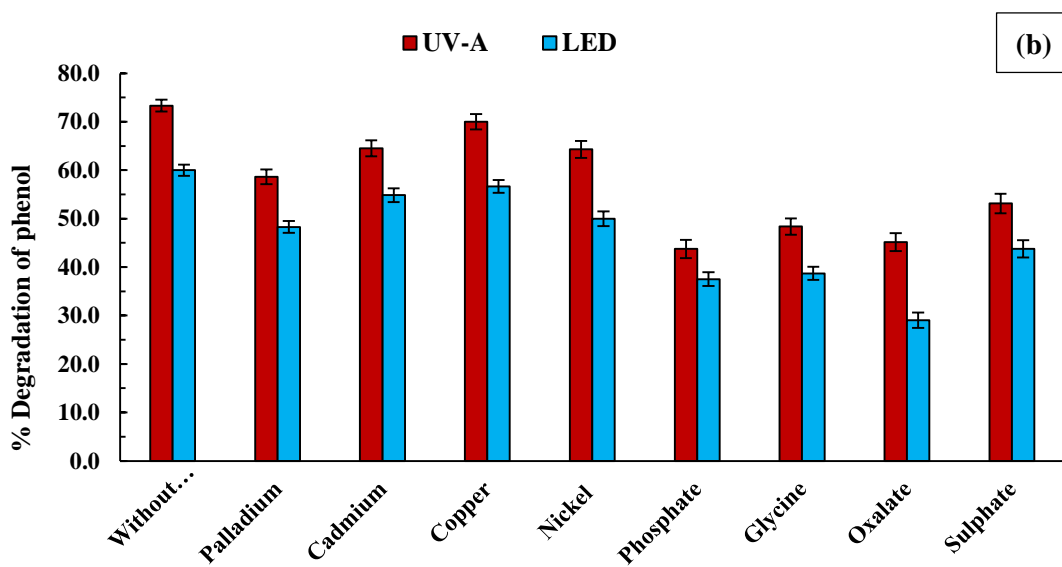
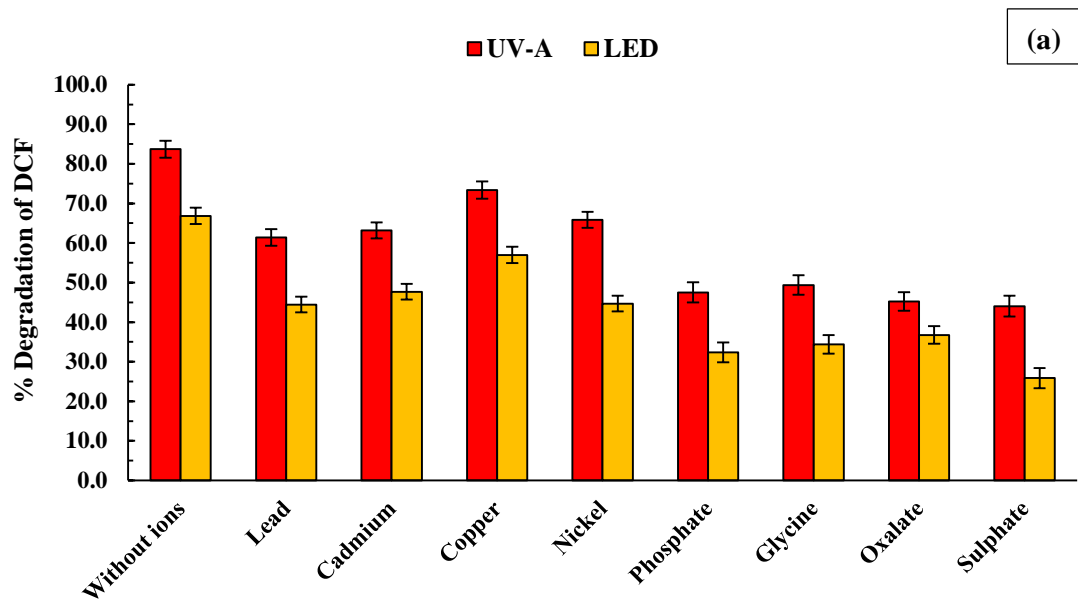
Figure 3.12: Percentage degradation vs initial concentration of (a) DCF [pH= 3.0; Catalyst dose = 250.0 mg/L; H₂O₂ dose = 0.4 mL/L; Reaction time = 2 hr]; (b) phenol [pH= 3.0; Catalyst dose = 100.0 mg/L; H₂O₂ dose = 0.15 mL/L; Reaction time = 2 hrs] & (c) NNPT [pH= 3.0; Catalyst dose = 125.0 mg/L; H₂O₂ dose = 0.1 mL/L; Reaction time = 2 hrs] in different light ambiance.

Figure 3.12 depicts the percentage efficiency of nanocatalysts as a function of pollutant concentrations utilizing different light conditions, i.e., dark, LED light, and UV-A light. Quantitatively, under UV-A irradiation, the Fenton-like reaction for the

percentage degradation was decreased from 83% to 50% whereas it was reduced from 70% to 41% using LED (visible) light irradiation on increasing the DCF concentration from 2.0 to 10.0 mgL⁻¹, respectively (Cf figure 3.12 (a)). Similarly, increasing the phenol concentration from 2.0 mg/L to 10.0 mg/L, the degradation percentage was decreased from 72.3% to 50.3% in the Fenton-like treatment under UV-A irradiation, whereas under LED irradiation, the degradation percentage was decreased from 60.0% to 35.2%, respectively (Cf figure 3.12 (b)). Increasing the NNPT concentration from 2.0 mg/L to 30.0 mg/L caused to lower in the degradation percentage from 95.1% to 61.3% in the Fenton-like treatment under UV-A irradiation and from 84.9% to 46.1% under the LED light irradiations, respectively (Cf figure 3.12 (c)). The decrease in degradation percentage of these pollutants i.e., DCF, phenol, and NNPT, at higher pollutant concentrations, was explained by the fact that a relatively lesser number of active sites are accessible on the nanocatalyst surface for a large number of pollutant species. Hence, relatively lesser degradation efficiency was recorded at increased pollutant concentrations (Sadeghi et al., 2019). Furthermore, these pollutant molecules adsorb on the surface of the nanocomposite, occupying a higher number of active sites, resulting in less leaching of active nanoparticles to react with H₂O₂, resulting in fewer hydroxyl radicals produced in the bulk of the solution. Hence, it caused a decrease in degradation efficiency at higher pollutant concentrations.

3.2.5 Presence of several cations/anions

In natural water samples, coexisting cations/anions are quite prevalent with organic or inorganic contaminants. As a result, the tests were performed to observe the simultaneous presence of a few cations, *viz.*, lead, cadmium, copper, nickel, and some anions, such as phosphate, glycine oxalate, and sulfate in the photo-Fenton-like degradation of targeted pollutants. A comparative elimination of pollutants was obtained under UV-A and LED light irradiations using the optimized reaction conditions. The pollutant and cations/anions concentrations were kept constant at 2.0 mg/L and 10.0 mg/L, respectively.



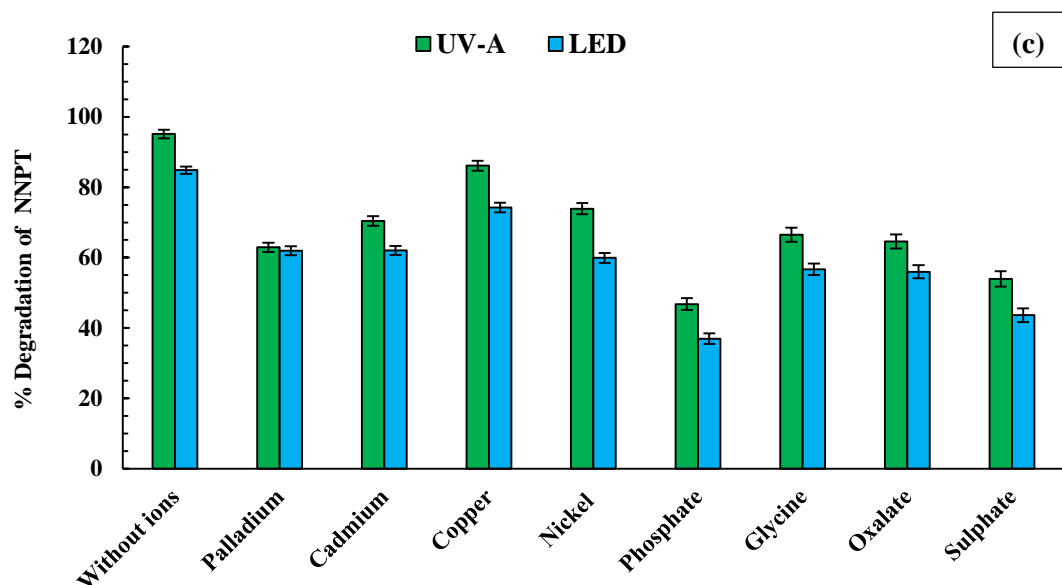


Figure 3.13: Effect of coexisting ions in different light conditions for (a) DCF [pH = 3.0; [DCF]= 2.0 mg/L; [Co-existing ion] = 10.0 mg/L; Catalyst dose = 250.0 mg/L; H₂O₂ dose = 0.4 mL/L; Reaction time = 2 hr]; (b) phenol [pH = 3.0; [phenol]= 2.0 mg/L; [Co-existing ion] = 10.0 mg/L; Catalyst dose = 100.0 mg/L; H₂O₂ dose = 0.15 mL/L; Reaction time = 2 hrs] & (c) NNPT [pH = 3.0; [NNPT]= 2.0 mg/L; [Co-existing ion] = 10.0 mg/L; Catalyst dose = 125.0 mg/L; H₂O₂ dose = 0.1 mL/L; Reaction time = 2 hrs].

Figure 3.13 depicts the degradation efficiency of nanocatalysts in the removal of DCF, phenol, and NNPT in the presence of various ions. In general, the presence of cations/or anions affected the percentage elimination of these two pollutants. However, the degradation of DCF, phenol, and NNPT was affected significantly in the presence of phosphate, oxalate, glycine, and sulfate. The decrease in degradation efficiency of pollutants is mainly because of two factors: the coexisting ions demonstrate competitive sorption towards the catalyst surface, preventing the target pollutants from being degraded; and second, some ions or compounds, such as sulfate, are known to be effective h⁺/•OH quenchers, posing a degradation barrier (Lalliansanga, Tiwari, Tiwari, Shukla, Shim, et al., 2020; Selvam et al., 2007). Furthermore, anions are generally effective complexing/chelating agents. These

anions are more likely to react and form complexes with iron/silver that is leached out of the Ben@[FeNPs+AgNPs] catalyst to the bulk of the solution. As a result, there is less formation of •OH radicals, which reduces the degradation efficiency.

3.2.6 Degradation kinetics of DCF, phenol, and NNPT

The Fenton or Fenton-like reactions are complicated, making kinetic investigations challenging. The Fenton or Fenton-like processes have multiple-step reactions, each with a specific rate constant. However, the reaction involving the degraded component and •OH radicals is regarded as the primary reaction for establishing the overall rate constant (Mitsika et al., 2013b). The degradation kinetics was investigated using both pseudo-first-order and pseudo-second-order kinetics models, with the best-fitted model being used to investigate the degradation kinetics of each pollutant. The plots are presented in Figure 3.14.

The pseudo-first-order (PFO) and pseudo-second-order (PSO) rate constants were obtained for the targeted pollutant's degradation in the photo-Fenton-like process utilizing the Ben@(FeNPs+AgNPs) nanocatalyst. Using a PFO kinetic model (*Cf* figure 3.14(a)), optimized reaction constant k_f and the R^2 value of degradation of pollutant DCF using the Ben@[FeNPs+AgNPs] the nanocomposite was determined to be 0.0137 min^{-1} and 0.9635, respectively. Whereas in the pseudo-second-order kinetic model (*Cf* figure 3.14(b)), the reaction constant k_s and R^2 value were determined to be $0.0149 \text{ Lmg}^{-1}\text{min}^{-1}$ and 0.8471, respectively. Based on the R^2 values, it is clear that the data for kinetics is better matched to the PFO kinetic model than the PSO method. Similarly, using the pseudo-first-order kinetic model (*Cf* figure 3.14(c)), the optimum reaction constant k_f and R^2 value for phenol degradation utilizing the Ben@(FeNPs+AgNPs) nanocomposite were 0.0119 min^{-1} and 0.9762, respectively. The reaction constant k_s and R^2 values in the pseudo-second-order kinetic model (*Cf* figure 3.14(d)), were $0.0109 \text{ Lmg}^{-1}\text{min}^{-1}$ and 0.9885, respectively. Similarly, in the case of NNPT, the optimum PFO reaction constant k_f and R^2 values were 0.0324 min^{-1} and 0.083, whereas the PSO rate constant k_s and R^2 values were $0.0789 \text{ Lmg}^{-1}\text{min}^{-1}$ and 0.9384 (*Cf* figure 3.14(e & f)). Results showed that the kinetic data fit the PSO model better than the PFO model based on the R^2 values.

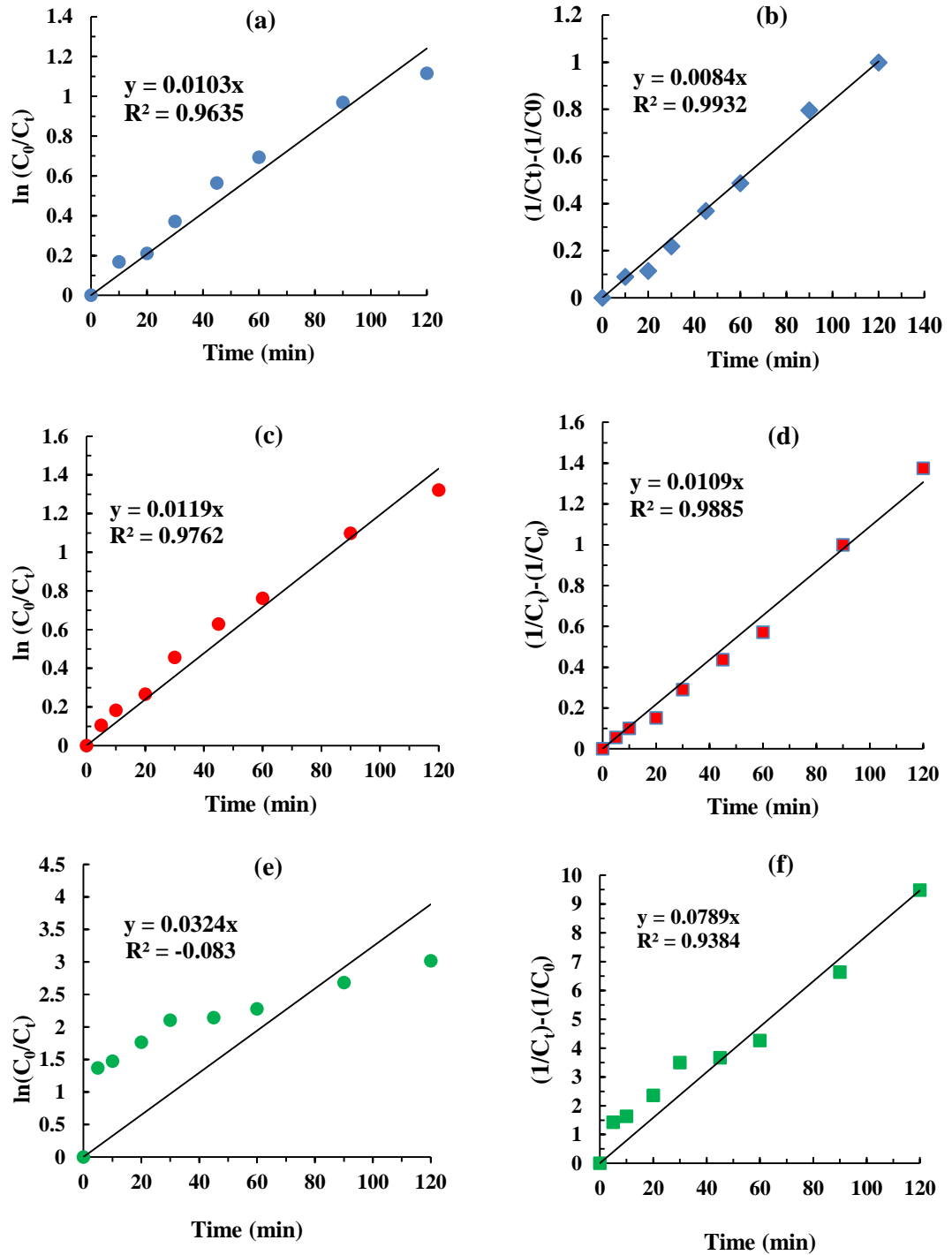


Figure 3.14: The kinetics of DCF [(a) and (b)], phenol [(c) and (d)], and NNPT [(e) and (f)] degradation using the PFO; and PSO models.

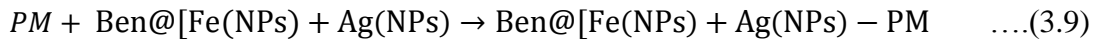
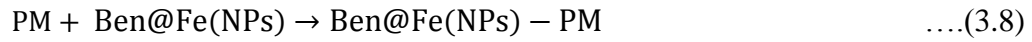
3.2.7 Involvement of •OH radical

Several well-known •OH radical quenchers are used to investigate the involvement of hydroxyl radicals in the degradation of micropollutants. The HCO_3^- and isopropanol effectively quench the •OH radicals (Lalliansanga et al., 2018b). Similarly, sodium azide (NaN_3) quenches the reactive oxygen species (ROS), singlet oxygen produced due to the reaction of $\bullet\text{O}_2^-$ radicals and photo-generated holes. The highly reactive nature of singlet oxygen towards organic molecules in aqueous media is well demonstrated elsewhere (Barka et al., 2010). To confirm the participation of •OH radicals in the photo Fenton-like degradation of 2.0 mg/L of pollutants was conducted in the presence of 1.0 mL (0.1 mol/L) isopropanol, HCO_3^- , and NaN_3 . Figure 3.15 shows the effect of quenchers in eliminating these three pollutants. The figure indicated that the presence of these quenchers significantly inhibited the degradation percentage of DCF, phenol, and NNPT. Photocatalytic degradation of Alizarin Yellow utilizing [Au(NPs)/Ag(NPs)] modified nanocomposites was studied and suggested that the involvement of •OH and $\bullet\text{O}_2^-$ radicals were predominantly involved in the degradation of pollutant molecules (Lalliansanga et al., 2020c; Lalliansanga et al., 2020). Similarly, Hofmann et al., proved that bicarbonates quench the •OH radicals. The presence of bicarbonate effectively transforms the •OH radicals into less active OH^- ions, preventing the synthesis of bromate (Hofmann and Andrews, 2006). These results inferred that the •OH and $\bullet\text{O}_2^-$ radical species are predominantly involved in the breakdown of these pollutant molecules in the photo-Fenton-like reactions.

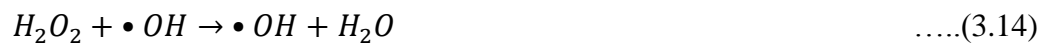
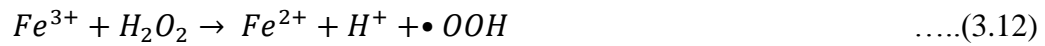
The probable Fenton-like degradation mechanisms of these pollutant molecules are suggested as (i) the pollutant molecules adsorb onto the catalyst surface Ben@FeNPs and Ben@(FeNPs+AgNPs); (ii) at the Ben@(FeNPs+AgNPs) nanocatalyst interface, Fe^{2+} and Fe^{3+} or Ag^+ leach out from the catalyst's surface, which accelerates the breakdown of H_2O_2 ; (iii) H_2O_2 produces hydroxyl radicals and attack on the pollutant molecule's unsaturated double bonds; and (iv) Hydroxyl radicals break down the conjugated system in macromolecules into tiny intermediates. Intermediates are readily mineralized as CO_2 and H_2O (Wu et al., 2015). Further, the TOC analyzer measures the apparent mineralization of organic pollutants at the end of

the reaction process. The degradation of these pollutant molecules (PM) (i.e., DCF, phenol, and NNPT) by the photo-Fenton-like processes is illustrated as:

a) Adsorption:



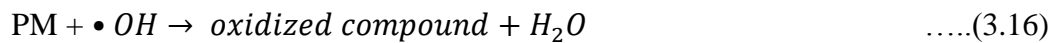
b) Generation of $\bullet\text{OH}$ radical:



c) Photo decomposition of H_2O_2 :



d) $\bullet\text{OH}$ radicals attack the pollutant on the catalyst surface:



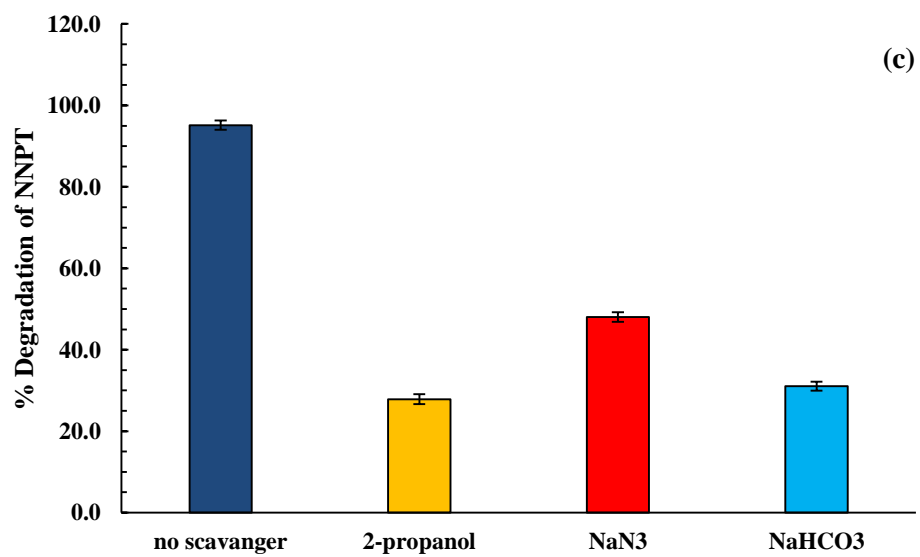
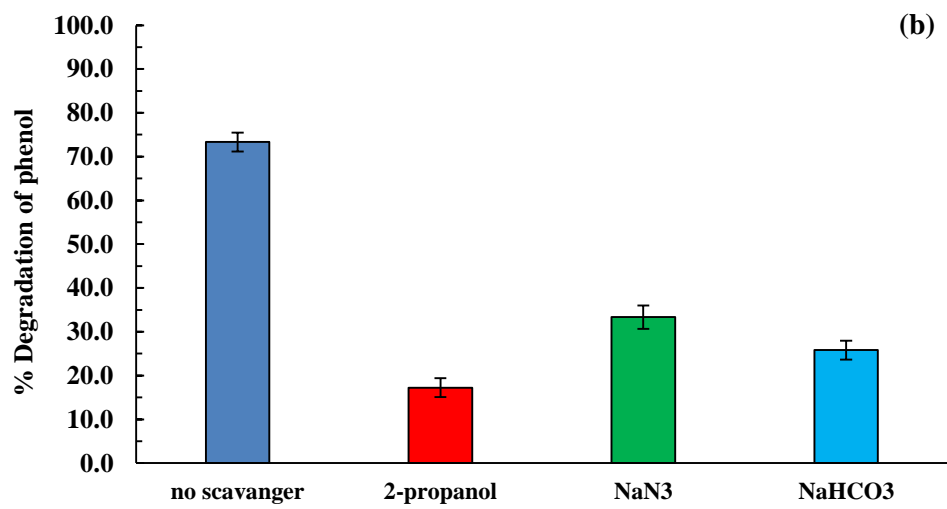
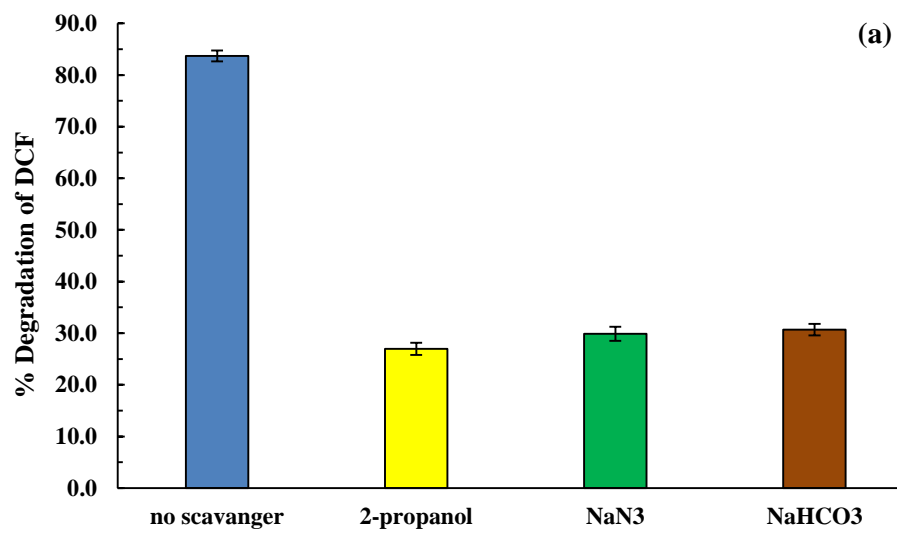


Figure 3.15: Effect on percentage degradation in the presence of scavengers [pH = 3.0; [pollutant] = 2.0 mg/L; [scavenger] = 0.1 mol/L (10 mL/L); Catalyst dose = 250.0 mg/L for DCF, 100.0 mg/L for phenol and 125.0 mg/L for NNPT; H₂O₂ dose = 0.4 mL/L for DCF, 0.15 mL/L for phenol and 0.1 mL/L for NNPT; Reaction time = 2 hrs].

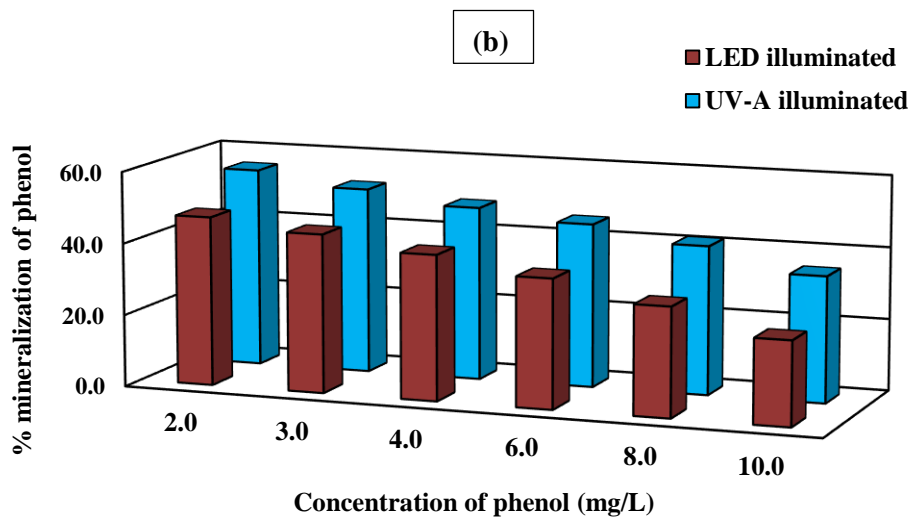
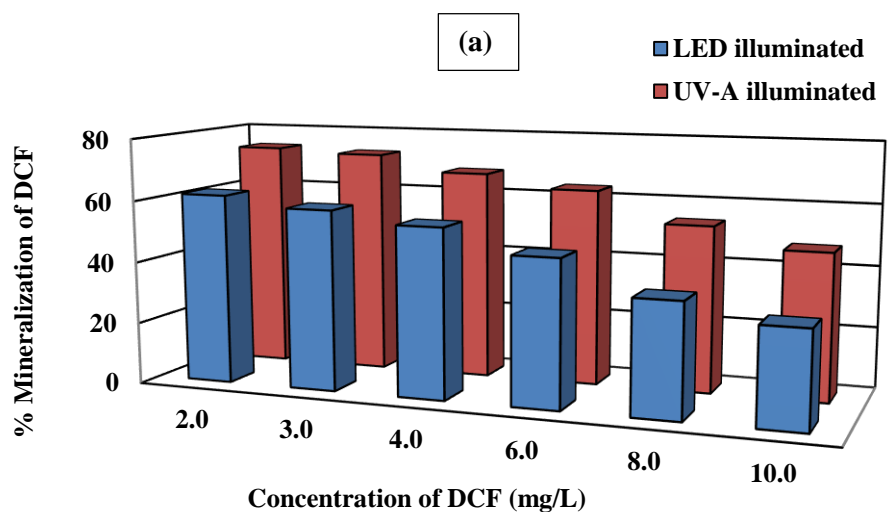
3.2.8 Mineralization of target organic pollutants

The study was further extended to obtain the percentage mineralization of DCF, phenol, and NNPT in the photo Fenton-like degradation utilizing the Ben@(FeNPS+AgNPs) nanocatalyst under the LED and UV light radiations for 2 hrs. The NPOC (Non-Purgeable Organic Carbon) data were obtained for the treated and untreated samples, which enabled us to obtain the percentage mineralization of these pollutant molecules.

Figure 3.16 (a, b &c) depicted the results, which demonstrated that as pollutant concentrations increased, the percentage mineralization of all these pollutants decreased significantly. Eventually, mineralization efficiency using the UV-A light was relatively more than the LED light irradiation. Moreover, the studies demonstrated that a considerable amount of these pollutants was mineralized during the photo-Fenton-like process.

Quantitatively, under UV-A light irradiation, the percentage mineralization of DCF was decreased from 74% to 47% with an increase of DCF concentration from 2.0 mg/L to 10.0 mg/L. Similarly, the LED light irradiation caused to decrease in the percentage mineralization of DCF from 62% to 31%, with a similar increase in DCF concentration, i.e., from 2.0 mg/L to 10.0 mg/L, respectively. Under UV-A light irradiation, 55.5% mineralization was accomplished at a phenol concentration of 2 mg/L, whereas 47.0% mineralization was obtained using LED light irradiation. Similarly, 64.0% of NNPT was mineralized at the NNPT concentration of 2.0 mg/L under UV-A irradiation, whereas LED light irradiation achieved 51.5% mineralization of NNPT. Overall, the results showed that the photo-Fenton-like process utilizing the Ben@(FeNPs+AgNPs) nanocatalyst mineralizes a considerable amount of DCF, phenol, and NNPT in aqueous solutions. In 10 mM H₂O₂ and 8W UV-C light, Feng et al. (Feng et al., 2006) showed roughly 50-60% mineralization of 0.2 mM orange II dye

compound utilizing bentonite clay supported nZVI. Similarly, Sétifi et al. used a goethite-montmorillonite nanocomposite to achieve 90% mineralization of naproxen (10^{-5} mol/L) in 5 hrs (Sétifi et al., 2019). Therefore, the novel Ben@(Fe^0+Ag^0) nanocomposite appears to be promising in the degradation of these pollutants in the photo-Fenton-like processes utilizing the less harmful UV-A or even visible light sources.



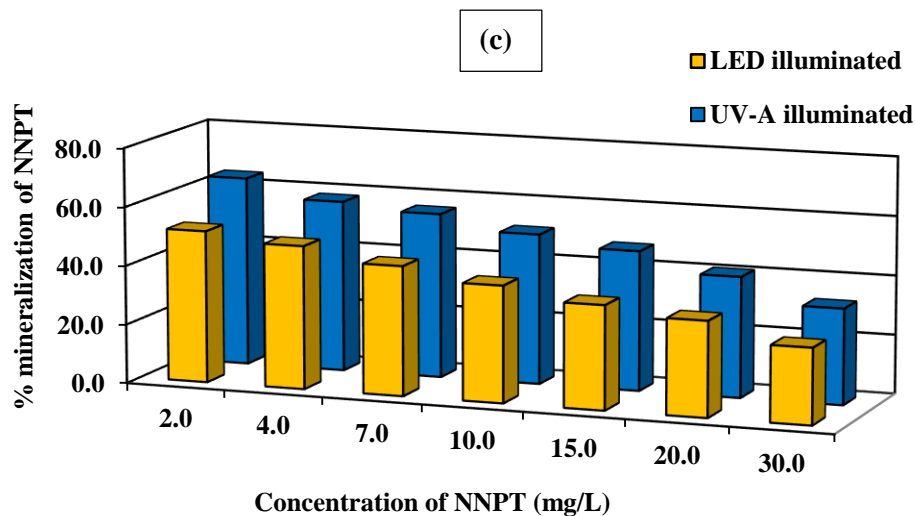


Figure 3.16: Mineralization(%) at different concentrations of (a) DCF [pH = 3.0; Catalyst dose = 250.0 mg/L; H₂O₂ dose = 0.4 ml/L; Reaction time = 2 hr]; (b) phenol [pH = 3.0; Catalyst dose = 100.0 mg/L; H₂O₂ dose = 0.15 ml/L; Reaction time = 2 hrs] and (c) NNPT [pH = 3.0; Catalyst dose = 125.0 mg/L; H₂O₂ dose = 0.1 ml/L; Reaction time = 2 hrs].

3.2.9 Determination of leached iron (II) concentrations

The Fenton-like reactions are always associated with the leaching of Fe(II) from the catalyst Ben@(FeNPs+AgNPs) during the reaction process. The participation of Fe(II) and H₂O₂ is the central notion of the traditional Fenton process. The concentration of Fe²⁺ increases as iron leaching advances (Cf Equation (3.1)), and the Fenton-like reaction of Fe²⁺/Fe³⁺ with H₂O₂ generates •OH radicals. In a heterogeneous system, the presence of H₂O₂ with Fe(NPs) or Ag(NPs) in Ben@(FeNPs+AgNPs) nanocatalyst is a primary source of ROS (reactive oxygen species) generation. As a result, the breakdown of H₂O₂ in the reaction is demonstrated by the H₂O₂ affinity for catalyst surfaces, the availability of surface sites for H₂O₂ adsorption, and the rate of ≡Fe(III) reduction. In addition, Ben@FeNPs releases less Fe in the Fe(NPs). As a result, using the Fe(NPs) poses minimal sludge production.

The C_t/C_0 values (C_t stands for concentration of the pollutant at time t and C_0 stands for initial concentration of the pollutant) for the elimination of targeted pollutants, on the other hand, are displayed in Figure 3.17. Iron leaching is closely connected with time-dependence removal, and higher iron leaching resulted in enhanced removal of both target pollutants. The Ben@(FeNPs+AgNPs) nanocatalyst was evaluated for Fe(II) leaching during the degradation of 2.0 mg/L DCF, phenol, and NNPT contaminants. After two hours of reaction time, a maximum of 68.80 $\mu\text{g/L}$, 53.33 $\mu\text{g/L}$, and 73.33 $\mu\text{g/L}$ of Fe(II) were leached out from the catalyst surface in the degradation of DCF, phenol, and NNPT, respectively. The catalyst Ben@(FeNPs+AgNPs) demonstrated potential in photo-Fenton-like processes due to significantly less iron leaching. The use of nanocatalysts enabled a significantly less release of iron leaching, hence; significantly controlling the release of excess sludge in the conventional Fenton processes.

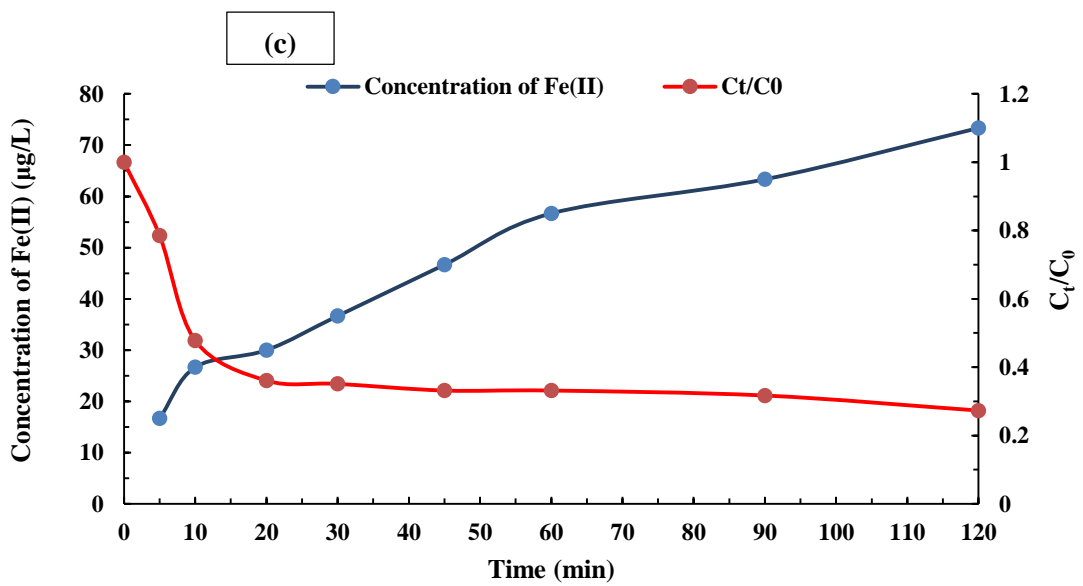
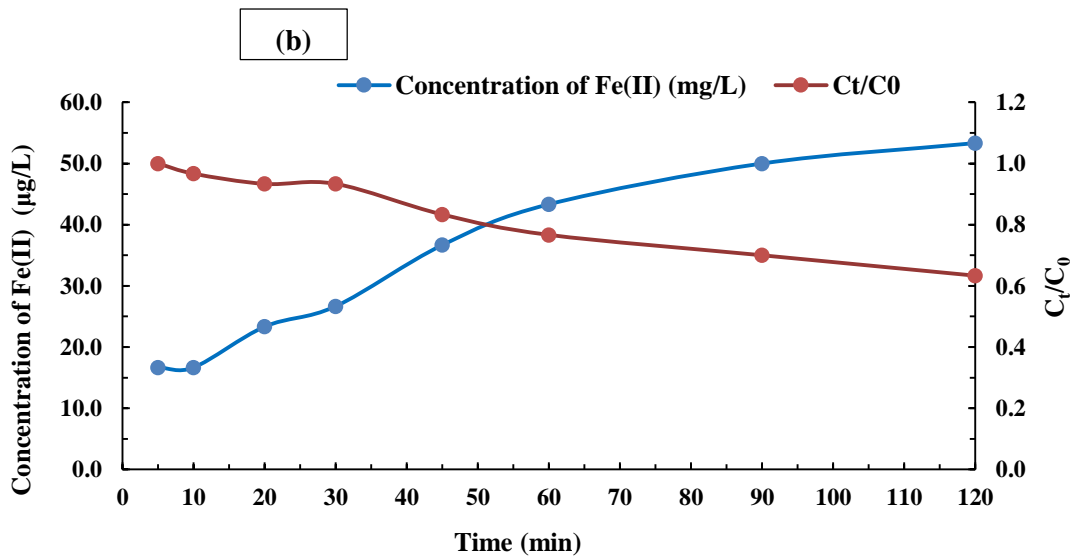
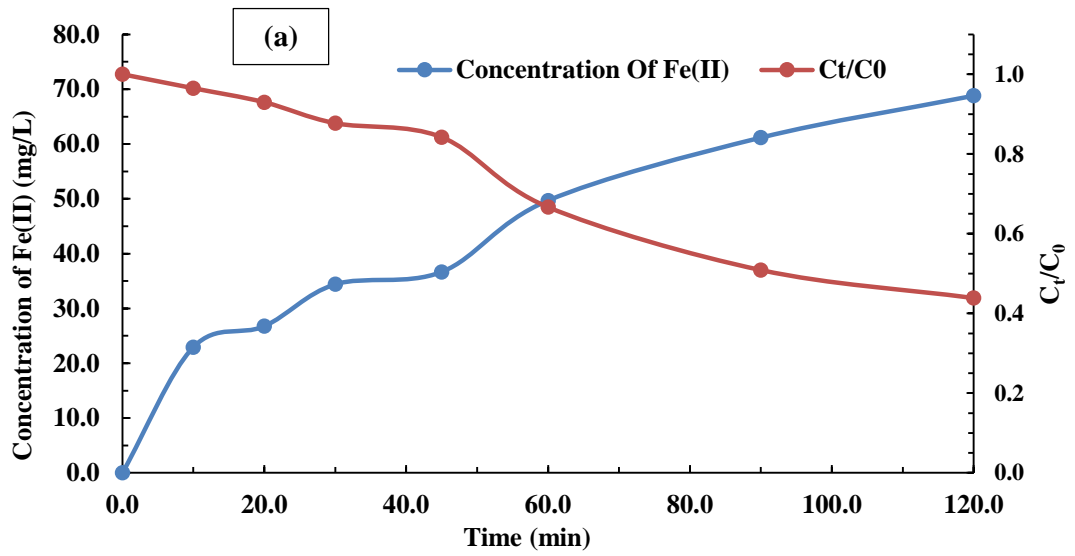


Figure 3.17: Leaching of iron concentration along with the disappearance of (a) DCF [pH = 3.0; Catalyst dose = 250.0 mg/L; H₂O₂ dose = 0.4 mL/L; Reaction time = 2 hr]; (b) phenol [pH = 3.0; Catalyst dose = 100.0 mg/L; H₂O₂ dose = 0.15 mL/L; Reaction time = 2 hrs] and (c) NNPT [pH = 3.0; Catalyst dose = 125.0 mg/L; H₂O₂ dose = 0.1 mL/L; Reaction time = 2 hrs] as a function of time.

3.2.10 Reutilization of nanocatalyst

From a practical standpoint, the reusability and stability of the catalyst are two essential parameters to study. The stability of nanocatalysts, particularly their reusability in repeated photo-Fenton-like processes, determines the practical implacability of catalysts. Studies allow nanocatalysts to be used for long and repeated operations. The tests were carried out to determine the stability of the Ben@(FeNPs+AgNPs) nanocatalyst in the photo-Fenton-like degradation of DCF, phenol, and NNPT. The nanocatalyst Ben@(FeNPs+AgNPs) was introduced for four repeated operations cycles. Figure 3.18 shows the results of the reusability of the Ben@(FeNPs+AgNPs) nanocatalyst for the degradation of these pollutants. Under UV-A irradiation, the degradation efficiency was investigated while maintaining optimal reaction conditions. In removing these pollutants for subsequent processes, the results showed a slight decrease in the removal efficiency of the catalyst (*Cf* Figure 3.18). Quantitatively, the removal efficiency of DCF decreased from 83% to 74% at the end of the 5th cycle of operation. On the other hand, at the end of the fourth cycle of operation, the removal efficiencies of phenol and NNPT dropped from 73% to 63%, and 95 to 89% only, respectively. From figure 3.18, results demonstrated that the photo-Fenton-like process allowed for a little amount of iron loss during oxidation cycles. Therefore, the catalyst is useful for longer use of operations at least in the removal of these pollutants under the photo-Fenton-like processes. Similar results were shown using the Fe₃O₄ particles adorned Zn pillared bentonite to treat the landfill leachate (Ma et al., 2018), and the reusability test revealed an insignificant change in mineralization percentage. Another bentonite-supported catalyst was used and the catalyst showed reasonably good stability in the Fenton-like removal of Orange II (Li et al., 2016).

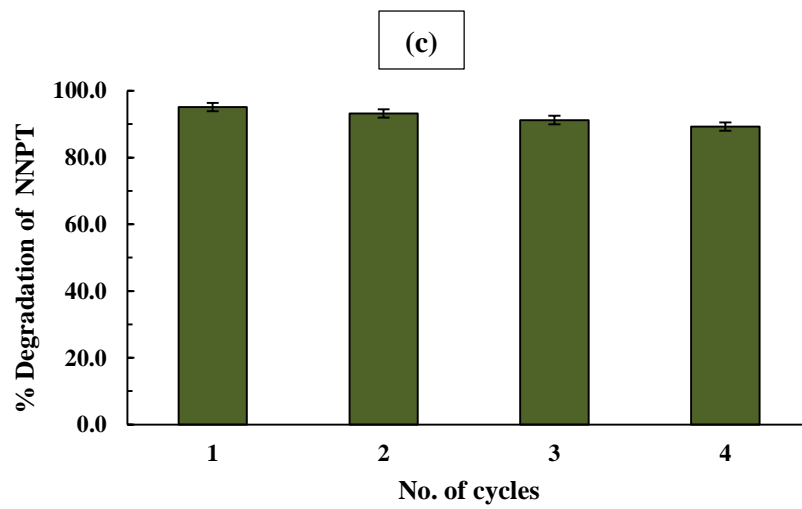
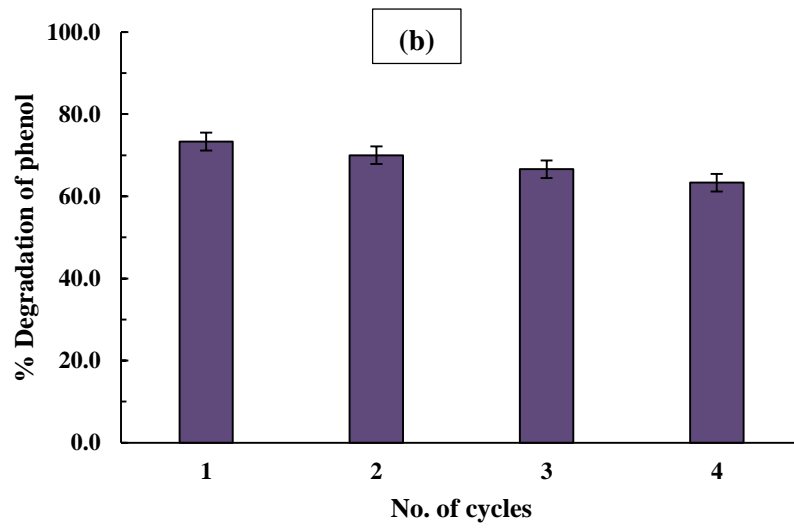
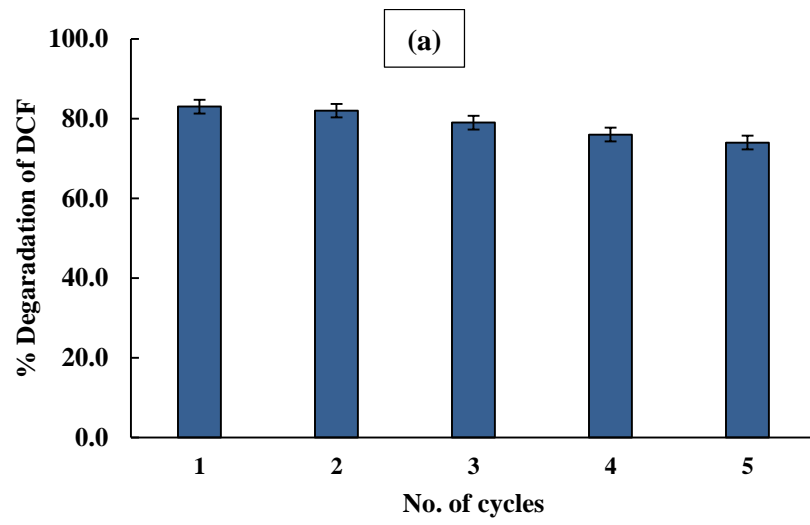
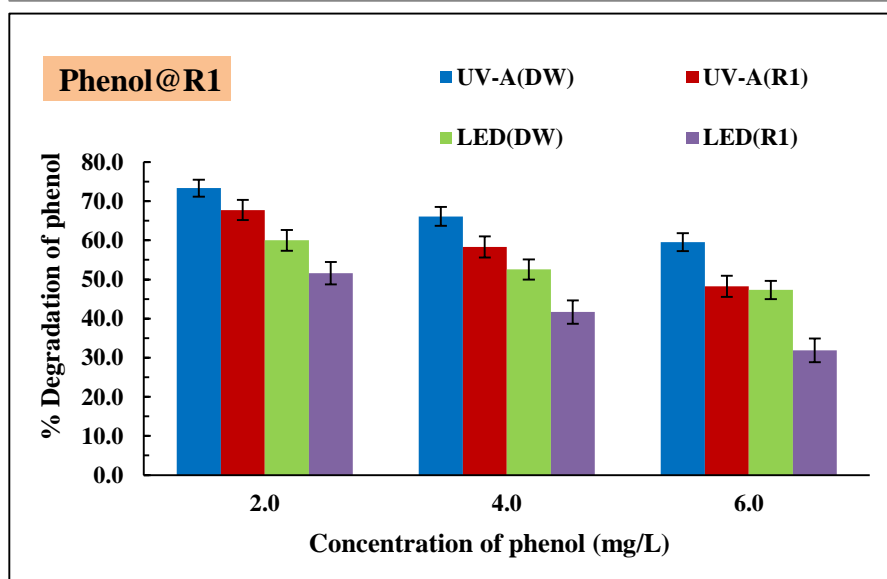
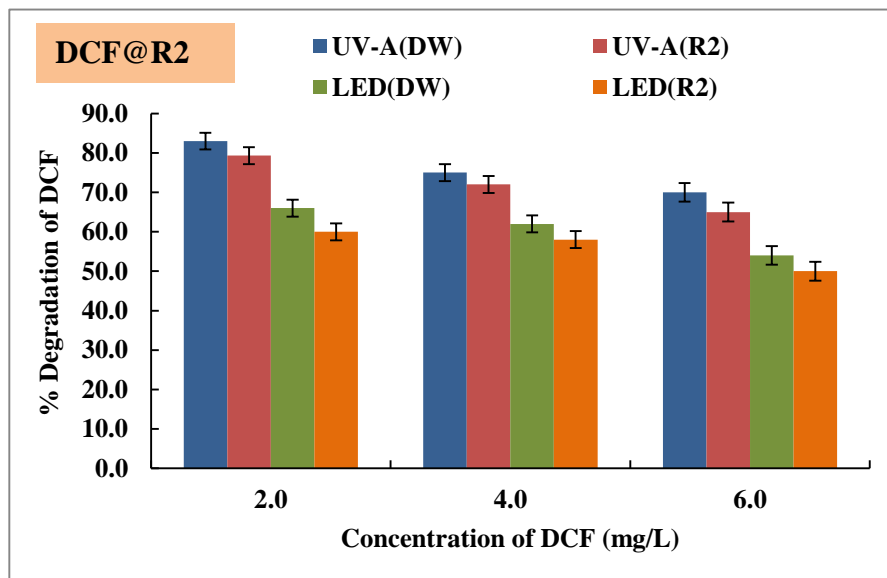
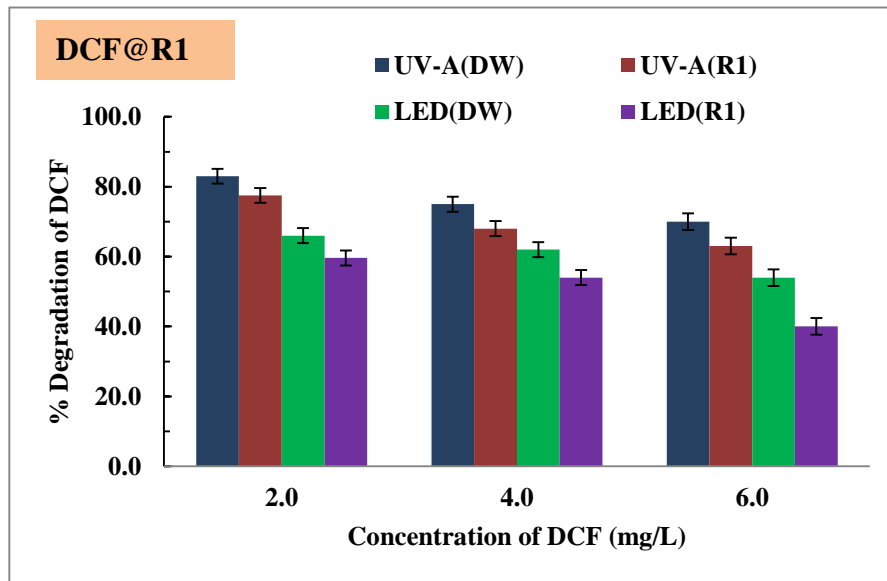


Figure 3.18: Reusability of the Ben@(FeNPs+AgNPs) nanocomposite in the degradation of (a) DCF [pH = 3.0; Catalyst dose = 250.0 mg/L; H₂O₂ dose = 0.4 mL/L; Reaction time = 2 hr]; (b) phenol [pH = 3.0; Catalyst dose = 100.0 mg/L; H₂O₂ dose = 0.15 mL/L; Reaction time = 2 hrs] and (c) NNPT [pH = 3.0; Catalyst dose = 125.0 mg/L; H₂O₂ dose = 0.1 mL/L; Reaction time = 2 hrs] as a function of time.

3.2.11 *Real matrix water experiments*

In the natural matrix treatment of DCF, phenol, and NNPT, Ben@(FeNPs+AgNPs) nanocatalyst was used in the photo-Fenton-like process. The experiments are extended to explore the possibility of scaling up the treatment process for DCF/phenol/or thiourea-contaminated water. Furthermore, it enables an examination of the nanocatalyst's appropriateness and selectivity in such a real matrix treatment. Water samples were taken from two different natural water sources and labeled as R1 (natural stream water) and R2 (groundwater) (Mizoram University supply water tank). The Physicochemical analyses of the water samples were performed, and the results are reported in Table 2.2. The supply water tank (R2) had a pH of 8.17, whereas the stream water sample (R1) had a pH of 7.8. Fe, Mn, Cu, Pb, Ni, and Zn were identified in trace amounts. However, the Ca level was relatively high in both water samples. Significant inorganic carbon (IC) and some non-purgeable organic carbon in both samples (NPOC) were present. The water samples were spiked with different concentrations of the pollutants (2.0, 4.0, and 6.0 mg/L) while keeping the pH at 3.0. For DCF, the catalyst dose was introduced as 250.0 mg/L with 0.4 mL/L of H₂O₂ (30%). For phenol, the photo-Fenton-like studies were carried out using the Ben@(FeNPs+AgNPs) nanocatalyst (100 mg/L) along with 0.15 mL/L H₂O₂ (30%), which was exposed to UV-A and LED light for 2 hrs. Similarly, for NNPT, the photo-Fenton-like studies proceeded using 125.0 mg/L of Ben@(FeNPs+AgNPs) nanocatalyst and 0.1 mL/L H₂O₂ (30%). Figure 3.19 shows the percentage efficiency results compared to the blank (purified water) results. When comparing the two actual water samples to the distilled water, the percentage efficiency of all these pollutants was not considerably reduced. Quantitatively, the degradation percentage of DCF (2.0 mg/L) was decreased from 83% to 78% under UV-A light-assisted reaction while the

percentage decreased from 66% to 59% under LED irradiation using the R1 real water sample. Similarly, the R2 real water sample of the degradation percentage for DCF (2.0 mg/L) was decreased from 83% to 79% under UV-A light irradiation, while under the LED (visible) light reaction condition, it declined from 66% to 60%. Similarly, the percentage degradation of phenol (2.0 mg/L) was decreased from 73% to 68% under UV-A light illumination and from 60% to 51% under LED light irradiation using the R1 water sample. Similarly, using the R2 water sample, the degradation of phenol (2.0 mg/L) was decreased from 73% to 69% under UV-A irradiation, whereas, under the LED light environment, it dropped from 60% to 52%. On the other hand, the degradation efficiency decreased from 95% to 89% in the case of NNPT under UV-A illumination and from 84% to 75% under LED light illumination using the R1 water sample. Further, using the R2 water sample, the percentage degradation of NNPT was decreased from 95% to 92% under UV-A irradiation and from 84% to 79% under LED irradiation. A change in the degradation efficiency of these pollutants using the actual matrix samples was due to the different Physico-chemical characteristics of water samples. However, even the presence of several ions and a relatively high value of IC could not significantly affect the removal efficiency of the catalyst in the photo-Fenton-like process. These results further showed the potential of the Ben@(FeNPs+AgNPs) nanocatalyst in the efficient removal of DCF, phenol, and NNPT from aqueous solutions under the photo-Fenton-like process using the visible (LED) or UV-A lights.



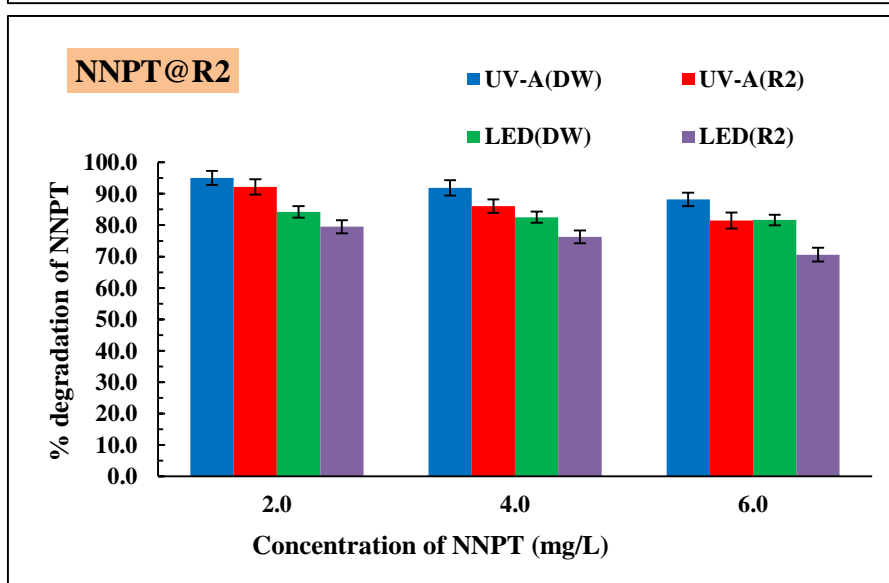
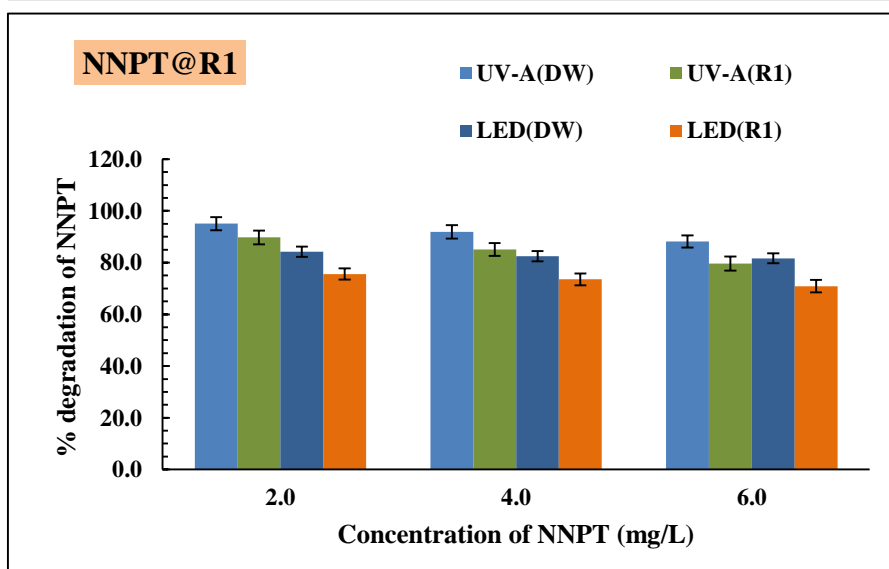
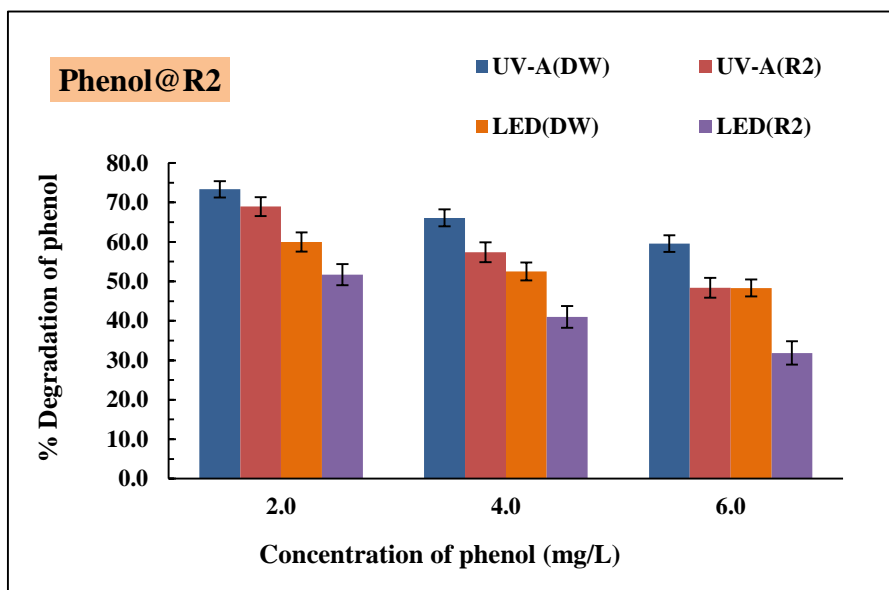


Figure 3.19: photo Fenton-like degradation in the real water system for DCF [pH = 3.0; Catalyst dose = 250.0 mg/L; H₂O₂ dose = 0.4 mL/L; Reaction time = 2 hr]; phenol [pH= 3; Catalyst dose = 100.0 mg/L; H₂O₂ dose = 0.15 mL/L; Reaction time = 2 hrs] and NNPT [pH= 3.0; Catalyst dose = 125.0 mg/L; H₂O₂ dose = 0.10 mL/L; Reaction time = 2 hrs].

3.3 Degradation of Amoxicillin (AMX) and Sulfamethazine (SMZ) using Ben@(CuNPs+AgNPs) nFLC

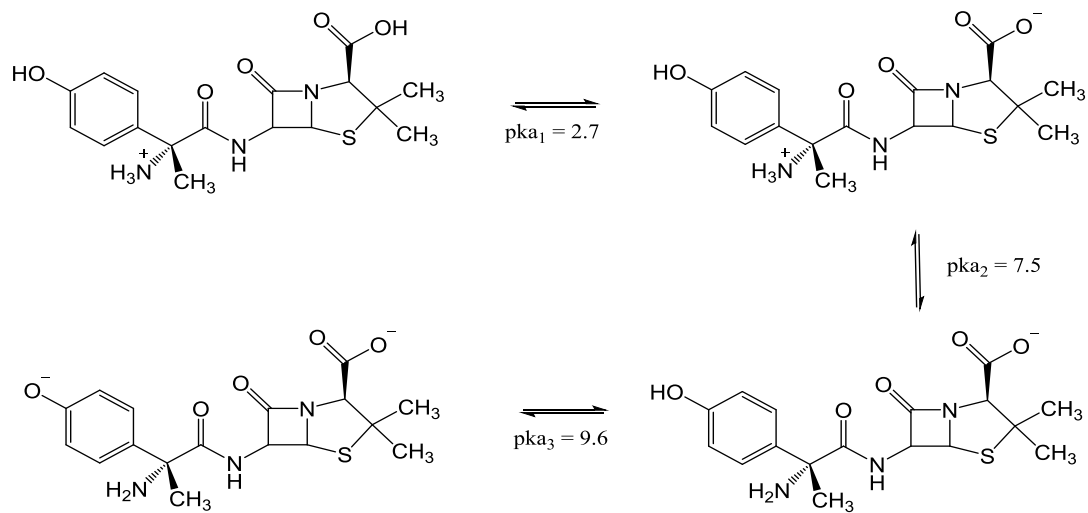
3.3.1 Effect of initial pH

The influence of the solution pH is a regulating parameter in deducing the process of pollutant degradation in aqueous media. The generation of •OH radicals and breakdown of zero-valent Cu(NPs) and the speciation of pollutant molecules are predominantly governed by the pH of the solution. Therefore, the solution pH strongly affects the degradation efficiency of organic pollutants in Fenton or Fenton-like reactions (Song et al., 2017). The pH-dependent experiments (pH 2.0-7.0) are carried out to assess the influence of pH on the elimination of AMX and SMZ using Ben@(CuNPs+AgNPs) nanocatalyst. A constant pollutant concentration (2.0 mg/L) with a fixed dosage of nanocatalyst (100.0 mg/L) and H₂O₂ (0.2 mL/L) was maintained in the reactor. Figure 3 shows the percentage degradation of AMX and SMZ in a dark environment. The acidic pH region (between pH 2.0-4.0) favors the degradation efficiency. Under dark conditions, AMX (2.0 mg/L) was eliminated to its moderate value of *ca.* 56% in 2 hours of reaction time. On the other hand, the elimination of SMZ obtained *ca.* 44% in similar dark conditions. Further, increase in pH from 5.0 to 7.0, both pollutants showed a significant decrease in their elimination rate.

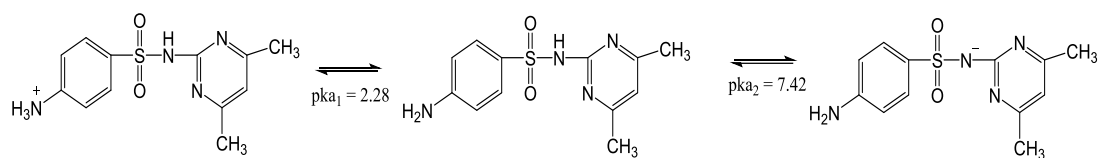
In aqueous solutions, the speciation of pollutant molecules and the surface properties of the catalyst play an important role in the catalytic performance (Bokare et al., 2008). The nanocomposite solids Ben@(CuNPs), and Ben@(CuNPs+AgNPs) showed a p*H*_{pzc} value of 6.2 and 6.4, respectively. This infers that the solids carry a net positive charge below this pH and a net negative charge above this pH. On the hand, amoxicillin has three dissociable hydrogens with the p*K*_a values of p*K*_{a1}, p*K*_{a2}, and p*K*_{a3} as 2.7, 7.5, and 9.6, respectively (*Cf* Equation 3.17) (Çağlar Yılmaz *et al.*, 2020).

Similarly, sulfamethazine has the pK_{a1} and pK_{a2} values of 2.28 and 7.42, respectively (Cf Equation 3.18) (Liu et al., 2017). Hence, the pollutants, viz., amoxicillin and sulfamethazine, are present predominantly in its anionic species within the pH region 2.5~7.0. Therefore, both the negatively charged pollutants molecules are electrostatically attracted by the positively charged solid surface within the pH region ~3.0 to 4.0 and are aggregated on the catalyst surface. This resulted in enhanced removal of AMX and SMZ within these regions. However, a significant but gradual decrease in the removal of AMX and SMZ is recorded with a further increase in the pH. This is because, with an increase in pH, the electropositive behavior of the surface is gradually decreasing hence, a gradual decrease in the aggregation of pollutants molecules on the surface, which causes for the decrease in the removal of these pollutants in the Fenton-like process. Additionally, the corrosion of CuNPs producing $\bullet\text{OH}$ radicals favors the acidic pH region. Hence the results indicated that acidic conditions (pH=3.0~4.0) were more favorable for the degradation of both pollutants. Furthermore, in alkaline solutions, the oxidation potential of $\bullet\text{OH}$ radicals decreases (Fida et al., 2017). Therefore, pH=3.0 was chosen for the rest of the studies.

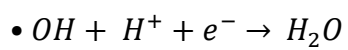
Similarly, at a much lower pH (pH~2.0), less elimination of AMX and SMZ was recorded. This decrease is due to the less attraction of neutral pollutant species by the positively charged catalyst surface, which lowers the removal of AMX and SMZ. The hydroxyl radicals induced by the abundant H^+ ions at low pH further prevent the degradation of the contaminants owing to the decomposition of $\bullet\text{OH}$ radical (Cf equation (3.19)).



...(3.17)



...(3.18)



...(3.19)

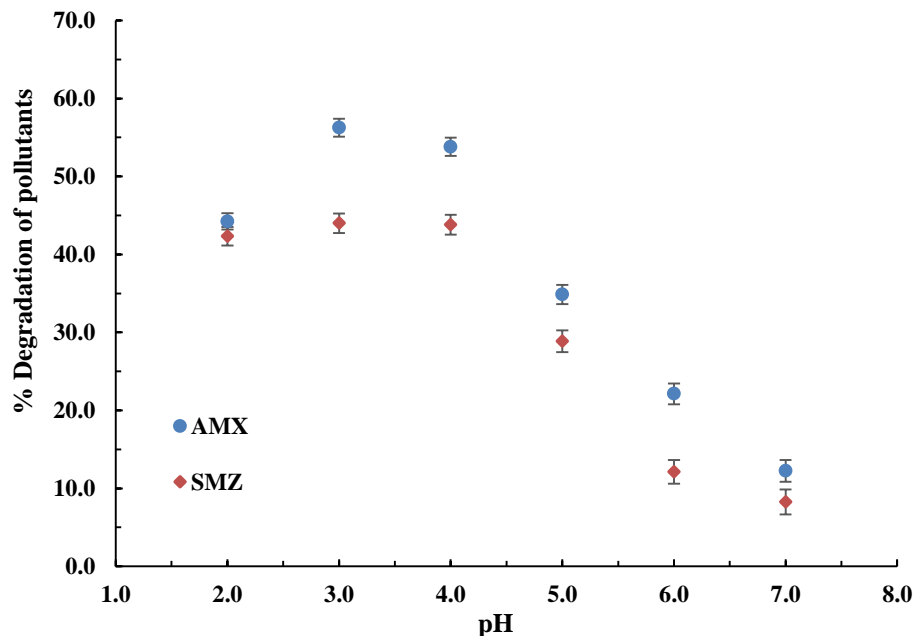
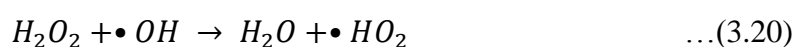


Figure 3.20: Degradation (%) of AMX and SMZ at different pH values under a dark environment [Catalyst dose = 300.0 mg/L; H₂O₂ dose (30%) = 0.2 mL/L; [Pollutant] = 2.0 mg/L; Reaction time = 2 hrs].

3.3.2 Effect of initial H₂O₂ dosage and nanocomposite dosage

The optimal dosage of hydrogen peroxide is a critical parameter for optimizing and maximizing degradation efficiency in the Fenton-like processes. Therefore, to monitor the effect of H₂O₂, different doses of H₂O₂ (30% v/v) (i.e., 0.1 to 0.2 mL/L) were employed at constant nFLC dose (300.0 mg/L), pollutant concentrations (2.0 mg/L), and pH (pH 3.0) (Cf figure 3.21(a & b)). The experiments were performed for each pollutant inside a dark box. With an increase in hydrogen peroxide dose from 0.01 mL/L to 0.2 mL/L, the degradation efficiency of AMX was slightly increased from *ca.* 54% to 56%. Further increase of peroxide dose >0.1 mL/L, had caused a slight decrease in the degradation efficiency. On the other hand, by increasing the H₂O₂ dose from 0.1 mL/L to 0.15 mL/L, the degradation efficiency of SMZ was almost constant, i.e., 43-44%. However, a further increase in H₂O₂ doses led to a significant decrease in the elimination efficiency of SMZ. Results inferred that an increase in H₂O₂

concentrations favors the generation of hydroxyl free radicals ($\bullet\text{OH}$ radicals). However, with much increase in H_2O_2 concentrations, the degradation percentage of these pollutants was decreased because hydrogen peroxide reacts with $\bullet\text{OH}$ radicals, producing water (H_2O) and hydroperoxyl radical ($\bullet\text{HO}_2$), as shown in Equation (3.20). As a result, the reactive $\bullet\text{OH}$ radicals were readily consumed before taking part in the Fenton-oxidation reaction (Hassan et al., 2020; Sétifi et al., 2019). Furthermore, Fida et al. (Fida et al., 2017) mentioned that the $\bullet\text{HO}_2$ radicals quench the $\bullet\text{OH}$ radicals.



Similarly, the nanocatalyst dosages (100.0 to 300.0 mg/L for AMX and SMZ) were studied to eliminate these pollutants under the Fenton-like process (Cf figure 3.21 (c & d)). The H_2O_2 amount, pollutant concentrations, and pH values of the solution were kept constant, i.e., H_2O_2 dose = 0.2 mL/L, pollutant concentrations (2.0 mg/L), and pH (pH 3.0). The degradation efficiency was increased by increasing the nanocatalyst dosages to the optimal dose of 300.0 mg/L for AMX and 250.0 mg/L for SMZ. The increase of the nanocatalyst amount provides enhanced available active sites at the catalyst surface, which favors the degradation efficiency. However, the percentage degradation of AMX and SMZ was decreased, increasing the dosages of Ben@(CuNPs+AgNPs) nanocatalyst (dose > 300.0 mg/L for AMX and dose > 250.0 mg/L for SMZ). The negative effect on the degradation of these pollutants at higher dosages of nanocatalysts was because of the scavenging effect, in which the generated $\bullet\text{OH}$ radicals are consumed by the excess catalysts' active sites (Hassan and Hameed, 2011). Similar findings were reported in the Fenton-like degradation of diethylene phthalate utilizing zero-valent copper (ZVC) (Wen et al., 2014b). Kurian et al. (Kurian and Sugunan, 2006) also observed that a minimum amount of catalyst is required for fast Fenton-like reactions to occur in the Fenton-like degradation of phenol.

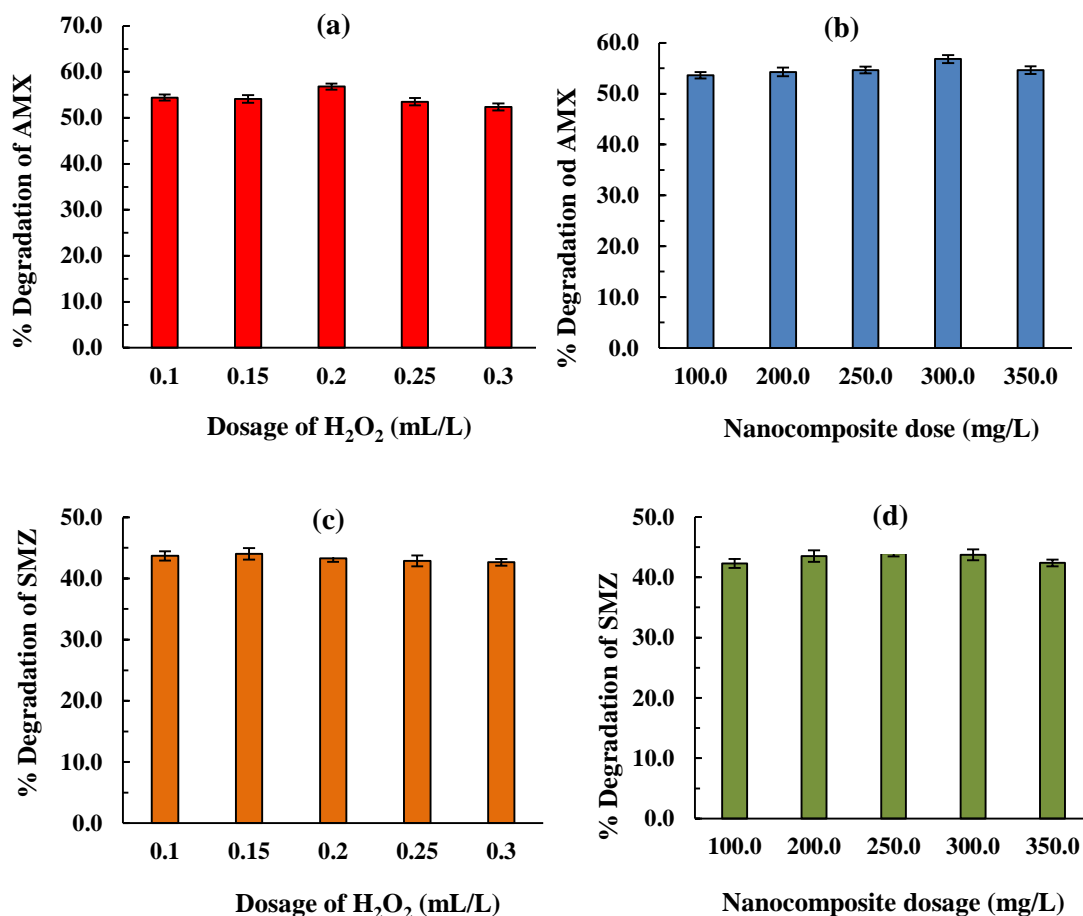


Figure 3.21: Percentage degradation of (a) AMX and (c) SMZ at different dosages of H₂O₂ in a dark environment under reaction condition as [pH = 3.0; [Pollutant] = 2.0 mg/L; Catalyst dose = 200.0 mg/L; Reaction time = 2 hrs]; Percentage degradation of (b) AMX, & (d) SMZ at different dosages of nanocatalyst in a dark environment under reaction condition as [pH = 3.0; [Pollutant] = 2.0 mg/L; peroxide dose = 0.2 ml/L; Reaction time = 2 hrs].

3.3.3 Photo-Fenton-like degradation of AMX and SMZ

The preoptimized conditions were utilized to investigate the elimination of AMX and SMZ under the photo-Fenton-like process utilizing the LED visible and UV-A light sources. It was observed that light irradiation synergized the removal efficiency of these two pollutants (*Cf* Figure 3.22). The comparison of the disappearance of AMX

and SMZ as a function of reaction time under different light environments is shown in Figure 3.22. The elimination efficiency of both pollutants followed the order: (Fenton-like/ UV-A) > (Fenton-like/ LED) > (Fenton-like/Dark). The photon energy stimulates the formation of •OH radicals (Sapach and Viraraghavan, 1997) as shown in (Eq. 3.21):



Under UV-A and LED (visible) light, the Fenton-like degradation of AMX (2mg/L) employing Ben@(CuNPs+AgNPs) nanocatalyst reached 84% and 72%, respectively, whereas, in the dark, the degradation percentage was only 56%. Similarly, the Fenton-like degradation of SMZ employing Ben@(CuNPs+AgNPs) nanocatalyst reached *ca.* 74% and 61% in UV-A and LED light, respectively, whereas the degradation, was only 44% in the absence of light. These results inferred that a slight increase in degradation of these two pollutants occurred in the UV-A light compared to the LED light illumination. However, LED light also synergizes the photo-Fenton-like process to a greater extent to achieve high percentage removal of these two pollutants.

The catalyst efficiency relates to the electron-hole pair reactions in the oxygenated environment or the rate of recombinations. The activity is improved by increasing the intensity of irradiated light, having energy roughly equal to or greater than the band gap energy or threshold energy. Free radicals are created when these electron-hole pairs interact with the substrate. The band gap energy of the catalyst was significantly reduced in the presence of noble metal nanoparticles, which favored the excitation of the catalyst at lower photon energy (Al-Hamdi et al., 2017; Tahir et al., 2020). On the other hand, *ca.* 41% and 39% degradation was obtained for the AMX and SMZ, respectively, utilizing the Ben@CuNPs nanocatalyst in a dark environment. These results inferred that the inclusion of Ag(NPs), enhanced the degradation efficiency significantly. It was previously reported that an acidic pH favors the formation of •OH radicals (He et al., 2014). The formation of complexes between the catalyst's surface and H₂O₂ results in the generation of •OH radicals. The photolysis of H₂O₂ is aided by light energy, which enhances the catalytic activity in the photo-

Fenton process with an increase in iron leaching from the nanocomposite (Sétifi et al., 2019).

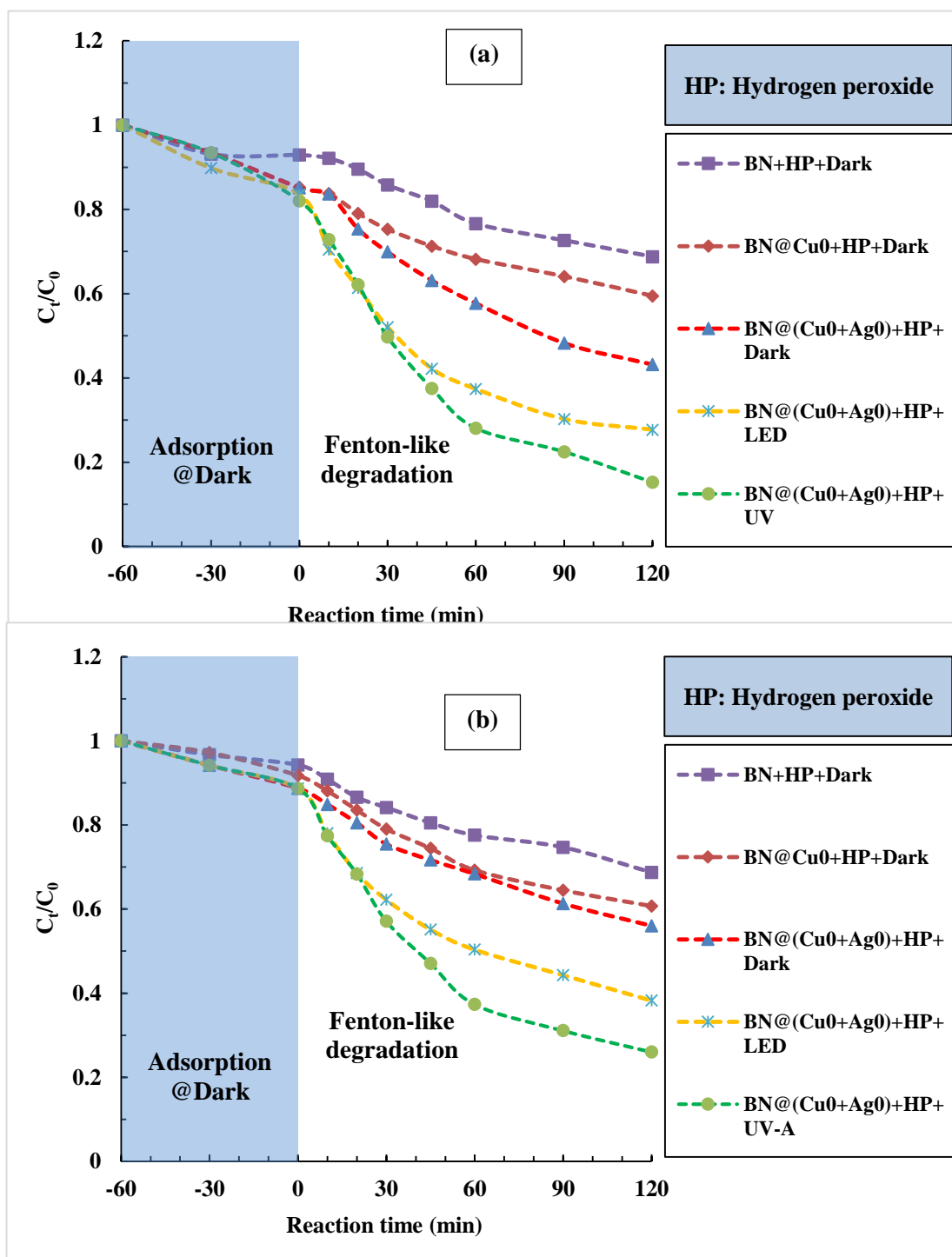


Figure 3.22. Removal of (a) AMX [pH = 3.0; [AMX] = 2.0 mg/L; catalyst dose = 300.0 mg/L; H₂O₂ dose = 0.2 mL/L; reaction time = 2 hrs]; and (b) SMZ [pH = 3;

[SMZ] = 2.0 mg/L; catalyst dose = 250.0 mg/L; H₂O₂ dose = 0.15 mL/L; reaction time = 2 hrs] vs. reaction time (min) at different reaction conditions in the photo-Fenton-like reactions.

3.3.4 Concentration dependence removal of AMX and SMZ

The effect of the initial concentration of pollutants on the degradation efficiency of the Ben@(CuNPs+AgNPs) nanocatalyst was studied. The pollutant concentration was increased from 2.0 to 20.0 mg/L (for AMX) and 2.0 to 15.0 (for SMZ) in the photo-Fenton-like process.

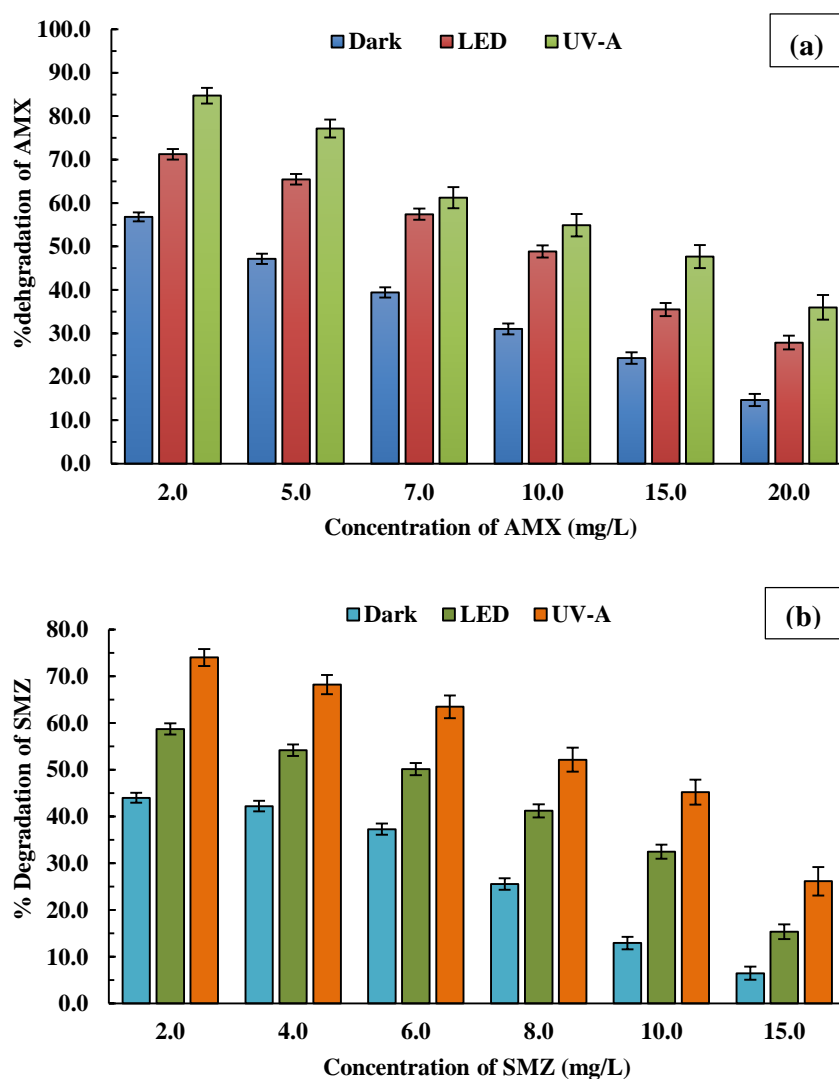


Figure 3.23: Percentage degradation vs initial concentration of (a) AMX [pH= 3.0; Catalyst dose = 300.0 mg/L; H₂O₂ dose = 0.2 mL/L; Reaction time = 2 hrs] & (b) SMZ

[pH= 3.0; Catalyst dose = 250.0 mg/L; H₂O₂ dose = 0.15 mL/L; Reaction time = 2 hrs] in different light ambiance.

Figure 3.23 depicts the percentage efficiency of nanocatalysts as a function of pollutant concentrations under varied conditions, i.e., dark, LED light, and UV-A light. Quantitatively, with increasing AMX concentration from 2.0 mg/L to 20.0 mg/L, the degradation percentage was decreased from 84% to 35% in the Fenton-like treatment under UV-A irradiation, whereas under LED irradiation, the degradation percentage was reduced from 71% to 27%. Similarly, raising the SMZ concentration from 2.0 mg/L to 15.0 mg/L lowered the degradation percentage from 74% to 26% in the Fenton-like treatment under UV-A irradiation. For a similar decrease in SMZ concentration, the degradation percentage decreased from 58% to 15% under LED irradiation. The decrease in degradation percentage in both cases with AMX and SMZ at higher pollutant concentrations explained that a relatively lesser number of active sites are accessible on the nanocatalyst surface for many pollutant species. Hence, lesser degradation efficiency was recorded at increased pollutant concentration (Sadeghi et al., 2019). Additionally, excess pollutants molecules on the surface of the nanocomposite and occupying the active sites, restrict the leaching of copper and silver nanoparticles, which reduces the number of hydroxyl radicals generated in the vicinity of the surface. Therefore, increasing pollutant concentrations resulted in a drop in degradation efficiency.

3.3.5 Presence of other cations/anions

Coexisting cations/anions (organic and inorganic) are quite prevalent in natural water samples. As a result, the tests were performed to assess the simultaneous presence of a few cations, viz., lead, cadmium, copper, nickel, and anions, such as phosphate, glycine oxalate, and sulfate in the photo-Fenton-like degradation of targeted pollutants. A comparative elimination of pollutants was obtained under UV-A and LED light irradiations and optimal reaction conditions. The concentrations of pollutant and cations/anions concentrations were taken at 2.0 mg/L and 10.0 mg/L, respectively.

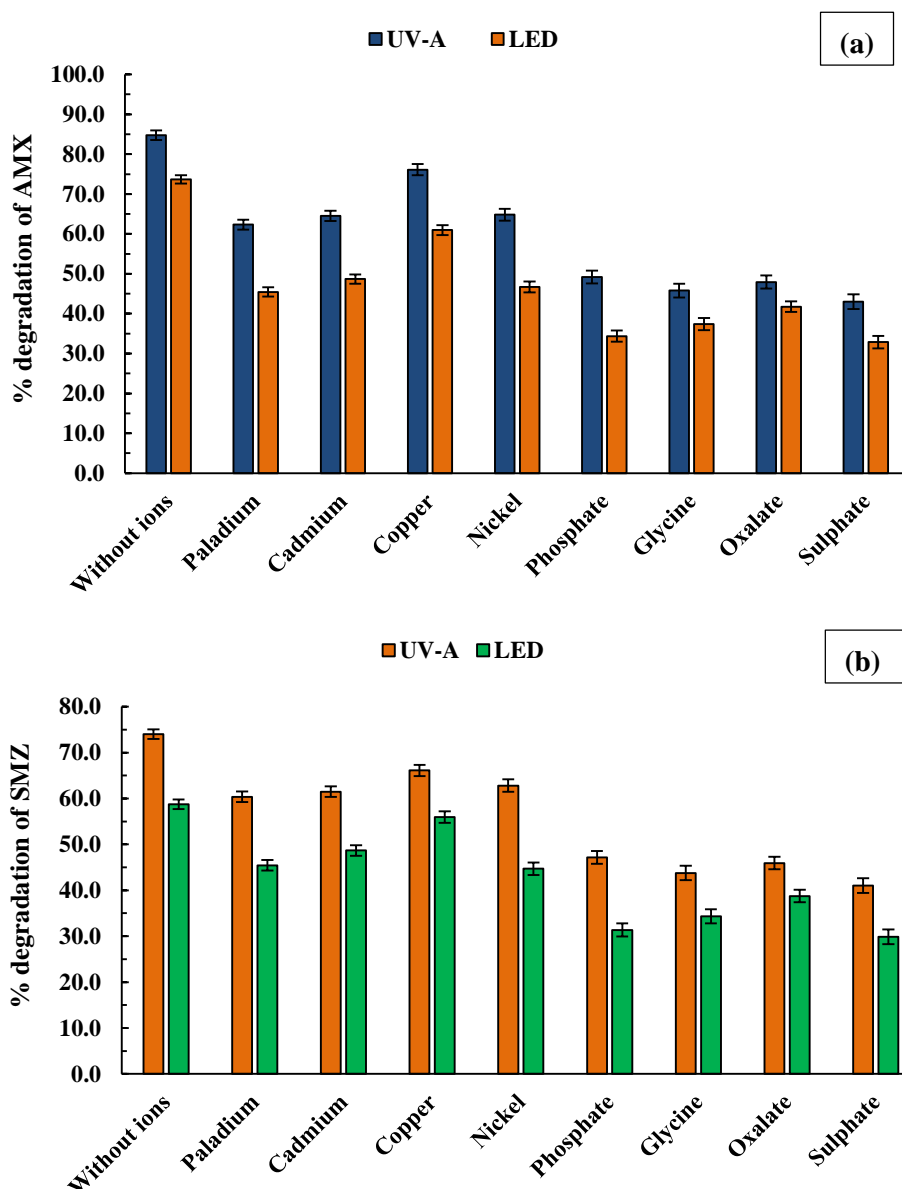


Figure 3.24: Effect of coexisting ions in different light conditions for (a) AMX [pH = 3.0; [AMX]= 2.0 mg/L; [Co-existing ion] = 10.0 mg/L; Catalyst dose = 300.0 mg/L; H₂O₂ dose = 0.2 mL/L; Reaction time = 2 hrs] & (b) SMZ [pH = 3.0; [SMZ]= 2.0 mg/L; [Co-existing ion] = 10.0 mg/L; Catalyst dose = 250.0 mg/L; H₂O₂ dose = 0.15 mL/L; Reaction time = 2 hrs].

Figure 3.24 shows the degradation efficiency of nanocatalysts in the removal of AMX and SMZ in the presence of various ions. In general, the presence of cations/or anions affected the percentage elimination of these two pollutants; however, the degradation of AMX and SMZ was affected significantly in the presence of phosphate,

oxalate, glycine, and sulfate. The decrease in degradation efficiency of pollutants is mainly because of two factors: the coexisting ions demonstrate competitive sorption towards the catalyst surface, preventing the target pollutant from aggregation and degradation at the catalyst surface; and second, some ions or compounds, such as sulfate, are known to be effective $h^+/\bullet OH$ quenchers, posing a degradation barrier (Lalliansanga et al., 2020; Selvam et al., 2007). Furthermore, anions are generally effective complexing/chelating agents. These anions are more likely to react and form complexes with copper/silver, leached out from the Ben@(CuNPs+AgNPs) catalyst and diffused into the bulk of the solution. As a result, reduced formation of $\bullet OH$ radicals prevented the degradation efficiency.

3.3.6 Degradation kinetics of AMX and SMZ

Kinetic studies are challenging because the Fenton or Fenton-like reactions are complex. The multiple steps are involved in the Fenton or Fenton-like processes, and each may regulate the reaction pathways and hence, controls the rate of reaction. However, the interaction between the degraded component and $\bullet OH$ radicals is the key reaction for determining the overall rate constant (Mitsika et al., 2013b). Both pseudo-first-order (PFO) and pseudo-second-order (PSO) kinetic models were employed to study the degradation kinetics based on the empirical data fitting (Butt et al., 2021).

The plots are presented in Figure 3.25 for the PSO and PFO models. Using the pseudo-first-order kinetic model, the optimum reaction constant K_f and R^2 value for AMX degradation utilizing the Ben@(CuNPs+AgNPs) nanocomposite were $7.60 \times 10^{-3} \text{ min}^{-1}$ and 0.9022, respectively. The reaction constant K_s and R^2 values in the pseudo-second-order kinetic model were $0.0192 \text{ L}\cdot\text{min}^{-1}\cdot\text{mg}^{-1}$ and 0.9753, respectively. Similarly, in the case of SMZ, the optimum PFO reaction constant K_f and R^2 values were $5.70 \times 10^{-3} \text{ min}^{-1}$ and 0.8622, whereas the PSO rate constant K_s and R^2 values were $0.0123 \text{ L}\cdot\text{min}^{-1}\cdot\text{mg}^{-1}$ and 0.9891. Based on the R^2 values, the results revealed that the kinetic data suited well to the PSO model than the PFO model.

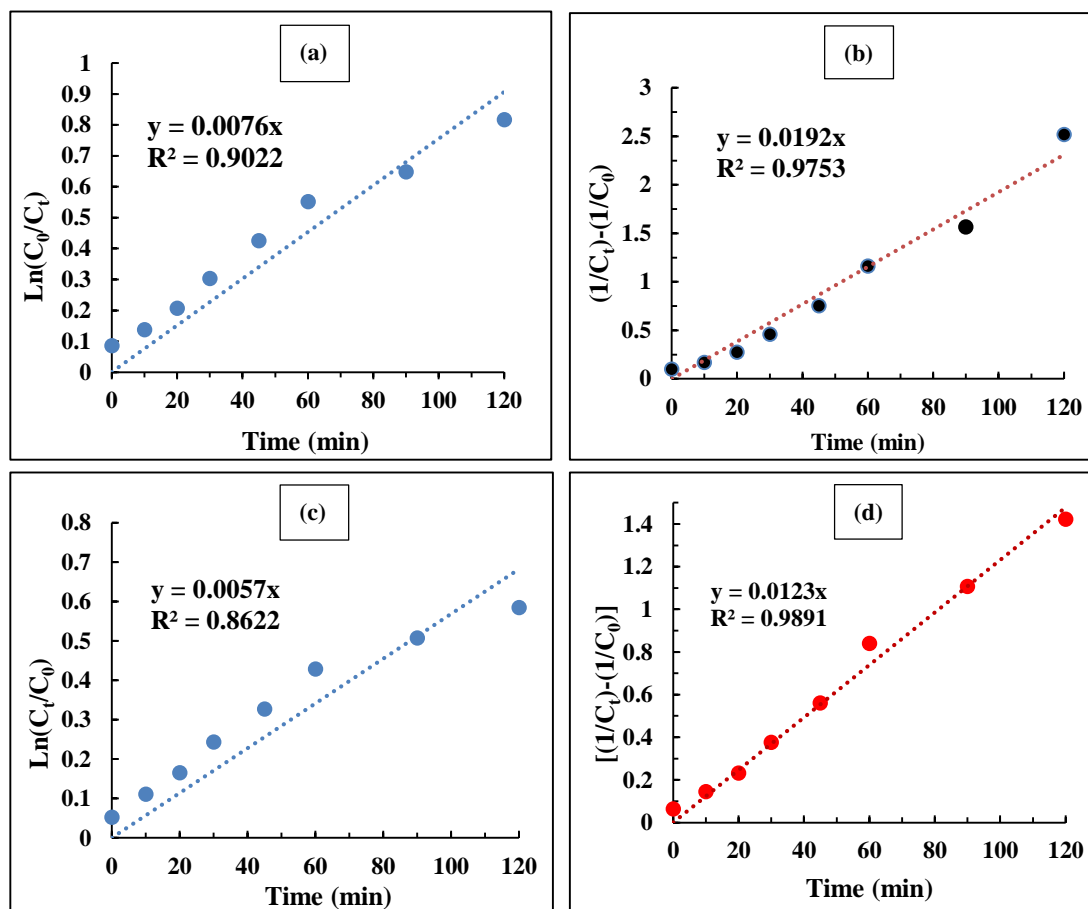


Figure 3.25: The kinetics of AMX [(a) and (b)] and SMZ [(c) and (d)] degradation using the PFO; and PSO models.

3.3.7 Involvement of $\bullet\text{OH}$ radical

The role of hydroxyl radicals in the bond cleavage of AMX and SMZ is investigated using the $\bullet\text{OH}$ radical quenchers. Isopropanol and HCO_3^- quench the $\bullet\text{OH}$ radicals (Lalliansanga, Tiwari, Tiwari, Shukla, Shim, et al., 2020; A. Tiwari et al., 2018b) effectively. The reactive oxygen species (ROS), or singlet oxygen created by the interaction of $\bullet\text{O}_2^-$ radicals with photo-generated holes, are quenched by sodium azide (NaN_3). The singlet oxygen's extremely reactive behavior against organic compounds in an aqueous medium was demonstrated elsewhere (Barka et al., 2010). To confirm the participation of $\bullet\text{OH}$ radicals in the photo-Fenton-like degradation of 2.0 mg/L of both targeted pollutants was conducted in the presence of 1.0 mL (0.1 mol/L) isopropanol, HCO_3^- , and NaN_3 . Figure 3.26 depicts the elimination of AMX

and SMZ in the presence of these quenchers under the photo-Fenton-like process under UV-A light. These quenchers considerably suppressed the removal of AMX and SMZ in the removal process. The isopropanol, sodium bicarbonate, and sodium azide showed the involvement of $\bullet\text{OH}$ and $\bullet\text{O}_2^-$ radicals in the degradation process during the photocatalytic degradation of Alizarin Yellow using [Au(NPs) or Ag(NPs)]/TiO₂ thin film (Lalliansanga et al., 2020c; Lalliansanga et al., 2020).

Moreover, Hofmann et al., (Hofmann and Andrews, 2006) showed that bicarbonates quench the $\bullet\text{OH}$ radicals. The presence of bicarbonate effectively transforms the $\bullet\text{OH}$ radicals into less active OH^- ions. In the present investigation, there was a significant decrease in the percentage degradation of the targeted pollutants in quenchers such as isopropanol and HCO_3^- . However, it was found that sodium azide showed considerably less impact than the isopropanol and HCO_3^- quenchers, indicating that the $\bullet\text{OH}$ radicals are the principal reactive species implicated in the degradation of AMX and SMZ (Cf Figure 3.26).

Therefore, these pharmaceuticals' probable Fenton-like degradation mechanisms are suggested as follows: the pollutant molecules adsorb onto the catalyst surface of Ben@(CuNPs+AgNPs). At the nanocatalyst interface, Cu^{2+} or Ag^+ ions leach out from the catalyst's surface, which accelerates the breakdown of H_2O_2 . H_2O_2 produces hydroxyl radicals and causes the cleavage of pollutant molecules' unsaturated double bonds. Hydroxyl radicals break down the macromolecule-conjugated system into intermediates (Wu et al., 2015). Intermediates are readily mineralized as CO_2 and H_2O . Further, the TOC analyzer measures the apparent mineralization of organic pollutants (OP) at the end of the reaction process.

a) Adsorption:



b) Generation of $\bullet\text{OH}$ radical:





c) Photo decomposition of H_2O_2 :



d) $\bullet OH$ radicals attack the pollutant on the catalyst surface:

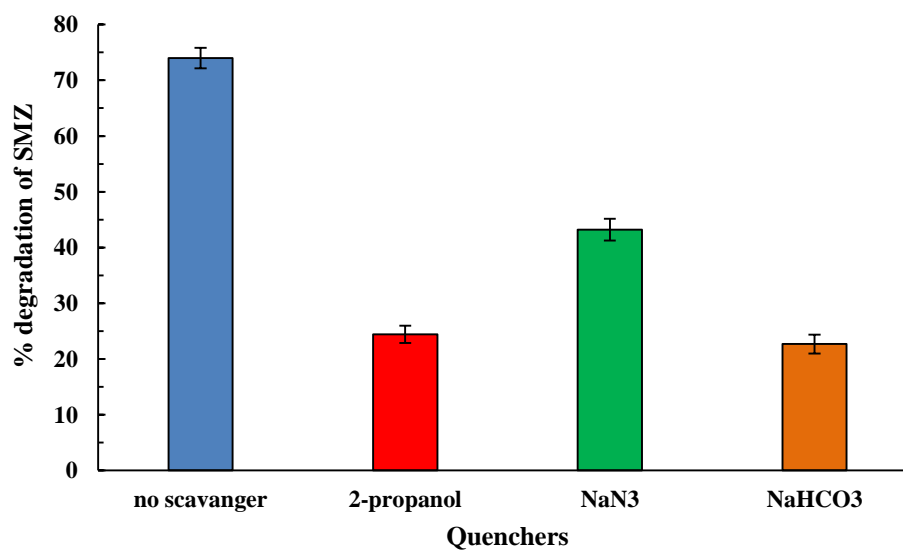
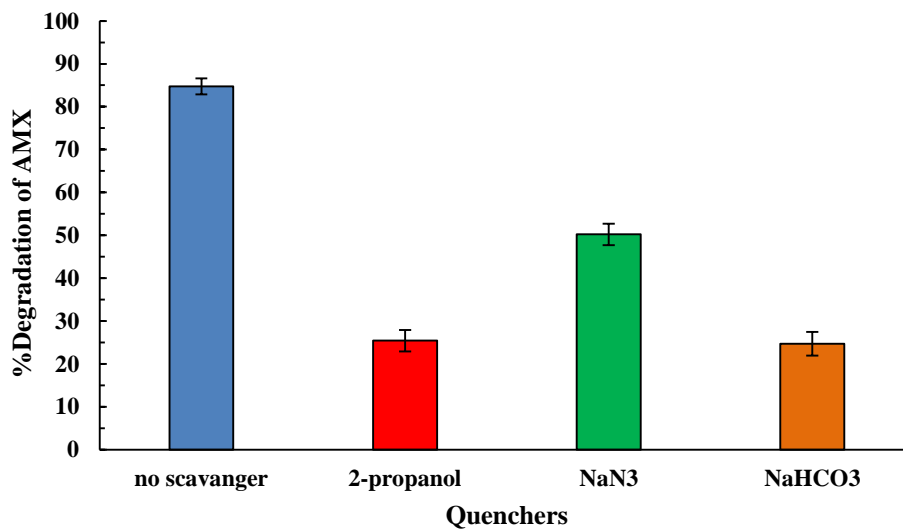
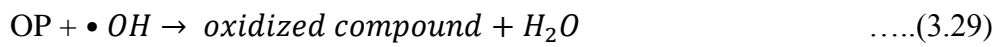


Figure 3.26: Effect on percentage degradation in the presence of scavengers [pH = 3.0; [pollutant] = 2.0 mg/L; [scavenger] = 0.1 mol/L (10 mL/L); Catalyst dose = 300.0 mg/L for AMX and 250.0 mg/L for SMZ; H₂O₂ dose = 0.2 mL/L for AMX and 0.15 mL/L for SMZ; Reaction time = 2 hrs].

3.3.8 Mineralization of target organic pollutants

Using the Ben@(CuNPs+AgNPs) nanocatalyst under LED and UV irradiations for two hours, the investigation was carried out to determine the percentage of mineralization of AMX and SMZ in the photo Fenton-like degradation. The NPOC (Non-Purgeable Organic Carbon) data were obtained for the treated and untreated samples, which enabled the percentage mineralization of SMX and SMZ.

Figure 3.27(a & b) depicted the results, demonstrating that as pollutant concentrations increased, the percentage mineralization of both pollutants decreased significantly. Moreover, the mineralization efficiency in the presence of UV-A light was slightly higher than the LED light-stimulated degradation. Under UV-A light irradiation, 66% mineralization was accomplished at an AMX concentration of 2.0 mg/L, whereas 53% mineralization was recorded using the LED light. Similarly, 62% of SMZ was mineralized at the concentration of SMZ 2.0 mg/L under UV-A irradiation, whereas LED light irradiation achieved 52% mineralization of SMZ. Overall, the results showed the photo-Fenton-like process utilizing the Ben@(CuNPs+AgNPs) nanocatalyst mineralizes a considerable amount of AMX and SMZ in aqueous solutions. In 10 mM H₂O₂ and 8W UV-C light, Feng et al. (J. Feng et al., 2006) showed roughly 50-60% mineralization of 0.2 mM orange II dye utilizing bentonite clay supported nZVI. Similarly, bentonite-supported superparamagnetic MnFe₂O₄ nanoparticles achieve 70% mineralization of oxytetracycline (1×10^{-4} mol dm⁻³) in 8 hrs (Gautam et al., 2017). Therefore, the novel Ben@(CuNPs+AgNPs) nanocomposite is promising for the degradation of both pollutants, as it mineralizes a significant amount of AMX and SMZ in aqueous solutions.

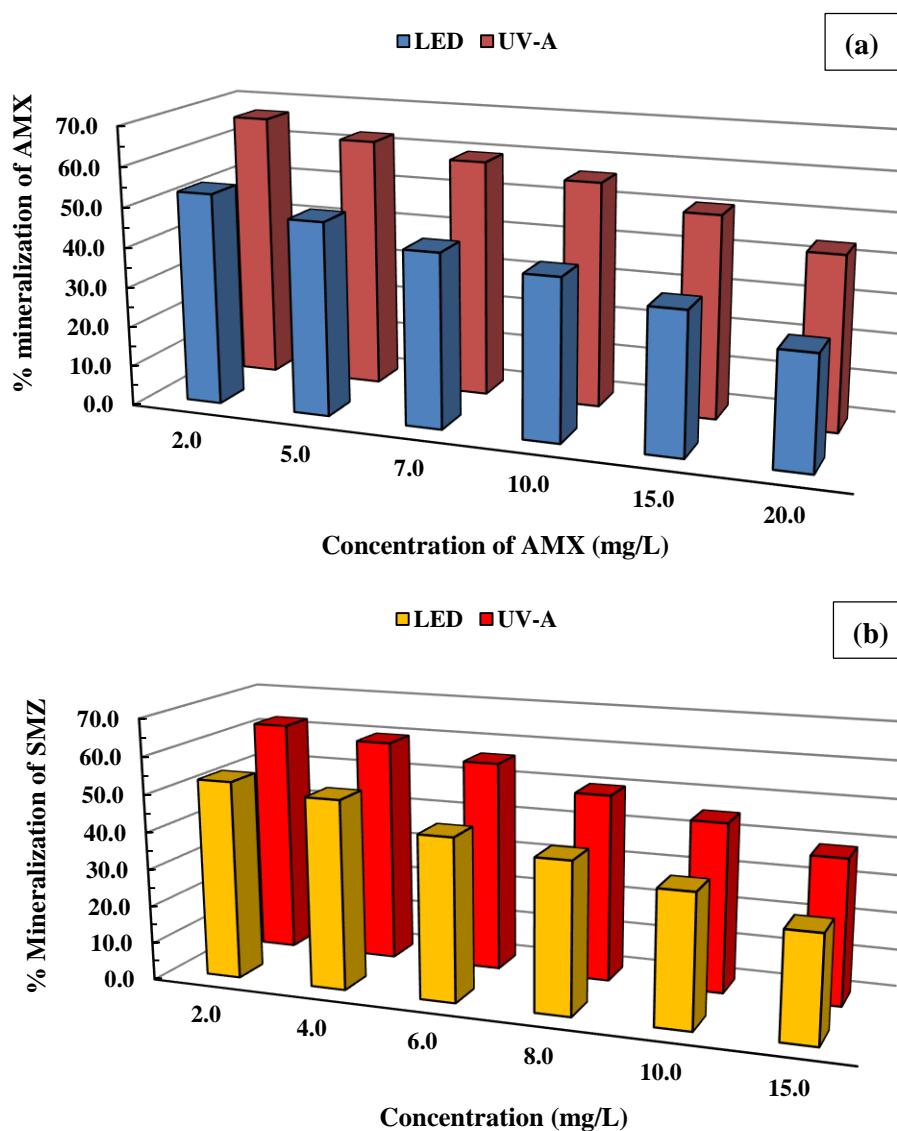


Figure 3.27: Mineralization (%) at different concentrations of (a) AMX [pH = 3.0; Catalyst dose = 300.0 mg/L; H₂O₂ dose = 0.2 ml/L; Reaction time = 2 hrs] and (b) SMZ [pH = 3.0; Catalyst dose = 250.0 mg/L; H₂O₂ dose = 0.15 ml/L; Reaction time = 2 hrs].

3.3.9 Determination of leached copper (II) concentrations

The elimination of AMX and SMZ in an aqueous medium under the photo-Fenton-like reactions using the Ben@(CuNPs+AgNPs) is associated with Cu²⁺ formation during the reaction process. The AAS [LOD= 10.0 µg/L] calculates the quantity of

Cu(II) corroded from the nFLCs and leached into the mixture. The participation of Cu^{2+} and H_2O_2 is the central notion of the Fenton process. The concentration of Cu^{2+} increases as leaching advances, and the Fenton-like reaction of $\text{Cu}^+/\text{Cu}^{2+}$ with H_2O_2 generates $\bullet\text{OH}$ radicals. In a heterogeneous system, the presence of H_2O_2 with Cu(NPs) or Ag(NPs) in Ben@(CuNPs+AgNPs) nanocatalyst is a primary source of reactive oxygen species generation.

The C_t/C_0 (C_t stands for concentration of the pollutant at time t and C_0 stands for the initial concentration of the pollutant) values for the elimination of both pollutants, on the other hand, are displayed in Figure 3.28. Copper leaching is closely connected with time-dependence removal and higher copper leaching results in enhanced removal of both target pollutants. The novel Ben@(CuNPs+AgNPs) nanocatalyst was evaluated for Cu(II) leaching during the degradation of 2.0 mg/L AMX and SMZ contaminants. After two hours of reaction time, a maximum of 77.0 $\mu\text{g/L}$ and 75.0 $\mu\text{g/L}$ of Cu(II) were leached out in AMX and SMZ-contaminated aqueous systems. Therefore, the catalyst Ben@(CuNPs+AgNPs) demonstrated potential in photo-Fenton-like processes due to significantly less copper leaching.

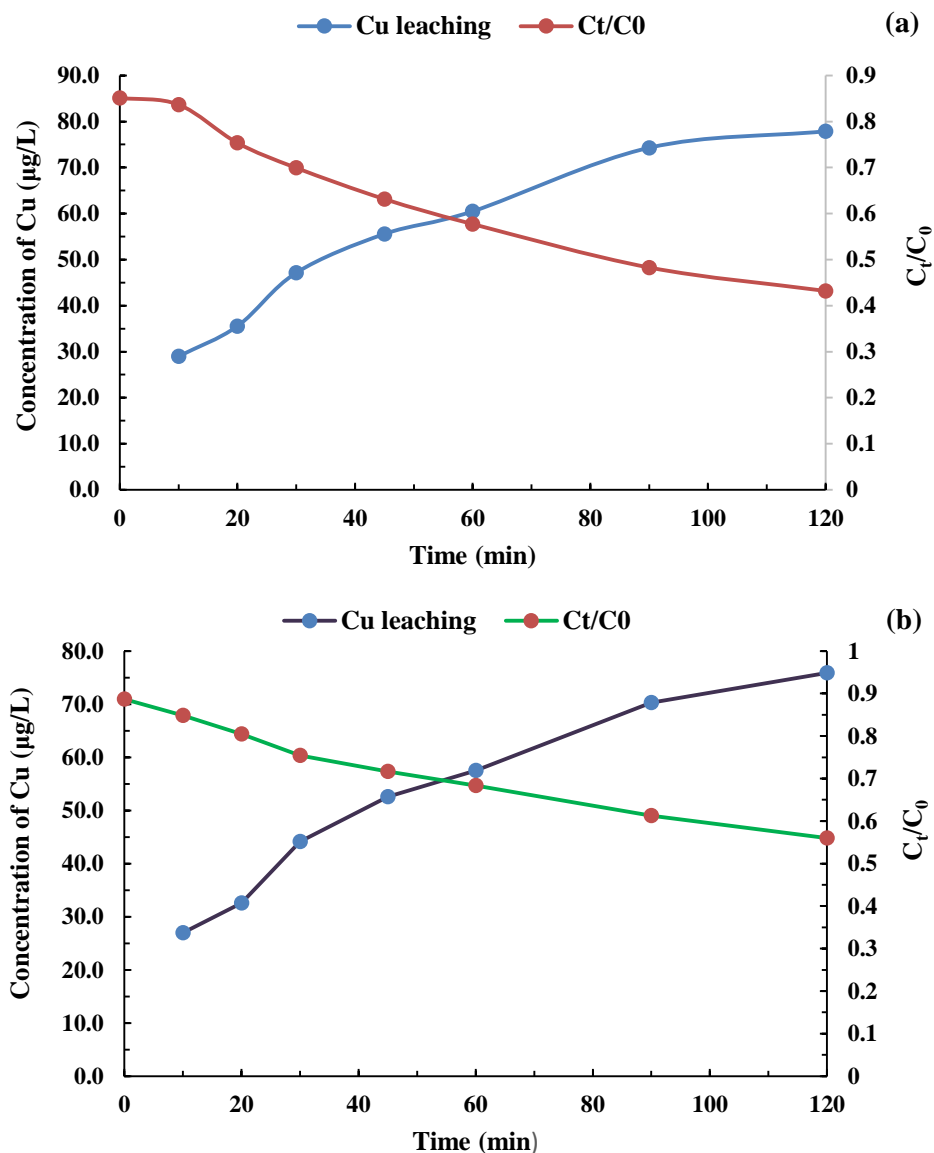


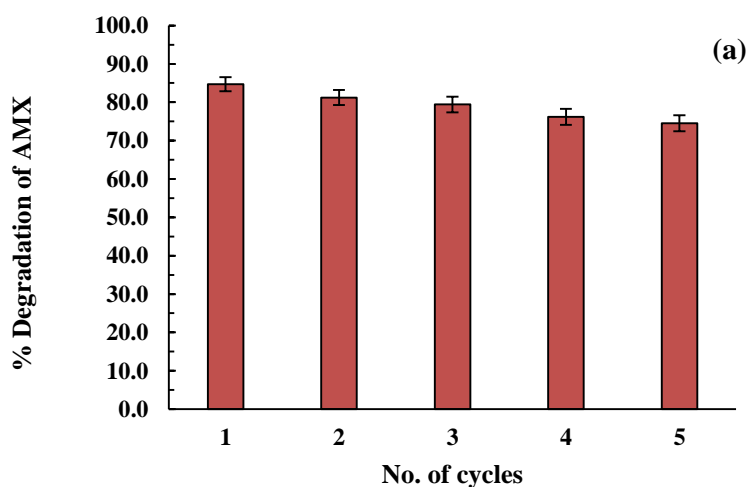
Figure 3.28: Leaching of copper concentration along with the disappearance of (a) AMX [pH = 3.0; Catalyst dose = 300.0 mg/L; H_2O_2 dose = 0.2 mL/L; Reaction time = 2 hrs] and (b) SMZ [pH = 3.0; Catalyst dose = 250.0 mg/L; H_2O_2 dose = 0.15 mL/L; Reaction time = 2 hrs] as a function of time.

3.3.10 Reutilization of the nanocatalyst

Reusability and stability are two crucial characteristics of a catalyst from a practical perspective. The practical implacability of nanocatalysts is determined by their stability, specifically their ability to be reused in repeated photo-Fenton-like

reactions. To ascertain the reusability of the Ben@(CuNPs+AgNPs) nanocatalyst in the photo-Fenton-like degradation of AMX and SMZ, experiments are conducted for five repeated runs.

The results of the reusability of the Ben@(CuNPs+AgNPs) nanocatalyst for the degradation of both the target pollutants were shown in figure 3.29. Under UV-A irradiation, the degradation efficiency was investigated while maintaining optimal reaction conditions, such as for AMX: pH = 3.0, catalyst dose = 300.0 mg/L, H₂O₂ dose = 0.2 mL/L, and reaction duration = 2 hrs and for SMZ: pH = 3.0, catalyst dose = 250.0 mg/L, H₂O₂ dose = 0.15 mL/L, and reaction duration = 2 hrs. In removing these pollutants for subsequent processes, the results revealed a slight drop in the removal efficiency. At the end of the fifth cycle of operation, the removal percentage of AMX dropped from 84% to 74%, whereas the efficiency of SMZ decreased from 74% to 63%, only. The results demonstrated that the photo Fenton-like process allowed a little copper content loss during oxidation cycles, which enables the use of the catalyst for a longer duration and more cycles of operations. A comparable catalyst, Fe₃O₄ particles doped with Zn pillared bentonite, was used to treat landfill leachate (Ma et al., 2018), and the reusability test revealed a decrease in mineralization percentage. Similarly, a bentonite-supported catalyst was used, and the catalyst showed stability in the Fenton-like destruction of Orange II (Li et al., 2016).



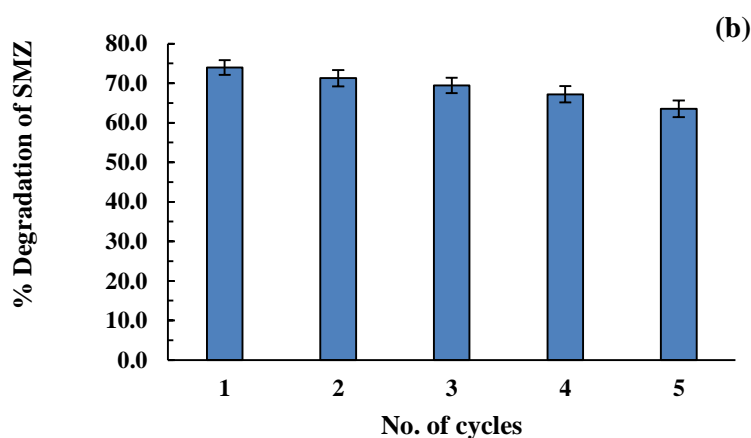
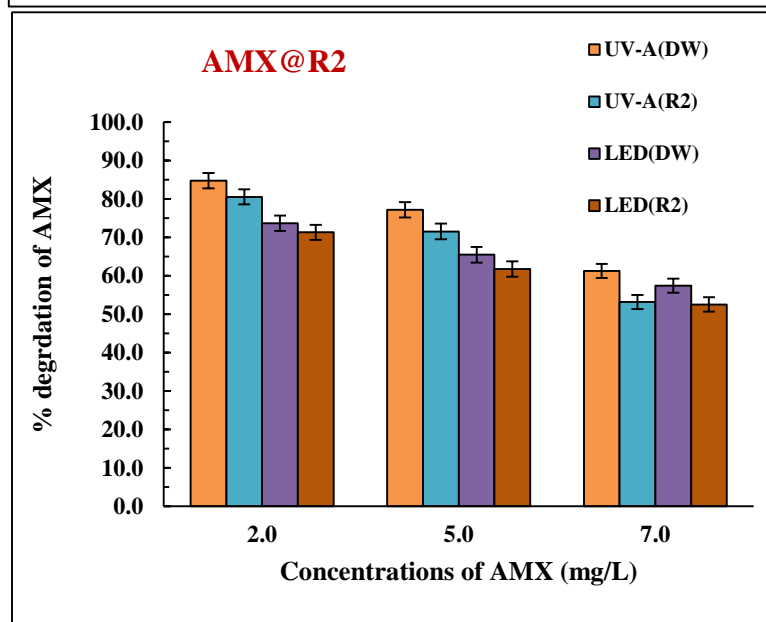
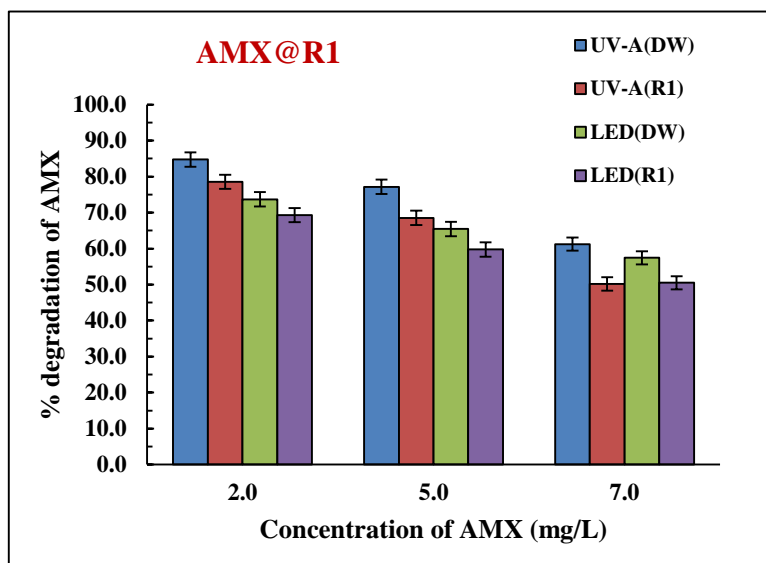


Figure 3.29: Reusability tests for Ben@(CuNPs+AgNPs) nanocatalyst in the degradation of (a) AMX and (b) SMZ

3.3.11 Real matrix water experiments

In the natural matrix treatment of AMX and SMZ, Ben@(CuNPs+AgNPs) nanocatalyst was used in the photo-Fenton-like processes. The experiments extend the possibility of scaling up the treatment process for AMX or SMZ-contaminated water. Furthermore, it enables an examination of nanocatalysts' appropriateness and selectivity in a real and complex matrix. Water samples were taken from two separate natural water sources and labeled R1 (natural stream water) and R2 (groundwater) (Mizoram University supply water tank). The supply water tank (R2) had a pH of 8.17, whereas the stream water sample (R1) had 7.8. Fe, Mn, Cu, Pb, Ni, and Zn were identified in trace amounts. However, the calcium level was relatively high in both water samples. Significant inorganic carbon (IC) and some non-purgeable organic carbon in both samples (NPOC) are present. Sulfate, phosphate, and nitrate concentrations in the R1 sample were 11.0 mg/L, 0.1 mg/L, and 1.97 mg/L, respectively. Similarly, the R2 sample contained 7.0 mg/L, 0.1 mg/L, and 20.0 mg/L sulfate, phosphate, and nitrate, respectively. The water samples were spiked with different concentrations of the pollutants, *viz.* (2.0, 5.0, and 7.0 mg/L) for AMX and (2.0, 4.0, and 6.0 mg/L) for SMZ while keeping the solution pH at 3.0. For AMX, the photo-Fenton-like processes were carried out using the Ben@(CuNPs+AgNPs)

nanocatalyst (300.0 mg/L) along with 0.2 mL/L H₂O₂ (35%), which was exposed to a UV-A and LED light for 2 hrs. Similarly, for SMZ, the photo-Fenton-like processes proceeded using 250.0 mg/L of Ben@(CuNPs+AgNPs) nanocatalyst and 0.15 mL/L H₂O₂ (35%). Figure 3.30 shows the percentage efficiency results compared to the blank (purified water) results. When comparing the two actual water samples to the distilled water, the percentage efficiency of both pollutants was not considerably affected. Quantitatively, the percentage degradation of AMX (2.0 mg/L) was decreased from 84% to 78% under UV-A light illumination and from 73% to 69% under LED light irradiation using the R1 water sample. Similarly, using the R2 water sample, the degradation of AMX (2.0 mg/L) was decreased from 84% to 80% under UV-A irradiation it dropped from 73% to 71% under the LED light environment. On the other hand, the degradation efficiency was decreased from 74% to 68% in the case of SMZ under UV-A illumination and from 58% to 55% under the LED light illumination using the R1 water sample. In the R2 water sample, the percentage degradation of SMZ decreased from 74% to 70% under UV-A irradiation and from 58% to 56% under LED irradiation. The reduction in the degradation of the pollutants using the actual matrix samples was due to the different physicochemical characteristics of water samples. However, despite the presence of several ions and a relatively high value of IC and TOC, the removal of AMX and SMZ was not significantly affected in the photo-Fenton-like process. These results further inferred the potential of nanocatalysts in the efficient removal of AMX and SMZ from aqueous solutions under the photo-Fenton-like process using visible (LED) or UV-A lights with enhanced suitability and selectivity.



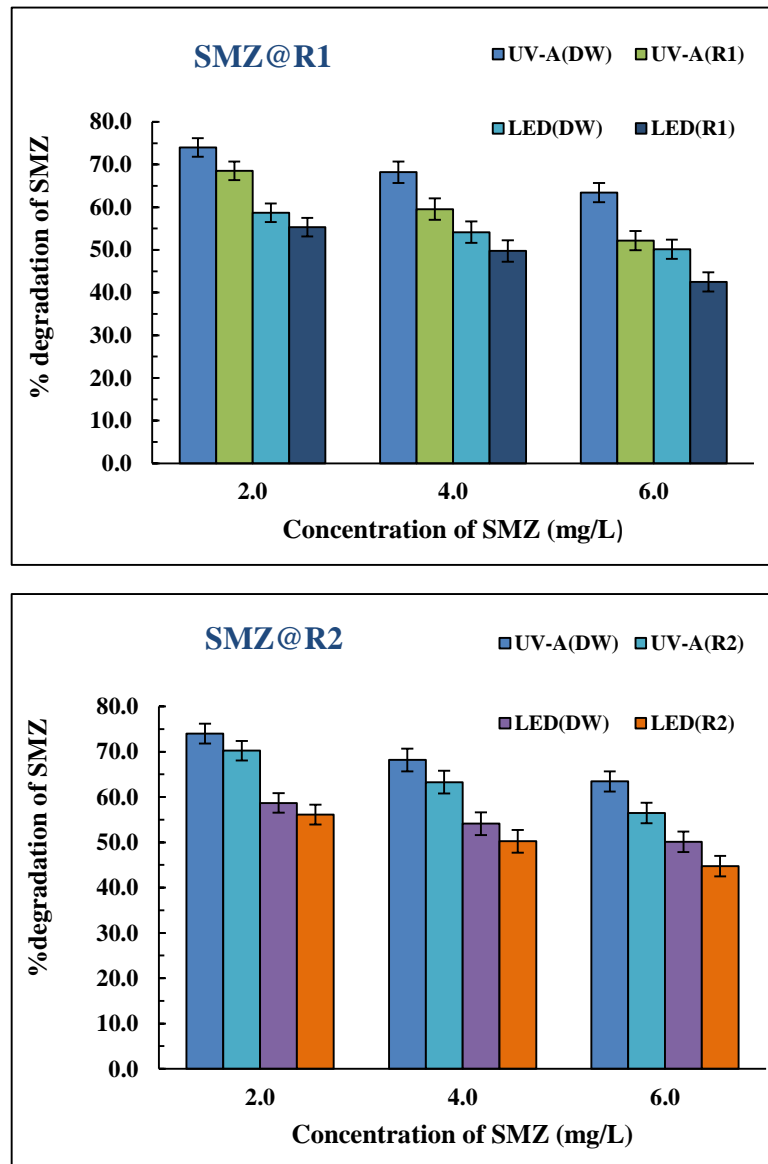


Figure 3.30: Photo Fenton-like degradation in the real water system for AMX [pH= 3.0; Catalyst dose = 300.0 mg/L; H₂O₂ dose = 0.2 mL/L; Reaction time = 2 hrs] and SMZ [pH= 3.0; Catalyst dose = 250.0 mg/L; H₂O₂ dose = 0.15 mL/L; Reaction time = 2 hrs].

CHAPTER 4
CONCLUSIONS

4. Conclusion

Waterbody contamination by emerging and enduring water pollutants is a serious environmental and health hazard. The aquatic environment is contaminated with several refractory organic chemicals. These contaminants are a serious hazard to both people and aquatic life. Due to their poor biodegradability and persistence, traditional wastewater treatment plants cannot effectively remove these contaminants. The Fenton, photo-Fenton, Fenton, and photo-Fenton-like processes are said to be among the prevalent AOPs (Advanced Oxidation Processes) that are found to be reasonably environment-friendly and promising methods for removing these contaminants from water bodies. Because of its low cost, easy processability, and scalability for small- to medium-scale renewable energy sources, the photo-Fenton-like process is consequently a useful approach. The introduction of nanotechnology paves newer dimensions to the Fenton processes. The use of nanomaterials showed widespread applications in wastewater treatment plants because of their high reactivity. Therefore, the primary goal of this research was to provide a straightforward, ecologically responsible process for synthesizing the novel bentonite-supported bimetallic heterogeneous nano-Fenton-like catalyst. The *in situ* nanoparticles, Fe⁰, Cu⁰, and Ag⁰, were produced using organic phytochemicals from *P. guajava* leaf extracts.

The nanocomposite materials were obtained in a facile and single-pot synthetic route. The Fe(NPs), Cu(NPs), and Ag(NPs) were synthesized *in situ* on the surface of the bentonite clay to obtain the novel composite materials, *viz.* (Ben@FeNPs, Ben@(FeNPs+AgNPs), Ben@CuNPs, and Ben@(CuNPs+AgNPs). Further, these materials were employed in the photo-Fenton-like degradation of some targeted micro-pollutants from aqueous solutions under batch studies. The materials were characterized by advanced analytical methods. The band gap energy of the materials was determined by converting the diffuse reflectance data into its adsorption coefficient (α) values using the Kubelka-Munk equation and Tauc's relationship. The diffuse reflectance spectra (DRS) for pristine bentonite along with all the modified nanocomposite materials, i.e. Ben@FeNPs, Ben@(FeNPs+AgNPs), Ben@CuNPs, and Ben@(CuNPs+AgNPs); were obtained using UV-Vis spectrophotometer. Band gap energies for Ben@FeNPs and Ben@(FeNPs+AgNPs) were 2.25 and 2.17 eV,

respectively, substantially lower than the 3.25 eV for pristine bentonite. Similarly, with a substantially lower band-gap energy (2.32 eV) than bentonite (3.25 eV), the catalyst Ben@(CuNPs+AgNPs) demonstrated its suitability for the visible-light-induced photo-Fenton-like reaction. The N₂ adsorption/desorption isotherms demonstrated that all of these solids have H3 hysteresis loops in their Type IV type isotherms. These findings demonstrated the presence of a mesoporous structure with a random pore-size distribution in the materials. Ben@FeNPs had pores that measured 91.086 cm³g⁻¹, whereas Ben@(FeNPs+AgNPs) had pores that measured 0.099 cm³g⁻¹. For bentonite, Ben@FeNPs, and Ben@(FeNPs+AgNPs), the corresponding BET-specific surface areas were 62.67, 36.50, and 8.61 m²g⁻¹. Additionally, the BET-specific surface areas for the Ben@CuNPs and Ben@(CuNPs+AgNPs) were 36.50 and 20.55 m²g⁻¹, respectively, whereas the pore diameters for the Ben@CuNPs and Ben@(CuNPs+AgNPs) were 13.02 nm and 5.86 nm, respectively. Ben@(FeNPs+AgNPs) XRD data exhibits distinctive diffraction peaks confirming the presence of Fe(NPs), Ag(NPs), along with quartz. The iron and silver nanoparticles were immobilized with bentonite according to the XRD measurements. According to the XPS data, the Ben@(FeNPs+AgNPs) solid has silver and iron in their zero-valent oxidation states. Similarly, in the case of Ben@(CuNPs+AgNPs) nanocomposite, the X-ray photoelectron spectroscopy and XRD analyses inferred the presence of zero-valent Cu and Ag in the nanocatalyst. The SEM images of bentonite revealed a heterogeneous and layered structure of each modified nanocomposite material. The surface has voids and uniform pores widely distributed on the surface. The bentonite, Ben@FeNPs, Ben@(FeNPs+AgNPs), Ben@CuNPs, and Ben@(CuNPs+AgNPs) nanocomposites showed a more dense surface structure, with the Fe, Cu, or Ag nanoparticles preferably occupying the pores. The EDX results revealed that these solids are contained the common elements of Si, Fe, Al, C, O, Na, K, Ti, etc. However, an additional peak of the Ag is obtained in the EDX spectrum of Ben@(FeNs+AgNPs), confirming the existence of Ag in the nanocomposite solid. The TEM image clearly demonstrated a specific distribution of nanoparticles on the surface of bentonite. The *in situ* generations of iron/silver nanoparticles, or copper/silver nanoparticles on the bentonite support media; enabled spatial distribution of nanoparticles that are not agglomerated on the surface. The average particle size of the Ben@(FeNPs+AgNPs)

nanocomposite was estimated to be around 10 nm. The d-spacing of Ag(NPs) was determined to be 0.1435 nm. The Ben@(CuNPs+AgNPs) nanocomposite showed a heterogenous surface structure, and the fringes indicated the d-values of 0.243 and 0.164 nm, respectively, for the Cu(NPs) and Ag(NPs). The calculated average particle size for the solids Ben@CuNPs and Ben@(CuNPs+AgNPs) was 4.207 nm and 2.518 nm, respectively.

Several physico-chemical parametric experiments are conducted to investigate the photo-Fenton-like degradation of micropollutants in order to get insight into the mechanisms involved in the degradation process. The nanocatalysts were utilized to degrade DCF, phenol and NNPT, AMX, SMZ in a photo-Fenton-like process under three different light environments (Dark, LED, and UV-A). The photo-Fenton-like process using the Ben@(FeNPs+AgNPs) nanocatalyst showed a very high percentage removal of DCF utilizing the LED (Visible) and UV-A light irradiations. The optimum reaction conditions i.e., pH~3; 250.0 mg/L Ben@(FeNPs+AgNPs) nanocatalyst dose; 0.4 mL/L of H₂O₂ (30%) provided 56% removal of DCF (2.0 mg/L) within 120 minutes of reaction time in dark conditions. Further, the UV-A and LED irradiations enhanced the degradation efficiency of the photo-Fenton-like process to 83% (UV-A) and 70% (LED) in the removal of DCF. Further, the photo-Fenton-like process enabled to mineralization of the DCF to 74% using the UV-A light in 2 hrs of reaction time. In 2 hrs of reaction time in a dark environment and under the optimum reaction conditions, 43.3% of phenol (2.0 mg/L) degradation was achieved. Moreover, the elimination efficiency was increased to 73.3% using UV-A and 60.0% using LED light irradiations. Similarly, in dark conditions, with the optimum reaction conditions, 72.7% elimination of 2.0 mg/L NNPT in 2 hrs was achieved. The degradation efficiency was increased to 95.1% (UV-A) and 84.9% (LED) using two different light sources. The reaction mechanism demonstrated that the •OH radical is predominantly involved in the reaction steps. A significant percentage of phenol and NNPT were mineralized in the photo-Fenton-like process i.e., 55.5% and 64.2%, of phenol and NNPT, respectively were mineralized utilizing UV-A irradiation. The degradation of these two pollutants followed pseudo-second-order reaction kinetics. Furthermore, the nanocatalyst showed significant stability in repeated catalytic operations conducted for 4 subsequent cycles. The catalyst showed reasonably high selectivity, and elimination

efficiency using the natural water sources in the photo-Fenton-like processes. Likewise, with the Ben@CuNPs, and Ben@(CuNPs+AgNPs) samples, the degradation of AMX and SMZ was conducted. Under UV-A, and LED (visible) light, the photo-Fenton-like degradation of AMX employing Ben@[CuNPs+AgNPs] nanocatalyst was obtained at 84% and 72%, respectively, whereas, in the dark, 56% degradation occurred during 2 hrs of reaction time. Similarly, during 2 hrs of reaction time, the Fenton-like degradation of SMZ employing Ben@(CuNPs+AgNPs) nanocatalyst was found 74% and 61% in UV-A and LED light, respectively, whereas, in the absence of light, the degradation was only 44%. Moreover, in a dark environment, 56% and 44% degradation was obtained for AMX and SMZ, respectively, utilizing the Ben@CuNPs nanocatalyst. Moreover, the nanomaterials show a greater efficiency of mineralization in the case of all the targeted nanomaterials.

Furthermore, the reusability of the nanocomposite material i.e., Ben@(CuNPs+AgNPs) was examined via several repeated cycles of degradation. The catalyst showed reasonably fair stability for 5 repeated cycles of operations at least in the degradation of AMX and SMZ. Moreover, the efficiency of the catalyst was not affected significantly in the real matrix water experiments. This showed greater applicability of catalysts for industrial purposes. The materials could be further employed in the large-scale treatment of wastewater contaminated with these pollutants at least at the ‘Pilot-Scale’ treatment and the treatment process would be, possibly, sustainable and extended implacability.

4.1 Future Perspective

The current study focuses on the comprehensive and economical treatment of water polluted with emerging water pollutants, including diclofenac (DCF), phenol, n-(n-propyl) thiourea (NNPT), amoxicillin (AMX), and sulfamethazine (SMZ) using bentonite supported bimetallic nanocomposite. The nanocomposite, which included Ben@FeNPs, Ben@(FeNPs+AgNPs), Ben@CuNPs, and Ben@(CuNPs+AgNPs), was obtained in a facile synthetic route and possibly sustainable. These micropollutants are effectively broken down to considerable mineralization in the aqueous medium by the efficient and selective application of these novel nanocatalysts. In a pilot plant setting for actual wastewater treatment, the encouraging

laboratory results could be used for large-scale treatment. The laboratory scale input data could enable us to demonstrate the unit operations in the large-scale treatment of wastewater contaminated with these emerging water pollutants.

The green synthesized bimetallic nanocomposites supported by bentonite demonstrated exciting and encouraging results in the effective treatment of water polluted with diverse contaminants. However, several challenges are lying which further be part of future studies:

- 1) In heterogeneous Fenton chemistry, the catalyst plays a major role in the performance of a Fenton-like reaction. In the case of nanocatalysts or nanocomposites, catalytic activity mainly depends upon the leaching rate, capability in the production of reactive oxygen species (ROS) from H_2O_2 , and availability of active sites on the catalyst surface. Hence, the development of such catalysts with minimal leaching (high stability) and high reactivity is desirable for minimizing sludge production.
- 2) The catalytic performance of nanocomposites categorically depends upon the properties of the supporting materials used. The supporting materials prevent the agglomeration of nanoparticles and allow the homogeneous distribution of the metal nanoparticles on the surface. Concerning the fact, modification of the supporting materials with coupling agents (e.g. silane) might be an advantageous way for achieving a stabilized structure of the nanocomposite and for enhancing the adsorption capability of the overall catalyst.

REFERENCES

- Abdullahi, S. S., Güner, S., Koseoglu, Y., Musa, I. M., Adamu, B. I., and Abdulhamid, M. I., (2016). Simple Method For The Determination of Band Gap of a Nanopowdered Sample Using Kubelka Munk Theory. *J. Niger Assoc. Math Phys.*, **35**: 13.
- Acuña, V., Ginebreda, A., Mor, J. R., Petrovic, M., Sabater, S., Sumpter, J., and Barceló, D., (2015). Balancing the health benefits and environmental risks of pharmaceuticals: Diclofenac as an example. *Environ. Int.*, **85**:327–333.
- Ahmed, S., Rasul, M. G., Martens, W. N., Brown, R., and Hashib, M. A., (2010). Heterogeneous photocatalytic degradation of phenols in wastewater: A review on current status and developments. *Desalination*, **261(1)**: 3–18.
- Ahsan, M. A., Puente Santiago, A. R., Rodriguez, A., Maturano-Rojas, V., Alvarado-Tenorio, B., Bernal, R., and Noveron, J. C., (2020). Biomass-derived ultrathin carbon-shell coated iron nanoparticles as high-performance tri-functional HER, ORR and Fenton-like catalysts. *J. Clean Prod.*, **275**:124141.
- Alfaya, E., Iglesias, O., Pazos, M., and Sanromán, M. A., (2015). Environmental application of an industrial waste as catalyst for the electro-Fenton-like treatment of organic pollutants. *RSC Adv.*, **5(19)**: 14416–14424.
- Al-Hamdi, A. M., Rinner, U., and Sillanpää, M., (2017). Tin dioxide as a photocatalyst for water treatment: A review. *Process Saf. Environ. Prot.*, **107**: 190–205.
- Almahri, A., (2022). The solid-state synthetic performance of bentonite stacked manganese ferrite nanoparticles: Adsorption and photo-Fenton degradation of MB dye and antibacterial applications. *J. Mater Res. Technol.*, **17**: 2935–2949.
- Amat, A. M., Arques, A., Beneyto, H., García, A., Miranda, M. A., and Seguí, S., (2003). Ozonisation coupled with biological degradation for treatment of

phenolic pollutants: A mechanistically based study. *Chemosphere*, **53(1)**:79–86

Archana, P., Samatha, T., Mahitha, B., and RamaSwamy, N., (2012). Preliminary phytochemical screening from leaf and seed extracts of *Senna alata* L. Roxb-an Ethnomedicinal plant. **3(3)**: 8.

Arya, D., Kumar, S., and Kumar, S., (2011). Biodegradation dynamics and cell maintenance for the treatment of resorcinol and p-cresol by filamentous fungus *Gliomastix indicus*. *J. Hazard. Mater.*, **198**:49–56.

Atta, A. Y., Jibril, B. Y., Al-Waheibi, T. K., and Al-Waheibi, Y. M., (2012). Microwave-enhanced catalytic degradation of 2-nitrophenol on alumina-supported copper oxides. *Catal. Commun.*, **26**: 112–116.

Auwal, M. S., Saka, S., Mairiga, I. A., Sanda, K. A., Shuaibu, A., and Ibrahim, A., (2014). Preliminary phytochemical and elemental analysis of aqueous and fractionated pod extracts of *Acacia nilotica* (Thorn mimosa). *Vet. Res. Forum Int. Q. J.*, **5(2)**:95–100.

Ayeni, O. (2014). A Preliminary Assessment of Phenol Contamination of Isebo River in South-western Nigeria.

Ayres, J. A. (1970). Decontamination of nuclear reactors and equipment. Ronald Press Company.

Babuponnusami, A., and Muthukumar, K., (2011). Degradation of Phenol in Aqueous Solution by Fenton, Sono-Fenton and Sono-photo-Fenton Methods. *CLEAN - Soil Air Water*. **39(2)**: 142–147. <https://doi.org/10.1002/clen.201000072>

Babuponnusami, A., and Muthukumar, K., (2012). Removal of phenol by heterogenous photo electro Fenton-like process using nano-zero valent iron. *Separation and Purification Technology*, **98**: 130–135.

Baghapour, M. A., Shirdarreh, M. R., and Faramarzian, M., (2014). Degradation of Amoxicillin by Bacterial Consortium in a Submerged Biological Aerated

- Filter: Volumetric Removal Modeling. *J. Health Sci. Surveill Syst.* **2(1)**: 15–25.
- Balakrishna, K., Rath, A., Praveenkumarreddy, Y., and Siri, K., (2020). A review of the occurrence of pharmaceuticals and personal care products in Indian water bodies. *Ecotoxicol Environ. Saf.* **137**: (April 2016), 113–120.
- Balci, B., Oturan, M. A., Oturan, N., and Sirés, I., (2009). Decontamination of Aqueous Glyphosate, (Aminomethyl)phosphonic Acid, and Glufosinate Solutions by Electro-Fenton-like Process with Mn²⁺ as the Catalyst. *J. Agric. Food Chem.* **57(11)**: 4888–4894.
- Bandara, J., Guasaquillo, I., Bowen, P., Soare, L., Jardim, W. F., and Kiwi, J., (2005). Photocatalytic Storing of O₂ as H₂O₂ Mediated by High Surface Area CuO. Evidence for a Reductive–Oxidative Interfacial Mechanism. *Langmuir* **21(18)**: 8554–8559.
- Bandara, J., Kiwi, J., Pulgarin, C., Peringer, P., Pajonk, G.-M., Elaloui, A., and Albers, P., (1996). Novel Cyclic Process Mediated by Copper Oxides Active in the Degradation of Nitrophenols: Implications for the Natural Cycle. *Environ. Sci. Technol.* **30(4)**: 1261–1267.
- Bao, T., Damtie, M. M., Hosseinzadeh, A., Wei, W., Jin, J., Phong Vo, H. N., Ye, J. S., Liu, Y., Wang, X. F., Yu, Z. M., Chen, Z. J., Wu, K., Frost, R. L., and Ni, B.-J., (2020). Bentonite-supported nano zero-valent iron composite as a green catalyst for bisphenol A degradation: Preparation, performance, and mechanism of action. *J. Environ. Manage.* **260**: 110105.
- Barb, W. G., Baxendale, J. H., George, P., and Hargrave, K. R., (1949). Reactions of Ferrous and Ferric Ions with Hydrogen Peroxide. *Nature* **163(4148)**: Article 4148.
- Barbosa, M. O., Moreira, N. F. F., Ribeiro, A. R., Pereira, M. F. R., and Silva, A. M. T., (2016). Occurrence and removal of organic micropollutants: An overview of the watch list of EU Decision 2015/495. *Water Res.* **94**: 257–279.

- Barka, N., Qourzal, S., Assabbane, A., Nounah, A., and Ait-Ichou, Y., (2010). Photocatalytic degradation of an azo reactive dye, Reactive Yellow 84, in water using an industrial titanium dioxide coated media. *Arab J. Chem.* **3(4)**: 279–283.
- Barra Caracciolo, A., Topp, E., and Grenni, P., (2015). Pharmaceuticals in the environment: Biodegradation and effects on natural microbial communities. A review. *J. Pharm. Biomed. Anal.* **106**: 25–36.
- Barron, V., and Torrent, J., (1986). Use of the Kubelka-Munk theory to study the influence of iron oxides on soil colour. *J. Soil Sci.* **37(4)**: 499–510.
- Bartrons, M., and Peñuelas, J., (2017). Pharmaceuticals and Personal-Care Products in Plants. *Trends Plant Sci.* **22(3)**: 194–203.
- Batt, A. L., Snow, D. D., and Aga, D. S., (2006). Occurrence of sulfonamide antimicrobials in private water wells in Washington County, Idaho, USA. *Chemosphere* **64(11)**: 1963–1971.
- Bebu, A., Szabó, L., Leopold, N., Berindean, C., and David, L., (2011). IR, Raman, SERS and DFT study of amoxicillin. *J. Mol. Struct.* **993(1)**: 52–56.
- Bell, A. T., (2003). The Impact of Nanoscience on Heterogeneous Catalysis. *Science* **299(5613)**: 1688–1691.
- Ben-Moshe, T., Dror, I., and Berkowitz, B., (2009). Oxidation of organic pollutants in aqueous solutions by nanosized copper oxide catalysts. *Appl. Catal. B Environ.* **85(3–4)**: 207–211.
- Bergendahl, J. A., and Thies, T. P., (2004). Fenton's oxidation of MTBE with zero-valent iron. *Water Res.* **38(2)**: 327–334.
- Bester, K., (2005). Fate of triclosan and triclosan-methyl in sewage treatment plants and surface waters. *Arch. Environ. Contam. Toxicol.*, **49(1)**: 9–17.

- Bokare, A. D., Chikate, R. C., Rode, C. V., and Paknikar, K. M., (2008). Iron-nickel bimetallic nanoparticles for reductive degradation of azo dye Orange G in aqueous solution. *Appl. Catal. B Environ.* **79(3)**: 270–278.
- Bokare, A. D., and Choi, W., (2014). Review of iron-free Fenton-like systems for activating H₂O₂ in advanced oxidation processes. *J. Hazard. Mater.* **275**: 121–135.
- Bounab, L., Draoui, K., Ahrouch, M., Hadri, M., Bouchta, D., and Barhoun, A., (2017). *An effective functionalized Moroccan bentonite: Application for a green remediation of m-Cresol*. 13.
- Bound, J. P., and Voulvoulis, N., (2006). Predicted and measured concentrations for selected pharmaceuticals in UK rivers: Implications for risk assessment. *Water Res.* **40(15)**: 2885–2892.
- Bozzi, A., Yuranova, T., Mielczarski, J., Lopez, A., and Kiwi, J., (2002). Abatement of oxalates catalyzed by Fe-silica structured surfaces via cyclic carboxylate intermediates in photo-Fenton reactions. *Chem. Commun.* **19**, 2202–2203.
- Bremner, D. H., Carlo, S. D., Chakinala, A. G., and Cravotto, G., (2008). Mineralisation of 2,4-dichlorophenoxyacetic acid by acoustic or hydrodynamic cavitation in conjunction with the advanced Fenton process. *Ultrason. Sonochem.* **15(4)**: 416–419.
- Brezina, P. R., Yunus, F. N., and Zhao, Y., (2012). Effects of Pharmaceutical Medications on Male Fertility. *J. Reprod. Infertil.* **13(1)**: 3–11.
- Brillas, E., and Garcia-Segura, S., (2020). Benchmarking recent advances and innovative technology approaches of Fenton, photo-Fenton, electro-Fenton, and related processes: A review on the relevance of phenol as model molecule. *Sep. Purif. Technol.* **237**: 116337.

- Brillas, E., Sirés, I., and Oturan, M. A., (2009). Electro-Fenton Process and Related Electrochemical Technologies Based on Fenton's Reaction Chemistry. *Chem. Rev.* **109(12)**: 6570–6631.
- Brooks, B. W., Turner, P. K., Stanley, J. K., Weston, J. J., Glidewell, E. A., Foran, C. M., Slattery, M., La Point, T. W., and Huggett, D. B., (2003). Waterborne and sediment toxicity of fluoxetine to select organisms. *Chemosphere* **52(1)**: 135–142.
- Butt, A. L., Mpinga, J. K., and Tichapondwa, S. M., (2021). Photo-Fenton Oxidation of Methyl Orange Dye Using South African Ilmenite Sands as a Catalyst. *Catalysts* **11(12)**: Article 12.
- Buxton, G. V., Greenstock, C. L., Helman, W. P., and Ross, A. B., (1988). Critical Review of rate constants for reactions of hydrated electrons, hydrogen atoms and hydroxyl radicals ($\cdot\text{OH}/\cdot\text{O}^-$ in Aqueous Solution. *J. Phys. Chem. Ref. Data.* **17(2)**: 513–886.
- Çağlar Yılmaz, H., Akgeyik, E., Bougarrani, S., El Azzouzi, M., and Erdemoğlu, S., (2020). Photocatalytic degradation of amoxicillin using Co-doped TiO₂ synthesized by reflux method and monitoring of degradation products by LC–MS/MS. *J. Dispers. Sci. Technol.* **41(3)**: 414–425.
- Campos, S., Salazar, R., Arancibia-Miranda, N., Rubio, M. A., Aranda, M., García, A., Sepúlveda, P., and Espinoza, L. C., (2020). Nafcillin degradation by heterogeneous electro-Fenton process using Fe, Cu and Fe/Cu nanoparticles. *Chemosphere* **247**, 125813.
- Cardoso, O., Porcher, J. M., and Sanchez, W., (2014). Factory-discharged pharmaceuticals could be a relevant source of aquatic environment contamination: Review of evidence and need for knowledge. *Chemosphere* **115(1)**, 20–30.
- Carless, J. E., (1966). Remington's Pharmaceutical Sciences, 13th Edition. *J. Pharm. Pharmacol.* **18(7)**, 479–480.

- Carta, R., and Desogus, F., (2013). The enhancing effect of low power microwaves on phenol oxidation by the Fenton process. *J. Environ. Chem. Eng.* **1(4)**: 1292–1300.
- Carter, L. J., Ryan, J. J., and Boxall, A. B. A., (2016). Effects of soil properties on the uptake of pharmaceuticals into earthworms. *Environ. Pollut.* **213**: 922–931.
- Cegarra, J., Gacén, J., Caro, M., and Pepió, M., (1988). Wool bleaching with thiourea dioxide. *J. Soc. Dye Colour.* **104(7–8)**: 273–279.
- Chand, R., Ince, N. H., Gogate, P. R., and Bremner, D. H., (2009). Phenol degradation using 20, 300 and 520kHz ultrasonic reactors with hydrogen peroxide, ozone and zero valent metals. *Sep. Purif. Technol.* **67(1)**: 103–109.
- Chandraker, S. K., Lal, M., Ghosh, M. K., Tiwari, V., Ghorai, T. K., and Shukla, R., (2020). Green synthesis of copper nanoparticles using leaf extract of *Ageratum houstonianum* Mill. And study of their photocatalytic and antibacterial activities. *Nano Express* **1(1)**: 010033.
- Chandraker, S., Lal, M., Ghosh, M., Tiwari, V., Ghorai, T., and Shukla, R., (2020). Green synthesis of copper nanoparticles using leaf extract of *Ageratum houstonianum* Mill. And study of their photocatalytic and antibacterial activities. *Nano Express* **1**.
- Chatterjee, D., and Dasgupta, S., (2005). Visible light induced photocatalytic degradation of organic pollutants. *J. Photochem. Photobiol. C. Photochem. Rev.* **6(2–3)**: 186–205.
- Chen, G., Den Braver, M. W., Van Gestel, C. A. M., Van Straalen, N. M., and Roelofs, D., (2015). Ecotoxicogenomic assessment of diclofenac toxicity in soil. *Environ. Pollut.* **199**: 253–260.
- Chen, L., Ni, R., Yuan, T., Gao, Y., Kong, W., Zhang, P., Yue, Q., and Gao, B., (2020). Effects of green synthesis, magnetization, and regeneration on ciprofloxacin

- removal by bimetallic nZVI/Cu composites and insights of degradation mechanism. *J. Hazard. Mater.*, **382**: 121008.
- Chiffre, A., Degiorgi, F., Buleté, A., Spinner, L., and Badot, P. M., (2016). Occurrence of pharmaceuticals in WWTP effluents and their impact in a karstic rural catchment of Eastern France. *Environ. Sci. Pollut. Res.* **23(24)**: 25427–25441.
- Chitra, M., Mangamma, G., Uthayarani, K., Neelakandeswari, N., and Girija, E. K., (2020). Band gap engineering in ZnO based nanocomposites. *Phys. E. Low-Dimens. Syst. Nanostructures.* **119**: 113969.
- Choi, K., and Lee, W., (2012). Enhanced degradation of trichloroethylene in nano-scale zero-valent iron Fenton system with Cu(II). *J. Hazard. Mater.* **211–212**: 146–153.
- Chong, M. N., Jin, B., Chow, C. W. K., and Saint, C., (2010). Recent developments in photocatalytic water treatment technology: A review. *Water Res.* **44(10)**: 2997–3027.
- Crane, M., Watts, C., and Boucard, T., (2006). Chronic aquatic environmental risks from exposure to human pharmaceuticals. *Sci. Total Environ.* **367(1)**: 23–41.
- Crane, R. A., and Scott, T. B., (2012). Nanoscale zero-valent iron: Future prospects for an emerging water treatment technology. *J. Hazard. Mater.* **211–212**: 112–125.
- Dai, C., Tian, X., Nie, Y., Lin, H.-M., Yang, C., Han, B., and Wang, Y., (2018). Surface Facet of CuFeO₂ Nanocatalyst: A Key Parameter for H₂O₂ Activation in Fenton-Like Reaction and Organic Pollutant Degradation. *Environ. Sci. Technol.* **52(11)**: 6518–6525.
- Dass, E., and Sattigeri, B. M., (2018). Hepatoprotective effect of DL-methionine on diclofenac-induced hepatotoxicity in albino rats: An experimental study. *Int. J. Res. Med. Sci.* **6(3)**: 802–807.

- Davidson, B., Soodak, M., Strout, H. V., Neary, J. T., Nakamura, C., And Maloof, F., (1979). Thiourea and Cyanamide as Inhibitors of Thyroid Peroxidase: The Role of Iodide*. *Endocrinology*, **104(4)**: 919–924.
- Davis, J. G., Truman, C. C., Kim, S. C., Ascough, J. C., and Carlson, K., (2006). Antibiotic Transport via Runoff and Soil Loss. *J. Environ. Qual.* **35(6)**: 2250–2260.
- De León, M. A., Castiglioni, J., Bussi, J., and Sergio, M., (2008). Catalytic activity of an iron-pillared montmorillonitic clay mineral in heterogeneous photo-Fenton process. *Catal. Today* **133–135**: 600–605.
- De Zacchini, M., and De Agazio, M., (2001). Dimethylthiourea, a hydrogen peroxide trap, partially prevents stress effects and ascorbate peroxidase increase in spermidine-treated maize roots: Dimethylthiourea prevents spermidine-induced stress effects. *Plant. Cell Environ.* **24(2)**: 237–244.
- Dehghani, M., Shahsavani, E., Farzadkia, M., and Samaei, M. R., (2014). Optimizing photo-Fenton like process for the removal of diesel fuel from the aqueous phase. *J. Environ. Health. Sci. Eng.*, **12(1)**: 87.
- Deng, B., Shi, A., Li, L., and Kang, Y., (2008). Pharmacokinetics of amoxicillin in human urine using online coupled capillary electrophoresis with electrogenerated chemiluminescence detection. *J. Pharm. Biomed. Anal.* **48(4)**: 1249–1253.
- Ding, R., Zhang, P., Seredych, M., and Bandosz, T. J., (2012). Removal of antibiotics from water using sewage sludge- and waste oil sludge-derived adsorbents. *Water Res.* **46(13)**: 4081–4090.
- Do, Q. C., Kim, D.-G., and Ko, S.-O., (2017). Nonsacrificial Template Synthesis of Magnetic-Based Yolk–Shell Nanostructures for the Removal of Acetaminophen in Fenton-like Systems. *ACS Appl. Mater. Interfaces.* **9(34)**: 28508–28518.

- Dolliver, H., and Gupta, S., (2008). Antibiotic losses in leaching and surface runoff from manure-amended agricultural land. *J. Environ. Qual.* **37(3)**: 1227–1237.
- Doong, R., and Chang, W., (1998). Photoassisted iron compound catalytic degradation of organophosphorous pesticides with hydrogen peroxide. *Chemosphere* **37(13)**: 2563–2572.
- Duan, W., Meng, F., Cui, H., Lin, Y., Wang, G., and Wu, J., (2018). Ecotoxicity of phenol and cresols to aquatic organisms: A review. *Ecotoxicol. Environ. Saf.* **157**: 441–456.
- Elmolla, E. S., and Chaudhuri, M., (2009). Improvement of Biodegradability of Synthetic Amoxicillin Wastewater by Photo-Fenton Process. *World Appl. Sci. J.* **5**: 53–58.
- ElShafei, G. M. S., Yehia, F. Z., Dimitry, O. I. H., Badawi, A. M., and Eshaq, Gh., (2014). Ultrasonic assisted-Fenton-like degradation of nitrobenzene at neutral pH using nanosized oxides of Fe and Cu. *Ultrason Sonochem.* **21(4)**: 1358–1365.
- ElShafei, G. M. S., Yehia, F. Z., Eshaq, Gh., and ElMetwally, A. E., (2017). Enhanced degradation of nonylphenol at neutral pH by ultrasonic assisted- heterogeneous Fenton using nano zero valent metals. *Sep. Purif. Technol.* **178**: 122–129.
- Escher, B. I., Bramaz, N., Richter, M., and Lienert, J., (2006). Comparative Ecotoxicological Hazard Assessment of Beta-Blockers and Their Human Metabolites Using a Mode-of-Action-Based Test Battery and a QSAR Approach †. *Environ. Sci. Technol.* **40(23)**: 7402–7408.
- Espinosa, J. C., Catalá, C., Navalón, S., Ferrer, B., Álvaro, M., and García, H., (2018). Iron oxide nanoparticles supported on diamond nanoparticles as efficient and stable catalyst for the visible light assisted Fenton reaction. *Appl. Catal. B Environ.* **226**, 242–251.

- Espinosa, J. C., and Navalón, S., (2015). Silver Nanoparticles Supported on Diamond Nanoparticles as a Highly Efficient Photocatalyst for the Fenton Reaction under Natural Sunlight Irradiation. *7*.
- Espinosa, J. C., Navalón, S., Álvaro, M., and García, H., (2016). Copper nanoparticles supported on diamond nanoparticles as a cost-effective and efficient catalyst for natural sunlight assisted Fenton reaction. *Catal. Sci. Technol.* **6(19)**: 7077–7085.
- Ezzatahmadi, N., Millar, G. J., Ayoko, G. A., Zhu, J., Zhu, R., Liang, X., He, H., and Xi, Y., (2019). Degradation of 2,4-dichlorophenol using palygorskite-supported bimetallic Fe/Ni nanocomposite as a heterogeneous catalyst. *Appl. Clay Sci.* **168**: 276–286.
- Fan, X., Hao, H., Wang, Y., Chen, F., and Zhang, J., (2013). Fenton-like degradation of nalidixic acid with Fe³⁺/H₂O₂. *Environ. Sci. Pollut. Res.* **20(6)**: 3649–3656.
- Fatta, D., Achilleos, A., Nikolaou, A., and Meriç, S., (2007). Analytical methods for tracing pharmaceutical residues in water and wastewater. *TrAC Trends Anal. Chem.* **26(6)**: 515–533.
- Fazelirad, H., Ranjbar, M., Taher, M. A., and Sargazi, G., (2015). Preparation of magnetic multi-walled carbon nanotubes for an efficient adsorption and spectrophotometric determination of amoxicillin. *J. Ind. Eng. Chem.* **21**: 889–892.
- Fei, B.-L., Yan, Q.-L., Wang, J.-H., Liu, Q.-B., Long, J.-Y., Li, Y.-G., Shao, K.-Z., Su, Z.-M., and Sun, W.-Y., (2014). Green Oxidative Degradation of Methyl Orange with Copper(II) Schiff Base Complexes as Photo-Fenton-Like Catalysts: Green Oxidative Degradation of Methyl Orange. *Z. Für Anorg. Allg. Chem.* **640(10)**: 2035–2040.

- Feng, J., Hu, X., and Yue, P. L., (2006). Effect of initial solution pH on the degradation of Orange II using clay-based Fe nanocomposites as heterogeneous photo-Fenton catalyst. *Water Res.* **40(4)**: 641–646.
- Feng, Y., Liao, C., and Shih, K., (2016). Copper-promoted circumneutral activation of H₂O₂ by magnetic CuFe₂O₄ spinel nanoparticles: Mechanism, stoichiometric efficiency, and pathway of degrading sulfanilamide. *Chemosphere.* **154**: 573–582.
- Fenton, H. J. H., (1894). LXXIII.—Oxidation of tartaric acid in presence of iron. *J. Chem. Soc. Trans.*, **65(0)**: 899–910.
- Fida, H., Zhang, G., Guo, S., and Naeem, A., (2017). Heterogeneous Fenton degradation of organic dyes in batch and fixed bed using La-Fe montmorillonite as catalyst. *J. Colloid. Interface Sci.*, **490**: 859–868.
- Fijalkowski, K., Rorat, A., Grobelak, A., and Kacprzak, M. J., (2017). The presence of contaminations in sewage sludge – The current situation. *J. Environ. Manage.*, **203**: 1126–1136.
- Finch, J. M., Osimitz, T. G., Gabriel, K. L., Martin, T., Henderson, W. J., Capen, C. C., Butler, W. H., and Lake, B. G., (2006). A mode of action for induction of thyroid gland tumors by Pyrethrins in the rat. *Toxicol. Appl. Pharmacol.*, **214(3)**: 253–262.
- Fink, L., Dror, I., and Berkowitz, B., (2012). Enrofloxacin oxidative degradation facilitated by metal oxide nanoparticles. *Chemosphere*, **86(2)**: 144–149.
- Flores, Y., Flores, R., and Gallegos, A. A., (2008). Heterogeneous catalysis in the Fenton-type system reactive black 5/H₂O₂. *J. Mol. Catal. Chem.*, **281(1–2)**: 184–191.
- Fontes, M. K., Gusso-choueri, P. K., Maranhão, L. A., Moledo, D., Abessa, D. S., Mazur, W. A., Campos, B. G. De, Guimarães, L., Toledo, M. S. De, Lebre, D., Marques, J. R., Felício, A., Cesar, A., Almeida, E. A., Dias, C., Pereira, S.,

- Guimarães, L. L., Toledo, M. S. De, Lebre, D., and Marques, J. R., (2018). A tiered approach to assess effects of diclofenac on the brown mussel *Perna perna*: A contribution to characterize the hazard. *Water Research*, **132**: 361–370
- Galeriková, A., Dávid, A., Materna, M., and Mako, P., (2021). Study of maritime accidents with hazardous substances involved: Comparison of HNS and oil behaviours in marine environment. *Transp. Res. Procedia.*, **55**: 1050–1064. <https://doi.org/10.1016/j.trpro.2021.07.182>
- Gautam, S., Shandilya, P., Priya, B., Singh, V. P., Raizada, P., Rai, R., Valente, M. A., and Singh, P., (2017). Superparamagnetic MnFe₂O₄ dispersed over graphitic carbon sand composite and bentonite as magnetically recoverable photocatalyst for antibiotic mineralization. *Sep. Purif. Technol.*, **172**: 498–511.
- Gaw, S., Thomas, K. V., and Hutchinson, T. H., (2014). Sources, impacts and trends of pharmaceuticals in the marine and coastal environment. *Philos. Trans. R. Soc. Lond. B. Biol. Sci.*, **369**(1656).
- Gianfreda, L., Iamarino, G., Scelza, R., and Rao, M. A., (2006). Oxidative catalysts for the transformation of phenolic pollutants: A brief review. *Biocatal. Biotransformation*, **24**(3): 177–187.
- Ginebreda, A., Muñoz, I., de Alda, M. L., Brix, R., López-Doval, J., and Barceló, D., (2010). Environmental risk assessment of pharmaceuticals in rivers: Relationships between hazard indexes and aquatic macroinvertebrate diversity indexes in the Llobregat River (NE Spain). *Environ. Int.*, **36**(2): 153–162.
- Giordano, G., Perathoner, S., Centi, G., De Rosa, S., Granato, T., Katovic, A., Siciliano, A., Tagarelli, A., and Tripicchio, F., (2007). Wet hydrogen peroxide catalytic oxidation of olive oil mill wastewaters using Cu-zeolite and Cu-pillared clay catalysts. *Catal. Today*, **124**(3): 240–246.

- Glaze, W. H., Kang, J. W., and Chapin, D. H., (1987). The chemistry of water treatment processes involving ozone, hydrogen peroxide and ultraviolet radiation. *Ozone: Sci. Eng.*, **9(4)**: 335–352.
- González, M., Fernández-lópez, C., Pedrero-salcedo, F., and Jose, J., (2018). Absorption of carbamazepine and diclofenac in hydroponically cultivated lettuces and human health risk assessment. *Agric. Water Manag.*, **206**: 42–47.
- Gopal, G., Sankar, H., Natarajan, C., and Mukherjee, A., (2020). Tetracycline removal using green synthesized bimetallic nZVI-Cu and bentonite supported green nZVI-Cu nanocomposite: A comparative study. *J. Environ. Manage.*, **254**: 109812.
- Guiloski, I. C., Stein Piancini, L. D., Dagostim, A. C., de Morais Calado, S. L., Fávoro, L. F., Boschen, S. L., Cestari, M. M., da Cunha, C., and Silva de Assis, H. C., (2017). Effects of environmentally relevant concentrations of the anti-inflammatory drug diclofenac in freshwater fish *Rhamdia quelen*. *Ecotoxicol Environ Saf.*, **139**: 291–300.
- Gumy, D., Fernández-Ibáñez, P., Malato, S., Pulgarin, C., Enea, O., and Kiwi, J., (2005). Supported Fe/C and Fe/Nafion/C catalysts for the photo-Fenton degradation of Orange II under solar irradiation. *Catalysis Today*, **101(3–4)**: 375–382.
- Guo, T., Wang, K., Zhang, G., and Wu, X., (2019). A novel α -Fe₂O₃@g-C₃N₄ catalyst: Synthesis derived from Fe-based MOF and its superior photo-Fenton performance. *Appl. Surf. Sci.*, **469**: 331–339.
- Guo, Y., Wen, M., and An, T., (2020). Recent advances in VOC elimination by catalytic oxidation technology onto various nanoparticles catalysts: A critical review. *Appl. Catal. B: Environ.*, **281**: 119447.
- Gupta, P., Lakes, A., and Dziubla, T., (2016). Chapter One—A Free Radical Primer. In T. Dziubla and D. A. Butterfield (Eds.), *Oxidative Stress and Biomaterials* (pp. 1–33). Academic Press.

- Hakimi, B., Ghorbanpour, M., and Feizi, A., (2018). ZnO/bentonite Nanocomposites Prepared with Solid-state Ion Exchange as Photocatalysts. *J. Ultrafine Grained Nanostructured Mater.*, **51(2)**.
- Hallare, A. V., Köhler, H. R., and Triebkorn, R., (2004). Developmental toxicity and stress protein responses in zebrafish embryos after exposure to diclofenac and its solvent, DMSO. *Chemosphere*, **56(7)**: 659–666.
- Hartmann, M., Kullmann, S., and Keller, H., (2010). Wastewater treatment with heterogeneous Fenton-type catalysts based on porous materials. *J. Mater. Chem.*, **20(41)**: 9002.
- Hass Caetano Lacerda, E., Monteiro, F. C., Kloss, J. R., and Fujiwara, S. T., (2020). Bentonite clay modified with Nb₂O₅: An efficient and reused photocatalyst for the degradation of reactive textile dye. *J. Photochem. Photobiol. Chem.*, **388**: 112084.
- Hassan, A. K., Al-Kindi, G. Y., and Ghanim, D., (2020). Green synthesis of bentonite-supported iron nanoparticles as a heterogeneous Fenton-like catalyst: Kinetics of decolorization of reactive blue 238 dye. *Water Sci. Eng.*, **13(4)**: 286–298.
- Hassan, H., and Hameed, B. H., (2011). Fenton-like Oxidation of Acid Red 1 Solutions Using Heterogeneous Catalyst Based on Ball Clay. *Int. J. Environ. Sci. Dev.*, 218–222.
- He, D., Miller, C. J., and Waite, T. D., (2014). Fenton-like zero-valent silver nanoparticle-mediated hydroxyl radical production. *J. Catal.*, **317**: 198–205.
- Heberer, T., (2002). Occurrence, fate, and removal of pharmaceutical residues in the aquatic environment: A review of recent research data. *Toxicol. Lett.*, **131(1–2)**: 5–17.
- Heidler, J., Sapkota, A., and Halden, R. U., (2006). Partitioning, Persistence, and Accumulation in Digested Sludge of the Topical Antiseptic Triclocarban during Wastewater Treatment. *Environ. Sci. Technol.*, **40(11)**: 3634–3639.

- Henglein, A., (1987). Sonochemistry: Historical developments and modern aspects. *Ultrasonics*, **25**(1): 6–16.
- Hernando, M. D., Gómez, M. J., Agüera, A., and Fernández-Alba, A. R., (2007). LC-MS analysis of basic pharmaceuticals (beta-blockers and anti-ulcer agents) in wastewater and surface water. *TrAC - Trends Anal. Chem.*, **26**(6): 581–594.
- Herney-Ramirez, J., Vicente, M. A., and Madeira, L. M., (2010). Heterogeneous photo-Fenton oxidation with pillared clay-based catalysts for wastewater treatment: A review. *Appl. Catal. B. Environ.*, **98**(1–2): 10–26.
- Hofmann, R., and Andrews, R. C., (2006). Impact of H₂O₂ and (bi)carbonate alkalinity on ammonia's inhibition of bromate formation. *Water Res.*, **40**(18): 3343–3348.
- Homem, V., Alves, A., and Santos, L., (2013). Microwave-assisted Fenton's oxidation of amoxicillin. *Chem. Eng. J.*, **220**: 35–44.
- Huang, C., Guo, B., Wang, X., Li, J., Zhu, W., Chen, B., Ouyang, S., and Yao, S., (2012). A generic approach for expanding homolog-targeted residue screening of sulfonamides using a fast matrix separation and class-specific fragmentation-dependent acquisition with a hybrid quadrupole-linear ion trap mass spectrometer. *Anal. Chim. Acta.*, **737**: 83–98.
- Hug, S. J., and Leupin, O., (2003). Iron-Catalyzed Oxidation of Arsenic(III) by Oxygen and by Hydrogen Peroxide: PH-Dependent Formation of Oxidants in the Fenton Reaction. *Environ. Sci. Technol.*, **37**(12): 2734–2742.
- Igberase, E., and Osifo, P., (2015). Equilibrium, kinetic, thermodynamic and desorption studies of cadmium and lead by polyaniline grafted cross-linked chitosan beads from aqueous solution. *J. Ind. Eng. Chem.*, **26**: 340–347.
- Iglesias Esteban, R., and Ortega de Miguel, E., (2008). Present and future of wastewater reuse in Spain. *Desalination*, **218**(1–3): 105–119.

- Iurascu, B., Siminiceanu, I., Vione, D., Vicente, M. A., and Gil, A., (2009). Phenol degradation in water through a heterogeneous photo-Fenton process catalyzed by Fe-treated Iaponite. *Water Res.*, **43(5)**: 1313–1322.
- Jain, S., Jain, A., Kachhawah, P., and Devra, V., (2015). Synthesis and size control of copper nanoparticles and their catalytic application. *Trans. Nonferrous Met. Soc. China*, **25(12)**: 3995–4000.
- Jo, E., Tahar, A., Mchugh, B., and Rowan, N. J., (2017). Science of the Total Environment Monitoring, sources, receptors, and control measures for three European Union watch list substances of emerging concern in receiving waters – A 20 year systematic review. *Sci. Total Environ.*, **574**: 1140–1163.
- Jones, O. A. H., Voulvoulis, N., and Lester, J. N., (2002). Aquatic environmental assessment of the top 25 English prescription pharmaceuticals. *Water Res.*, **36(20)**: 5013–5022.
- Joo, S. H., Feitz, A. J., and Waite, T. D., (2004). Oxidative Degradation of the Carbothioate Herbicide, Molinate, Using Nanoscale Zero-Valent Iron. *Environ. Sci. Technol.*, **38(7)**: 2242–2247.
- Jun, L. Y., Yon, L. S., Mubarak, N. M., Bing, C. H., Pan, S., Danquah, M. K., Abdullah, E. C., and Khalid, M., (2019). An overview of immobilized enzyme technologies for dye and phenolic removal from wastewater. *J. Environ. Chem. Eng.*, **7(2)**: 102961.
- Kaczala, F., and Blum, S. E., (2016). The Occurrence of Veterinary Pharmaceuticals in the Environment: A Review. *Curr. Anal. Chem.*, **12(3)**: 169–182.
- Kallel, M., Belaid, C., Mechichi, T., Ksibi, M., and Elleuch, B., (2009). Removal of organic load and phenolic compounds from olive mill wastewater by Fenton oxidation with zero-valent iron. *Chem. Eng. J.*, **150(2)**: 391–395.
- Kanakaraju, D., Kockler, J., Motti, C. A., Glass, B. D., and Oelgemöller, M., (2015). Titanium dioxide/zeolite integrated photocatalytic adsorbents for the degradation of amoxicillin. *Appl. Catal. B. Environ.*, **166–167**: 45–55.

- Karunakaran, C., and Anilkumar, P., (2007). Semiconductor-catalyzed solar photooxidation of iodide ion. *J. Mol. Catal. Chem.*, **265(1)**: 153–158.
- Kasprzyk-Hordern, B., Dinsdale, R. M., and Guwy, A. J., (2008). The occurrence of pharmaceuticals, personal care products, endocrine disruptors and illicit drugs in surface water in South Wales, UK. *Water Res.*, **42(13)**: 3498–3518.
- Kiliç, N. K., (2009). Enhancement of phenol biodegradation by *Ochrobactrum* sp. Isolated from industrial wastewaters. *Int. Biodeterior. Biodegrad.*, **63(6)**: 778–781.
- Kim, S. D., Cho, J., Kim, I. S., Vanderford, B. J., and Snyder, S. A., (2007). Occurrence and removal of pharmaceuticals and endocrine disruptors in South Korean surface, drinking, and waste waters. *Water Res.*, **41(5)**: 1013–1021.
- Kitis, M., and Kaplan, S. S., (2007). Advanced oxidation of natural organic matter using hydrogen peroxide and iron-coated pumice particles. *Chemosphere*, **68(10)**: 1846–1853.
- Kolpin, D. W., Furlong, E. T., Meyer, M. T., Thurman, E. M., Zaugg, S. D., Barber, L. B., and Buxton, H. T., (2002). Pharmaceuticals, Hormones, and Other Organic Wastewater Contaminants in U.S. Streams, 1999–2000: A National Reconnaissance. *Environ. Sci. Technol.*, **36(6)**: 1202–1211.
- Kremer, M. L., (1999). Mechanism of the Fenton reaction. Evidence for a new intermediate. *Phys. Chem. Chem. Phys.*, **1(15)**: 3595–3605.
- Kumar, B., Smita, K., Cumbal, L., and Debut, A., (2017). Green synthesis of silver nanoparticles using Andean blackberry fruit extract. *Saudi J. Biol. Sci.*, **24(1)**: 45.
- Kurian, M., and Sugunan, S., (2006). Wet peroxide oxidation of phenol over mixed pillared montmorillonites. *Chem. Eng. J.*, **115(3)**: 139–146.

- L, A. K., and L, H. G., (1971). A method for determining need for chemical cleaning of high-pressure boilers. *Proc. Am. Power. Conf.*, **33**: 710–720.
- Lado Ribeiro, A. R., Moreira, N. F. F., Li Puma, G., and Silva, A. M. T., (2019). Impact of water matrix on the removal of micropollutants by advanced oxidation technologies. *Chem. Eng. J.*, **363**: 155–173.
- Lalchhingpuii, Tiwari, D., Lalhmunsiam, and Lee, S. M., (2017). Chitosan templated synthesis of mesoporous silica and its application in the treatment of aqueous solutions contaminated with cadmium(II) and lead(II). *Chem. Eng. J.*, **328**: 434–444.
- Lalhriatpuia, C., Tiwari, D., Tiwari, A., and Lee, S. M., (2015). Immobilized Nanopillars-TiO₂ in the efficient removal of micro-pollutants from aqueous solutions: Physico-chemical studies. *Chem. Eng. J.*, **281**: 782–792.
- Lalhriatpuia, C., Tiwari, D., Tiwari, A., and SeungMok, L., (2015). Immobilized Nanopillars-TiO₂ in the efficient removal of micro-pollutants from aqueous solutions: Physico-chemical studies. *Chem. Eng. J.*, **281**: 782–792.
- Lalliansanga, Tiwari, D., Tiwari, A., Shukla, A., Kim, D.-J., Yoon, Y.-Y., and Lee, S.-M., (2020a). Facile synthesis and characterization of nanocomposite Au⁰(NPs)/titanium dioxide: Photocatalytic degradation of Alizarin Yellow. *J. Ind. Eng. Chem.*, **82**: 153–163.
- Lalliansanga, Tiwari, D., Tiwari, A., Shukla, A., Kim, D.-J., Yoon, Y.-Y., and Lee, S.-M., (2020b). Facile synthesis and characterization of nanocomposite Au⁰(NPs)/titanium dioxide: Photocatalytic degradation of Alizarin Yellow. *J. Ind. Eng. Chem.*, **82**: 153–163.
- Lalliansanga, Tiwari, D., Tiwari, A., Shukla, A., Kim, D.-J., Yoon, Y.-Y., and Lee, S.-M., (2020c). Facile synthesis and characterization of nanocomposite Au⁰(NPs)/titanium dioxide: Photocatalytic degradation of Alizarin Yellow. *J. Ind. Eng. Chem.*, **82**: 153–163.

- Lalliansanga, Tiwari, D., Tiwari, A., Shukla, A., Shim, M. J., and Lee, S.-M., (2020). Facile synthesis and characterization of Ag(NP)/TiO₂ nanocomposite: Photocatalytic efficiency of catalyst for oxidative removal of Alizarin Yellow. *Catal. Today*,.
- Lapworth, D. J., Baran, N., Stuart, M. E., and Ward, R. S., (2012). Emerging organic contaminants in groundwater: A review of sources, fate and occurrence. *Environ. Pollut.*, **163**: 287–303.
- Larsbo, M., Fenner, K., Stoob, K., Burkhardt, M., Mikayilov, F., and Stamm, C., (2008). Simulating Sulfadimidine Transport in Surface Runoff and Soil at the Microplot and Field Scale. *J. Environ. Qual.*, **37**: 788–797.
- Lee, E., Lee, H., Kim, Y. K., Sohn, K., and Lee, K., (2011). Hydrogen peroxide interference in chemical oxygen demand during ozone based advanced oxidation of anaerobically digested livestock wastewater. *Int. J. Environ. Sci. Technol.*, **8(2)**: 381–388.
- Lee, S.-M., Laldawngliana, C., and Tiwari, D., (2012). Iron oxide nano-particles-immobilized-sand material in the treatment of Cu(II), Cd(II) and Pb(II) contaminated waste waters. *Chem. Eng. J.*, **195–196**: 103–111.
- Lehutso, R. F., Daso, A. P., and Okonkwo, J. O., (2017). Occurrence and environmental levels of triclosan and triclocarban in selected wastewater treatment plants in Gauteng Province, South Africa. *Emerg. Contam.*, **3(3)**: 107–114.
- Lewis, R. J., (1996). *Sax's dangerous properties of industrial materials*. New York : Van Nostrand Reinhold.
- Li, P., Song, Y., Wang, S., Tao, Z., Yu, S., and Liu, Y., (2015). Enhanced decolorization of methyl orange using zero-valent copper nanoparticles under assistance of hydrodynamic cavitation. *Ultrason. Sonochem.*, **22**: 132–138.

- Li, W., Wan, D., Wang, G., Chen, K., Hu, Q., and Lu, L., (2016). Heterogeneous Fenton degradation of Orange II by immobilization of Fe₃O₄ nanoparticles onto Al-Fe pillared bentonite. *Korean J. Chem. Eng.*, **33**(5): 1557–1564.
- Li, Y., Zhang, L., Liu, X., and Ding, J., (2019). Ranking and prioritizing pharmaceuticals in the aquatic environment of China. *Sci. Total Environ.*, **658**: 333–342.
- Lin, C.-C., and Chen, Y.-H., (2018). Feasibility of using nanoscale zero-valent iron and persulfate to degrade sulfamethazine in aqueous solutions. *Sep. Purif. Technol.*, **194**: 388–395.
- Lin, C.-C., and Wu, M.-S.,(2018). Feasibility of using UV/H₂O₂ process to degrade sulfamethazine in aqueous solutions in a large photoreactor. *J. Photochem. Photobiol. Chem.*, **367**: 446–451.
- Lindholm-Lehto, P. C., Ahkola, H. S. J., Knuutinen, J. S., and Herve, S. H., (2016). Widespread occurrence and seasonal variation of pharmaceuticals in surface waters and municipal wastewater treatment plants in central Finland. *Environ. Sci. Pollut. Res.*, **23**(8): 7985–7997.
- Lindsey, M. E., Meyer, M., and Thurman, E. M., (2001). Analysis of trace levels of sulfonamide and tetracycline antimicrobials in groundwater and surface water using solid-phase extraction and liquid chromatography/mass spectrometry. *Anal. Chem.*, **73**(19): 4640–4646.
- Liou, R.-M., Chen, S.-H., Hung, M.-Y., Hsu, C.-S., and Lai, J.-Y., (2005). Fe (III) supported on resin as effective catalyst for the heterogeneous oxidation of phenol in aqueous solution. *Chemosphere*, **59**(1): 117–125.
- Lissemore, L., Hao, C., Yang, P., Sibley, P. K., Mabury, S., and Solomon, K. R., (2006). An exposure assessment for selected pharmaceuticals within a watershed in Southern Ontario. *Chemosphere*, **64**(5), 717–729.

- Litter, M., (1999). Heterogeneous photocatalysis Transition metal ions in photocatalytic systems. *Appl. Catal. B: Environ.*, **23(2–3)**: 89–114.
- Liu, C.-M., Diao, Z.-H., Huo, W.-Y., Kong, L.-J., and Du, J.-J., (2018). Simultaneous removal of Cu²⁺ and bisphenol A by a novel biochar-supported zero valent iron from aqueous solution: Synthesis, reactivity and mechanism. *Environ. Pollut. Barking Essex*, **239**: 698–705.
- Liu, H., Cao, X., Liu, G., Wang, Y., Zhang, N., Li, T., and Tough, R., (2013). Photoelectrocatalytic degradation of triclosan on TiO₂ nanotube arrays and toxicity change. *Chemosphere*, **93(1)**: 160–165.
- Liu, Y., Liu, X., Dong, W., Zhang, L., Kong, Q., and Wang, W., (2017). Efficient Adsorption of Sulfamethazine onto Modified Activated Carbon: A Plausible Adsorption Mechanism. *Sci. Rep.*, **7(1)**: 12437.
- Liu, Y., and Wang, J., (2013). Degradation of sulfamethazine by gamma irradiation in the presence of hydrogen peroxide. *J. Hazard. Mater.*, **250–251**: 99–105.
- Liu, Y., Zha, S., Rajarathnam, D., and Chen, Z., (2017). Divalent cations impacting on Fenton-like oxidation of amoxicillin using nZVI as a heterogeneous catalyst. *Sep. Purif. Technol.*, **188**: 548–552.
- Lonappan, L., Brar, S. K., Das, R. K., Verma, M., and Surampalli, R. Y., (2016a). Diclofenac and its transformation products: Environmental occurrence and toxicity—A review. *Environ. Int.*, **96**: 127–138.
- Lonappan, L., Brar, S. K., Das, R. K., Verma, M., and Surampalli, R. Y., (2016b). Diclofenac and its transformation products: Environmental occurrence and toxicity—A review. *Environ. Int.*, **96**: 127–138.
- Lucas, M. S., and Peres, J. A., (2009). Removal of COD from olive mill wastewater by Fenton's reagent: Kinetic study. *J. Hazard. Mater.*, **168(2–3)**: 1253–1259.

- Lücking, F., Köser, H., Jank, M., and Ritter, A., (1998). Iron powder, graphite and activated carbon as catalysts for the oxidation of 4-chlorophenol with hydrogen peroxide in aqueous solution. *Water Res.*, **32(9)**: 2607–2614.
- Lv, X., Xu, Y., Lv, K., and Zhang, G., (2005). Photo-assisted degradation of anionic and cationic dyes over iron(III)-loaded resin in the presence of hydrogen peroxide. *J. Photochem. Photobiol. Chem.*, **173(2)**: 121–127.
- Ma, C., He, Z., Jia, S., Zhang, X., and Hou, S., (2018). Treatment of stabilized landfill leachate by Fenton-like process using Fe₃O₄ particles decorated Zr-pillared bentonite. *Ecotoxicol, Environ. Saf.*, **161**: 489–496.
- Ma, X., Cheng, Y., Ge, Y., Wu, H., Li, Q., Gao, N., and Deng, J., (2018). Ultrasound-enhanced nanosized zero-valent copper activation of hydrogen peroxide for the degradation of norfloxacin. *Ultrason. Sonochem.*, **40**: 763–772.
- Madani, M., Aliabadi, M., Nasernejad, B., Kermanj Abdulrahman, R., Yalili Kilic, M., and Kestioglu, K., (2015). Treatment of olive mill wastewater using physico-chemical and Fenton processes. *Desalination. Water. Treat.*, **53(8)**: 2031–2040.
- Maekawa, J., Mae, K., and Nakagawa, H., (2014). Fenton•Cu²⁺ system for phenol mineralization. *J. Environ. Chem. Eng.*, **2(3)**: 1275–1280.
- Maletzky, P., Bauer, R., Lahnsteiner, J., and Pouresmael, B., (1999). Immobilisation of iron ions on nafion® and its applicability to the photo-fenton method. *Chemosphere*, **38(10)**: 2315–2325.
- Malsawmdawngzela, R., and Tiwari, D., (2021). Facile synthesis and implications of novel hydrophobic materials: Newer insights of pharmaceuticals removal. *Indian j. Biochem. Biophys.*, **58**: 12.
- Markets, R. and., (2019). World Phenol Market Outlook and Forecast up to 2023. GlobeNewswire News Room.

- Marshall, W. D., (2002). Oxidative degradation of ethylenethiourea (ETU) and ETU progenitors by hydrogen peroxide and hypochlorite (world). *ACS Publications; American Chemical Society*.
- Martinez, J. L., (2009). Environmental pollution by antibiotics and by antibiotic resistance determinants. *Environ. Pollut.*, **157(11)**: 2893–2902.
- Mei, W., Song, H., Tian, Z., Zuo, S., Li, D., Xu, H., and Xia, D., (2019). Efficient photo-Fenton like activity in modified MIL-53(Fe) for removal of pesticides: Regulation of photogenerated electron migration. *Mater. Res. Bull.*, **119**: 110570.
- Meneses, M., Pasqualino, J. C., and Castells, F., (2010a). Environmental assessment of urban wastewater reuse: Treatment alternatives and applications. *Chemosphere*, **81(2)**: 266–272.
- Meneses, M., Pasqualino, J. C., and Castells, F., (2010b). Environmental assessment of urban wastewater reuse: Treatment alternatives and applications. *Chemosphere*, **81(2)**: 266–272.
- Miranda-García, N., Maldonado, M. I., Coronado, J. M., and Malato, S., (2010). Degradation study of 15 emerging contaminants at low concentration by immobilized TiO₂ in a pilot plant. *Catal. Today*, **151(1–2)**: 107–113.
- Mitsika, E. E., Christophoridis, C., and Fytianos, K., (2013a). Fenton and Fenton-like oxidation of pesticide acetamiprid in water samples: Kinetic study of the degradation and optimization using response surface methodology. *Chemosphere*, **93(9)**: 1818–1825.
- Mitsika, E. E., Christophoridis, C., and Fytianos, K., (2013b). Fenton and Fenton-like oxidation of pesticide acetamiprid in water samples: Kinetic study of the degradation and optimization using response surface methodology. *Chemosphere*, **93(9)**: 1818–1825.

- Molina, R., Martínez, F., Melero, J. A., Bremner, D. H., and Chakinala, A. G., (2006). Mineralization of phenol by a heterogeneous ultrasound/Fe-SBA-15/H₂O₂ process: Multivariate study by factorial design of experiments. *Appl. Catal. B: Environ.*, **66(3–4)**: 198–207.
- Morales, A. E., Mora, E. S., and Pal, U., (2007). Use of diffuse reflectance spectroscopy for optical characterization of un-supported nanostructures. **6**.
- Morshed, M. N., Bouazizi, N., Behary, N., Guan, J., and Nierstrasz, V., (2019). Stabilization of zero valent iron (Fe⁰) on plasma/dendrimer functionalized polyester fabrics for Fenton-like removal of hazardous water pollutants. *Chem. Eng. J.*, **374**: 658–673.
- Muthuvel, I., and Swaminathan, M., (2008). Highly solar active Fe(III) immobilised alumina for the degradation of Acid Violet 7. *Sol. Energy Mater. Sol. Cells*, **92(8)**: 857–863.
- Mzukisi, L., Tawanda, N., and Chimuka, L., (2017). Status of pharmaceuticals in African water bodies: Occurrence, removal and analytical methods. *J. Environ. Manage.*, **193**: 211–220.
- Nägele, E., and Moritz, R., (2005). Structure Elucidation of Degradation Products of the Antibiotic Amoxicillin with Ion Trap MSn and Accurate Mass Determination by ESI TOF. *J. Am. Soc. Mass Spectrom.*, **16(10)**:1670–1676.
- Navalon, S., Alvaro, M., and Garcia, H., (2010). Heterogeneous Fenton catalysts based on clays, silicas and zeolites. *Appl. Catal. B. Environ.*, **99(1–2)**:1–26.
- Navalon, S., Sempere, D., Alvaro, M., and Garcia, H., (2013). Influence of Hydrogen Annealing on the Photocatalytic Activity of Diamond-Supported Gold Catalysts. *ACS Appl. Mater. Interfaces.*, **5(15)**: 7160–7169.
- Neyens, E., and Baeyens, J., (2003). A review of classic Fenton's peroxidation as an advanced oxidation technique. *J. Hazard. Mater.*, **98(1–3)**: 33–50.

- Nidheesh, P. V., Gandhimathi, R., and Ramesh, S. T., (2013). Degradation of dyes from aqueous solution by Fenton processes: A review. *Environ. Sci. Pollut. Res.*, **20(4)**:2099–2132.
- Nogueira, I., and Pliego, J., (2018). Theoretical Study of the Mechanism and Regioselectivity of the Alkylation Reaction of the Phenoxide Ion in Polar Protic and Aprotic Solvents. *Comput. Theor. Chem.*, 1138.
- Noradoun, C. E., and Cheng, I. F., (2005). EDTA Degradation Induced by Oxygen Activation in a Zerovalent Iron/Air/Water System. *Environ. Sci. Technol.*, **39(18)**: 7158–7163.
- Noradoun, C., Engelmann, M. D., McLaughlin, M., Hutcheson, R., Breen, K., Paszczyński, A., and Cheng, I. F., (2003). Destruction of Chlorinated Phenols by Dioxygen Activation under Aqueous Room Temperature and Pressure Conditions. *Environ. Sci. Technol.*, **42(21)**: 5024–5030.
- Obouayeba, A. P., Diarrassouba, M., Soumahin, E. F., and Kouakou, H., (2015). Phytochemical Analysis, Purification and Identification of Hibiscus Anthocyanins. **3(2)**: 156–168.
- Pan, X., Deng, C., Zhang, D., Wang, J., Mu, G., and Chen, Y., (2008). Toxic effects of amoxicillin on the photosystem II of *Synechocystis* sp. Characterized by a variety of in vivo chlorophyll fluorescence tests. *Aquat. Toxicol. Amst. Neth.*, **89(4)**: 207–213.
- Pang, S.-Y., Jiang, J., and Ma, J., (2011). Oxidation of Sulfoxides and Arsenic(III) in Corrosion of Nanoscale Zero Valent Iron by Oxygen: Evidence against Ferryl Ions (Fe(IV)) as Active Intermediates in Fenton Reaction. *Environ. Sci. Technol.*, **45(1)**: 307–312.
- Parashar, U. K., Kumar, V., Bera, T., Saxena, P. S., Nath, G., Srivastava, S. K., Giri, R., and Srivastava, A., (2011). Study of mechanism of enhanced antibacterial

- activity by green synthesis of silver nanoparticles. *Nanotechnology*, **22(41)**: 415104.
- Paschoalino, M., Guedes, N. C., Jardim, W., Mielczarski, E., Mielczarski, J. A., Bowen, P., and Kiwi, J., (2008). Inactivation of *E. coli* mediated by high surface area CuO accelerated by light irradiation >360nm. *J. Photochem. Photobiol. Chem.*, **199(1)**: 105–111.
- Paul, B., Martens, W. N., and Frost, R. L., (2011). Organosilane grafted acid-activated beidellite clay for the removal of non-ionic alachlor and anionic imazaquin. *Appl. Surf. Sci.*, **257(13)**: 5552–5558.
- Perez, J. M. (2007). A catalytic property widely used for laboratory tests and the treatment of waste water has been discovered in iron oxide nanoparticles and could lead to many applications in medical diagnostics. **2**.
- Petala, M., Tsiridis, V., Samaras, P., Zouboulis, A., and Sakellaropoulos, G. P., (2006). Wastewater reclamation by advanced treatment of secondary effluents. *Desalination*, **195(1–3)**: 109–118.
- Petrovic, M., and Barceló, D. (2006). Application of liquid chromatography/quadrupole time-of-flight mass spectrometry (LC-QqTOF-MS) in the environmental analysis. *J. Mass. Spectrom.*, **41(10)**: 1259–1267.
- Pham, V. L., Kim, D. G., and Ko, S. O., (2018). Cu@Fe₃O₄ core-shell nanoparticle-catalyzed oxidative degradation of the antibiotic oxytetracycline in pre-treated landfill leachate. *Chemosphere*, **191**: 639–650.
- Phillips, P. J., Smith, S. G., Kolpin, D. W., Zaugg, S. D., Buxton, H. T., Furlong, E. T., Esposito, K., and Stinson, B., (2010). Pharmaceutical formulation facilities as sources of opioids and other pharmaceuticals to wastewater treatment plant effluents. *Environ. Sci. Technol.*, **44(13)**: 4910–4916.

- Pignatello, J. J., Oliveros, E., and MacKay, A., (2006). Advanced Oxidation Processes for Organic Contaminant Destruction Based on the Fenton Reaction and Related Chemistry. *Crit. Rev. Environ. Sci. Technol.*, **36(1)**: 1–84.
- Pirsaheb, M., Moradi, S., Shahlaei, M., Wang, X., and Farhadian, N., (2019). A new composite of nano zero-valent iron encapsulated in carbon dots for oxidative removal of bio-refractory antibiotics from water. *J. clean. Pod.*, **209**: 1523–1532.
- Planas, C., Caixach, J., Santos, F. J., and Rivera, J., (1997). Occurrence of pesticides in Spanish surface waters. Analysis by high resolution gas chromatography coupled to mass spectrometry. *Chemosphere*, **34(11)**: 2393–2406.
- Prieto, P., Nistor, V., Nouneh, K., Oyama, M., Abd-Lefdil, M., and Díaz, R., (2012). XPS study of silver, nickel and bimetallic silver–nickel nanoparticles prepared by seed-mediated growth. *Appl. Surf. Sci.*, **258(22)**: 8807–8813.
- Putra, E. K., Pranowo, R., Sunarso, J., Indraswati, N., and Ismadji, S., (2009). Performance of activated carbon and bentonite for adsorption of amoxicillin from wastewater: Mechanisms, isotherms and kinetics. *Water Res.*, **43(9)**: 2419–2430.
- Rahim Pouran, S., Abdul Aziz, A. R., and Wan Daud, W. M. A., (2015). Review on the main advances in photo-Fenton oxidation system for recalcitrant wastewaters. *J. Ind. Eng. Chem.*, **21**: 53–69.
- Rahim Pouran, S., Abdul Raman, A. A., and Wan Daud, W. M. A., (2014). Review on the application of modified iron oxides as heterogeneous catalysts in Fenton reactions. *J. clean Pod.*, **64**: 24–35.
- Rajesh Banu, J., Godvin Sharmila, V., Gayathri devi, M., Adish Kumar, S., Kumar, G., Nguyen, D. D., and Dattatraya Saratale, G., (2019). Cost effective sludge reduction using synergetic effect of dark fenton and disperser treatment. *J. clean. Pod.*, **207**: 261–270.

- Raji, M., Mirbagheri, S. A., Ye, F., and Dutta, J., (2021). Nano zero-valent iron on activated carbon cloth support as Fenton-like catalyst for efficient color and COD removal from melanoidin wastewater. *Chemosphere*, **263**: 127945.
- Ramirez, J. H., Maldonado-Hódar, F. J., Pérez-Cadenas, A. F., Moreno-Castilla, C., Costa, C. A., and Madeira, L. M. (2007). Azo-dye Orange II degradation by heterogeneous Fenton-like reaction using carbon-Fe catalysts. *Appl. Catal. B: Environ.*, **75(3–4)**: 312–323.
- Rasheed, H. U., Lv, X., Zhang, S., Wei, W., ullah, N., and Xie, J., (2018). Ternary MIL-100(Fe)@Fe₃O₄/CA magnetic nanophotocatalysts (MNPCs): Magnetically separable and Fenton-like degradation of tetracycline hydrochloride. *Adv. Powder Technol.*, **29(12)**: 3305–3314.
- Ribas, J. L. C., Zampronio, A. R., and Silva de Assis, H. C., (2016). Effects of trophic exposure to diclofenac and dexamethasone on hematological parameters and immune response in freshwater fish. *Environ. Toxicol. Chem.*, **35(4)**: 975–982.
- Rios-Enriquez, M., Shahin, N., Durán-de-Bazúa, C., Lang, J., Oliveros, E., Bossmann, S. H., and Braun, A. M., (2004). Optimization of the heterogeneous Fenton-oxidation of the model pollutant 2,4-xylydine using the optimal experimental design methodology. *Solar Energy*, **77(5)**: 491–501.
- Rodríguez, M., Timokhin, V., Contreras, S., Chamarro, E., and Esplugas, S., (2003). Rate equation for the degradation of nitrobenzene by ‘Fenton-like’ reagent.
- Rostami-Vartooni, A., Alizadeh, M., and Bagherzadeh, M., (2015). Green synthesis, characterization and catalytic activity of natural bentonite-supported copper nanoparticles for the solvent-free synthesis of 1-substituted 1 H -1,2,3,4-tetrazoles and reduction of 4-nitrophenol. *Beilstein J. Nanotechnol.*, **6**: 2300–2309.
- S, J. P., and Evan Prince, S., (2018). Diclofenac-induced renal toxicity in female Wistar albino rats is protected by the pre-treatment of aqueous leaves extract

of *Madhuca longifolia* through suppression of inflammation, oxidative stress and cytokine formation. *Biomed. Pharmacother.*, **98**: 45–51.

Sabhi, S., and Kiwi, J., (2001). Degradation of 2,4-dichlorophenol by immobilized iron catalysts. *Water Res.*, **35(8)**: 1994–2002.

Sadeghi, M., Mehdinejad, M. H., Mengelizadeh, N., Mahdavi, Y., Pourzamani, H., Hajizadeh, Y., and Zare, M. R., (2019). Degradation of diclofenac by heterogeneous electro-Fenton process using magnetic single-walled carbon nanotubes as a catalyst. *J. Water Process Eng.*, **31**: 100852.

Sahoo, P. R., Sahu, S., Patel, S., and Mishra, B. K., (2010). Oxidation kinetics of arylthioureas by cetyltrimethylammonium dichromate. *IJC-A Vol.* **49A(11)**.

Sahu, S., Rani Sahoo, P., Patel, S., and Mishra, B. K., (2011). Oxidation of thiourea and substituted thioureas: A review. *J. Sul. Chem.*, **32(2)**: 171–197.

Salgado, P., Melin, V., Contreras, D., Moreno, Y., and Mansilla, H. D., (2013). Fenton reaction driven by iron ligands. *J. Chil. Chem. Soc.*, **58(4)**: 2096–2101.

Sanabria, N., Álvarez M, A., Molina, R., and Moreno, S., (2008). Synthesis of pillared bentonite starting from the Al–Fe polymeric precursor in solid state, and its catalytic evaluation in the phenol oxidation reaction. *Catalysis Today*, **133**: 530–533.

Sangami, S., and Manu, B., (2017). Synthesis of Green Iron Nanoparticles using Laterite and their application as a Fenton-like catalyst for the degradation of herbicide Ametryn in water. *Environ. Technol. Innov.*, **8**: 150–163.

Sapach, R., and Viraraghavan, T., (1997). An introduction to the use of hydrogen peroxide and ultraviolet radiation: An advanced oxidation process. *J Environ Sci. Health Part Environ. Sci. Eng. Toxicol.*, **32(8)**: 2355–2366.

- Scaria, J., Gopinath, A., and Nidheesh, P. V., (2021). A versatile strategy to eliminate emerging contaminants from the aqueous environment: Heterogeneous Fenton process. *J. Clean. Prod.*, **278**: 124014.
- Sdiri, A., Khairy, M., Bouaziz, S., and El-Safty, S., (2016). A natural clayey adsorbent for selective removal of lead from aqueous solutions. *Appl. Clay. Sci.*, **126**: 89–97.
- Segura, Y., Martínez, F., and Melero, J. A., (2013). Effective pharmaceutical wastewater degradation by Fenton oxidation with zero-valent iron. *Appl. Catal. B: Environ.*, **136–137**: 64–69.
- Seibig, S., and van Eldik, R., (1997). Kinetics of [Fe^{II}(edta)] Oxidation by Molecular Oxygen Revisited. New Evidence for a Multistep Mechanism. *Inorg. Chem.*, **36(18)**: 4115–4120.
- Selvam, K., Muruganandham, M., Muthuvel, I., and Swaminathan, M., (2007). The influence of inorganic oxidants and metal ions on semiconductor sensitized photodegradation of 4-fluorophenol. *Chem. Eng. J.*, **128(1)**: 51–57.
- Sempere, D., Navalon, S., Dančíková, M., Alvaro, M., and Garcia, H., (2013). Influence of pretreatments on commercial diamond nanoparticles on the photocatalytic activity of supported gold nanoparticles under natural Sunlight irradiation. *Appl. Catal. B: Environ.*, **142–143**: 259–267.
- Sétifi, N., Debbache, N., Sehili, T., and Halimi, O., (2019). Heterogeneous Fenton-like oxidation of naproxen using synthesized goethite-montmorillonite nanocomposite. *J. Photochem. Photobiol. Chem.*, **370**: 67–74.
- Shah, N. S., Khan, J. A., Sayed, M., Iqbal, J., Khan, Z. U. H., Muhammad, N., Polychronopoulou, K., Hussain, S., Imran, M., Murtaza, B., Usman, M., Ismail, I., Shafique, A., Howari, F., and Nazzal, Y., (2020). Nano-zerovalent copper as a Fenton-like catalyst for the degradation of ciprofloxacin in aqueous solution. *J. Water Process Eng.*, **37**: 101325.

- Shahid, M. K., Kashif, A., Fuwad, A., and Choi, Y., (2021). Current advances in treatment technologies for removal of emerging contaminants from water – A critical review. *Coord. Chem. Rev.*, **442**: 213993.
- Shahwan, T., Üzüm, Ç., Eroğlu, A. E., and Lieberwirth, I., (2010). Synthesis and characterization of bentonite/iron nanoparticles and their application as adsorbent of cobalt ions. *Appl. Clay. Sci.*, **47(3–4)**: 257–262.
- Shinya, A., and Bergwall, L., (n.d.). Pyrite Oxidation: Review and Prevention Practices. **27**: 145A-145A.
- Silva, P. J., (2009). Inductive and Resonance Effects on the Acidities of Phenol, Enols, and Carbonyl α -Hydrogens. *J. Org. Chem.*, **74(2)**: 914–916.
- Sirés, I., Oturan, N., Oturan, M. A., Rodríguez, R. M., Garrido, J. A., and Brillas, E., (2007). Electro-Fenton degradation of antimicrobials triclosan and triclocarban. *Electrochimica Acta*, **52(17)**: 5493–5503.
- Snell, F. D. (1978). Photometric and fluorometric methods of analysis: Metals. Wiley.
- Song, Shikun., Su, Yiming., Adeleye, A. S., Zhang, Yalei., and Zhou, Xuefei., (2017). Optimal design and characterization of sulfide-modified nanoscale zerovalent iron for diclofenac removal. *Appl. Catal. B: Environ.*, **201**: 211–220.
- Sousa, J. C. G., Ribeiro, A. R., Barbosa, M. O., Pereira, M. F. R., and Silva, A. M. T., (2018). A review on environmental monitoring of water organic pollutants identified by EU guidelines. *J. Hazard. Mater.*, **344**: 146–162.
- Sriuttha, P., Sirichanchuen, B., and Permsuwan, U., (2018). Hepatotoxicity of Nonsteroidal Anti-Inflammatory Drugs: A Systematic Review of Randomized Controlled Trials. *Int. J. Hepatol.* 2018, e5253623.
- Stumm, W., and Morgan, J. J., (2012). *Aquatic chemistry: Chemical equilibria and rates in natural waters* (Vol. **126**). John Wiley & Sons.

- Sulaiman, S., and Al-Jabari, M., (2021). Enhanced adsorptive removal of diclofenac sodium from aqueous solution by bentonite- supported nanoscale zero-valent iron. *Arab. J. Basic Appl. Sci.*, **28**: 51–63.
- Sun, J., Li, W., Zheng, P., and Zhu, J., (2012). Toxicity evaluation of antibiotics in piggery wastewater by luminescent bacteria. *Pol. J. Environ. Stud.*, **21(3)**: 741–747.
- Tahir, M. B., Sohaib, M., Sagir, M., and Rafique, M., (2020). Role of Nanotechnology in Photocatalysis. *Ref. Module Mater. Sci. Mater. Eng.*, B978-0-12-815732-9.00006-1.
- Tamilvanan, A., Balamurugan, K., Ponappa, K., and Kumar, B. M. (2014). Copper Nanoparticles: Synthetic Strategies, Properties and Multifunctional Application. *Int. J. Nanosci.*, **13(02)**: 1430001.
- Tang, J., and Wang, J., (2018). Fenton-like degradation of sulfamethoxazole using Fe-based magnetic nanoparticles embedded into mesoporous carbon hybrid as an efficient catalyst. *Chem. Eng. J.*, **351**: 1085–1094.
- Tang, J., and Wang, J., (2019). MOF-derived three-dimensional flower-like FeCu@C composite as an efficient Fenton-like catalyst for sulfamethazine degradation. *Chem. Eng. J.*, 375:122007.
- Tang, S. C. N., and Lo, I. M. C., (2013). Magnetic nanoparticles: Essential factors for sustainable environmental applications. *Water Res.*, **47(8)**: 2613–2632.
- Teijon, G., Candela, L., Tamoh, K., Molina-Díaz, A., and Fernández-Alba, A. R., (2010). Occurrence of emerging contaminants, priority substances (2008/105/CE) and heavy metals in treated wastewater and groundwater at Depurbaix facility (Barcelona, Spain). *Sci. Total Environ.*, **408(17)**: 3584–3595.

- Thelusmond, J., Kawka, E., Strathmann, T. J., and Cupples, A. M., (2018). Science of the Total Environment Diclofenac , carbamazepine and triclocarban biodegradation in agricultural soils and the microorganisms and metabolic pathways affected. *Sci .Total Environ.*, **640–641**: 1393–1410.
- Theng, B. K. G., and Yuan, G., (2008). Nanoparticles in the Soil Environment. *Elements.*, **4(6)**: 395–399.
- Thomas, C., Mackey, M. M., Diaz, A. A., and Cox, D. P., (2009). Hydroxyl radical is produced via the Fenton reaction in submitochondrial particles under oxidative stress: Implications for diseases associated with iron accumulation. *Redox Report: Commun. Free Radic. Res.*, **14(3)**: 102–108.
- Tiwari, A., Shukla, A., Lalliansanga, null, Tiwari, D., and Lee, S. M., (2018a). Nanocomposite thin films Ag0(NP)/TiO2 in the efficient removal of micro-pollutants from aqueous solutions: A case study of tetracycline and sulfamethoxazole removal. *J. Environ. Manage.*, **220**: 96–108.
- Tiwari, A., Shukla, A., Lalliansanga, Tiwari, D., and Lee, S. M., (2018b). Nanocomposite thin films Ag0(NP)/TiO2 in the efficient removal of micro-pollutants from aqueous solutions: A case study of tetracycline and sulfamethoxazole removal. *J. Environ. Manage.*, **220**:96–108.
- Tiwari, D., Laldanwngliana, C., Choi, C.-H., and Lee, S. M., (2011). Manganese-modified natural sand in the remediation of aquatic environment contaminated with heavy metal toxic ions. *Chem. Eng. J.*, **171(3)**: 958–966.
- Tiwari, D., Lalhriatpuia, C., Lalhmunsiama, Lee, S.-M., and Kong, S.-H., (2015). Efficient application of nano-TiO2 thin films in the photocatalytic removal of Alizarin Yellow from aqueous solutions. *Appl. Surf. Sci.*, **353**:275–283.
- Tiwari, D., Lalhriatpuia, C., and Lee, S.-M., (2015). Hybrid materials in the removal of diclofenac sodium from aqueous solutions: Batch and column studies. *J Ind. Eng. Chem.*, **30**:167–173.

- Tomic, Z., Milijasevic, B., Sabo, A., Dusan, L., Jakovljevic, V., Mikov, M., Majda, S., and Vasovic, V., (2008). Diclofenac and ketoprofen liver toxicity in rat. *Eur. J. Drug Metab. Pharmacokinet.*, **33(4)**:253.
- Triebkorn, R., Casper, H., Scheil, V., and Schwaiger, J., (2007). Ultrastructural effects of pharmaceuticals (carbamazepine, clofibrac acid, metoprolol, diclofenac) in rainbow trout (*Oncorhynchus mykiss*) and common carp (*Cyprinus carpio*). *Anal. Bioanal. Chem.*, **387(4)**: 1405–1416.
- Tryba, B., (2008). Immobilization of TiO₂ and Fe–C–TiO₂ photocatalysts on the cotton material for application in a flow photocatalytic reactor for decomposition of phenol in water. *J. Hazard. Mater.*, **151(2–3)**: 623–627.
- Tzeng, T.-W., Wang, S.-L., Chen, C.-C., Tan, C.-C., Liu, Y.-T., Chen, T.-Y., Tzou, Y., and Hung, J. T., (2016). Photolysis and photocatalytic decomposition of sulfamethazine antibiotics in an aqueous solution with TiO₂. *RSC Advances.*, **6**: 69301–69310.
- United Nations Environment Programme and Earthscan., (2002). *Global environment outlook 3 3*. Earthscan [on behalf of] UNEP.
- Utset, B., Garcia, J., Casado, J., Domènech, X., and Peral, J., (2000). Replacement of H₂O₂ by O₂ in Fenton and photo-Fenton reactions. *Chemosphere.*, **41(8)**.
- Van scnte, P. M., and Young, L. Y., (2000). Biodegradation of phenol: Mechanisms and applications. *Bioremediation J.*, **4(1)**: 1–18.
- Vaz-Moreira, I., Nunes, O. C., and Manaia, C. M., (2014). Bacterial diversity and antibiotic resistance in water habitats: Searching the links with the human microbiome. *FEMS Microbiol. Rev.*, **38(4)**:761–778.
- Vieno, N., and Sillanpää, M., (2014). Fate of diclofenac in municipal wastewater treatment plant—A review. *Environ. Int.*, **69**:28–39.

- Wan, Z., and Wang, J., (2016). Ce-Fe-reduced graphene oxide nanocomposite as an efficient catalyst for sulfamethazine degradation in aqueous solution. *Environ. Sci. Pollut. Res. Int.*, **23**.
- Wang, C., and Shih, Y., (2015). Degradation and detoxification of diazinon by sono-Fenton and sono-Fenton-like processes. *Sep. Purif. Technol.*, **140**: 6–12.
- Wang, C., Sun, R., and Huang, R., (2021). Highly dispersed iron-doped biochar derived from sawdust for Fenton-like degradation of toxic dyes. *J. Clean. Prod.*, **297**:126681.
- Wang, J., Zhuan, R., and Chu, L., (2019). The occurrence, distribution and degradation of antibiotics by ionizing radiation: An overview. *Sci. Total Environ.*, **646**:1385–1397.
- Wang, L., Lu, F., Liu, Y., Wu, Y., and Wu, Z., (2018). Photocatalytic degradation of organic dyes and antimicrobial activity of silver nanoparticles fast synthesized by flavonoids fraction of *Psidium guajava* L. leaves. *J. Mol. Liq.*, **263**:187–192.
- Wang, N., Zheng, T., Zhang, G., and Wang, P., (2016). A review on Fenton-like processes for organic wastewater treatment. *J. Environ. Chem. Eng.*, **4**(1): 762–787.
- Watkinson, A. J., Murby, E. J., Kolpin, D. W., and Costanzo, S. D., (2009). The occurrence of antibiotics in an urban watershed: From wastewater to drinking water. *J. Environ. Chem. Eng.*, **407**(8): 2711–2723.
- Weisburger, J. H., (1992). Mutagenic, carcinogenic, and chemopreventive effects of phenols and catechols: The underlying mechanisms. *ACS Symp. Ser. (USA)*.
- Wen, D., Wu, Z., Tang, Y., Li, M., and Qiang, Z., (2018). Accelerated degradation of sulfamethazine in water by VUV/UV photo-Fenton process: Impact of sulfamethazine concentration on reaction mechanism. *J. Hazard. Mater.*, **344**: 1181–1187.

- Wen, G., Wang, S.-J., Ma, J., Huang, T.-L., Liu, Z.-Q., Zhao, L., and Xu, J.-L., (2014a). Oxidative degradation of organic pollutants in aqueous solution using zero valent copper under aerobic atmosphere condition. *J. Hazard. Mater.*, **275**:193–199.
- Wen, G., Wang, S.-J., Ma, J., Huang, T.-L., Liu, Z.-Q., Zhao, L., and Xu, J.-L., (2014b). Oxidative degradation of organic pollutants in aqueous solution using zero valent copper under aerobic atmosphere condition. *J. Hazard. Mater.*, **275**:193–199.
- Wen, T., Zhao, Y., Jiao, X., Yang, G., Zhang, Z., Wang, W., Zhang, T., Zhang, Q., and Song, S., (2021). Use of posnjakite containing sludge as catalyst for decoloring dye via photo-Fenton-like process. *J. Clean. Prod.*, **293**:126184.
- WHO, and UNICEF., (2013). *Sanitation and Drinking-water Progress on 2013 UPDATE WHO Library Cataloguing-in-Publication Data Progress on sanitation and drinking-water-2013 update*. 40.
- Windholz, M., (1976). *The Merck Index: An encyclopedia of chemicals, drugs, and biologicals*. Merck.
- Wu, Y., Zeng, S., Wang, F., Megharaj, M., Naidu, R., and Chen, Z., (2015). Heterogeneous Fenton-like oxidation of malachite green by iron-based nanoparticles synthesized by tea extract as a catalyst. *Sep. Purif. Technol.*, **(154)**:161–167.
- Xu, F., Lu, Q., Li, K., Zhu, T.-T., Wang, W.-K., and Hu, Z.-H., (2021). Green synthesis of magnetic mesoporous carbon from waste-lignin and its application as an efficient heterogeneous Fenton catalyst. *J. Clean. Prod.*, **285**: 125363.
- Xu, H.-Y., Liu, W.-C., Qi, S.-Y., Li, Y., Zhao, Y., and Li, J.-W., (2014). Kinetics and optimization on discoloration of dyeing wastewater by schorl-catalyzed fenton-like reaction. *J. Serbian. Chem .Soc.*, **79(3)**:361–377.

- Xu, L., and Wang, J., (2011). A heterogeneous Fenton-like system with nanoparticulate zero-valent iron for removal of 4-chloro-3-methyl phenol. *J. Hazard. Mater.*, **186(1)**:256–264.
- Xu, L., Yang, Y., Li, W., Tao, Y., Sui, Z., Song, S., and Yang, J., (2019). Three-dimensional macroporous graphene-wrapped zero-valent copper nanoparticles as efficient micro-electrolysis-promoted Fenton-like catalysts for metronidazole removal. *Sci. Total Environ.*, **658**: 219–233.
- Xu, W., Zhang, G., Zou, S., Li, X., and Liu, Y., (2007). Determination of selected antibiotics in the Victoria Harbour and the Pearl River, South China using high-performance liquid chromatography-electrospray ionization tandem mass spectrometry. *Environ. Pollut. Barking. Essex : 1987.*, **145(3)**: 672–679.
- Xue, X., Hanna, K., Despas, C., Wu, F., and Deng, N., (2009). Effect of chelating agent on the oxidation rate of PCP in the magnetite/H₂O₂ system at neutral pH. *J. Mol. Catal. Chem.*, **311(1–2)**: 29–35.
- Yang, H., and Abbaspour, K. C., (2007). Analysis of wastewater reuse potential in Beijing. *Desalination.*, **212(1–3)**: 238–250.
- Yang, X., Moats, M. S., Miller, J. D., Wang, X., Shi, X., and Xu, H., (2011). Thiourea–thiocyanate leaching system for gold. *Hydrometallurgy.*, **106(1)**: 58–63.
- Yang, Y., Xu, L., Li, W., Fan, W., Song, S., and Yang, J., (2019). Adsorption and degradation of sulfadiazine over nanoscale zero-valent iron encapsulated in three-dimensional graphene network through oxygen-driven heterogeneous Fenton-like reactions. *Appl. Catal. B. Environ.*, **259**:118057.
- Yao, H., Hu, S., Wu, Y., and Fan, L., (2019). The Synergetic Effects in a Fenton-like System Catalyzed by Nano Zero-valent Iron (nZVI). *Pol. J. Environ. Stud.*, **28(4)**: 2491–2499.

- Ye, J., Luo, Y., Sun, J., and Shi, J., (2021). Nanoscale Zero-Valent Iron Modified by Bentonite with Enhanced Cr(VI) Removal Efficiency, Improved Mobility, and Reduced Toxicity. *Nanomaterials.*, **11**: 2580.
- Yogesh J. Sanghani., (2017). (PDF) *Handbook of chemistry lab reagent*.
_Handbook_of_chemistry_lab_reagent
- Yurt, K. K., Kaplan, S., and Kivrak, E. G., (2017). The neuroprotective effect of melatonin on the hippocampus exposed to diclofenac sodium during the prenatal period. *J Chem Neuroanat.*,
- Yuval, A., Eran, F., Janin, W., Oliver, O., and Yael, D., (2017). Photodegradation of micropollutants using V-UV/UV-C processes; Triclosan as a model compound. *Sci Total Environ.*, **601–602(Supplement C)**: 397–404
- .Zelmanov, G., and Semiat, R., (2008). Iron(3) oxide-based nanoparticles as catalysts in advanced organic aqueous oxidation. *Water. Res.*, **42(1–2)**: 492–498.
- Zhang, H., Choi, H. J., and Huang, C.-P., (2005). Optimization of Fenton process for the treatment of landfill leachate. *J. Hazard. Mater.*, **125(1–3)**: 166–174.
- Zhang, M.-H., Dong, H., Zhao, L., Wang, D.-X., and Meng, D., (2019). A review on Fenton process for organic wastewater treatment based on optimization perspective. *Sci. Total. Environ.*, **670**: 110–121.
- Zhang, W., Gao, H., He, J., Yang, P., Wang, D., Ma, T., Xia, H., and Xu, X., (2017). Removal of norfloxacin using coupled synthesized nanoscale zero-valent iron (nZVI) with H₂O₂ system: Optimization of operating conditions and degradation pathway. *Sep. Purif. Technol.*, **172**: 158–167.
- Zhang, Y., Zhao, L., Yang, Y., and Sun, P., (2020). Fenton-Like Oxidation of Antibiotic Ornidazole Using Biochar-Supported Nanoscale Zero-Valent Iron as Heterogeneous Hydrogen Peroxide Activator. *Int. J. Environ. Res. Public Health*, **17(4)**: 1324.

- Zhao, H., Cao, Z., Liu, X., Zhan, Y., Zhang, J., Xiao, X., Yang, Y., Zhou, J., and Xu, J., (2017). Seasonal variation, flux estimation, and source analysis of dissolved emerging organic contaminants in the Yangtze Estuary, China. *Mar. Pollut. Bull.*, **125(1)**: 208–215.
- Zhou, P., Zhang, J., Liu, J., Zhang, Y., Liang, J., Liu, Y., Liu, B., and Zhang, W., (2016). Degradation of organic contaminants by activated persulfate using zero valent copper in acidic aqueous conditions. *RSC Adv.*, **6(101)**: 99532–99539.
- Zhou, P., Zhang, J., Zhang, Y., Liang, J., Liu, Y., Liu, B., and Zhang, W., (2016). Activation of hydrogen peroxide during the corrosion of nanoscale zero valent copper in acidic solution. *J. Mol. Catal. Chem.*, **424**: 115–120.
- Zhou, T., Lim, T.-T., Lu, X., Li, Y., and Wong, F.-S., (2009). Simultaneous degradation of 4CP and EDTA in a heterogeneous Ultrasound/Fenton like system at ambient circumstance. *Sep. Purif. Technol.*, **68(3)**: 367–374.
- Zia, H., Shalchian, N., and Borhanian, F., (1977). Kinetics of amoxicillin degradation in aqueous solutions. *Can. J. Pharm. Sci.*, **12(3)**: 80–83.
- Zuo, Y., (1995). Kinetics of photochemical/chemical cycling of iron coupled with organic substances in cloud and fog droplets. *Geochim. Cosmochim. Acta.*, **59(15)**: 3123–3130.

BIO-DATA

- 1. NAME** : Himangshu Dihingia
- 2. DATE OF BIRTH** : 26th June, 1994.
- 3. FATHER'S NAME** : Late. Nripen Dihingia
- 4. PERMANENT ADDRESS** : Bokata Dihingia Gaon, P.O : Charubhanga
Sivasagar, Assam-785674

5. EDUCATIONAL QUALIFICATIONS:

Qualification	Year of Passing	Board/University	Subjects	Marks %	Division
HSLC	2010	Board of Secondary Education, Assam	English, Assamese, Mathematics, Science, Social sciences Adv. Math.	78.5	First
HSSLC	2012	Assam Higher Secondary Education Council	English, Assamese, Computer-Science, Physics, Chemistry	68.2	First
B.Sc (Chemistry)	2015	Gargaon College, Dibrugarh University	Chemistry, Physics, mathematics	63.65	First
M.Sc (Chemistry)	2017	Mizoram University	Chemistry (Specialization in physical Chemistry)	76.5	First

List of publications

A. Journals

1. **Dihingia, H., & Tiwari, D.** (2022). Impact and implications of nanocatalyst in the Fenton-like processes for remediation of aquatic environment contaminated with micro-pollutants: A critical review. *Journal of Water Process Engineering*, **45**:102500. <https://doi.org/10.1016/j.jwpe.2021.102500>
2. **Dihingia, H., & Tiwari, D.** (2022). Green synthesis of bimetallic nanocomposite: Efficient use of nanocomposite in the removal of phenol and n-(n-Propyl) thiourea by photo-Fenton-like process. *Journal of cleaner production*, **374**: 133913. <https://doi.org/10.1016/j.jclepro.2022.133913>
3. **Dihingia, H., & Tiwari, D.** (2023). Green and facile synthesis of heterojunction nanocatalyst: Insights and mechanism of antibiotics removal. *Separation and purification technology*, **306**: 122641. <https://doi.org/10.1016/j.seppur.2022.122641>
4. **Dihingia, H., Lalmalsawmdawngliani & Tiwari, D.** (2022). New insights in the removal of diclofenac sodium from aqueous solutions: Efficient use of bentonite supported bimetallic Fe⁰/Ag⁰ nanocomposite. (communicated- *Journal of Industrial and Engineering Chemistry*)

B. Conference/ Seminar

1. Presented “Heterogeneous Fenton-like Degradation of N-(n-Propyl)Thiourea from Aqueous Solution using synthesized(Bentonite/Fe⁰/Ag⁰) Nanocomposite” at 2nd Annual Convention of North East (India) Academy of Science and Technology (NEAST) & International Seminar on Recent Advances in Science and Technology (ISRAST), 16th -18th November 2020, Organized by NEAST, Mizoram University, Aizawl, Mizoram, India.
2. Presented “Heterogeneous Fenton-like Degradation of Diclofenac sodium from Aqueous Solution using synthesized Bentonite/FeNPs/AgNPs Nanocomposite” at the National conference on Emerging trends in environmental research (NACTER 2019), organized by the Department of Environmental Science, Pachhunga University College, Aizawl in collaboration with Environment, Forest & climate change department, Government of Mizoram, During 31 October-2 November 2019



ELSEVIER

ISSN 2214-7144

JOURNAL OF

WATER PROCESS ENGINEERING



Impact and implications of nanocatalyst in the Fenton-like processes for remediation of aquatic environment contaminated with micro-pollutants: A critical review

Himangshu Dihingia, Diwakar Tiwari^{*}

Department of Chemistry, School of Physical Sciences, Mizoram University, Aizawl 796004, India

ARTICLE INFO

Keywords:
Micro-pollutants
Fenton-like process
Insights of mechanism
Bimetallic
Nanocomposites

ABSTRACT

Nanomaterials-mediated Fenton-like processes have received global interest because of their unique and efficient degradation efficacy towards potential micro-pollutants in aquatic environments. The Fenton-like approach is relatively promising, greener, and interestingly, the micro-pollutants are degraded to their end products efficiently. The conventional Fenton-like methods are concomitant with several limitations, including the high operational costs, risk possibility in handling, and the significant leaching of iron that causes indirect contamination. The advanced and newer nanocomposite materials have shown unique and advanced technological inputs in the development and optimized use of Fenton-like processes. Therefore, this communication's inherent objective is to critically review the role of various nanocomposite catalysts in the Fenton-like process. Further, the review extensively demonstrated the critical aspects of homogeneous chemistry to heterogeneous chemistry using nanomaterials and nanoparticles to degrade a wide range of emerging micro-pollutants. The critical parameters, viz., the support media, light energy, ultrasound, which significantly affect the efficiency of Fenton-like processes, are extensively demonstrated in the review for greater applicability of study. Moreover, the challenges and commercial implications are outlined and discussed for possible future perspectives.

1. Introduction

Polluting the water bodies by a range of micro-pollutants is becoming a severe ecological concern requiring urgent monitoring and implementation of proper and adequate remediation plans for its agreeable solutions. The primary problem is the unfettered discharge of wastewaters (WW) from a variety of industries along with the agricultural runoffs contained with several herbicides/pesticides into the receiving water bodies and led to the widespread contamination of aquatic environments. A wide range of organic contaminants viz., pharmaceuticals, personal care products (PCPs), endocrine-disrupting chemicals (EDCs), dyes, nitrogen-containing compounds, halogenated aliphatic and aromatic hydrocarbons, agrochemicals, etc. are readily detected in measurable quantity in the water bodies and posing a serious threat to the ecological system [1–6].

The advanced treatment technologies including membrane filtration, wet chemical oxidation, biodegradation, flocculation, adsorption, precipitation, reduction, reverse osmosis, etc. are proposed to eliminate emerging water contaminants from aqueous wastes. However, these

methods are sometimes inadequate to eliminate the recalcitrant and emerging pollutants from aqueous solutions or found exceedingly expensive for possible implications. Additionally, expensive equipment, high operating costs, and high maintenance limited these methods' utilization further [7]. Moreover, the environmentally sustainable remediation process is demonstrated with low energy consumption [8], less harmful byproducts that are greatly preferred. Therefore, the researchers propose newer and advanced methods for the efficient treatment of potential recalcitrant that need to be reviewed for greater understanding.

Among numerous treatment technologies, advanced oxidation processes (AOPs) are utilized as an innovative method for efficient and enhanced degradation of recalcitrant micropollutants. The process is simply based on the in situ hydroxyl radicals ($\cdot\text{OH}$) generation. The hydroxyl radicals hence provide enhanced oxidation ability (standard potential: 2.80 V vs SHE) as well as high rate constants for bimolecular reactions ($10^8\text{--}10^{11} \text{ M}^{-1} \text{ s}^{-1}$) and non-selective reactivity [9–11]. It is interesting to note that the $\cdot\text{OH}$ radical either oxidize the complex organic molecules to smaller by-products or degrade completely to their

^{*} Corresponding author.

E-mail address: diw.tiwari@yahoo.com (D. Tiwari).

<https://doi.org/10.1016/j.jwpe.2021.102500>

Received 22 October 2021; Received in revised form 1 December 2021; Accepted 3 December 2021
2214-7144/© 2021 Elsevier Ltd. All rights reserved.

Volume 381P2, 25 December 2022 ISSN 0959-6526



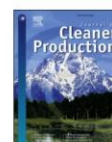
Journal of Cleaner Production

- Pollution Prevention
- Source Reduction
- Industrial Ecology
- Life Cycle Assessment
- Waste Minimisation
- Sustainable Development



Contents lists available at ScienceDirect

Journal of Cleaner Production

journal homepage: www.elsevier.com/locate/jclepro

Green synthesis of bimetallic nanocomposite: Efficient use of nanocomposite in the removal of phenol and n-(n-Propyl) thiourea by photo-Fenton-like process

Himangshu Dihingia, Diwakar Tiwari^{*}

Department of Chemistry, School of Physical Sciences, Mizoram University, Aizawl, 796004, India

ARTICLE INFO

Handling Editor: Mingzhou Jin

Keywords:
Bimetallic Fe⁰/Ag⁰ catalyst
Phytochemicals
Photo-fenton-like process
Reusability of nanocatalyst
Degradation mechanism
Real matrix treatment

ABSTRACT

The contamination of water bodies with emerging and persistent water contaminants, viz., phenol and n-(n-propyl) thiourea (NNPT) is a severe environmental and health concern. This study aims to obtain the novel bimetallic heterogeneous nanocatalyst supported with natural bentonite using a facile greener route. The *in situ* bimetallic nanoparticles, i.e., Fe⁰ and Ag⁰, were obtained utilizing natural phytochemicals from leaf extracts of *P. guajava*. The XPS and XRD analyses inferred the presence of Ag⁰(NPs) and Fe⁰(NPs) in the composite material. Moreover, the bandgap energy of nanocomposite material (Ben@(Fe⁰+Ag⁰)) was 2.25 eV compared to the pristine bentonite of 3.25 eV. Further, the nanocatalyst was efficiently employed in the photo-Fenton-like process to eliminate phenol and NNPT in an aqueous medium. The degradation efficiency of the catalyst for targeted pollutants was found to be 73% (for phenol) and 95% (for NNPT) in the photo-Fenton-like process for 2 h of UV-A illumination. Similarly, a significant efficiency (Ca. 60% for phenol and Ca. 90% for NNPT) was achieved utilizing the LED (Visible) light illumination in a similar photo-Fenton-like process. The degradation of these two pollutants has predominantly proceeded through the •OH radicals. The photo-Fenton-like process mineralized these two pollutants significantly. Several parameters optimized the Fenton-like process, including pH, catalyst dose, and H₂O₂ concentration. The repeated photo-Fenton-like processes for 4 consecutive cycles showed an insignificant decrease in the efficiency of nanocatalyst, at least in the elimination of these two contaminants. The process was further employed to eliminate phenol and NNPT in the natural water samples spiked with known concentrations of these pollutants. The promising approach is excellent for the removal of recalcitrant environmental pollutants.

1. Introduction

Several recalcitrant organic compounds are widely detected in aquatic ecosystems. They pose a severe threat to humans and marine life. Moreover, the identification and exclusion of such perilous compounds from aquatic environments are continuously noticed as a persistent concern. It is noticed that various toxic chemicals are detected in the natural water bodies, which are due to the indiscriminate discharge of treated or untreated industrial and agricultural wastes (Norouzi et al., 2020). These toxic compounds enter the water bodies through different sources (Heberer, 2002). Micro-pollutants, which include pharmaceuticals, personal care products, etc., are detected in the surface or ground waters at ppb to ppm levels and significantly impact human health and marine life (Sharma et al., 2020).

The presence of phenolic compounds in the aquatic environment is identified as a biologically noxious and recalcitrant pollutant that requires serious attention. Phenols and their derivatives are often detected in petroleum refinery wastewater. In 1976, the Environmental Protection Agency (EPA) designated phenol as one of 129 priority pollutants. The World Health Organization (WHO) designated it as the third form of carcinogen in 2017 (Boruah et al., 2017). Phenol affects the nervous system, suppressing blood cell development and leading to the cancer cell activity at ppb (µg L⁻¹) levels. (Abussaud et al., 2016). Furthermore, due to their resistant and persistent character, phenolic compounds are challenging to remove from aqueous wastes using conventional treatment methods (Kumar et al., 2020).

Similarly, thiourea is a cancer-causing agent ("Sixth annual report on carcinogens," 1991) and has been found to be a very toxic compound

^{*} Corresponding author.

E-mail address: diw_tiwari@yahoo.com (D. Tiwari).

<https://doi.org/10.1016/j.jclepro.2022.133913>

Received 2 April 2022; Received in revised form 25 August 2022; Accepted 27 August 2022

Available online 6 September 2022

0959-6526/© 2022 Elsevier Ltd. All rights reserved.



Volume 308PB, 15 February 2023 ISSN 1383-5866

Separation and Purification Technology





Green and facile synthesis of heterojunction nanocatalyst: Insights and mechanism of antibiotics removal

Himangshu Dihingia, Diwakar Tiwari*

Department of Chemistry School of Physical Sciences, Mizoram University, Tanhril Campus, Aizawl 796004, India

ARTICLE INFO

Keywords:

Heterojunction bimetallic nanocatalyst
Elimination of antibiotics
Stability of nanocatalyst
Photo-Fenton-process
Real water implications
Insights of the reaction mechanism

ABSTRACT

Detecting of antibiotics in the aquatic environment is a serious health concern due to the development of antibiotic-resistant genes in humans and marine life. The current investigation aims to synthesize highly efficient heterojunction bimetallic nanocatalyst ($\text{Cu}^0 + \text{Ag}^0$)@Bentonite in a facile and 'greener' route. *In situ*, the phytochemicals of *P. guajava* leaves synthesize the Cu^0 and Ag^0 nanoparticles onto the bentonite support media. The advanced analytical methods characterize the nanomaterials extensively. The potential antibiotics (amoxicillin and sulfamethazine) are treated in photo-Fenton-like processes utilizing the UV-A and LED (Visible) light sources. The bimetallic ($\text{Cu}^0 + \text{Ag}^0$)@Bentonite exhibited a synergized in the photo-induced degradation of amoxicillin and sulfamethazine. The effect of pH, initial pollutant concentrations, and the presence of interfering ions optimize the removal efficiency and demonstrate insights into the reaction mechanism. The photo-Fenton-like degradation of AMX and SMZ was found to be 84 % and 74 %, respectively, under the UV-A illumination employing ($\text{Cu}^0 + \text{Ag}^0$)@Bentonite nanocatalyst. Similarly, the process mineralizes a significant amount of these pollutants, i.e., 66 % and 62 % of SMX and SMZ, respectively, using UV-A irradiation., enhancing the applicability of the catalyst. The nanocatalyst showed greater stability in the reactor operations, and Cu(II) leaches very minimally extent in the reaction pathways. The real water implications inferred the potential of novel nanocatalysts in scaling up the process for the decontamination of water contaminated with amoxicillin and sulfamethazine.

1. Introduction

Environmental pharmaceuticals are one of the growing threats to the ecological system. The use of antibiotics significantly increased worldwide from 2000 to 2015, contaminating the terrestrial and aquatic environment [1,2]. Among the developing countries, India is the world's biggest consumer of antibiotics, with a consumption rise of almost 100 % from 2000 to 2015, with a base consumption of 3.2 billion defined daily doses (DDD) [3]. The use of antibiotics received serious attention since bacterial resistance and harmful effects on various species, including algae and crustaceans, were discovered mostly at high concentrations and low concentrations of antibiotic exposure. The intake of these antibiotics leads to several chronic effects in humans and livestock [4].

Amoxicillin (AMX), a semi-synthetic drug of β -lactam groups of penicillin derivatives, is widely used in human and veterinary medicines and is effective for Gram-positive and Gram-negative bacteria [5]. Sulfamethazine (SMZ) is a heterocyclic sulphonamide antibacterial drug

broadly prescribed to veterinary and humans. It showed broad antimicrobial activity and was relatively less expensive to use [6]. Extensive use of these drugs causes their existence in surface water, groundwater, and soils [7]. A continued discharge into aquatic habitats gives rise antibiotic-resistant bacteria and genes (ARGs) preponderance, lowering their therapeutic value and limiting infection treatment options [8]. Effluent discharged from municipal/industrial wastewater, hospital wastewater, and treatment facilities are the significant sources of these pharmaceuticals contaminating the aquatic environment [9]. Due to the requirements for antibiotic removal, typical physical, chemical, and biological treatment procedures in industrial and pharmaceutical wastewater treatment need to remove antibiotics better [10].

Moreover, a significant fraction of antibiotics are discarded from the biological system through urine or feces, only Ca. 10–20 % is metabolized [9], and unmetabolized fraction further contaminates the water bodies. Traditional wastewater treatment plants do not efficiently eliminate these drugs due to antibiotics' limited biodegradability and persistence. This poses a greater threat to the ecosystem and needs

* Corresponding author.

E-mail address: diw_tiwari@yahoo.com (D. Tiwari).

<https://doi.org/10.1016/j.seppur.2022.122641>

Received 9 August 2022; Received in revised form 30 October 2022; Accepted 9 November 2022

Available online 15 November 2022

1383-5866/© 2022 Elsevier B.V. All rights reserved.

PARTICULARS OF THE CANDIDATE

NAME OF THE CANDIDATE : Himangshu Dihingia
DEGREE : Doctor of Philosophy (Ph.D.)
DEPARTMENT : Department of Chemistry
TITLE OF THESIS : Photo-mediated Fenton-like Process in
the Removal of Micro-pollutants from
Aqueous Solutions using Highly Active
Nano-catalyst
DATE OF ADMISSION : 18th August, 2017

APPROVAL OF RESEARCH PROPOSAL:

1. DRC : 5th April, 2018
2. BOS : 13th April, 2018
3. SCHOOL BOARD : 24th April, 2018
4. MZU REGISTRATION NUMBER : 1506749
5. Ph.D. REGISTRATION NO. & DATE : MZU/Ph.D./1103 of 24.04.2018
6. EXTENSION : NA

Head

Department of Chemistry

ABSTRACT

PHOTO-MEDIATED FENTON-LIKE PROCESS IN THE REMOVAL OF MICRO-POLLUTANTS FROM AQUEOUS SOLUTIONS USING HIGHLY ACTIVE NANO-CATALYST

**AN ABSTRACT SUBMITTED IN PARTIAL FULFILMENT OF
THE REQUIREMENTS FOR THE DEGREE OF DOCTOR OF
PHILOSOPHY**

HIMANGSHU DIHINGIA

MZU REGISTRATION NUMBER : 1506749

Ph.D. REGISTRATION NUMBER: MZU/Ph.D./1103 of 24.04.2018



**DEPARTMENT OF CHEMISTRY
SCHOOL OF PHYSICAL SCIENCES
DECEMBER, 2022**

**PHOTO-MEDIATED FENTON-LIKE PROCESS IN THE
REMOVAL OF MICRO-POLLUTANTS FROM AQUEOUS
SOLUTIONS USING HIGHLY ACTIVE NANO-CATALYST**

BY
HIMANGSHU DIHINGIA
Department of Chemistry

Under the supervision of
Prof. DIWAKAR TIWARI

Submitted
In partial fulfilment of the requirement of the Degree of Doctor of Philosophy in
Chemistry of Mizoram University, Aizawl.

ABSTRACT

Water is one of the most essential resources, and its continued exploitation for human requirements of economic and social growth, along with the crises created by climate change, has resulted in ever-increasing environmental repercussions. The majority of human activities require water and end with wastewater. As a result, worldwide demand for freshwater increases hence, the volume of wastewater generated and the pollutant burden is increasing significantly. Globally, the amount of wastewater generated and the overall pollution stockpile are increasing, owing mostly to population increase, rapid urbanization, and economic development. Water usage in the industry is estimated to account for 19% of total world water consumption. Due to its numerous uses for drinking, food, electricity, navigation, irrigation, industries, and recreation, water bodies including rivers, oceans, lakes, and ponds, among others, are under tremendous pressure. Furthermore, the discharge of municipal and industrial wastewater with variable degrees of treatment adds to the pollution load in the aquatic environment. Marine life appears to be harmed by pollutants dumped into the water bodies, and drinking natural water supplies is also rendered with pollutants load. Wastewater from diverse sources, whether fully or partially treated, returns to the natural water bodies. More than 80% of wastewater is produced worldwide, and more than 95% in some underdeveloped nations, usually discharge the wastewater into the terrestrial aquatic environment.

Waterbody pollution caused by a variety of micropollutants is developing serious environmental concerns that need immediate monitoring and the implementation of appropriate remediation programs for workable solutions. The primary cause is the unrestricted discharge of wastewater (WW) from several industries as well as agricultural runoffs containing numerous herbicides and pesticides into the receiving water bodies. This has caused a significant imbalance in the aquatic ecosystem. The ecological system is seriously threatened by micropollutants that include pharmaceuticals, personal care products (PCPs), endocrine-disrupting chemicals (EDCs), dyes, nitrogen-containing compounds, halogenated aliphatic and aromatic hydrocarbons, agrochemicals, sulphur, etc.

Diclofenac is a nonsteroidal anti-inflammatory drug having pain-relieving qualities, which is widely used in both humans and domestic animals. In general, pharmaceutical businesses, hospitals, and home drain regularly transfer diclofenac into the environment, which pollutes the environment as a parent molecule or in its metabolite forms and is thus a cause of concern. Diclofenac accumulates in edible fruits and vegetables, having a direct influence on human health. Furthermore, partial diclofenac degradation in WWTP treatment operations leaves residual diclofenac in effluent waterways, resulting in record-high diclofenac levels that threaten inland aquatic ecosystems. Phenol is one of the most prevalent organic pollutants found in industrial effluent. The most prevalent sources of phenol are textile processing, coal gasification, petroleum refining, leather production, resin synthesis, coconut retting, perfume creation, and pharmaceutical manufacturing. When introduced into aquatic ecosystems, phenol poses a significant ecological danger due to its toxicity, even at low levels. Dermatitis of the eyes, skin, and respiratory system are caused by phenol. Long-term phenol exposure has been related to health problems affecting the central nervous system, heart, liver, and kidneys. Thiourea, an antioxidant, is completely absorbed and excreted unchanged by the kidneys after oral administration to humans and animals. Because thiourea is dangerous and a cancer-causing chemical, environmental concerns have driven studies towards its efficient elimination. Amoxicillin (AMX) is a beta-lactam antibiotic that is one of the most often used antibiotics in both animal and human medicine. Because of its pharmacological properties, ingestion rate, environmental toxicity, chemical makeup, and solubility, it is considered a serious water pollutant. Amoxicillin and its hydrolyzed and metabolized compounds are found in both urine and feces, posing danger to many aquatic creatures. Sulfamethazine (SMZ) is a regularly used drug for the treatment of infectious diseases in humans and animals. It is also a very hydrophilic chemical that bacteria do not metabolize well. Through surface run-off/leaching, the SMZ is reintroduced into ground and drinking waters, surface water, and eventually aquatic ecosystems. Furthermore, it is known that sulfonamide antibiotics may impede the growth of certain *Gram-negative* bacteria as well as the majority of *Gram-positive* bacteria.

Traditional wastewater treatment plants are insufficient to remove resistant and emerging contaminants from aqueous solutions. As a result, researchers try to investigate efficient and advanced approaches for the effective treatment of prospective recalcitrants. A remediation procedure is considered ecologically sustainable if it uses less energy and produces less toxic byproducts/or sludge, hence avoiding secondary contamination. Among several treatment approaches, “Advanced Oxidation Processes (AOPs)” is used as a promising innovation for the efficient and increased destruction of stubborn micropollutants. The method relies on *in situ* generations of highly reactive hydroxyl radicals ($\bullet\text{OH}$), which gives improved oxidation capacity (standard potential: 2.80 V vs SHE). It is fascinating to observe that the $\text{OH}\bullet$ radicals either oxidize complex organic molecules to produce smaller byproducts or mineralize completely into the end products i.e., CO_2 and H_2O .

The Fenton, photo-Fenton, and photo-Fenton-like processes are some of the common AOPs that are known to be promising approaches for eliminating these toxins from water bodies. The photo-Fenton-like process, thus, is a beneficial method since it is inexpensive, simple to process, and scalable for small to medium-scale renewable methods. The development of nanotechnology opens up new possibilities for the Fenton processes. Considering the high reactivity of nanoparticles, wastewater treatment facilities have used them extensively. Similarly, the surface properties of the nanoparticles allow significantly the bulk properties of catalysts. The catalytic performance, and the nature of nanocatalysts, such as activity and selectivity, are strongly dependent on the shape, size, and surface structure, as well as on bulk compositions of catalysts. Nanotechnology-engineered materials are found to have broad applications in upgrading existing Fenton-like processes.

The Fenton-like procedures for the remediation of organic pollutants frequently make use of nano-zero-valent iron (nZVI). For the activation of H_2O_2 to produce $\bullet\text{OH}$ radicals, it is an essential slow-releasing source of soluble Fe^{2+} . However, the bimetallic nanocomposites (M/nZVI) of nZVI and other metals enhance the reactivity of nZVI and prevent iron from oxidizing on the surface. Similarly, Cu has been employed in a wider variety of catalytic applications since it is substantially less costly than other noble metal nanoparticles. Compared to monometallic catalysts, Cu-based bimetallic nano-catalysts demonstrated enhanced

catalytic activity. The reactivity of Cu is enhanced by the bimetallic nanocomposites of Cu(NPs) with other metals (M/CuNPs). The exterior surface of the catalyst is shielded from copper oxidation by this bimetallic arrangement. Silver nanoparticles (Ag(NPs)) are investigated for numerous of today's water purification technologies since they are less dangerous to people and are simple to impregnate on many substrates for a variety of functions. Even though these nanoparticles are having a wide range of applications, employing them might be challenging since they frequently oxidize or aggregate. Therefore, improving the stability and reactivity of nanocatalysts with a support medium is a good substitute for the essential consequences of catalysts. Pillared interlayered clays, mesoporous materials, biochar, activated carbon, ashes, zeolites, polymeric resins, Nafion films, etc. are some of the supporting materials used. Alternative support media include natural clay materials, which have a high specific surface and are porous by nature. The kaolinite form of clay comprises layers, whereas bentonite is smectite. Two layers of tetrahedral silicon $[\text{SiO}_4]^{4-}$ and one layer of octahedral aluminum (magnesium) oxygen $[\text{AlO}_3(\text{OH})_3]^{6-}$ sheets, in a 2:1 ratio, make up the interlaminar structure of bentonite. Possibly a useful substance for support medium in the impregnation of nanocatalysts is bentonite. As a result, the main objective of this research was to obtain a simple, environment-friendly method for making the novel bimetallic heterogeneous nano-Fenton-like catalyst that is supported by bentonite. Fe(NPs), Cu(NPs), and Ag(NPs) *in situ* nanoparticles were obtained in a more environment-friendly manner.

Simple and one-pot synthetic methods were used to produce the nanocomposite materials. The composite materials named as Ben@FeNPs, Ben@(FeNs+AgNPs), Ben@CuNPs, and Ben@(CuNs+AgNPs), the Fe(NPs), Cu(NPs), and Ag(NPs) were synthesized by *in situ* generations of respective nanoparticles on the surface of bentonite clay. Additionally, these materials were used in batch investigations to photo-Fenton-like degradation of several targeted micro-pollutants from aqueous solutions. The materials were characterized by advanced analytical methods. The diffuse reflectance data were converted into the materials' absorption coefficient (α) values using the Kubelka-Munk equation and Tauc's relationship, and the band gap energy of the material was then calculated. The diffuse reflectance spectra (DRS) for unmodified bentonite and all of the modified

nanocomposite materials, including Ben@FeNPs, Ben@(FeNPs+AgNPs), Ben@CuNPs, and Ben@(CuNPs+AgNPs), were obtained using a UV-Vis spectrophotometer. Ben@FeNPs and Ben@(FeNPs+AgNPs) have band gap energies of 2.25 and 2.17 eV, which are significantly lower than the 3.25 eV of pristine bentonite. The catalyst Ben@(CuNPs+AgNPs), similarly showed the visible-light-induced photo-Fenton-like reaction by having a significantly lower band-gap energy (2.32 eV) than bentonite (3.25 eV). All these materials feature H3 hysteresis loops in their Type IV type isotherms, as shown by the N₂ adsorption/desorption isotherms. These results showed that the materials have a mesoporous structure with a random distribution of pore sizes. The pore size for Ben@FeNPs was 91.086 cm³g⁻¹, whereas Ben@(FeNPs+AgNPs) had a pores size of 0.099 cm³g⁻¹. The corresponding BET-specific surface areas for bentonite, Ben@FeNPs, and Ben@(FeNPs+AgNPs) were 62.67, 36.50, and 8.61 m²g⁻¹, respectively. Additionally, the pore diameters of the Ben@CuNPs and Ben@(CuNPs+AgNPs) were 13.02 nm and 5.86 nm, respectively, whilst the BET-specific surface areas were 36.50 and 20.55 m²g⁻¹ for the Ben@CuNPs and Ben@(CuNPs+AgNPs), respectively. The Ben@(FeNPs+AgNPs) XRD data showed different diffraction peaks that confirm the presence of quartz, Fe(NPs), and Ag(NPs). The Ben@(FeNPs+AgNPs) solid has silver and iron in their zero-valent oxidation states, based on the XPS results. The existence of zero-valent Cu and Ag in the nanocatalyst was also implied by X-ray photoelectron spectroscopy and XRD investigations of the Ben@(CuNPs+AgNPs) nanocomposite. The heterogeneous and layered structures of each modified nanocomposite material were visible in the bentonite SEM images. The surface structure of the bentonite, Ben@FeNPs, Ben@(FeNPs+AgNPs), Ben@CuNPs, and Ben@(CuNPs+AgNPs) nanocomposites was denser, with the Fe, Cu, or Ag nanoparticles preferentially occupied the pores. These solids contain common elements including Si, Fe, Al, C, O, Na, K, Ti, etc., according to the EDX findings. However, the EDX spectrum of Ben@(FeNs+AgNPs) shows an extra peak of Ag, indicating that the nanocomposite solid contains Ag. The spatial distribution of nanoparticles on the surface of the bentonite was seen in the TEM images of these nanocomposite materials and nanoparticles are not agglomerated on the surface. The Ben@(FeNPs+AgNPs) nanocomposite's average particle size was found to be about 10 nm. Ag(NPs) are

found to have a d-spacing of 0.1435 nm. The Ben@(CuNPs+AgNPs) nanocomposite displayed a heterogenous surface structure, and the fringes showed that the Cu(NPs) and Ag(NPs) had respective d-values of 0.243 and 0.164 nm (NPs). The solids Ben@CuNPs and Ben@(CuNPs+AgNPs) are having average particle sizes of 4.207 nm and 2.518 nm, respectively.

In order to gain insights into the mechanisms of the degradation process, several physicochemical parametric studies are carried out to look into the photo-Fenton-like degradation of micropollutants. Under various light conditions, the nanocatalysts were used in a photo-Fenton-like procedure to degrade DCF, phenol, NNPT, AMX, and SMZ. Utilizing LED (Visible) and UV-A light irradiations, the photo-Fenton-like process using the Ben@(FeNPs+AgNPs) nanocatalyst demonstrated a very high percentage elimination of DCF. The best reaction conditions, which included a pH of 3.0, 250.0 mg/L of Ben@(FeNPs+AgNPs) nanocatalyst, and 0.4 mL/L of 30% H₂O₂, enabled 56% of DCF (2.0 mg/L) removal in 2 hrs of reaction time in the dark. Additionally, the degrading efficiency of the photo-Fenton-like process was increased by the UV-A and LED irradiations to 83% (UV-A) and 70% (LED), respectively, for the elimination of DCF. Additionally, the photo-Fenton-like procedure allowed the DCF to mineralize to 74% utilizing UV-A light in 2 hrs of reaction time. 43.3% of phenol (2.0 mg/L) degradation was accomplished after 2 hrs of reaction time in a dark environment under ideal reaction conditions. Furthermore, the UV-A and LED light irradiations improved the elimination efficiency to 73.3% and 60.0%, respectively. Similar to this, 72.7% of the 2.0 mg/L NNPT was eliminated after 2 hrs in the dark environment. However, the use of light radiations enhanced the degradation efficiency to 95.1% (UV-A) and 84.9% (LED). The mechanism of the reaction showed that the •OH radical is predominantly involved in the reaction stages. A large amount of phenol and NNPT i.e., 55.5% and 64.2%, respectively, were mineralized by UV-A irradiation in the photo-Fenton-like processes. Likewise, AMX and SMX degradation was carried out using the Ben@CuNPs and Ben@(CuNPs+AgNPs) solids. Ben@[CuNPs+AgNPs] nanocatalyst enabled the photo-Fenton-like degradation of AMX under UV-A and LED (visible) light at 84% and 72%, respectively. In contrast, in the absence of light, only 56% degradation is obtained in 2 hrs of reaction time. Similar to this, after 2 hrs

of reaction time, the Fenton-like degradation of SMZ using the Ben@(CuNPs+AgNPs) nanocatalyst was found to be 74% and 61%, respectively, in UV-A and LED light, but the degradation was only 44% in the absence of light. Additionally, using the Ben@CuNPs nanocatalyst in a dark environment, degradation of AMX and SMZ was achieved at a rate of 56% and 44%, respectively. All of the targeted nanoparticles exhibit a higher mineralization efficiency for these pollutants in the photo-Fenton-like reactions.

Furthermore, via several repeated cycles of degradation, the reusability of the nanocomposite materials, viz. Ben@(FeNPs+AgNPs) and Ben@(CuNPs+AgNPs) was investigated. During repeated catalytic operations carried out throughout four successive cycles, the Ben@(FeNPs+AgNPs) nanocatalyst showed remarkable stability against the degradation of DCF, phenol, and NNPT. Similarly, the degradation of AMX and SMZ demonstrated very acceptable stability at least for 5 repeated cycles of operations. Moreover, in the actual matrix water studies, these catalysts' effectiveness was not significantly impacted. This demonstrated the broader industrial applications of the catalysts, at least for the "Pilot-Scale" unit operations.